

TG-1034A
DECEMBER 1968
Copy No. 1



Technical Memorandum

**DODGE SATELLITE PERFORMANCE
1 JULY 1967 — 1 OCTOBER 1968**

Prepared by SPACE DEVELOPMENT DEPARTMENT

**COLOR ILLUSTRATIONS REPRODUCED
IN BLACK AND WHITE**



THE JOHNS HOPKINS UNIVERSITY • APPLIED PHYSICS LABORATORY

This document has been approved for public
release and sale; its distribution is unlimited.

TG-1034A
DECEMBER 1968

Technical Memorandum

**DODGE SATELLITE PERFORMANCE
1 JULY 1967 — 1 OCTOBER 1968**

Prepared by SPACE DEVELOPMENT DEPARTMENT

THE JOHNS HOPKINS UNIVERSITY ■ APPLIED PHYSICS LABORATORY
8621 Georgia Avenue, Silver Spring, Maryland 20910
Operating under Contract NOw 68-0604-c with the Department of the Navy

This document has been approved for public
release and sale; its distribution is unlimited.

ABSTRACT

This report defines the mission of the Department of Defense Gravity Experiment (DODGE) satellite program, describes briefly the design of each of the satellite systems, and describes in detail the performance of each of the systems from the time the satellite was launched into orbit on 1 July 1967 to 1 October 1968. The systems include attitude control, attitude detection, electric power, telemetry, command, thermal control, and doppler tracking. It also includes ground station operations. The report summarizes the magnetic field measurements made to date and the performance of the satellite's attitude control systems. It presents conclusions on the attitude performance and on how well the objectives of the mission were met.

Volume B is an Appendix and contains pitch-roll, yaw, and in-plane-cross-plane plots for APL passes 2 through 39 and ORRORAL passes 2, 9, 14, 16, and 17.

CONTENTS

	Page
ILLUSTRATIONS	xiii
TABLES	xxi
1. INTRODUCTION	1-1
1.1 Mission Objectives	1-1
1.2 Mission Plan	1-2
1.2.1 Satellite Design	1-2
1.2.2 Ground Stations for Data Acquisition and Tracking	1-4
1.3 Launch and Immediate Post-Launch Operations	1-8
1.4 Satellite Tracking	1-12
2. ATTITUDE CONTROL SYSTEM DESIGN AND PERFORMANCE	2-1
2.1 Magnetic Damping and Stabilization System	2-4
2.1.1 System Design	2-4
2.1.1.1 Hysteresis Damping	2-6
2.1.1.2 Sample-and-Hold Damping	2-6
2.1.1.3 Power Amplifiers, Electromagnets, and Z Coil	2-7
2.1.1.4 Hardware	2-8
2.1.2 Magnetic Despin System	2-8
2.1.2.1 Spin-Despin Mode	2-8
2.1.2.2 Enhanced Hysteresis Rod	2-10
2.1.2.3 Demagnetization Capability	2-12
2.1.2.4 In-Orbit Performance of Magnetic Angular Rate Damping System	2-13
2.1.3 Magnetic Stabilization System	2-15
2.1.3.1 Fixed X-Z Magnetic Moment	2-15
2.1.3.2 Variable X-Z Magnetic Moment	2-17
2.1.3.3 Z Axis Fixed Magnetic Moment	2-17
2.2 Gravity-Gradient Stabilization Systems	2-18
2.2.1 Extendible Booms	2-23

	Page
2.2.1.1 System Description and Performance	2-23
2.2.1.2 Thermal Bending	2-27
2.2.2 Angular Momentum Flywheel	2-39
2.2.3 Magnetic Damping Systems	2-42
2.2.3.1 Time-Lag Damping	2-42
2.2.3.2 Enhanced Hysteresis Damping	2-48
2.2.3.3 Magnetometer Performance	2-49
2.2.4 Torsion Wire Damping System	2-51
2.2.4.1 Damper Booms	2-55
2.2.4.2 Torsion Wire Suspension System	2-55
2.2.4.3 Caging Mechanisms	2-55
2.2.4.4 Electrical System	2-59
2.2.4.5 Angle Sensor	2-59
2.2.4.6 Eddy-Current Damper	2-59
2.2.4.7 Magnetic Hysteresis Damper	2-61
2.2.4.8 In-Orbit Performance	2-64
2.2.5 Manual Damping Using the Angular Momentum Flywheel	2-66
2.3 Prelaunch Computer Simulation of Time-Lag Magnetic Damping and Torsion Wire Gimbal Damping, Neglecting External Effects	2-68
2.3.1 Simulation Objectives	2-68
2.3.2 Simulation of the Torsion Wire Gimbal Damping System	2-69
2.3.2.1 Development of Rotational Equations of Motion	2-70
2.3.2.2 Stability Analysis--Application of Lyapunov's Second Method	2-80
2.3.2.3 Numerical Results	2-85
2.3.3 Simulation of Time-Lag Magnetic Damping	2-92
2.3.3.1 Equations of Motion	2-94
2.3.3.2 Analysis of the Damping	2-97
2.3.3.3 Numerical Analysis	2-101
2.3.4 Conclusions	2-108

	Page
2.4 Comparison of Theoretical and Experimental Data for Time-Lag Damping Systems in the Presence of an Apparent Time Dependent Magnetic Field	2-110
2.4.1 Conclusion	2-114
2.5 Prelaunch Computer Simulation of Time-Lag Magnetic Damping, Including External Effects	2-114
2.5.1 Equations of Motion	2-116
2.5.2 Magnetic Torques	2-121
2.5.3 Thermal Bending of Stabilizing Booms	2-124
2.5.4 Radiation Pressure Torques	2-129
2.5.5 Prelaunch Performance Evaluation	2-130
2.6 Comparison of Theoretical Experimental DODGE Attitude Data with DAS Program	2-136
2.6.1 Simulation for Days 260-275, 1967	2-142
2.6.2 Simulation for Days 318-338, 1967	2-142
2.6.3 Simulation for Days 352-363, 1967	2-143
2.6.4 Simulation for Days 033-048, 1968	2-143
2.6.5 Conclusion	2-144
2.7 References	2-145
3. ATTITUDE DETECTION SYSTEM	3-1
3.1 Dual Television Camera System	3-1
3.1.1 TV System Configuration	3-1
3.1.2 Camera Design	3-3
3.1.2.1 Electronic Design	3-7
3.1.2.2 Mechanical Design	3-14
3.1.2.3 Optical Design	3-21
3.1.3 In-Orbit Performance	3-23
3.1.3.1 Attitude Measurement	3-27
3.1.3.2 Multispectral Experiment	3-31
3.1.3.3 Engineering Performance	3-31

	Page
3.2 Solar Attitude Detectors	3-33
3.2.1 Cosine Detectors	3-33
3.2.2 Linear Detectors	3-33
3.2.3 Bias Voltage Regulator	3-34
3.2.4 Detector Construction	3-34
3.2.5 Detector Calibration	3-37
3.2.5.1 Normal Incidence Calibration	3-37
3.2.5.2 Calibration for Output With Variations in Incidence Angle	3-38
3.2.5.3 Temperature Calibration	3-38
3.2.5.4 Correction to Mean Solar Intensity	3-38
3.2.6 In-Orbit Performance	3-38
3.3 The Use of the Vector Magnetometer System In Attitude Detection	3-42
3.4 DODGE Attitude Detection Procedure	3-43
3.4.1 Pitch and Roll Determination - Reduction of Televised Earth Pictures	3-43
3.4.2 Yaw Determination	3-46
3.4.2.1 Operational Method Using Analog Solar Attitude Detectors	3-46
3.4.2.2 Alternate Method Using Terminator Cusps	3-48
3.4.2.3 Alternate Method Using Identifiable Geographic Features	3-48
3.4.3 Data Reduction	3-49
3.4.4 Summary and Conclusions	3-50
3.5 References	3-50
4. ELECTRIC POWER SYSTEM	4-1
4.1 Solar Array	4-1
4.1.1 Design Characteristics	4-1
4.1.2 In-Orbit Performance	4-4

	Page
4.2 Battery	4-7
4.2.1 Design Characteristics	4-7
4.2.2 In-Orbit Performance	4-9
4.3 Voltage Limiting	4-13
4.3.1 Low Voltage Sensing Switch	4-13
4.3.2 High Voltage Zeners	4-13
4.4 Converters and Inverters	4-13
5. TELEMETRY SYSTEM	5-1
5.1 System Design	5-1
5.2 In-Orbit Performance	5-10
6. COMMAND SYSTEM	6-1
6.1 Description	6-1
6.2 Command Function Descriptions	6-10
6.3 In-Orbit Performance	6-31
7. THERMAL CONTROL SYSTEM	7-1
7.1 Description	7-1
7.2 In-Orbit Performance	7-4
8. DOPPLER TRACKING SYSTEM	8-1
8.1 Near-Synchronous Orbit Tracking	8-1
8.2 DODGE Doppler Data	8-2
8.3 Data Compression	8-3
8.4 Tracking Program	8-6
8.5 Tracking Results	8-7
8.6 Solar Detector Data	8-10
8.7 Antenna Pointings	8-11
8.8 Conclusions	8-12
8.9 References	8-14
9. GROUND STATIONS OPERATION	9-1
9.1 APL Command and Telemetry Station	9-1
9.1.1 Operating Modes	9-3

	Page
9.1.2 Data Output	9-6
9.1.2.1 Analog Strip Charts	9-6
9.1.2.2 Analog Data Tapes	9-6
9.1.2.3 Telemetry Printouts	9-6
9.1.2.4 Digital Data Tapes	9-12
9.1.2.5 TV Picture Data	9-12
9.1.3 Hardware	9-14
9.1.3.1 RF and Analog Hardware	9-14
9.1.3.2 Digital Hardware	9-14
9.1.3.3 TV Recovery System Hardware	9-18
9.1.4 Software	9-21
9.1.4.1 Programming Approach.	9-21
9.1.4.2 Real-Time Decommutation Program	9-22
9.1.4.3 Sequential Operation of the Decommutation Program (Refer to Fig. 9-12)	9-25
9.1.4.4 DODGE Non-Real Time Program	9-29
9.1.4.5 Data Tape File Handling Program	9-29
9.1.5 Performance Evaluation	9-30
9.2 DODGE Satellite Time Tracking System	9-30
9.2.1 Description	9-30
9.2.2 Establishing An Epoch	9-32
9.2.3 Time Recovery Accuracy vs. Signal to Noise Ratios	9-34
9.2.4 Measurement and Stability of Equipment Delays	9-35
9.2.5 Tracking Results	9-36
9.3 References	9-36
10. TV PICTURE STUDY	10-1
10.1 Processing System	10-1
10.1.1 Hardware Configuration	10-2
10.1.2 Software Description	10-6

	Page
10.1.2.1 Synchronization and Input Conversion	10-7
10.1.2.2 Repair and Quality Enhancement	10-8
10.1.2.3 Video Display Routines	10-13
10.1.2.4 Analysis of Picture Content	10-14
10.1.2.5 Data Handling, Conversion, and Storage	10-15
10.2 Picture Characterization	10-17
10.2.1 Camera Limitations	10-18
10.2.2 Reproducer Limitations	10-23
10.3 Data Analysis	10-26
10.3.1 Picture Distortion	10-26
10.3.2 Photometric Calibration	10-31
10.4 Picture Correction Procedures	10-31
10.4.1 Prestorage Processing	10-33
10.4.2 Special Processing	10-38
10.5 Photographic Procedures	10-40
10.6 Optical Processing	10-41
10.7 References	10-43
11. MAGNETIC FIELD MEASUREMENTS	11-1
12. CONCLUSIONS	12-1
13. BIBLIOGRAPHY	13-1
APPENDIX A. RESULTS OF ATTITUDE CONTROL EXPERIMENTS	Vol. B

BLANK PAGE

ILLUSTRATIONS

Figure		Page
Front.	The Earth as Seen From 20,000 Miles Taken by the DODGE Satellite. Received at the Johns Hopkins University, Applied Physics Laboratory, September 23, 1968 .	xxiii
1-1	DODGE - Artist's Concept . . .	1-3
1-2	Location of Data Acquisition and Tracking Stations . . .	1-5
2-1	"Times" Configuration for DODGE . . .	2-2
2-2	Simplified Block Diagram of DODGE Enhanced Magnetic Damping System . . .	2-5
2-3	Functional Block Diagram of Enhanced Hysteresis Damping System . . .	2-11
2-4	DODGE Detumble History . . .	2-14
2-5	Hysteresis Loops from TM Data . . .	2-16
2-6	"Plus" Boom Configuration With Damper Booms Extended . . .	2-19
2-7	"Times" Boom Configuration With Damper Booms Extended . . .	2-20
2-8	External Arrangement . . .	2-21
2-9	DODGE Extendible Boom . . .	2-24
2-10	"Plus" Configuration . . .	2-26
2-11	Displacement of DODGE End Mass Due to Thermal and Dynamic Bending of -Z Boom, Pass 10-Days 283, 284, 1967 . . .	2-29
2-12	Displacement of DODGE End Mass Due to Thermal and Dynamic Bending of -Z Boom, Pass 24 - Days 076, 077, 078, 1968 . . .	2-30
2-13	Displacement of DODGE End Mass Due to Thermal and Dynamic Bending of -Z Boom, Pass 24 - Day 076, 1968 . . .	2-31

Figure		Page
2-14	Thermal Boom Bending	2-38
2-15	Flywheel Motor Current After a 235 Second Turn-Off	2-41
2-16	Libration History of Pass No. 3	2-43
2-17	Libration History of Pass No. 4	2-44
2-18	Libration History of Pass No. 8	2-47
2-19	Libration History of Pass No. 9	2-47
2-20	Magnetic Field Observed During Pass No. 8	2-50
2-21	Magnetic Field Observed During Pass No. 7	2-50
2-22	DODGE Magnetic Field Data through Solar Eclipse	2-52
2-23	Torsion Wire Damper Assembly	2-53
2-24	DODGE Showing Damper Assembly and Booms	2-54
2-25	Torsion Wire Damper Assembly Cross Section	2-56
2-26	Launch Lock Clamping System	2-58
2-27	Vane and Magnet	2-60
2-28	Magnetic Hysteresis Damper	2-63
2-29	Hysteresis Damper Performance	2-65
2-30	Manual Damping By Flywheel Reversal	2-67
2-31	Primary Configuration with Torsion Wire Damper.	2-71
2-32	Transient Response to Initial 10° Pitch Displacement	2-86

Figure		Page
2-33	Study to Optimize Damping Constant K .	2-87
2-34	Effect of Ratio I_d/I_ξ on Damping Time .	2-88
2-35	Effect of Torsion Wire Constant .	2-90
2-36	Effect of Damper Boom Offset Angle .	2-91
2-37	Time Lag Magnetic Damping System (Single Axis).	2-93
2-38	Energy Damping Time Constant as a Function of Holding Time and Initial Phasing (Initial Yaw Perturbation). .	2-102
2-39	Energy Damping Time Constant as a Function of Holding Time and Initial Phasing (Initial Roll Perturbation). .	2-103
2-40	Energy Damping Time Constant as a Function of Holding Time (Yaw Perturbation of Maximum Amplitude, $\alpha = \pi/2$)	2-104
2-41	Energy Damping Time Constant as a Function of Holding Time (Roll Pertur- bation of Maximum Amplitude, $\alpha = \pi/2$) .	2-105
2-42	Study to Optimize Holding Time for Initial Roll Perturbations	2-107
2-43	Transient Response to an Initial 10° Yaw Angle with 15 Hour Time Lag Holding Period	2-109
2-44	DODGE Attitude Analysis - Eighth Pass- Correlation of Average Predicted Attitude Energy With Actual Attitude Energy	2-111
2-45	DODGE Attitude Analysis - Ninth Pass- Correlation of Predicted Attitude Energy With Measured Values	2-113

Figure		Page
2-46	Reference Frames Used to Define Orientations of Spacecraft . . .	2-118
2-47	Local Vertical Reference Frame . . .	2-119
2-48	Time Lag Magnetic Damping . . .	2-122
2-49	Thermal Bending Reference Systems .	2-126
2-50	Least Squares Constant Curvature Fit of a Thermally Deformed Boom ($\phi = 2\pi$ Rad/150ft., $\psi = 0$, Overlap = 98.6°)	2-128
2-51	Simulation Results for Plus Configuration of DODGE Spacecraft in Inclined Orbit	2-132
2-52	Simulation Results for Times Configuration of DODGE Spacecraft in Inclined Orbit	2-133
2-53	Simulation Results for Dumbbell Configuration of DODGE Spacecraft in Inclined Orbit	2-134
2-54	Comparison of Flight and Theoretical Data for Days 260-275, 1967. . .	2-138
2-55	Comparison of Flight and Theoretical Data for Days 318-330, 1967. . .	2-139
2-56	Comparison of Flight and Theoretical Data for Days 352-363, 1967. . .	2-140
2-57	Comparison of Flight and Theoretical Data for Days 033-048, 1968. . .	2-141
3-1	Artist's Conception of DODGE, Showing Its Two Cameras And Their Picture Characteristics	3-2
3-2	TV System Block Diagram	3-4
3-3	DODGE Camera System	3-5

Figure		Page
3-4	Functional Block Diagram of Camera Electronics	3-8
3-5	Beam Modulation in the DODGE Cameras .	3-11
3-6	Temporal Relationship of Sampling .	3-13
3-7	60° Shutter Assembly	3-15
3-8	22° Shutter Assembly	3-16
3-9	Vidicon Mounting Hardware	3-19
3-10	Vidicon Tube Assembly, 22° and 60° Camera	3-20
3-11	22° Camera Head Assembly With Cover Removed.	3-22
3-12	Color Channel Spectral Characteristics	3-24
3-13	Haze Filter Characteristics.	3-25
3-14	Optical Calibration Setup	3-26
3-15	Earth From the 60° DODGE Camera . .	3-28
3-16	Earth From the 22° DODGE Camera . .	3-29
3-17	Earth Through the Blank Position of the 22° DODGE Camera	3-30
3-18	DODGE Camera Performance Data-Days 233 and 234, 1968.	3-32
3-19	DODGE Type Solar Attitude Detector .	3-35
3-20	DODGE +Z Axis Solar Attitude Detector Output at 77°F as a Function of Solar Incidence Angle (Prelaunch Calibration)	3-36
3-21	Coordinate Grid Template for 60° Camera	3-44
3-22	Coordinate Grid Template for 22° Camera	3-44

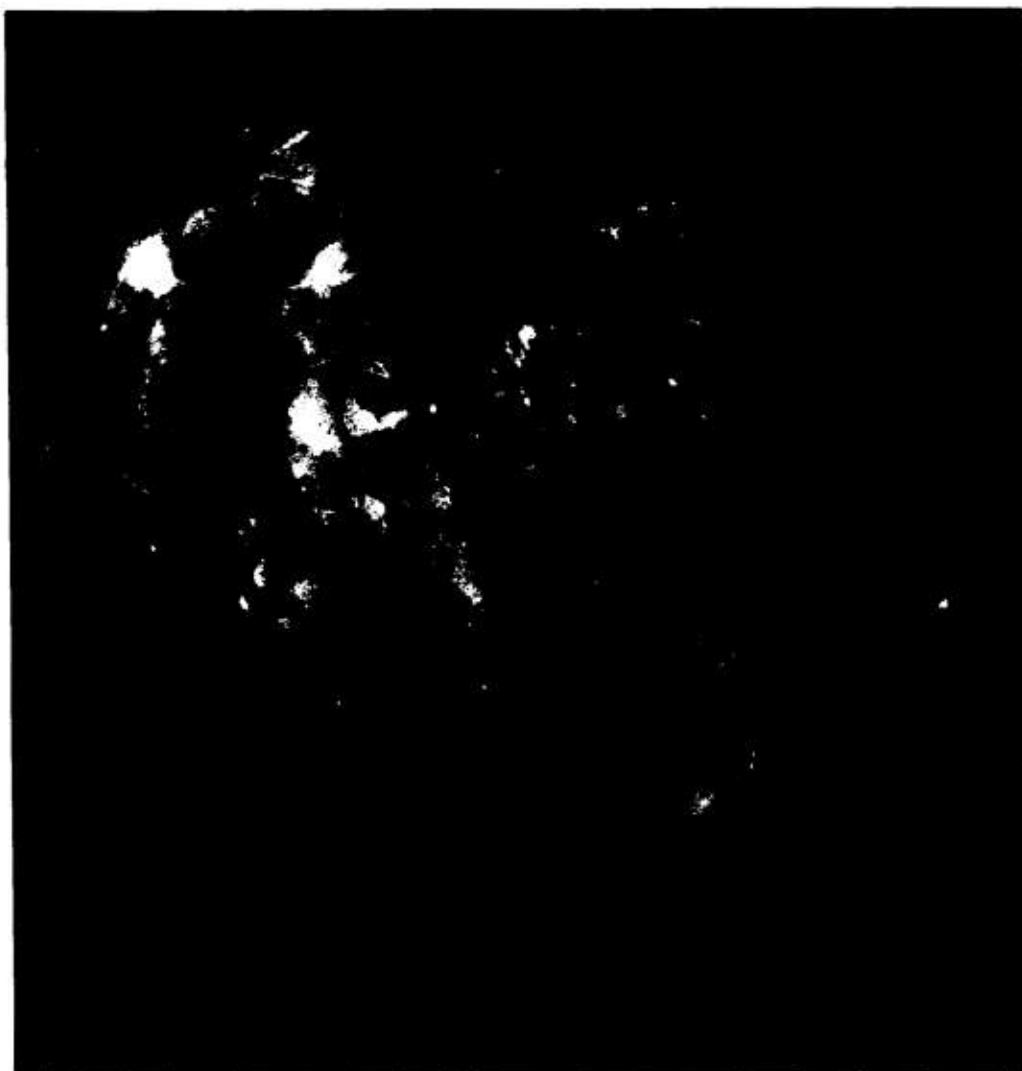
Figure		Page
3-23	Typical Horizon - Subpoint Overlays for Various Local Vertical Angles	3-45
3-24	Reduction of DODGE Television Picture of Earth	3-47
4-1	Block Diagram of Satellite Electrical System	4-2
4-2	Preflight Data for DODGE Solar Cell Array	4-2
4-3	DODGE +X Equatorial Solar Panel	4-5
4-4	DODGE Solar Array Current (Main Circuit)	4-6
4-5	DODGE Main Solar Array Current Vs Time	4-8
4-6	DODGE Satellite Battery	4-10
4-7	DODGE Battery Capacity Measurements	4-11
4-8	DODGE Battery Performance Data Day 234, 1968	4-12
5-1	Block Diagram of the Telemetry System for the DODGE Satellite	5-3
5-2	Modulation Index Control.	5-5
5-3	DODGE Time Burst Waveform	5-9
5-4	DODGE Automatic Mode Timing Diagram	5-9
6-1	Block Diagram of DODGE Command System	6-2
6-2	Power Switching Matrix	6-3
7-1	Thermal Vacuum Test Results Compared With Orbit Predictions (Minimum Sun Orbit, Day 081, 1967)	7-3

Figure		Page
7-2	Telemetered Battery Cell Temperature Compared With Analytical Prediction (Minimum Sun Orbit, Day 284-285, 1967)	7-3
8-1	Typical 10-Minute Block of DODGE Doppler Versus Time	8-4
8-2	Real Doppler Curve From DODGE Pass: Day 214 to 219, 1967.	8-4
8-3	Tracking Accuracy Measures From All Available Sources Versus Time	8-8
8-4	Modeled Ionospheric Refraction Contribution to Doppler Signal From a Near-Synchronous Satellite	8-13
8-5	Doppler Residuals After Tracking From DODGE Pass: Day 214 to 219, 1967	8-13
9-1	Station 502 Functional Diagram.	9-2
9-2	Analog Strip Chart Recording	9-7
9-3	Real Time Telemetry Printout	9-8
9-4	Non-Real Time Telemetry Printout	9-9
9-5	Real Time TV Pictures	9-13
9-6	RF and Analog Section Hardware.	9-15
9-7	Digital Section Hardware	9-16
9-8	Video Section Hardware	9-19
9-9	DODGE TV Reproduction Equipment	9-20
9-10	Simplified Flow Chart Real Time Program.	9-23
9-11	Computation of Calibration Equations	9-24
9-12	DODGE Decommutation Program Timing	9-26
9-13	Typical Station Clock System	9-33

Figure		Page
9-14	Station 112 DODGE Timing Points First Differences	9-37
10-1	Block Diagram of DODGE Video Processor.	10-3
10-2	Conventional Digital Data Tape Format .	10-9
10-3	An Uncorrected DODGE Picture. . . .	10-19
10-4	Comparison of the DODGE Camera "Haze 4" Position and the Standard Visual Response.	10-22
10-5	Reproducer Warm-Up Characteristic. .	10-24
10-6	Reproducer Film Batch Variance . .	10-25
10-7	Data Distribution for Picture of Fig. 10-3	10-27
10-8	Page 2 of TVSTAT Output.	10-29
10-9	Section of the Line Average Graph From TVSTAT	10-30
10-10	Output of FRAME	10-32
10-11	Uncorrected Picture and its Data Distribution	10-34
10-12	Picture and Data Distribution After Background Correction	10-35
10-13	Picture and Data Distribution After Prestorage Corrections	10-36
10-14	Enlarged Picture After Prestorage Corrections	10-39
10-15	Schematic of Basic Optical System. .	10-42
10-16	Optical Line Removal	10-44
11-1	An Example of Geomagnetic Micropulsations	11-2
A-1	Matrix Representation of Attitude Angles	A-2

TABLES

Table		Page
2-1	Sun to Satellite Angles, APL Pass No. 10, Days 283-284, 1967 . . .	2-33
2-2	Sun to Satellite Angles, APL Pass No. 24, Days 076-078, 1968 . . .	2-34
2-3	Sun to Satellite Angles, APL Pass No. 24, Day 076, 1968.	2-37
2-4	Spacecraft Characteristics	2-131
3-1	Summary of DODGE Camera System Characteristics	3-6
3-2	DODGE Solar Attitude Detectors Prelaunch Calibration Constants . .	3-39
3-3	DODGE Solar Attitude Detectors Normalized Detector Outputs as a Function of Solar Incidence Angle. .	3-40
3-4	DODGE Solar Attitude Detectors Temperature Correction Factors . . .	3-41
5-1	DODGE Telemetry Modulation Modes . .	5-6
5-2	DODGE Telemetry Functions (Attitude Commutator A).	5-11
5-3	DODGE Telemetry Functions (Attitude Commutator B).	5-13
5-4	DODGE Telemetry Functions (House- keeping Commutator)	5-15
5-5	DODGE Telemetry Register Functions. .	5-19
6-1	DODGE Command Assignments.	6-5
8-1	Summary of Orbit Errors for DODGE Tracks	8-10
8-2	Comparison of Antenna Pointings With Direction of Maximum Signal Strength .	8-12



THE EARTH AS SEEN FROM 20,000 MILES
TAKEN BY THE DODGE SATELLITE
RECEIVED AT THE JOHNS HOPKINS UNIVERSITY
APPLIED PHYSICS LABORATORY
SEPTEMBER 23, 1968

**COLOR ILLUSTRATIONS REPRODUCED
IN BLACK AND WHITE**

1. INTRODUCTION

1.1 Mission Objectives

The DODGE Satellite Program was initiated by the Bureau of Naval Weapons (now the Naval Air Systems Command) in response to a request from the Department of Defense to perform a gravity-gradient stabilization experiment that would provide supporting technology for the military communication satellite program.

The primary objectives of the DODGE satellite program are as follows:

- a. Achieve two-axis and three-axis gravity-gradient stabilization at near-synchronous altitude.
- b. Obtain comparatively fast damping of satellite librations.
- c. Steady stabilization--to within less than 2° rms in pitch and roll and less than 4° rms in yaw. (Plus that error due to orbit eccentricity.)
- d. To explore the effect of variations in boom configuration and damping systems on the attitude of the satellite, and thus obtain basic data that can be used for designing future gravity-gradient stabilized satellites.
- e. Develop computer programs that can predict the behavior of gravity-gradient stabilized satellites and compare experimental results with those obtained by a computer simulation.

The secondary objectives are as follows:

- a. Study boom bending characteristics resulting from solar (thermal) radiation.

- b. Measure the earth's magnetic field at near-synchronous altitude.
- c. Take color television (TV) pictures of the full earth disc.
- d. To measure the output of different types of solar cells.

1.2 Mission Plan

1.2.1 Satellite Design

To meet the objectives described in Section 1.1 above, the DODGE satellite was designed with an emphasis on flexibility and reliability by means of system redundancy. Some of the redundant systems which provided for the purpose of assuring to the highest degree that the mission objectives would be met are as follows:

- a. Two entirely separate sets of four extendible booms, one called the "+" configuration, the other called the "X" configuration.
- b. Two different schemes for providing libration damping by means of interacting with the earth's magnetic field.
- c. Two different schemes for providing damping by means of an articulated boom mounted on a torsion wire.
- d. Two different TV cameras, either of which could provide the required attitude information.
- e. Two different telemetry transmitters, either of which could provide the required rf power for telemetry.

Fig. 1-1 is an artist's concept of the DODGE satellite in orbit.

THE JOHNS HOPKINS UNIVERSITY
APPLIED PHYSICS LABORATORY
SILVER SPRING MARYLAND



Fig. 1-1 DODGE-ARTIST'S CONCEPT

The satellite was provided with 152 telemetry channels to provide the large variety of information required to determine satellite performance. The satellite responds to 128 different commands, thereby providing a great flexibility in its operating modes. A total of 26^4 (approximately 10^{12}) different command modes are possible with the DODGE satellite.

1.2.2 Ground Stations for Data Acquisition and Tracking

The mission plan prepared by APL includes requirements for tracking the satellite, determining its orbit, sending commands, and acquiring telemetry data. These stations are located on the map of Fig. 1-2.

Most of the above requirements are being met through the tracking, TM acquisition, computing, and command facilities located at the Applied Physics Laboratory, Howard County, Maryland.

The prelaunch nominal, 18,200 nautical mile altitude, equatorial orbit indicated a satellite period of approximately 22 hours. Since the earth period is 24 hours, the satellite period with respect to a point on the earth is approximately 12 days. The satellite is visible at the APL Howard County Station for about 5 days and is below the horizon for approximately 7 days. Therefore, the NASA, STADAN Station at Ororral, Australia and USAF, Indian Ocean Station (IOS) through its Satellite Control Facility (SCF) Sunnyvale, California were selected as sites from which the satellite could be monitored during the interval the satellite is not visible from APL.

TRANET stations 008 in Brazil, 112 in Australia, and 013 in Japan can also receive doppler and timing data on the 240 MHz carrier when the satellite is within range of these stations. The Satellite Control Center (SCC) at the Howard County laboratory provides the interface between APL and all other data acquisition facilities.

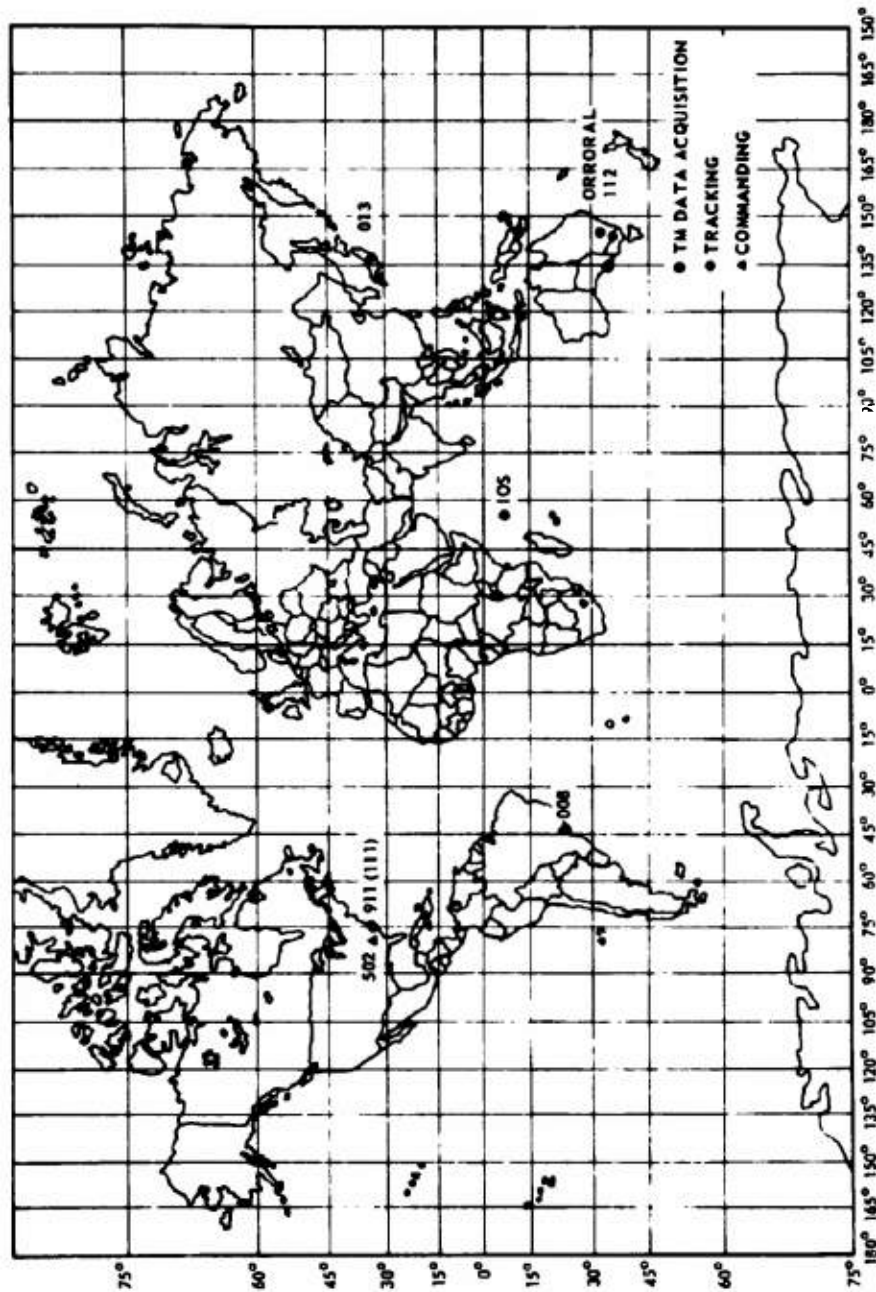


Fig. 1-2 LOCATION OF DATA ACQUISITION AND TRACKING STATIONS

A summary of the APL operations and the SCF Sunnyvale and NASA support requirements is given in the following paragraphs.

The Applied Physics Laboratory performs the following operations:

- a. Determines and executes commands and acquires telemetry (TM) and TV data required for the primary experiments while the satellite is in view of Station 502, Howard County, Maryland.
- b. Specifies and directs via the Goddard Space Flight Center (GSFC) the TM and command operations to be conducted at the NASA Orroal, Australia station.
- c. Determines and submits to SCF, Sunnyvale, the TM data acquisition requirements for the Indian Ocean station.
- d. Tracks and determines satellite orbit elements by an extension of the doppler technique and by new techniques involving satellite time marks. Specifies the equipment and procedures to be employed at DODGE tracking stations and exercises technical control over the acquisition of tracking data. Supplies alerts and antenna pointings, satellite ephemerides, and Kepler orbital elements as required by tracking stations.
- e. Conducts the experiment and necessary analysis to achieve the mission objectives.

SCF Sunnyvale, California. SCF support consists of receiving a VHF telemetry signal on 136.8 MHz and recording the composite data on magnetic tape at the Indian Ocean Station (IOS) during the periods when only IOS can see the satellite, approximately 2 out of every 12 days. The satellite normally transmits telemetry data for 602 seconds every 60 minutes when the 136.8 MHz transmitter

is on. IOS will record a minimum of 2 transmissions a day, or as requested they provide increased support during critical periods. A maximum of 24 observations a day may be requested, subject to the availability of time and the priority of all programs requiring IOS support.

The station continued to record TM data until the end of January 1968 when APL began turning off the 136.8 MHz transmitter before the satellite set below the horizon to conserve power for attitude experiments. TM data were recorded on the GR-2800 recorder, together with timing, voice, and flutter reference signals. The tapes were mailed to APL where the data were processed by the computer in Station 502. The station has again been requested to record TM data on 26 and 27 August 1968.

NASA STADAN STATION, Orroral, Australia

NASA support consists of receiving a VHF telemetry signal on 136.8 MHz and recording the composite data on magnetic tape at the Orroral, Australia Station during the period when the satellite is in view; approximately 5 days out of every 12 days. When the TM transmitter is on, Orroral will record a minimum of 4 transmissions every other day, with increased support during any critical period; a maximum of 24 observations a day may be requested subject to the availability of time and the priority of all programs requiring Orroral support. Except for the first 30 days after launch, data came to APL on magnetic tape. The Orroral station was also equipped to command the satellite as directed by APL.

During the first 30 days after launch an APL representative was present at Orroral, and an additional APL representative was present during the satellite's first 5-day pass only. These men were responsible for the acquisition and reduction of the TM data and for commands sent to the satellite. The TM reduction consisted of demodulating the 625 Hz, 859 Hz, and 1090 Hz subcarrier oscillator outputs, which contain attitude and housekeeping data, recording these data on a strip chart, and reducing the data to

engineering units. The reduced data were then sent by teletypewriter message to SCC APL via GSFC.

The station continued to record TM data until the end of January 1968 when APL began turning off the 136.8 MHz transmitter before the satellite set below the horizon to conserve power for attitude experiments. The TM data recorded on magnetic tapes were mailed to APL/JHU via GSFC.

In mid-August 1968 APL requested that the station again record and send to APL via magnetic tape DODGE telemetry data.

1.3 Launch and Immediate Post-Launch Operations

DODGE was launched into orbit on 1 July 1967 by an Air Force TITAN IIIC vehicle from Cape Kennedy, Florida. The trajectory included a park orbit, a transfer ellipse, and a final orbit. Lift-off time was 9:15 AM EDT (1315:01.111 Z).

At launch the satellite was in a "solar-only" mode, i.e., the satellite was operating only on solar cells, with the 136.8 MHz transmitter on and commanded to low rf power. The output of the transmitter was radiated by means of an omnidirectional antenna.

The APL ground station at Cape Kennedy acquired the signal at the time of vehicle fairing separation. Signal lock-on was achieved five seconds later, and the satellite was tracked to the horizon. At that time all satellite systems were operating normally and there had been no change in the launch mode status of the command system.

A successful park orbit was achieved with a perigee of 78 nautical miles and an apogee of 95 nautical miles.

After vehicle third stage burn the satellite was injected into the transfer orbit and the 136.8 MHz signals of the satellite were again acquired by the APL Cape Kennedy station. The

time of acquisition was 85 minutes after lift-off. The telemetry data confirmed that there had been no change from the launch mode.

The APL Command Telemetry station (Station 502) at Howard County, Md., acquired the satellite's telemetry signals a few minutes later. Station 502 tracked the satellite telemetry signals throughout the time of the transfer orbit and injection into final orbit at 3:15 PM EDT. The telemetry data showed that all temperatures, power levels, voltages, and currents were nominal throughout the entire launch trajectory. The -Z solar panel of the satellite faced toward the sun during the transfer orbit and reached a temperature of 192°F; the prelaunch predicted temperature was 188°F. Temperatures of the battery at lift-off and at injection into the final orbit were 70°F and 75°F, respectively, both of which are ideal for operation.

The orbit achieved was nominal with an apogee of 18,161 nautical miles, a perigee of 17,959 nautical miles, and an inclination angle of 7.027 degrees.

A satellite separation anomaly was observed at injection into orbit. The launch vehicle telemetry indicated that DODGE did not separate from the vehicle until 283 seconds later. Two telltales monitored this function in the satellite. One indicated clamp strap separation occurred immediately at the time of command; the other, a lift-off switch, indicated actual separation occurred some five minutes later. This discrepancy is believed to be caused by the adhesion of a rubber, protective cushion to the +Z end mass located in the spacecraft/launch vehicle adapter, thereby impeding the action of the one foot per second separation springs. Ground tests after launch confirmed that this cushion, after being linked to the +Z end mass for many hours, could adhere to the end mass with a force sufficient to overcome the thrust of the separation springs. However, the tests showed that in time the separation springs overcome this force and the satellite separates from the launch vehicle.

At 4:00 PM on 1 July 1967 Station 502 at APL commanded the television camera on and obtained the first pictures. The station also confirmed the operability of the flywheel and many other operational characteristics of the satellite.

Between 5:45 and 10:30 PM EDT the booms were checked out. Nine of the 10 booms were successfully unlocked and extended a minimum length. It was noted that while the +Z boom was being extended the counter stopped turning and the inverter current increased simultaneously to a value that would indicate a stalled motor.

The distance that each boom was extended is as follows:

<u>Boom Designation</u>	<u>Length (Inches)</u>
-Z	67.1
+Y	24.8
-Y	25.6
+X+Z	29.3
-X-Z	28.1
+X-Z	26.6
-X+Z	29.2
+Z	13.9
-X+Y (damper booms)	23.2
+X-Y (damper booms)	23.2

The damper boom torsion wire launch cage was successfully unlocked and recaptured in the orbit cage mode.

At 11:55 PM EDT, Station 502 sent commands to the satellite that verified the operability of the hysteresis and sample-and-hold magnetic damping systems. The satellite was then placed in a mode that would cause it to despin about each of its three axes. The telemetry data indicated satisfactory operation of the magnetometers. The data from the magnetometers and solar attitude detectors were within the anticipated ranges.

The satellite was then commanded to the automatic programmer mode. In this mode the satellite is turned on automatically for 10 minutes (602 seconds) every hour.

On 2 July proper operation of the 240 MHz transmitter was confirmed, and on 3 July Station 502 commanded the transmitter on again to check out its receiving equipment and to enable Station 111 at APL and Station 008 at Brazil to obtain doppler data. Although the equipment in all the stations operated properly, only Station 008 obtained data.

The Air Force station in the Indian Ocean observed the 136 MHz signals on 3 and 4 July and obtained a magnetic tape recording of the data.

A spin rate of 0.29 rpm was recorded on 2 July and 0.25 rpm on 3 July. The enhanced hysteresis damping system was functioning properly. The satellite was despining at the rate of 0.04 rpm a day, as expected. The initial spin rate was slightly higher than anticipated due to the separation anomaly.

The satellite set at APL on 4 July about 10 AM EDT. At that time the satellite was commanded to the automatic, programmed mode.

The satellite rose at the NASA station at Ororral, Australia on 6 July. The initial telemetry data obtained at the station confirmed that the satellite had remained in the programmed mode.

Command operations were conducted by APL representatives at the Ororral station to enhance the despin of the satellite.

The satellite rose again at APL on 11 July. Telemetry data obtained indicated that all temperatures and voltages were nominal. Television pictures were also obtained.

Station 111 at APL recovered timing data using the specially designed DODGE time recovery unit. The data indicated nominal performance of the satellite oscillator.

The satellite spin rate was observed to be zero at 2:00 AM EDT on 13 July. Station 502

then commanded the satellite to obtain magnetic stabilization. When the satellite was magnetically stabilized, the station extended the times booms to achieve gravity-gradient stabilization. This attempt was not successful; however the second attempt on 14 July was successful. The operations to achieve gravity-gradient stabilization of the satellite in various configurations are described in detail in Section 2 below.

Since 14 July, all of the other satellite systems were checked out and proved to be operable.

1.4 Satellite Tracking

Stations 111 and 008 continue to obtain doppler data from DODGE when the satellite is within range of the stations and the 240 MHz transmitter is on. On 27 July 1967 the Indian Ocean station received the 240 MHz signals for the first time; during previous passes the satellite was radiating on 136 MHz only. Beginning 29 July, Station 112 in Australia and Station 013 in Japan obtained doppler data. Station 112 also obtained timing data with specially designed equipment provided by APL.

APL accumulated the doppler data prior to running the satellite tracking program. Two weeks of data were required to begin the program operation. In the interim, APL updated the prelaunch orbit to provide improved alerts by determining the pointing angles for maximum strength signals as received at the APL, 60-foot dish antenna. Based on these data, the following DODGE orbit parameters were calculated:

Epoch	Day 182 (1 July 1967)
Semimajor Axis	6.24770 earth radii
Eccentricity	0.00522
Inclination	7 degrees
Longitude of Ascending Node	296 degrees
Argument of Perigee	0.985363 degrees
Time of Perigee	28508 seconds

Later APL tracked the satellite using doppler data obtained by the four stations from 23 July to 8 August 1967. During that time DODGE orbited the earth approximately 1.5 times and completed 18 orbital revolutions. The orbit parameters resulting from this tracking program were as follows:

Semimajor Axis	6.2463740 earth radii or 21,511.887 miles
Eccentricity	.0048482972
Inclination	6.9660605 degrees
Longitude of Ascending Node	297.50302 degrees
Argument of Perigee	268.04401 degrees
Precession of Ascending Node	-.016349 degrees/day
Precession of Perigee	+.032276 degrees/day
Time of Perigee	7864.9228 seconds on Day 204, 1967
Mean Anomaly	0
Period	79140.01 seconds or 21.983 hours.
Apogee Altitude	18165.889 nautical miles
Perigee Altitude	17970.085 nautical miles

Doppler data obtained in May 1968 were used to update the orbit. The Kepler parameters for this orbit, which is the most recent determination of the orbit parameters, are as follows:

Epoch	Day 143 (22 May 1968)
Semimajor Axis	6.2468173 earth radii
Eccentricity	0.0047707612
Inclination	6.3448376 degrees
Longitude of Ascending Node	294.98994 degrees
Argument of Perigee	281.48578 degrees
Precession of Ascending Node	-0.007200 degrees/day
Precession of Perigee	0.009549 degrees/day
Time of Perigee	19843.090 seconds or 330.718 minutes
Mean Anomaly	0
Period	1319.148 minutes or 21.9858 hours
Apogee Altitude	18172.329 nautical miles
Perigee Altitude	17967.056 nautical miles

2. ATTITUDE CONTROL SYSTEM DESIGN AND PERFORMANCE

Since the major objective of the DODGE satellite is to perform experiments in gravity-gradient stabilization in a near-synchronous orbit, a large number of extendible booms and libration damping systems were provided. The total of 10 booms, each adjustable to better than ± 1.0 inch over a total length as long as 150 feet, provide virtually an infinite variety of moments of inertia for obtaining gravity-gradient restoring torques to various degrees. Unfortunately, the failure of the +Z boom to extend limited the satellite to the (still infinite) variety of boom configurations employing the "X" configuration shown in Fig. 2-1.

The principle libration damping systems on the satellite are as follows:

a. Magnetic Damping Systems

- (1) Magnetic sample-and-hold
- (2) Enhanced hysteresis

b. Torsion Wire Damping Systems

- (1) With eddy current damper
- (2) With hysteresis damper

The parameters for each of these systems can be varied by command.

The sample-and-hold magnetic damping can be operated to sample automatically every three hours or six hours and manually can be set to any time duration (longer than approximately one minute). Also, the output gain can be set to either high strength or low strength.

The enhanced hysteresis damping system can be operated in four different gain states.

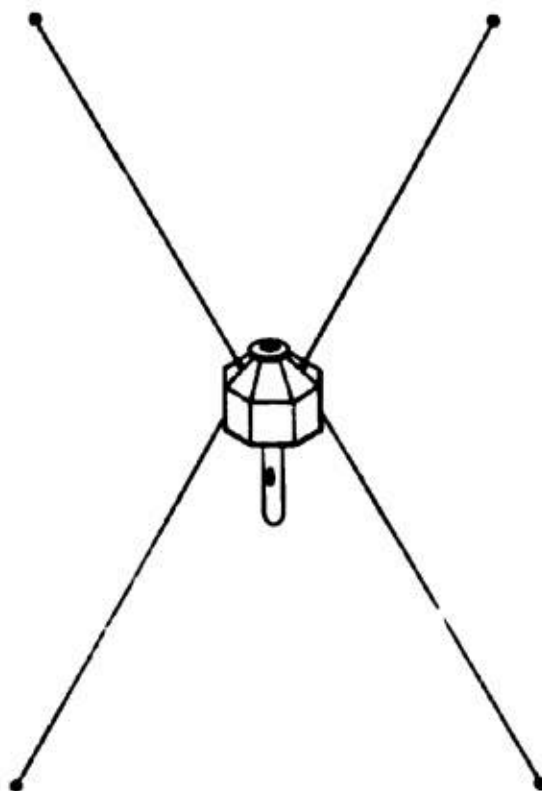


Fig. 2-1 "TIMES" CONFIGURATION FOR DODGE

Using the eddy current mode with the torsion wire damper, the satellite can be commanded to an infinite number of different damping states; from zero damping to approximately five times optimum.

With the hysteresis damper mode of the torsion wire damping, one can command eight different states of damping.

All the dampers described above can be activated in any combination.

A magnetic system for despinning the satellite about its Z axis is provided. A magnetic detumble system is used to remove satellite angular rates about any of the three principal satellite axes. If desired, the satellite could also be spun-up to angular rates.

The satellite can be magnetically stabilized with either its +Z, -Z, +X or -X axis aligned along the earth's magnetic field. In this mode, one can also obtain damping of the oscillations about the local magnetic field direction.

The satellite also includes the capability of stabilizing by gravity-gradient in pitch and roll and by a magnetic dipole in yaw.

Still another form of stabilization utilizes an angular momentum wheel to augment the roll and yaw stabilizing torques and gravity-gradient booms to provide the pitch stabilizing torque. This system can be combined with any of the libration damping systems described above.

After injection into orbit the satellite is first despun (or detumbled) to essentially zero angular rate about all three axes. The satellite is then magnetically stabilized with its +X axis aligned along the earth's magnetic field. The booms are then deployed to obtain gravity-gradient stabilization.

All these various systems and their performance in orbit are described in Sections 2.1 to 2.6, inclusive, and in Appendix A.

2.1 Magnetic Damping and Stabilization System

The DODGE satellite includes a no-moving-parts magnetic damping and stabilization system. The principal uses of this system are to:

- a. Damp rotations of the satellite following separation from the launch vehicle
- b. Magnetically stabilize the satellite so that its X axis is roughly horizontal
- c. Damp the oscillations associated with magnetic stabilization, and
- d. Damp the oscillations associated with librations during the gravity stabilization phase.

2.1.1 System Design

A simplified block diagram of the system is shown in Fig. 2-2. The primary elements are:

- a. Three-axis vector magnetometer
- b. Three-channel hysteresis generator
- c. Three channel sample-and-hold (time-lag) generator
- d. Three channel power amplifier
- e. X and Y permeable core electro-magnets and a Z coil

Each axis of the magnetometer provides a continuous DC signal proportional to the component of the magnetic field along that sensor axis. This device will produce +8 volts of output for +250 gamma of applied field with a nominal accuracy and linearity of 2.5 gamma (1 gamma = 10^{-5} gauss). The signals go to the hysteresis generator and the sample-and-hold generator, as well as to telemetry for transmission to the earth.

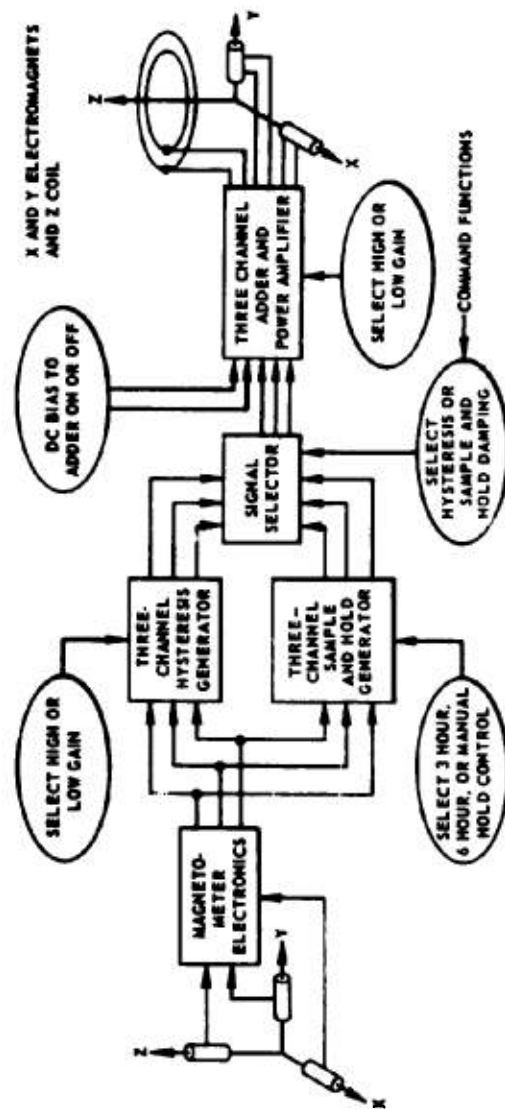


Fig. 2-2 SIMPLIFIED BLOCK DIAGRAM OF DODGE ENHANCED
MAGNETIC DAMPING SYSTEM

By command from the ground, either the hysteresis or the sample-and-hold mode of damping can be selected.

2.1.1.2 Hysteresis Damping

The hysteresis generator produces three output signal voltages that are related to its input voltages as flux density B is related to magnetizing force H in a toroid of magnetic material. The magnetic material is highly hysteretic; i.e., the output voltage has a non-linear phase delay as compared to the input voltage. These signals are amplified and used to energize the X and Y electromagnets and the Z₀ coil, which produce a net magnetic dipole moment \vec{M} that reacts with the external magnetic field \vec{H} to produce a torque \vec{T} given in vector notation, by $\vec{T} = \vec{M} \times \vec{H}$. This torque damps satellite motions in a fashion analogous to the passive hysteresis rods of the Oscar satellites, but with the important advantage that the effectiveness can be boosted by the application of more power to the electromagnets and coil, thereby compensating for the very weak external magnetic field that is encountered by the DODGE satellite. This system is used in DODGE for despin, detumble, damping of magnetic oscillations, and damping of gravity librations.

2.1.1.3 Sample-and-Hold Damping

This is the principal scheme used for damping gravity librations. The magnetic field components are sampled periodically, and proportional output voltages are produced. This is accomplished by the three-channel sample-and-hold generator. The output voltages are amplified and used to energize the electromagnets and coil. A magnetic dipole is produced, with components proportional to the external field. Therefore, \vec{M} and \vec{H} are collinear and there is no torque. If the satellite then undergoes an angular displacement, \vec{M} will be moved away from \vec{H} , and a torque will develop to oppose the motion, hence damping is provided. The dipole is held fixed for a certain "hold" time before the magnetic field is sampled again. Automatic sampling at 3 or 6 hour hold times can be selected by

command. Sampling can be speeded up or slowed down by a manual command override to achieve other hold times. The natural period of gravity librations is on the order of 24 hours. The 6 hour hold time then is roughly a quarter of an oscillation cycle; thus, the magnetic dipole tends to lag the motion by approximately 90° . This scheme has been shown to be quite effective in damping gravity libration in computer analyses and has been effective in orbit.

2.1.1.4 Power Amplifiers, Electromagnets, and Z Coil

The power amplifiers are designed to produce an output current proportional to the input voltage. The X and Y channels produce ± 200 ma output current for an input of ± 8 volts. The X and Y electromagnets consist of copper wire windings on 26-inch-long, Mu-metal cores. When energized with 200 ma, they produce a magnetic dipole moment of 8.64×10^4 pole-cm. The outputs of the X and Y amplifiers are provided with current limiters that prevent the output current from exceeding ± 205 ma. In this way the electromagnets are prevented from exceeding the linear range of the cores.

The Z amplifier has an output of ± 800 ma for ± 8 volt input. This current energizes the Z coil which consists of 80 turns of wire wound around the periphery of the satellite just beneath the solar cell panels. This coil produces a Z axis dipole of 8.64×10^4 pole-cm when energized at 800 ma. No current limiter is used on the Z amplifier since there is no saturatable core.

Additional signals can be added at the input to the power amplifiers. DC bias voltages are applied to the X and Z channels, primarily the X channel to produce a DC magnetic dipole along the X axis. This is used to achieve magnetic stabilization, with the X axis aligned with the magnetic field as a prelude to capture in gravity stabilization.

2.1.1.5 Hardware

The electronics system comprises four electronic books, the magnetometer sensor assembly the X and Y electromagnets, and the Z coil. The approximate weights are:

4 electronic books	8 pounds
magnetometer sensor assembly	1.5 pounds
X and Y electromagnets	12.5 pounds
Z coil	4.0 pounds

Total system weight is about 26 pounds.

2.1.2 Magnetic Despin System

The DODGE magnetic despin system includes two modes of operation referred to as (a) spin-despin mode and (b) enhanced hysteresis damping mode. The spin-despin mode is intended to remove residual spin (rotation about Z axis) following injection into orbit. In this mode, a torque vector in the +Z or -Z direction can be impressed on the satellite to despin or spin-up the satellite. The enhanced hysteresis damping mode is a three-channel system which is used to remove angular motions about any satellite axis. Even though the enhanced hysteresis system is capable of providing general despin or detumble, the spin-despin mode is included because it affords faster despin rates about the Z axis and provides a means for generating magnetic torques about the Z axis which can be used to control the yaw motions of the spacecraft in the gravity stabilized mode.

2.1.2.1 Spin-Despin Mode

In the spin-despin mode, the X magnetometer drives the Y channel amplifier and the Y magnetometer drives the X channel amplifier with a 180° phase lag. In this mode a magnetic dipole moment is generated in the satellite X-Y plane which lags by 90° the X-Y component of magnetic field intensity. This spin-despin system has been used successfully in controlling the spin rate of the DME-A, AE-B, and RAE-A satellites. The advantage of this system is that a

maximum despin torque is developed by the 90° phase shift between the dipole moment and the earth's magnetic field projected into the satellite's X-Y plane.

Two commands are used in conjunction with the spin-despin mode: a spin torque sense select and a two-state amplifier gain select. Spin torque sense is determined by the state of reversing relays which control the amplifier outputs. Gain select is achieved by changing the input impedance to an operational amplifier.

The despin rate for this system is given by:

$$\dot{\omega} = (k H^2 \sin^2 \theta) / I \quad 2.1 (1)$$

where

k = gain of damping system (pole-cm/oersted)

H = earth's magnetic field intensity (oersted)

θ = angle between H and the spin axis (radians)

I = spin axis moment of inertia (gm-cm²)

The despin rate for DODGE in high gain is:

$$\dot{\omega} = 0.16 \text{ rpm/day} \quad 2.1 (2)$$

for

$k = 3.24 \times 10^7$ pole-cm/oersted

$\theta = 90^\circ$

$H = 1.25 \times 10^{-3}$ oersted

$I = 2.54 \times 10^8$ gm-cm² (18.7 slug-ft²)

The spin-despin mode was not used during the DODGE detumble phase since rotations were principally about the X and Y axes and not about the Z axis. The spin-despin mode, however, was used considerably during the gravity stabilization phase for controlling yaw. For the spacecraft

nominally stabilized in roll and pitch and with a predominately North ambient magnetic field, the spin-despin mode will produce a torque about the Z axis. By direct ground command this control torque has been successfully employed in aligning the satellite in yaw. On Day 009, 1968, for example, the spin-despin system was used in conjunction with a fixed X-Z magnetic moment to align the +X axis normal to the orbit plane before the rotor was energized.

2.1.2.2 Enhanced Hysteresis Rod

Enhanced magnetic hysteresis damping is the second mode of operation of the DODGE magnetic despin system. In operation it is equivalent to having in the satellite a set of passive hysteresis rods with the inherent ability to remove spin energy via magnetic hysteresis. In DODGE, the hysteresis rod effect is greatly enhanced by active electronics. A block diagram of one channel of the enhanced hysteresis damping system is shown in Fig. 2-3. DODGE includes three identical channels - one each for the X, Y, and Z body axes.

In use the component of magnetic field along an axis is detected and converted into a proportional DC voltage. This voltage is processed by the hysteresis generator which produces a voltage proportional to the flux density B in a magnetic hysteresis material. This voltage drives a transconductance amplifier which powers a linear electromagnet or a coil. The net result is that a magnetic dipole moment is produced which lags the applied magnetic field in such a way as to produce a simulated hysteresis loop.

A command function is provided to adjust the shape of the hysteresis loop. This command, referred to as the input shape-select, changes the gain of the input amplifier to the hysteresis generator. A high gain command amplifies the magnetometer voltage so that the hysteresis generator saturates at low field levels (about 30 gamma). Low gain does not allow the loop to saturate before 120 gamma.

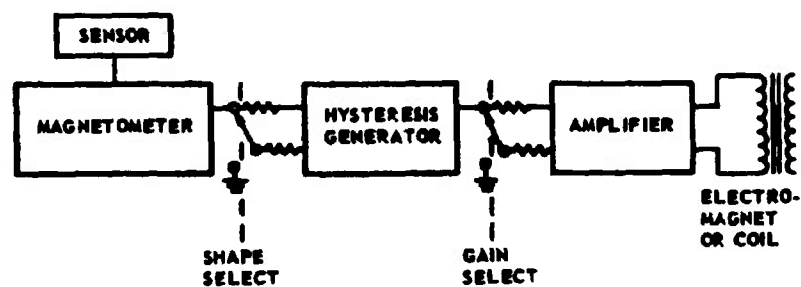


Fig. 2-3 FUNCTIONAL BLOCK DIAGRAM OF ENHANCED
HYSTERESIS DAMPING SYSTEM

An output gain-select command is also provided. It determines the amplitude of the hysteresis loop. This command adjusts the current gain to the power amplifiers; the output current at high gain is four times that at low gain.

Design and evaluation of the magnetic hysteresis damping system was performed using an analog computer. In general it is exceedingly difficult to simulate spacecraft magnetic hysteresis damping. The analog computer performs the simulation by including three flight-type hysteresis generators as computer elements. Computer studies of despin and detumble dynamics were performed during the satellite design phase and enabled APL to design a system that would produce the best damping. The flight electronics, when completed, were similarly coupled to the computer to evaluate the electronic as well as the dynamical performance. In this way the effect of gain change and demagnetization could be readily evaluated and an optimum post launch operation procedure developed. Results of analog computer simulation indicated detumble rates of 0.038 to 0.049 rpm/day.

2.1.2.3 Demagnetization Capability

A command exists that provides for the demagnetization of the hysteresis generators. The demagnetizer produces a low frequency sinusoidal voltage of decreasing amplitude. This signal drives the generators through smaller and smaller loops thereby removing all previous hysteresis. In operation the demagnetizer can be used whenever the hysteresis generators become biased and do not generate loops of significant area. When the hysteresis damping system is turned back on, satellite motions would again produce major loops necessary for despin.

This system can also be used for demagnetizing the entire spacecraft body to assure that there is no residual dipole after it has been placed in orbit.

2.1.2.4 In-Orbit Performance of Magnetic Angular Rate Damping System

A summary of the performance of the enhanced magnetic damping system is indicated in the tumble history curve of Fig. 2-4. Following injection into orbit at 1920 UT on Day 182, 1967 DODGE was observed to be tumbling at 0.6 rpm. Between 2200 UT, Day 182 and 0200 UT, Day 183, all booms were partially extended. The resulting increase in moment of inertia reduced the spin rate to 0.34 rpm. At 0400 UT, Day 183, the enhanced magnetic system was turned on and commanded to the hysteresis mode. During the first APL pass, DODGE appeared to be detumbling at about 0.044 rpm/day. This result compares well with analog simulations of detumble, using enhanced hysteresis damping. Near the set time of the APL pass, a spin rate of 2.25 rpm was observed. The enhanced hysteresis damping system was left on following set of the pass.

The next data were received at the Orroal Tracking Station near Canberra, Australia. On Day 188 a tumble rate of 0.22 rpm was observed, which indicated that little damping had occurred since set of the APL pass. It was suspected that the hysteresis generators had become saturated; thus, several demagnetization commands were sent. Shortly thereafter, the detumble rate improved to about 0.035 rpm/day and remained at that rate throughout the remainder of the detumble phase. A zero rotation rate was observed at 0500 UT, Day 194. The X-Z fixed dipole moment was then turned on for magnetic stabilization.

The telemetry records covering the period during the detumble phase were studied in order to understand the anomalous detumble behavior during Days 185-188. The character of the hysteresis loop during the period was of particular concern. If the system were severely biased, only minor hysteresis loops would be generated and little damping could be expected. In general it was noted that both the X and Y channels were producing major hysteresis loops, even during the period of poor detumble. The Z channel was slightly biased; its loop area was 1/5 the major loop area. Hysteresis

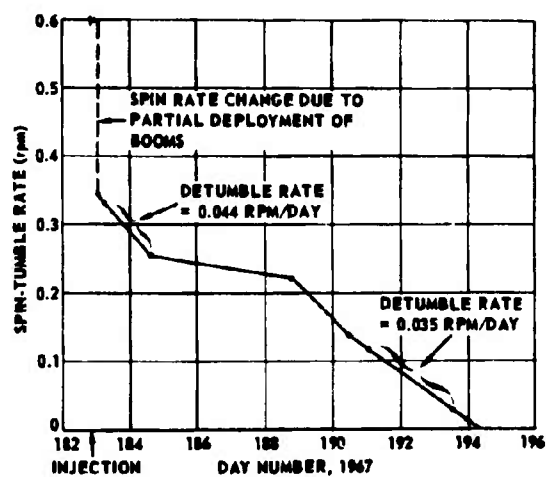


Fig. 2-4 DODGE DETUMBLE HISTORY

loops, as determined from telemetry data, are shown in Fig. 2-5. The average torque generated by the hysteresis damping system is about 40 dyne-cm for the detumble rate of 0.040 rpm/day and the satellite moment of inertia of 60 slug-ft². The fact that hysteresis loops were being generated throughout detumble indicates that the hysteresis generators were functioning properly. The anomalous despin behavior was due not to a malfunction of the hysteresis damping system but was more likely caused by erratic magnetometer signals.

2.1.3 Magnetic Stabilization System

The magnetic stabilization system is intended to (a) stabilize the spacecraft following the despin and detumble phase into an attitude where gravity capture can be implemented, (b) to provide additional control torques during the gravity stabilization phase, and (c) to produce perturbing moments so that the transient damping performance can be evaluated when changing from one configuration to another. Magnetic hysteresis damping can be used in conjunction with these modes to provide damping of oscillations. Operating modes of the magnetic stabilization include:

- a. fixed X-Z magnetic moment,
- b. variable X-Z magnetic moment, and
- c. fixed Z-axis moment.

2.1.3.1 Fixed X-Z Magnetic Moment

The fixed X-Z magnetic moment configuration provides for initial magnetic stabilization prior to deployment of the gravity booms. In this mode constant magnetic dipole moments of

$$M_x = 8.64 \times 10^4 \text{ pole-cm} \quad 2.1 (3)$$

and

$$M_z = \sim 3.28 \times 10^4 \text{ pole-cm} \quad 2.1 (4)$$

are generated. The resultant dipole moment

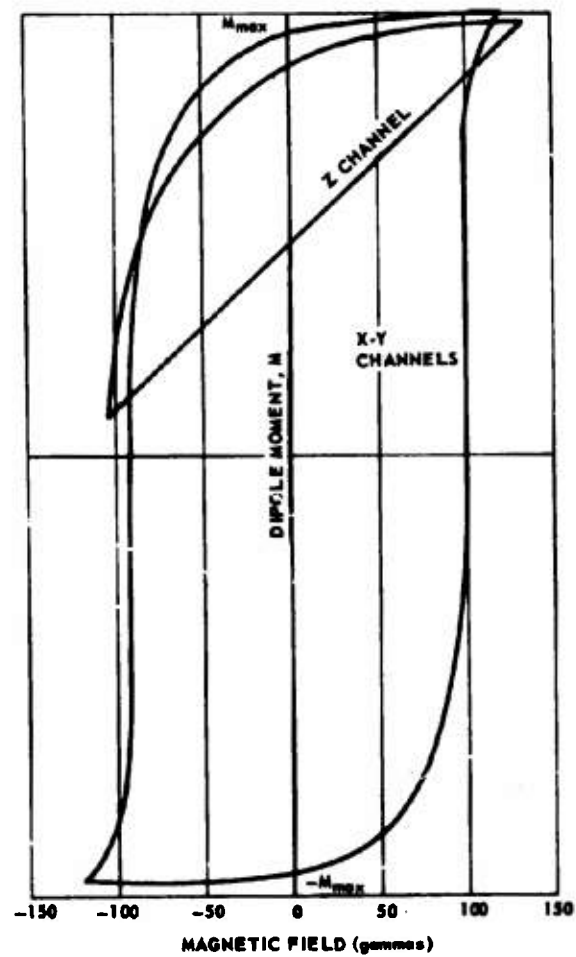


Fig. 2-5 HYSTERESIS LOOPS FROM TM DATA

(predominately X axis) tends to line up with the earth's magnetic field. Over the Eastern United States, the ratio of X to Z moment and inclination of magnetic field combine to align the spacecraft +X axis North and the +Z axis along the outbound local vertical. Since there is no control moment about the dipole moment axis, the spacecraft will slowly rotate about this axis. When it is determined by TV picture attitude data that the +Z axis is aligned outward along the local vertical, a gravity capture sequence is initiated.

Magnetic stabilization using the fixed X-Z magnetic moment was employed following the despin and detumble phase. It assisted in aligning the Z axis with local vertical prior to gravity capture.

2.1.3.2 Variable X-Z Magnetic Moment

The variable X-Z magnetic moment was to be used in conjunction with the "+" or Z dumbbell gravity-gradient boom configuration for providing a magnetic torque which assists in controlling yaw. In operation X and Z axis magnetometers supply signals to the power amplifiers which generate a magnetic moment in the spacecraft X-Z plane. This dipole moment is aligned with the component of ambient magnetic field in the X-Z plane. The resultant magnetic torque attempts to align this plane with the local field direction which is predominately North. The net effect is that additional yaw torque is generated which tends to assist gravity gradient torques. Due to the anomalous behavior of the magnetometers, however, yaw control using the variable X-Z magnetic moment has not been attempted.

2.1.3.3 Z Axis Fixed Magnetic Moment

The fixed Z axis magnetic moment is intended to produce a magnetic torque about the nominal roll axis. This torque could be used for additional manual roll control or as a perturbing torque so that transient gravity-gradient damping behavior can be investigated. In operation, a Z axis dipole moment of $\pm 1.0 \times 10^5$ pole-cm or zero is generated. For a nominally stabilized spacecraft with a North ambient magnetic field direction,

this dipole produces a torque about the roll axis. In the case of serious roll error, this moment could be manually controlled so as to produce roll torque assisting gravity stabilization.

A second use of the fixed Z axis magnetic moment is that of producing a controlled perturbing torque on the spacecraft. It was anticipated that accurate gravity stabilization would be achieved for some particular boom configuration. The boom lengths or configuration would then be altered for a new experiment and the Z axis fixed moment energized so as to produce a 10° to 20° roll error. In this manner the transient damping performance for the new configuration could be evaluated.

The fixed Z axis moment was used in one attempt to manually damp librations by direct ground command on Day 228, 1967.

2.2 Gravity-Gradient Stabilization Systems

The basic concept in the gravity-gradient stabilization of DODGE is to take advantage of the earth's gravity field to produce a restoring torque tending to bring the satellite to the local vertical. The theory of gravity-gradient stabilization shows that the pitch restoring torque is proportional to the moment of inertia difference, $I_{\text{roll}} - I_{\text{yaw}}$, and that the roll restoring torque is proportional to $I_{\text{pitch}} - I_{\text{yaw}}$. Therefore large inertia in roll and pitch is needed to achieve adequate restoring torque. This is achieved by the use of motorized extendible booms with heavy end masses, which are extended from the main satellite body in symmetrical pairs to retain a balanced configuration to minimize solar radiation pressure torques. For this purpose eight extendible booms were incorporated in DODGE, four of which form the so-called "+" configuration, sketched in Fig. 2-6; four others form the "X" (or "times") configuration, Fig. 2-7. Also shown are an additional two booms which are mounted on a torsion-wire suspension and are essential elements of one of the satellite damping schemes. Maximum boom lengths and end mass weights are indicated on Figs. 2-6 and 2-7. The external arrangement is shown in Fig. 2-8.

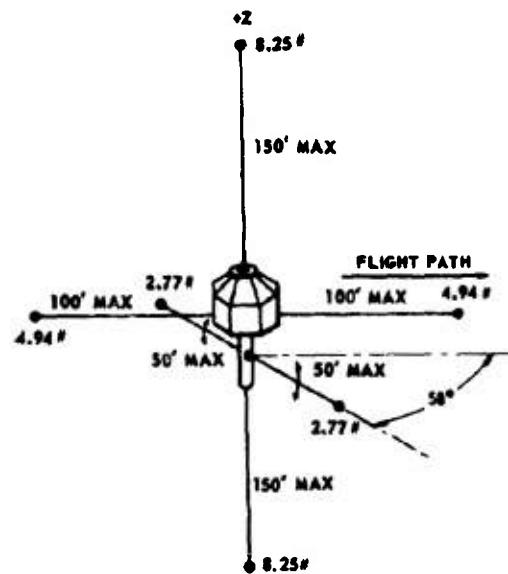


Fig. 2-6 "PLUS" BOOM CONFIGURATION WITH
DAMPER BOOMS EXTENDED

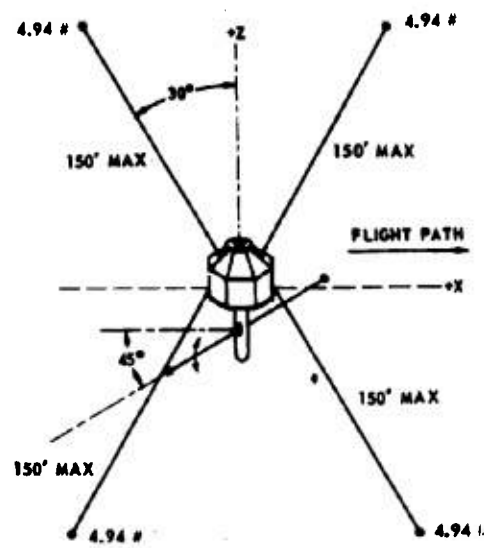


Fig. 2-7 "TIMES" BOOM CONFIGURATION WITH
DAMPER BOOMS EXTENDED

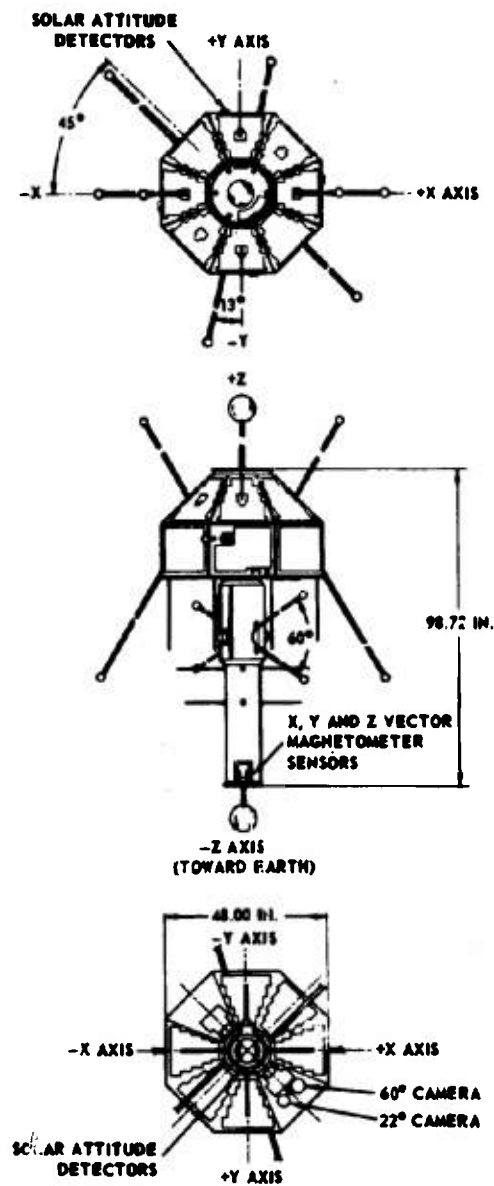


FIG. 2-8 EXTERNAL ARRANGEMENT

The gravity-gradient restoring torque tends to bring the satellite into alignment with the local vertical, but without damping, oscillations about the local vertical would continue indefinitely. One of the major purposes of DODGE is to experiment with different damping schemes to find satisfactory techniques and make comparisons in performance.

Two basic types of damping systems are available in DODGE, the torsion wire damper system and the magnetic damping system.

- a. The Torsion-Wire Damper System. This system uses extendible booms supported on a delicate torsion-wire suspension (Ref. 2-1). As the satellite librates, the suspended booms experience gravity-gradient torques and tend to oscillate relative to the satellite. This relative motion between suspended booms and the satellite is damped by an eddy-current damper and/or a hysteresis damper, as selected by command. Therefore as the satellite librates, energy is dissipated in the eddy-current damper and/or hysteresis damper, and the libration amplitude decays.

Theoretical analysis of this concept shows that it has the advantages of rapid transient damping (a few days), good steady-state accuracy in pitch and roll (a few degrees), and modest accuracy in yaw (10 degrees). A disadvantage is the mechanical complexity.

- b. Magnetic Damping System. This system uses the three axis vector magnetometer, the electronic system and the magnetic torques shown in the block diagram of Fig. 2-2. Damping torques are derived by interaction with the earth's magnetic field. Two types of interaction are available, one producing a type of artificial hysteresis damping, the other

producing time-lag damping by the sample and hold technique. Both modes have various operating parameters that can be selected and changed by command in the search for better performance.

Dodge also has a momentum wheel for yaw control. Both the "+" and "X" configurations in any of the damping modes described above have a natural yaw stabilization tendency by virtue of the planar boom configuration. However, it is a relatively weak tendency and is easily disturbed by extraneous torque. To enhance the yaw stability a small momentum wheel was installed in DODGE, with the spin axis parallel to the satellite X axis. When this device is in use the X axis tends to align itself parallel to the orbit normal. The yaw stability is enhanced by virtue of the gyrostabilizing effect of the momentum wheel.

2.2.1 Extendible Booms

2.2.1.1 System Description and Performance

The extendible boom system on DODGE consists of ten deHavilland P/N 5489F1 gravity-gradient booms designed specifically for DODGE (see Fig. 2-9). The boom tape was made of 2 mil thick beryllium copper sheet formed into a tubular shape with a highly polished silver plated external surface exhibiting a reflectivity of 0.90.

An indication of deployed boom length is furnished by a magnetic reed switch that is tripped by four small equally spaced bar magnets mounted on a wheel attached to one of the boom mechanism drive shafts (see Fig. 2-9). As tape is unreeled from the storage drum, each magnet in turn passes the reed switch and actuates it. Each actuation corresponds to approximately 1/2 inch of boom length; from this one obtains the total length of deployed boom. This information, which is telemetered, furnishes the operator with an accurate record of deployed lengths.

It is unfortunate that the first boom to be extended (+Z) malfunctioned after partial deployment (about 14 inches). The fact that this

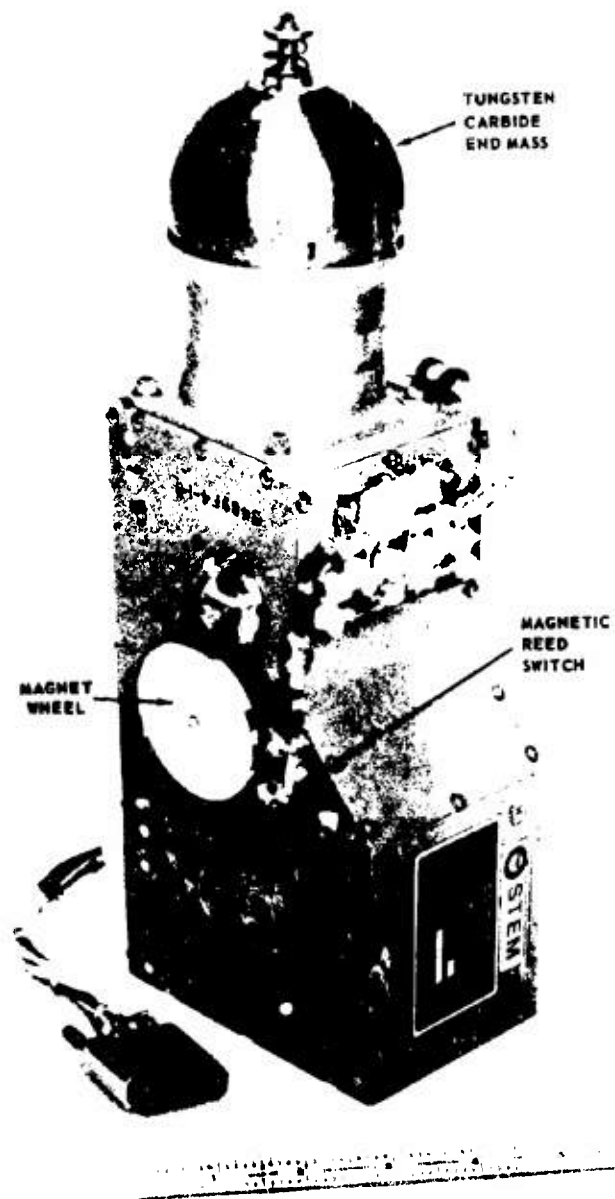


Fig. 2-9 DODGE EXTENSIBLE BOOM

boom operated satisfactorily just prior to launch threw suspicion on the launch environment. A condition where a drive spring jumped its track under abnormal vibrations was observed during the environmental testing program prior to launch. The proximity of the boom to the satellite-launch vehicle interface, where it was difficult to introduce effective vibration isolation, tends to support this theory.

The remaining nine booms were uncaged and partially extended (approximately 2 feet) between 0043 UT and 0223 UT on Day 183, 1967. Failure of the (+Z) boom precluded the deployment of the "plus" configuration (see Fig. 2-10). Consequently, a decision was made to use the "times" configuration (see Fig. 2-7). The four "times" booms were extended to approximately 70 feet to establish the initial configuration for gravity-gradient stabilization.

The four booms that comprise this configuration have been extended and retracted nearly a dozen times each. A "dead-beat" capture following an inversion maneuver necessitated a boom retraction to 20 feet of exposed length and a precisely timed extension to 100 feet. A maximum extension to 110 feet and a retraction to 3 feet are the extreme lengths to which the booms have been driven thus far.

On one occasion, while a pair of booms was being extended simultaneously, and unexpected overload of the inverter caused a phase reversal that made them retract instead. Before the condition was discovered, the satellite orbited for a number of days with an unbalanced configuration. The ensuing unbalance of solar radiation pressure was quite pronounced and appreciably degraded the stabilization of the satellite. This unbalance was corrected and manual damping consisting of boom retraction and extension was used to dissipate the undesired attitude energy.

The torsion wire damper booms were extended to 30 feet early in the post-launch program. Under the conditions that prevailed at the time, the damper was ineffective in dissipating libration

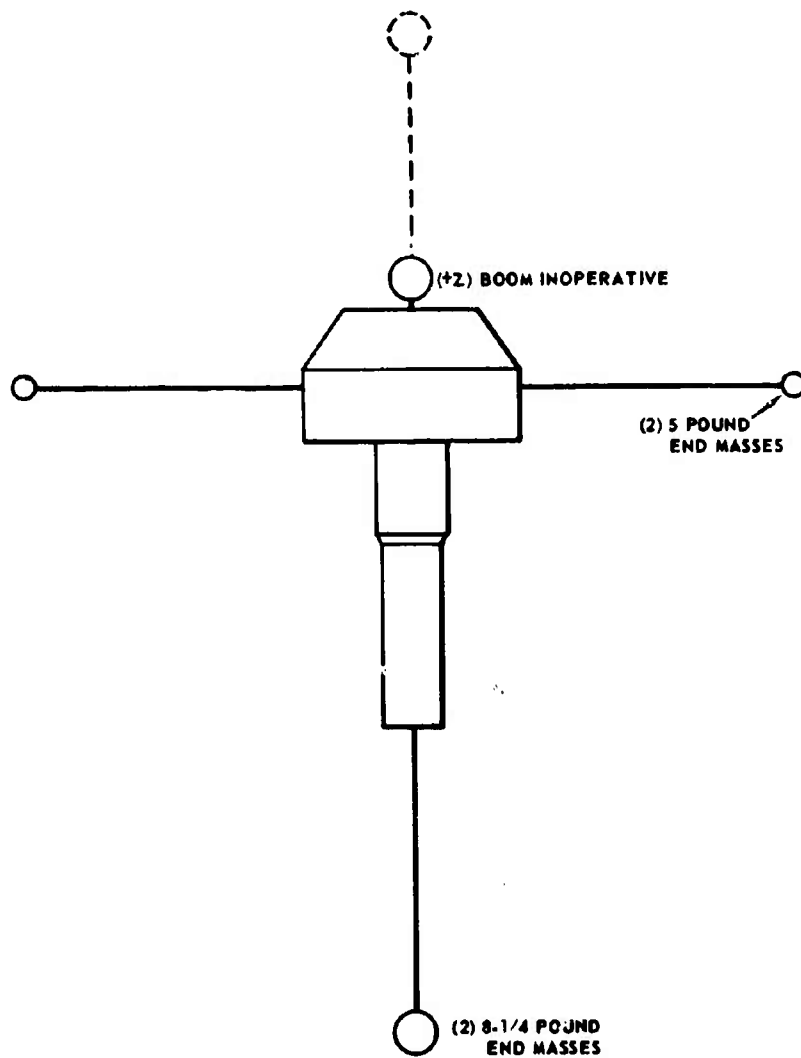


Fig. 2-10 "PLUS" CONFIGURATION

energy. For this reason the booms were retracted, and the experiment was postponed. The (-Z) boom was extended approximately 17 feet a few days after injection and subsequently retracted. Later, this boom was extended to 36 and 80 feet, for the sake of studying solar induced thermal distortion (see Sec. 2.2.1.2).

Considerable confidence relative to the functioning of electromechanical devices in a hard vacuum has been acquired since DODGE was placed into orbit. The AC hysteresis-synchronous type boom motor-gearhead combinations (Kearfott) and length measuring rotary potentiometers (Bourns) have operated faultlessly as have the many special high vacuum roller bearings (New Hampshire with "Duroid" separators) in over 150 boom extensions and retractions.

The end mass release mechanisms that are actuated by boom motion are electrically passive. Those associated with the nine booms that operated satisfactorily functioned as expected. The tenth one, it is believed, also operated properly; the malfunction caused by a damaged boom was discussed previously.

These background data will have a significant influence on the use of such devices on future satellites.

2.2.1.2 Thermal Bending

One of the major objectives of the DODGE experiment was the study of solar induced thermal bending of an extendible gravity gradient boom. Since a cylindrical boom at best can receive sunlight from one direction at a time, it stands to reason that the illuminated side will attain a temperature somewhat greater than that of the leeward side. The hot side, therefore, will elongate relative to the cold side and cause the boom to bend. This condition has a direct bearing on the stability of satellite attitude or the precision with which it can be pointed if this is a requirement.

There are two conditions that are of concern here: (a) steady state bending and (b) transient response. The former condition is really an extremely long term transient response and occurs while the boom rotates slowly in the sun. When the boom passes into the shadow of the earth and out again the latter condition prevails. And aside from the solar induced effect there is also some contribution from earth albedo and infra-red emission.

On DODGE the 22 1/2-degree and 60-degree television cameras are used primarily for attitude sensing. Their secondary mission is to provide the means for studying thermal bending of the -Z boom. Fig. 2-11, 2-12, and 2-13 are plots of data obtained from the 22 1/2° camera. Fig. 2-11 shows the dispersion of the -Z end mass: a 9 inch diameter aluminum sphere, with the boom extended to 80 feet which corresponds to an exposed length of 76 feet. This experiment took place during pass 10 on Days 283 and 284, 1967. The "times" booms were retracted to 20 feet.

With the exception of point 11, all of the data points fall within a rectangular envelope measuring 18 x 21 inches. Point 11, it is believed, carries a dynamic component substantially greater than that of the other points. The test duration was 29 hours.

Fig. 2-12 shows the results of a similar experiment conducted during pass 24 on Days 076, 077, and 078, 1968. During this period the times booms were extended to 78 feet on the +Z side and 62 feet on the -Z side of the satellite. The data points fall into a narrower dispersion pattern measuring 11 x 24 inches. The test duration was 40 hours.

The major difference between the conditions under which these two tests were conducted was in the stability of satellite attitude. In the latter case, dynamically, the satellite was more quiescent and, therefore the data probably contain a larger thermal bending component.

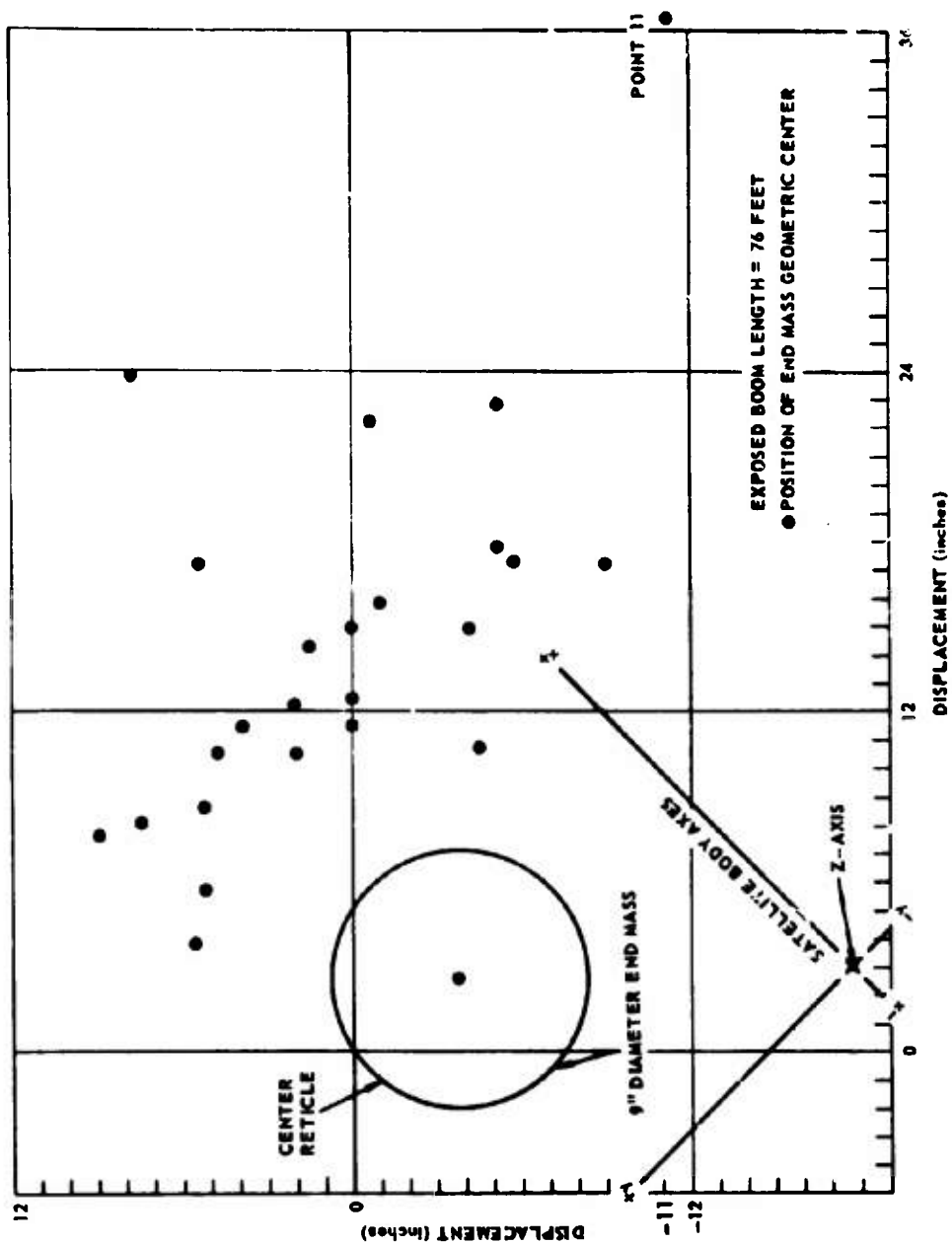


Fig. 2-11 DISPLACEMENT OF DODGE END MASS DUE TO
THERMAL AND DYNAMIC BENDING OF -Z BOOM,
PASS 10 - DAYS 283, 284, 1967

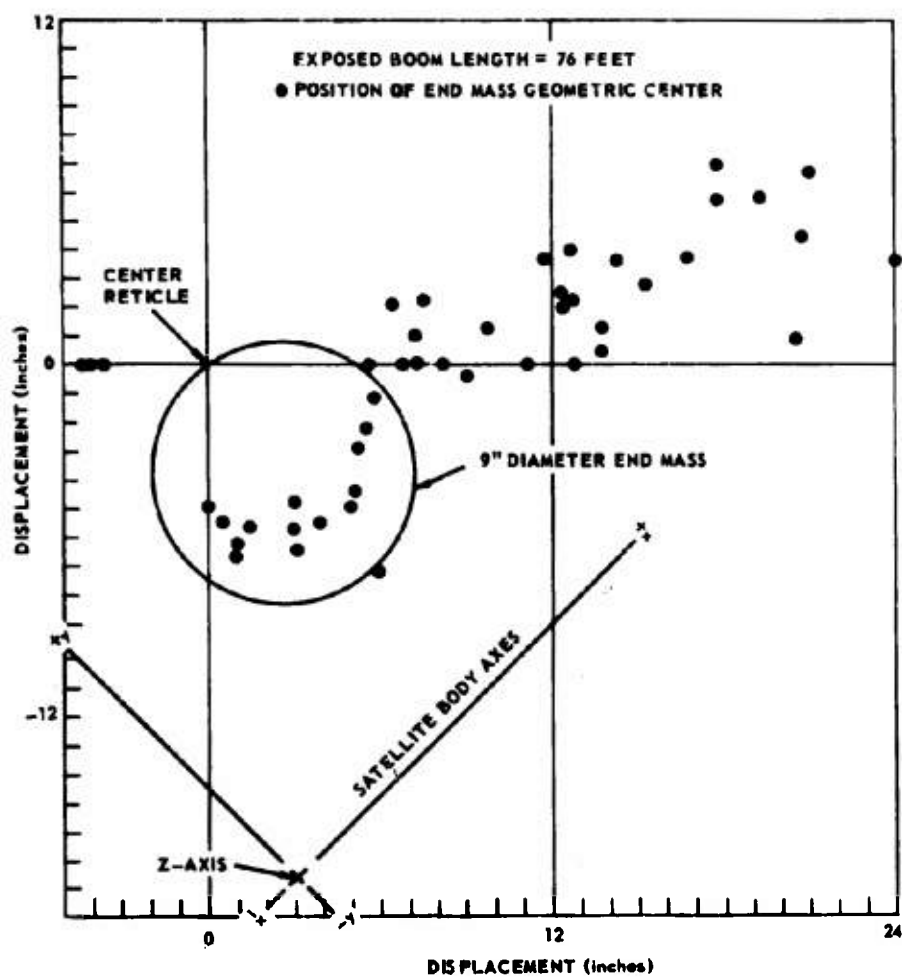


Fig. 2-12 DISPLACEMENT OF DODGE END MASS DUE TO
THERMAL AND DYNAMIC BENDING OF -Z BOOM
PASS 24- DAYS 076, 077, 078 1968

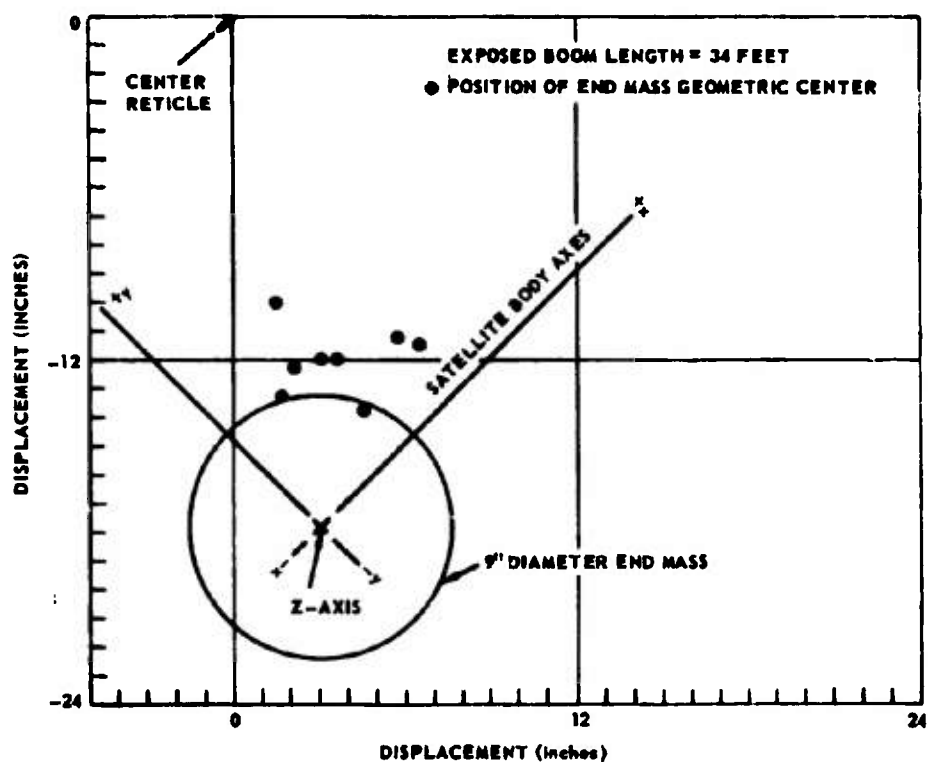


Fig. 2-13 DISPLACEMENT OF DODGE END MASS DUE TO THERMAL
AND DYNAMIC BENDING OF -Z BOOM, PASS 24-DAY 076, 1968

Fig. 2-13 illustrates the magnitude of bending with 34 feet of the -Z boom exposed. It can be seen that the dispersion pattern is very small. All of the points are contained within a 5 inch square. The test duration was 5 1/2 hours.

Tables 2-1, 2-2, and 2-3 give angles of the sun with respect to the satellite. Using these data and the right handed coordinate system shown in each of the figures one can establish the direction of the sun relative to the boom and its end mass.

Fig. 2-14 shows how pronounced boom bending can appear even though the displacement of the end mass is small compared to the length of the boom.

On the basis of what has been presented thus far, one might reach the preliminary conclusion that thermal bending is insignificant and for some applications this could be true. What is not known, however, is whether or not consecutive data points represent the same cycle of motion. For instance two consecutive points could represent different cycles if the boom were whirling around. This condition is impossible to detect from the photographs. If this were the case, then substantial amounts of energy could be stored in this mode. The transfer of this energy from mode to mode would have some effect on attitude stability. And not to be discounted is the gyroscopic effect of the whirling end mass. Fluid dampers contained in the end mass, it is felt, helped damp transient boom vibrations, but nothing quantitative can be said about their performance. In any event their presence was not detrimental to the performance of the satellite.

The data collected during these experiments are still undergoing interpretation and much more study lies ahead before one can ascertain how large a role boom bending plays in gravity gradient stabilization.

TABLE 2-1

SUN TO SATELLITE ANGLES
APL PASS NO. 10, DAYS 283-284, 1967

<u>Data Point</u>	<u>Day</u>	<u>Time</u>	<u>θ_x</u>	<u>θ_y</u>	<u>θ_z</u>
4	283	1842	58.5	72.0	45.0
7		2050	62.0	18.0	73.0
9		2137	75.0	6.0	78.0
11		2337	129.0	43.0	76.0
13	284	0037	156.0	81.0	76.0
15		0137	170.0	105.0	83.0
18		0837	124.0	47.0	106.0
19		0937	157.0	71.0	76.0
20		1037	150.0	97.0	53.0
22		1243	93.0	114.0	34.0
25		1300	86.0	108.0	32.0
28		1307	85.5	107.0	32.5
29		1313	85.0	106.5	32.0
31		1320	84.5	106.0	31.0
32		1328	84.0	105.0	30.0
33		1437	85.0	92.0	28.0
35		1537	88.0	80.0	27.0
36		1637	93.0	70.0	28.0
38		1737	98.0	69.0	29.0
40		1837	103.0	76.0	27.0
42		1937	106.0	91.0	8.0
44		2037	100.0	113.0	30.0
46		2137	89.0	133.0	52.0
48		2237	70.0	154.0	78.0
49		2337	59	138.0	114.0

TABLE 2-2
SUN TO SATELLITE ANGLES
APL PASS NO. 24, DAYS 076-078, 1968

<u>Data Point</u>	<u>Day</u>	<u>Time</u>	<u>θ_x</u>	<u>θ_y</u>	<u>θ_z</u>
17	076	2235	22.0	111.0	92.0
18		2242	21.0	109.0	93.0
19		2249	20.0	108.0	94.0
20		2339	15.0	100.0	102.0
21	077	0039	04.0	83.0	113.0
22		0139	35.0	78.0	125.0
23		0239	48.0	70.0	136.0
24		0737	139.0	101.0	133.0
25		0837	160.0	105.0	108.0
26		0937	176.0	107.0	86.0
27		1137	130.0	108.0	39.0
28		1237	107.0	107.0	15.0
29		1337	92.0	105.0	4.0
30		1430	84.0	101.0	13.0
31		1503	76.0	98.0	19.0
32		1509	75.0	97.0	20.0
33		1516	74.0	96.0	21.0
34		1525	73.0	96.0	22.0
35		1529	72.0	95.0	23.0
36		1543	71.5	94.5	24.0
37		1549	71.0	94.0	24.5
38		1556	70.5	93.5	25.0
39		1603	70.0	93.0	26.0
40		1610	69.0	92.0	27.0
41		1616	68.0	91.0	28.0
42		1630	66.0	89.0	30.0
43		1637	65.0	88.0	29.0
44		1734	62.0	83.0	37.0

TABLE 2-2 (continued)
SUN TO SATELLITE ANGLES
APL PASS NO. 24, DAYS 076-078, 1968

<u>Data Point</u>	<u>Day</u>	<u>Time</u>	<u>θ_x</u>	<u>θ_y</u>	<u>θ_z</u>
46		1741	61.0	82.0	38.0
47		1748	60.0	81.0	39.0
48		1755	59.0	80.0	40.0
49		1802	58.0	79.0	41.0
50		1906	56.0	78.0	45.0
51		1913	54.0	77.0	49.0
52		1920	52.0	75.0	51.0
53		1927	50.0	73.0	53.0
54		1933	47.0	72.0	55.0
55		2037	40.0	69.0	67.0
56		2135	31.0	68.5	80.0
57		2256	24.0	69.0	99.0
58		2303	25.0	69.5	103.0
59		2317	26.0	70.0	107.0
60		2325	27.0	71.0	111.0
61		2337	28.0	72.0	113.0
62	078	0039	47.0	75.0	135.0
64		0637	164.0	75.0	85.0
65		0737	154.0	74.0	66.0
66		0837	143.0	75.0	55.0
67		0937	133.0	77.0	44.0
68		1309	100.0	90.0	14.0
69		1316	99.0	90.0	13.0
70		1323	96.0	90.0	12.0
71		1401	93.0	90.0	8.0
72		1408	92.0	90.0	7.0
73		1415	92.0	90.0	7.0
74		1421	92.0	90.0	6.5

TABLE 2-2 (continued)
SUN TO SATELLITE ANGLES
APL PASS NO. 24, DAYS 076-078, 1968

<u>Data Point</u>	<u>Day</u>	<u>Time</u>	<u>θ_x</u>	<u>θ_y</u>	<u>θ_z</u>
75		1428	91.0	90.0	6.0
77		1448	91.0	90.0	6.0
78		1455	85.0	90.0	21.0

TABLE 2-3
SUN TO SATELLITE ANGLES
APL PASS NO. 24, DAY 076, 1968

<u>Data Point</u>	<u>Day</u>	<u>Time</u>	<u>θ_x</u>	<u>θ_y</u>	<u>θ_z</u>
1	076	1635	102	82	24
2		1642	90	84	18
7		1817	56	109	50
8		2056	44	120	73
9		2114	42	120	78
10		2120	39	120	80
11		2138	33	118	83
12		2139	33	118	83
13		2146	31	117	84
15		2201	18	116	86

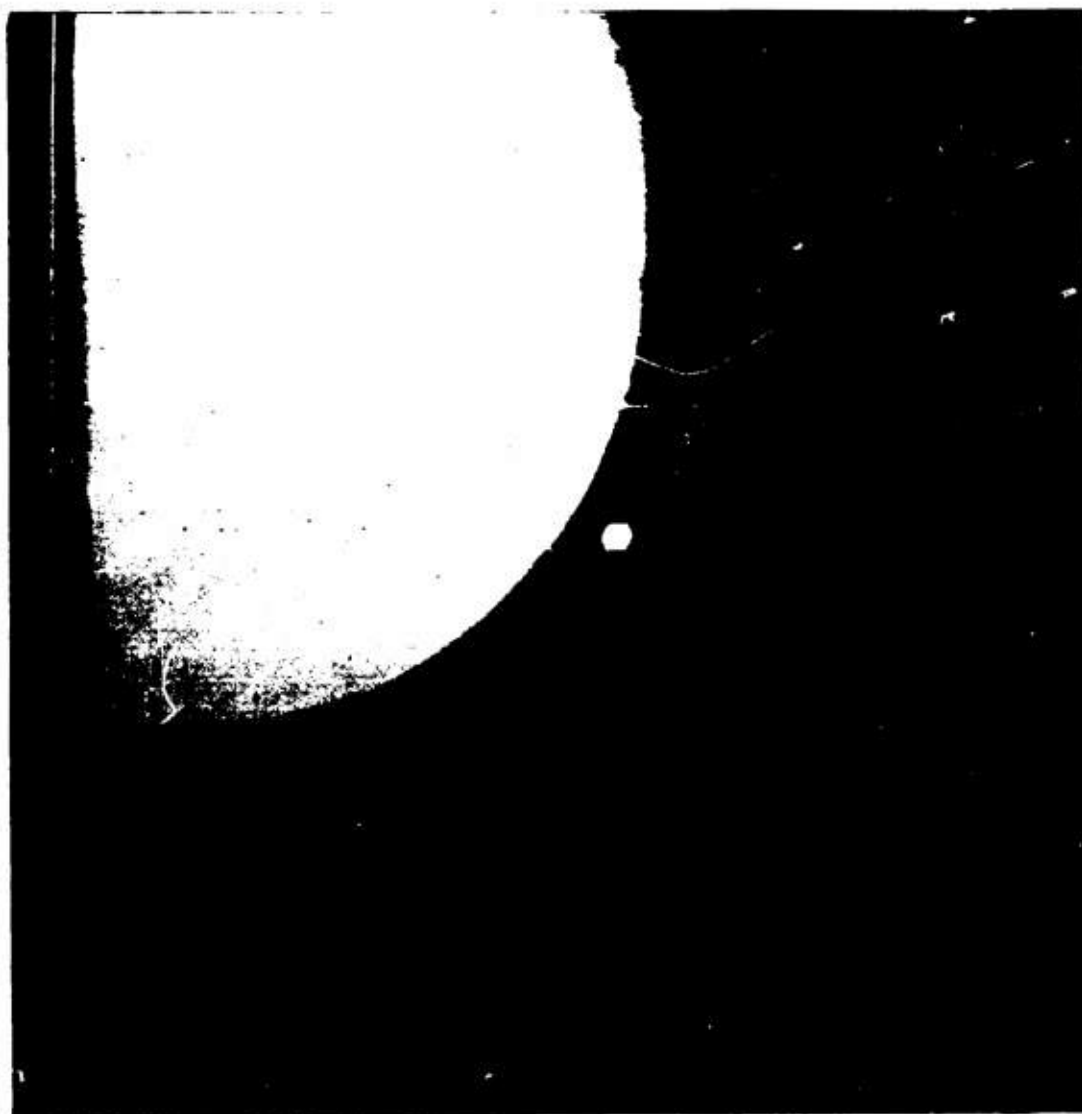


Fig. 2-14 THERMAL BOOM BENDING

2.2.2 Angular Momentum Flywheel

Very late in the design of the DODGE satellite it was decided to include an angular momentum flywheel to provide a stabilizing torque in yaw and in roll. The rotor for this flywheel is driven by a 400 Hz AC hysteresis synchronous motor. The electric power for the motor is obtained from the same source as that for the motorized boom units. Some other significant features of the flywheel are as follows:

- | | |
|-------------------------------------|--|
| a. Size: | 4-inch diameter x
6-inches long. |
| b. Weight: | 2.0 pounds. |
| c. Flywheel Moment-
of-Inertia: | $2.84 \text{ by } 10^{-4}$
slug-ft ² . |
| d. Synchronous Rate: | 8,400 rpm. |
| e. Angular Momentum: | 0.25 pound-foot-
second. |
| f. Electric Power
Configuration: | 2.1 watts. |

The flywheel is oriented with its angular momentum vector along the satellite's X axis, i.e., along the pitch axis of the satellite.

Results from ground measurements indicate that the bearing friction decreased during the first several trial runs in a vacuum. A further slight reduction in bearing friction was observed in tests with the orbiting satellite.

On 9 January 1968, the first in-orbit experiments using an angular momentum flywheel in conjunction with gravity-gradient booms to obtain three-axis stabilization was initiated. Results to date are encouraging. The satellite has stabilized in yaw with the flywheel rotation axis normal to the orbit plane. Yaw oscillations are approximately ± 40 degrees; the increased yaw stiffness is apparent in the observed decrease

in yaw period of oscillation. Turning on the flywheel did not result in loss of capture in pitch and roll. Each of these has a peak angle of approximately 20 degrees.

After one day of flywheel operation, a test was performed to compare the friction in the flywheel in orbit as compared to that observed in DODGE satellite thermal vacuum tests. The results are shown in Fig. 2-15. Several aspects of the two curves indicate that flywheel friction is less in orbit now than it was in the thermal vacuum tests. These indications are as follows:

- a. The boom motor current was less immediately after and during the time that the motor was approaching synchronous speed.
- b. Synchronous speed was obtained in 13 seconds in the in-orbit tests compared to 18 seconds in thermal vacuum tests.
- c. The steady state motor current was 220 milliamperes in thermal vacuum tests, but decreased to 210 milliamperes in orbit.

From the above data it appears that the friction in the flywheel bearings was less than that obtained in ground measurements. This may be due partially to running in, but may be due entirely to the zero gravity conditions in orbit compared to the one g experienced in thermal vacuum tests.

As can be seen in the attitude data of Appendix A, the use of the angular momentum flywheel greatly increased the yaw stiffness of the satellite and somewhat increased the roll stiffness, thus reducing yaw/roll motions with resulting cross coupling to the pitch axis. As of 30 September 1968 the angular momentum flywheel has operated for a total of approximately three months continuous operation. Most of the three months occurred during the summer of 1968. At the end of this length of operation the bearing friction seemed to be the same as measured after the first week the satellite was placed into orbit.

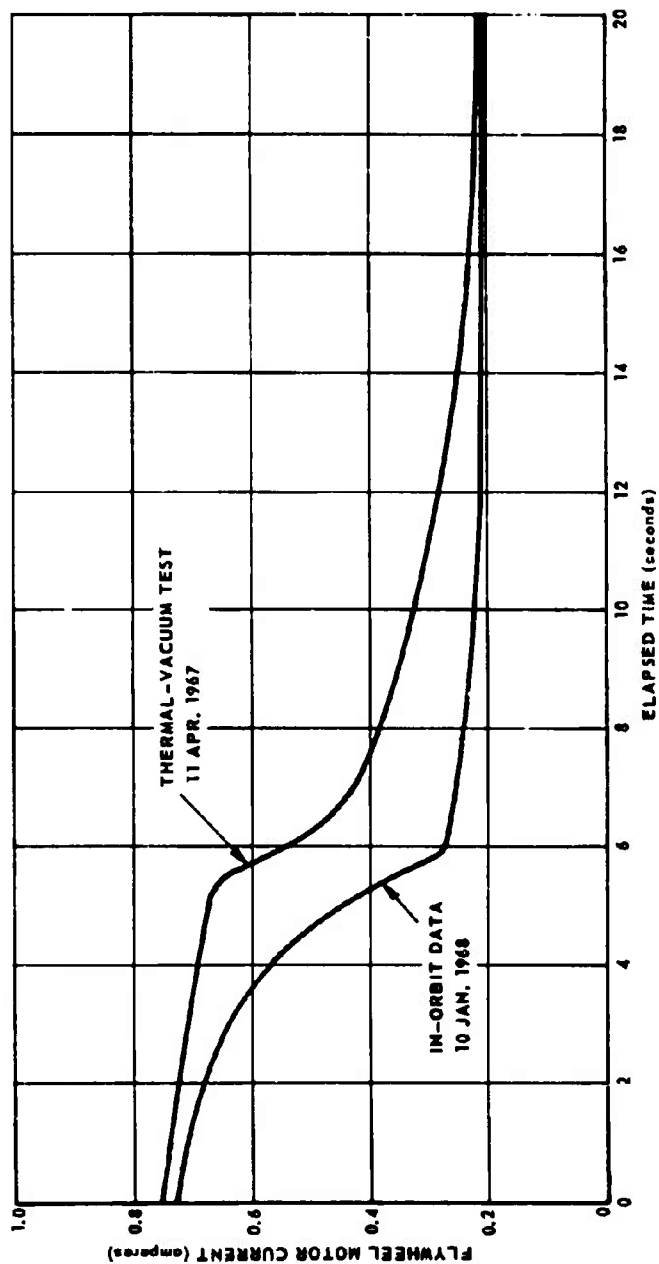


Fig. 2-15 FLYWHEEL MOTOR CURRENT AFTER A 235 SECOND TURN-OFF

2.2.3 Magnetic Damping Systems

The magnetic damping systems consisting of electronics for producing time-lag and artificial hysteresis damping modes and a three-axis vector magnetometer are used in conjunction with the gravity-gradient boom stabilization system. These systems (discussed in Section 2.1) provide for the damping of librations via magnetic torquing.

2.2.3.1 Time-Lag Damping

The first system to be tried for damping gravity librations was the time-lag mode. As DODGE approached the "set" time of the 2nd APL pass the magnetic damping system was turned on in the 6 hour, low output gain mode. Shortly before rise of the 3rd APL pass the output gain of the damping system was changed from low to high by command from the Orroal station at Canberra, Australia.

At rise at APL on Day 203 the satellite was clearly captured to the vertical, and subsequent analysis confirmed that it was captured in yaw also. The libration angles for the entire pass are given in Fig. 2-16. By Day 204 roll and pitch angle peaks were less than 15 degrees and yaw peaks less than 30 degrees.

These results confirmed that three-axis stabilization had been achieved, and that the time-lag magnetic damping system was functioning to damp librations. The ultimate desired stabilization was not achieved at this time.

During the next seven satellite passes APL experimented extensively with various modes of magnetic time-lag damping and boom lengths in an effort to find a combination of satellite parameters that would produce better stabilization.

As Pass #4 approached its end on Day 219, roll and pitch libration appeared to be increasing with final peak roll of 22 degrees. Yaw peaks of about 30 degrees were observed (see Fig. 2-17).

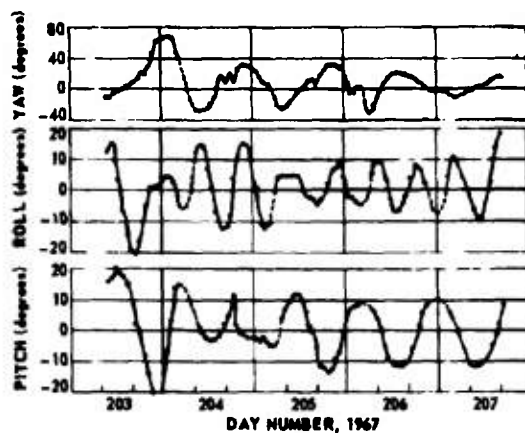


Fig. 2-16 LIBRATION HISTORY OF PASS NO. 3

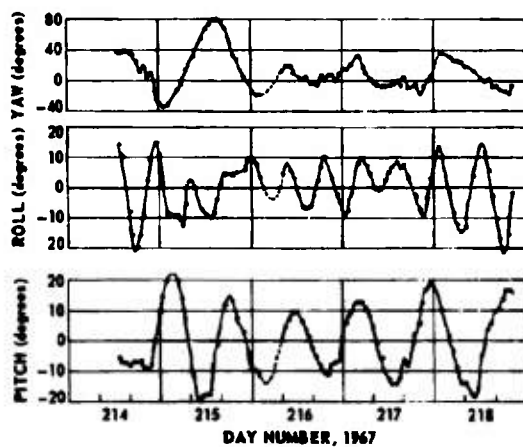


Fig. 2-17 LIBRATION HISTORY OF PASS NO. 4

In the first few days of Pass #5 (Days 225-227) time-lag damping in 6 hour, high gain was used, and peak pitch angles of about 20 degrees were observed. On Day 228 magnetic damping was turned off and a large Z axis dipole turned on manually in an attempt to damp librations by direct ground command. The satellite responded by flipping 180 degrees in yaw and producing a pitch angle of 23 degrees. At the end of Day 228 the manual "damping" was abandoned and magnetic damping in the 3 hour, high gain mode was established.

The satellite continued in this mode into the 6th pass which began on Day 237. An attempt to reduce pitch libration by extension of the "X" booms from 75 feet to 87 feet led to inexplicable (at the time) librations. Further boom length changes were made on Day 238 and on Day 240 in attempts to reduce librations, but the final change caused the satellite to tumble in pitch.

Early in Pass #7 it was discovered that the "X" booms had unsymmetrical lengths. This state was traced to the boom operation on Day 237 when the booms were "extended" in separate pairs. One pair in fact extended, but the other pair had retracted. All commands had been properly sent and received by the satellite for extension. The two-phase inverter was however overloaded and apparently suffered severe phase shift in its output, causing the boom motors to run backwards, as noted in Section 2.2.1.1. After discovery of this fact the boom lengths were corrected.

During Pass #7 the satellite continued to tumble until capture was achieved on Day 251. Eight boom operations were necessary to stop the satellite tumble and re-achieve a state of capture with the vertical. The final boom extension on Day 251 achieved a form of "dead-beat" capture in that subsequent librations did not exceed 20 degrees in pitch and roll. At satellite "set", magnetic damping in the 3 hour, low gain mode was in effect.

Pass #8 covered the period from Day 259 to 264. Fig. 2-18 shows the libration angle history of this pass. Pitch and roll showed peculiar anomalies at the beginning of the pass, then settled into damped sinusoids with peaks less than 3 degrees by Day 264. Yaw was less well behaved with a peak of 25 degrees.

The results of Pass #8 were very striking and encouraging. The stabilization accuracy was comparable to the expectations based on theoretical analysis. Magnetic damping in the 3 hour, low gain mode seemed to be working very well.

Our elation was somewhat deflated by the results of the next pass given in Fig. 2-19. Pitch librations were up to 20-30 degrees, roll peaks were about 20 degrees and a peak yaw of 40 degrees was observed. The cause of the buildup in libration amplitude is not known at this time. Yaw oscillations continued to build up, until a full 180° reversal occurred on Day 274.

At rise of Pass #10 on Day 282 libration angles had built up to 60 to 70 degrees. Most of the time the earth's image was outside of the field-of view of the 60° camera. In this case determination of libration angles rests on solar attitude detector data and magnetic field observations. The resultant determinations are crude at best, sufficient primarily to tell whether the satellite is tumbling or not.

The very large librations at the start of the 10th pass discouraged further efforts with magnetic damping at that time.

Pass #8 exemplified exceptionally good stabilization, and it has been suggested that the results were due to a fortuitous phasing of librations with magnetometer signals.

Results comparable to Pass #9 were achieved both before and after that time, in particular Passes #3, #5, #11, and #17. So it appears that stabilization on the order of 20° in pitch and roll can be

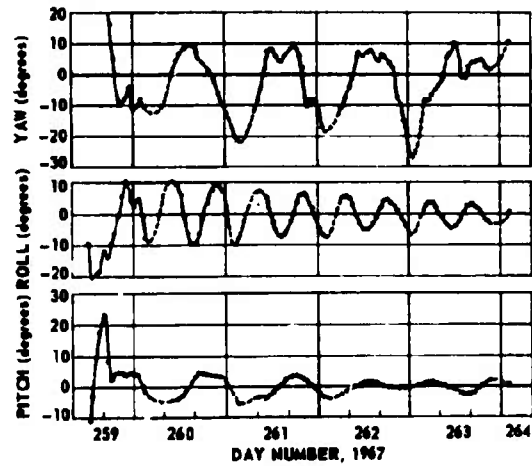


Fig. 2-18 LIBRATION HISTORY OF PASS NO. 8

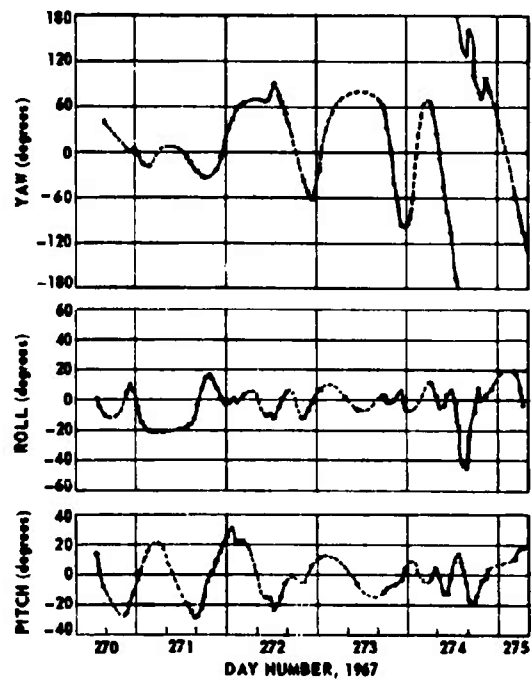


Fig. 2-19 LIBRATION HISTORY OF PASS NO. 9

routinely achieved with DODGE using magnetic damping. If boom operations were halted that degree of stabilization could probably be maintained for many months.

Anomalies in the magnetometer signals may be degrading the steady-state accuracy. With correction of these problems in future satellites better steady-state performance should be achieved.

2.2.3.2 Enhanced Hysteresis Damping

Enhanced hysteresis damping was successfully used for initial despin and detumble following injection of the satellite into orbit. Input-output telemetered signal characteristics indicated that the hysteresis generators functioned as designed.

The demagnetizer used in conjunction with the hysteresis damping system was used on several occasions to demagnetize the hysteresis generators and remove extraneous permanent moments from the spacecraft. An attempt was also made to demagnetize the torsion wire assembly and hopefully reduce the damper boom bias. It is noted that the demagnetizer and hysteresis damping system was not originally intended to perform this function. The demagnetization cycle was effective in removing residual magnetism from the hysteresis generators and probably the spacecraft but not from the torsion wire assembly.

Enhanced hysteresis damping was tried as a means of damping librations on Passes #28 through #29. Here, the "X" booms were extended 80 feet and the hysteresis damping system set at low input - low output gain state. Pitch and roll were nominally maintained within $\pm 30^\circ$ but yaw was not well controlled. The system was turned off on Pass #30. As a consequence of magnetometer behavior, magnetic torque perturbations reduce the enhanced hysteresis damping system effectiveness in damping gravity librations.

2.2.3.3 Magnetometer Performance

The DODGE magnetometer is a three-axis vector magnetometer operating on the fluxgate principle. As noted in Section 2.1.1 it has a full scale range of ± 250 gamma (1 gamma = 10^{-5} oersted), and was designed to achieve a basic accuracy of a few gamma over the temperature and supply voltage range of the satellite. The sensor was placed at the end of the satellite mast to reduce the effect of satellite hardware and currents on the magnetometer sensor. Nevertheless, some degradation in magnetometer accuracy due to satellite-generated bias was expected, specifically from residual magnetization of the X and Y electromagnets. Variable biases on the order of 5 gamma are due to known sources. Fixed biases of 5 to 15 gamma were measured in final systems tests at the magnetic facility of the Naval Ordnance Laboratory, White Oak, Md.

Operation of the magnetometer in orbit has appeared to be quite normal. In-flight checks of the magnetometer sensitivity have confirmed pre-launch measurements. Satisfactory operation of the magnetic damping system implies a good measure of magnetometer performance. Nevertheless careful observation of the magnetometer data over many passes at APL shows some extraordinary and unexpected results. Briefly summarized, when the satellite is well captured the magnetometer data indicate a periodic variation in total magnetic field with peak at satellite sunset, and minimum at satellite sunrise. But when the satellite is tumbling this periodicity disappears. This phenomenon is illustrated by comparison of the data of Figs. 2-20 and 2-21. The curves show the total magnetic field as measured by the three-axis vector magnetometer. Fig. 2-20 shows the typical variation of field which appears when the satellite is well stabilized. These data were taken during Pass #8 when stabilization better than 5 degrees was achieved. A minimum field strength is observed near satellite sunrise, and a maximum field near sunset. The data of Fig. 2-21 were taken in the previous pass during which the satellite was tumbling slowly. The distinct periodicity does not appear until after capture was achieved on

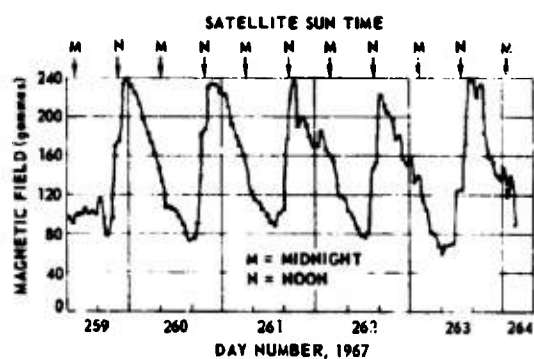


FIG. 2-20 MAGNETIC FIELD OBSERVED DURING PASS NO. 8

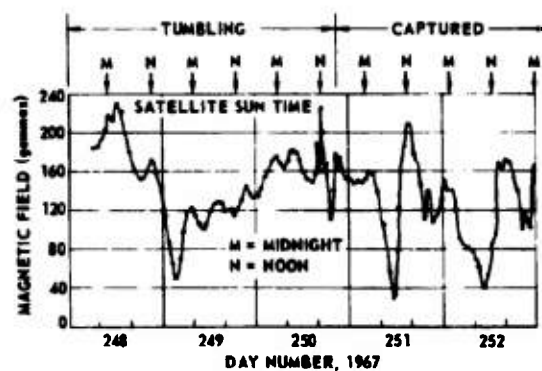


Fig. 2-21 MAGNETIC FIELD OBSERVED DURING PASS NO. 7

Day 250. The telemetry data also indicated rapid changes in field strength over an interval of a few hours on Day 250.

There is little doubt at this time that the magnetometer is responding to a spurious bias being generated by the satellite. Its amplitude is sometimes over ± 50 gamma, and it is dependent on the satellite orientation relative to the sun.

A possible source of the variable bias would seem to be currents in the satellite solar arrays. In an attempt to confirm this hypothesis a number of series of continuous data were taken through eclipse periods of the satellite. If solar array currents were a major source of bias then the magnetometer readings should change rapidly as the satellite passes into eclipse, and again change rapidly as the satellite emerges from eclipse. The results of a particular test are given in Fig. 2-22. Here the "apparent" total field is plotted versus time. No abrupt transients appear at the beginning or end of the eclipse. Furthermore the apparent total field is not constant during the eclipse as one might expect if solar array currents were the source of bias. The final rise in the total magnetic field prior to emerging from the eclipse seems to imply that the satellite "anticipated" coming out of the eclipse. These phenomena are as yet unexplained.

2.2.4 Torsion Wire Damping System

Several variations of damping systems were flown on DODGE to demonstrate which technique would be best suited for damping satellite libration energy at near synchronous altitudes. Two of these systems -- a magnetic hysteresis damper and an eddy current damper along with two transversely mounted extendible booms suspended from a very fine torsion wire -- constitute what is known as the torsion wire damper (see Fig. 2-23). This subsystem is mounted in a mast that protudes from the main body of the satellite (see Fig. 2-24). The torsion wire permits planar oscillations of the booms relative to the satellite body to occur. This action moves certain damper elements through corresponding

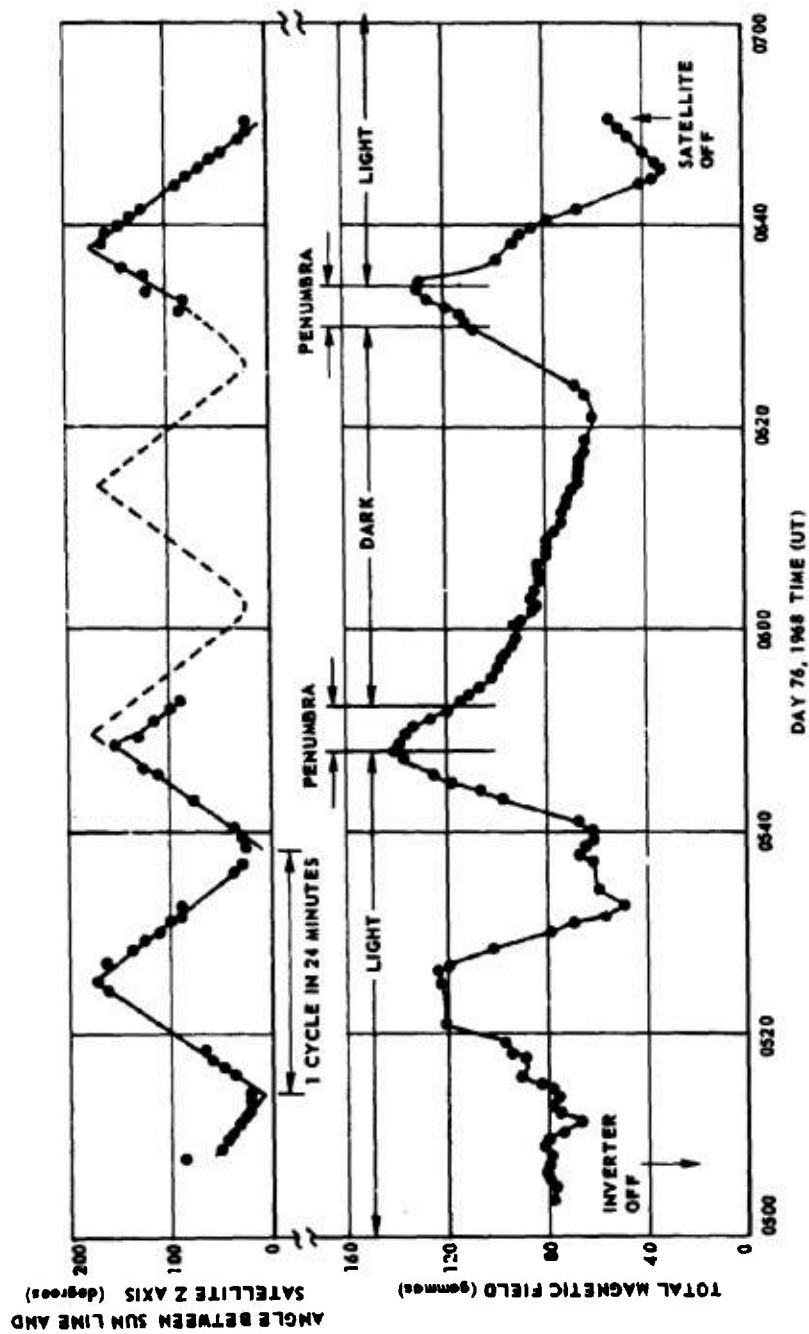


Fig. 2-22 DODGE MAGNETIC FIELD DATA THROUGH SOLAR ECLIPSE

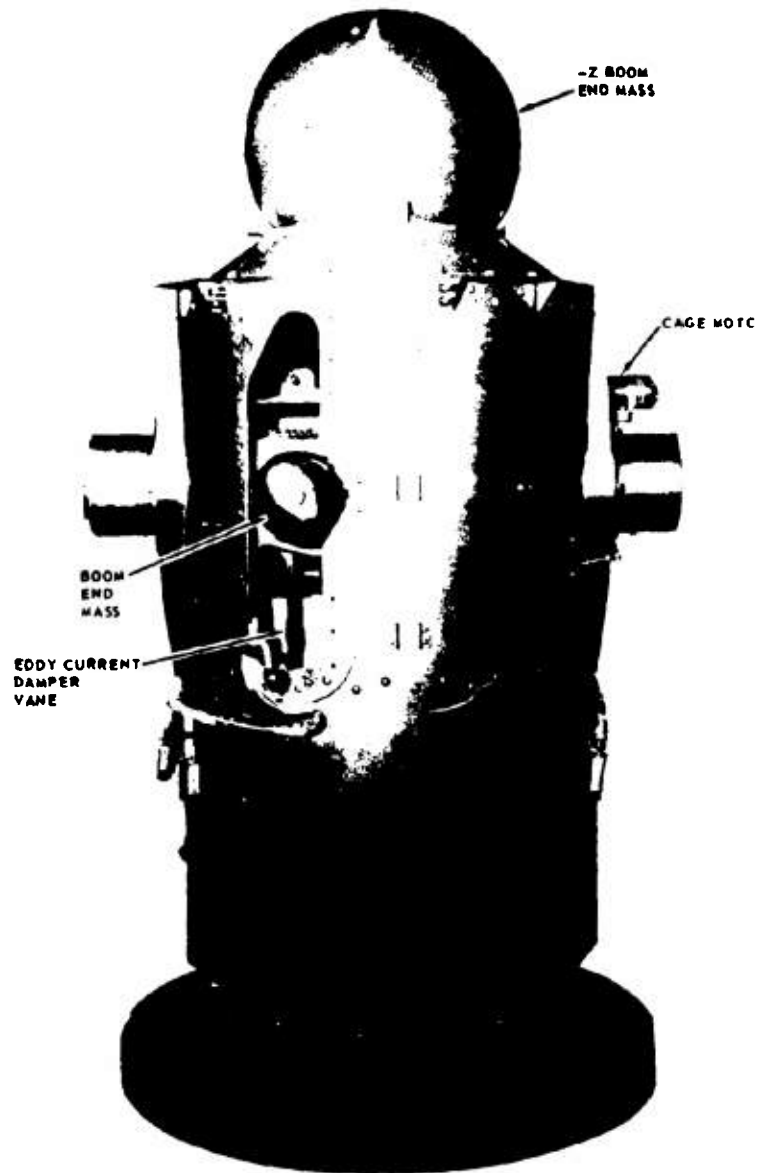


Fig. 2-23 TORSION WIRE DAMPER ASSEMBLY

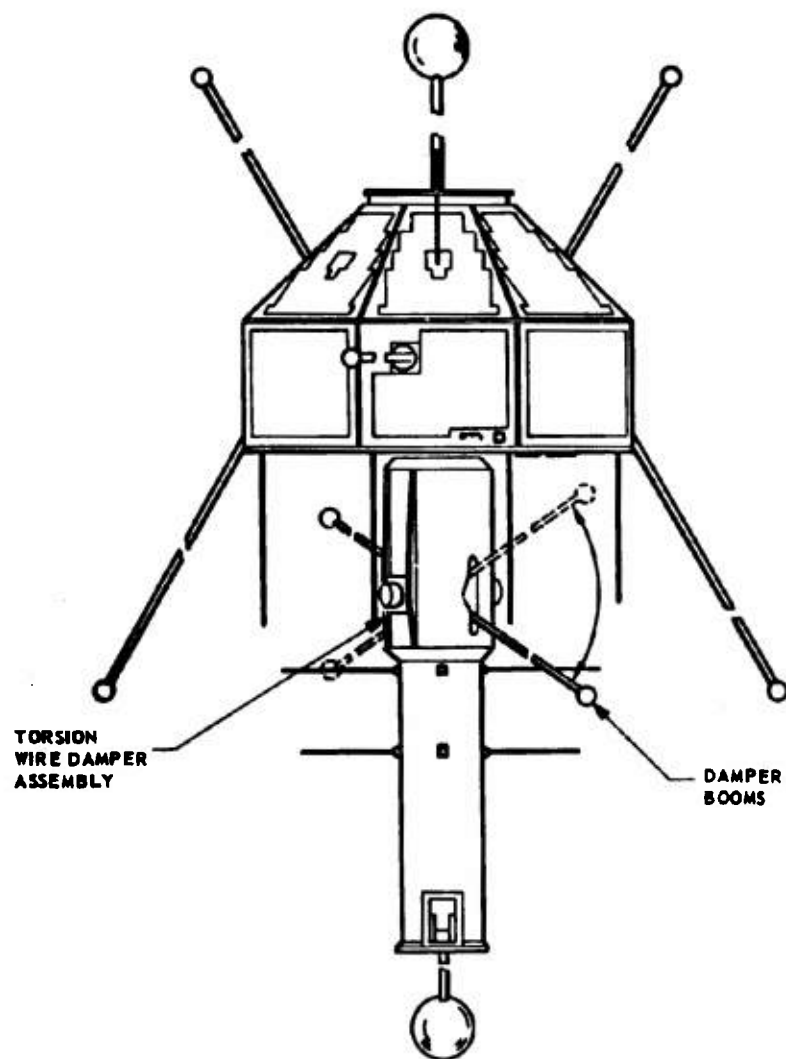


Fig. 2-24 DODGE SHOWING DAMPER ASSEMBLY AND BOOMS

elements fixed to the satellite body thereby providing the necessary environment for the removal of libration energy.

2.2.4.1 Damper Booms

The damper boom mechanisms are identical to the other eight gravity gradient booms on DODGE; namely, deHavilland Model 5489F1 motorized stem units with 1/2 inch diameter, 2 mil thick beryllium copper boom tape with a highly polished silver plated external surface exhibiting a reflectivity of approximately 0.90. A boom mechanism with end mass caged for launch is shown in Fig. 2-9. Maximum extension capability of these booms is 50 feet.

2.2.4.2 Torsion Wire Suspension System

The torsion wire suspension system consists of a boom mechanism housing and two fine torsion wires which tie the housing to the mast. The entire damper system including the wire suspension is shown in cross section in Fig. 2-25.

Both torsion wires are made of 3 mil music wire. Tapered chuck grips machined from soft brass secure the wires at their ends. Considerable care was exercised in the design of the grips to minimize stress concentrations which could produce fatigue failure during launch and to a lesser extent during the operational phase of the satellite's existence. Damper boom oscillations are limited to ± 30 degrees from the mid-position by mechanical stops.

2.2.4.3 Caging Mechanisms

There are two separate caging mechanisms. The first, the launch lock, protects the entire torsion wire damper from damage during launch. The second, caging mechanism, the orbit lock, prevents oscillation of the torsion wire system in orbit. Both locking systems are operated by command and from a common shaft driven by a hysteresis synchronous motor with a gearhead whose output shaft turns at 1 rpm.

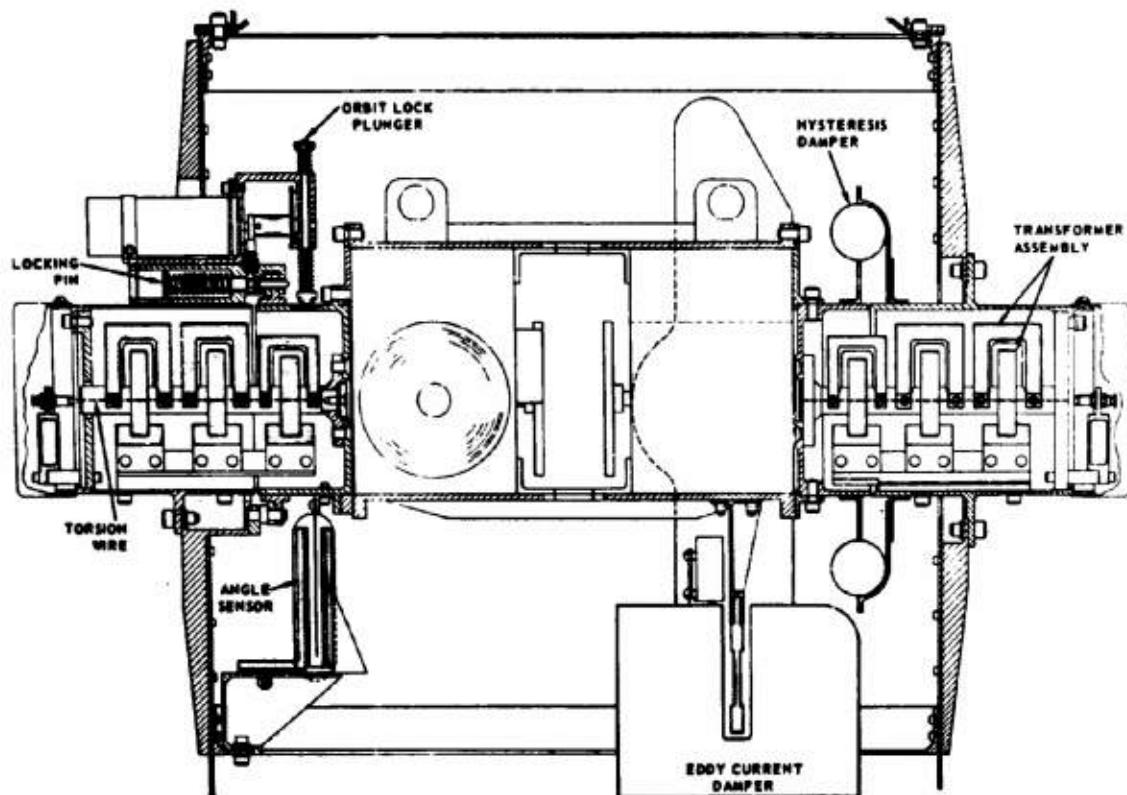


Fig. 2-25 TORSION WIRE DAMPER ASSEMBLY CROSS SECTION

The launch lock operates at one of the suspension system. It consists of two semicircular clamp halves sharing a common pivot (see Fig. 2-26). When closed the clamp halves secure a cylinder which is an integral part of the damper boom housing. During the clamping operation, the suspension system is manually displaced off-center until a cylinder at the opposite end of the assembly is captured in a tapered seat. The clamp is then engaged. In this condition the suspension system is caged.

The clamp is held in place by a spring loaded pin (see Fig. 2-25). When the cage motor is started it rotates a cam which eventually releases a small ball which normally keeps the pin in the locked position. A spring then retracts the pin, releasing the clamp halves which are quickly sprung away from the cylinder they gripped securely. The suspended booms and damper elements are then free to oscillate in a zero-g environment. The launch lock is a manually resettable single function device. It is set before launch or test and once released serves no further function.

The orbit lock consists of a spring loaded plunger that when activated applies a lateral load to the suspended subassembly, which bottoms-out against a tubular limit stop. Motion of the plunger is controlled by a cam mounted to the same motor gearhead combination used for the launch lock.

The head of the orbit lock has a hemispherical tip which seats in a hole in the damper assembly. This hole enables the lock to stop the damper in its equilibrium position if this is desirable. Locking action can occur at any position within ± 30 degrees of equilibrium. The cam actuates the plunger through a spring to prevent jamming. This also eliminates the need for limit switches since rotation can be continuous and unidirectional. Since the orbit lock does not require manual resetting, it can be activated remotely and as often as necessary.

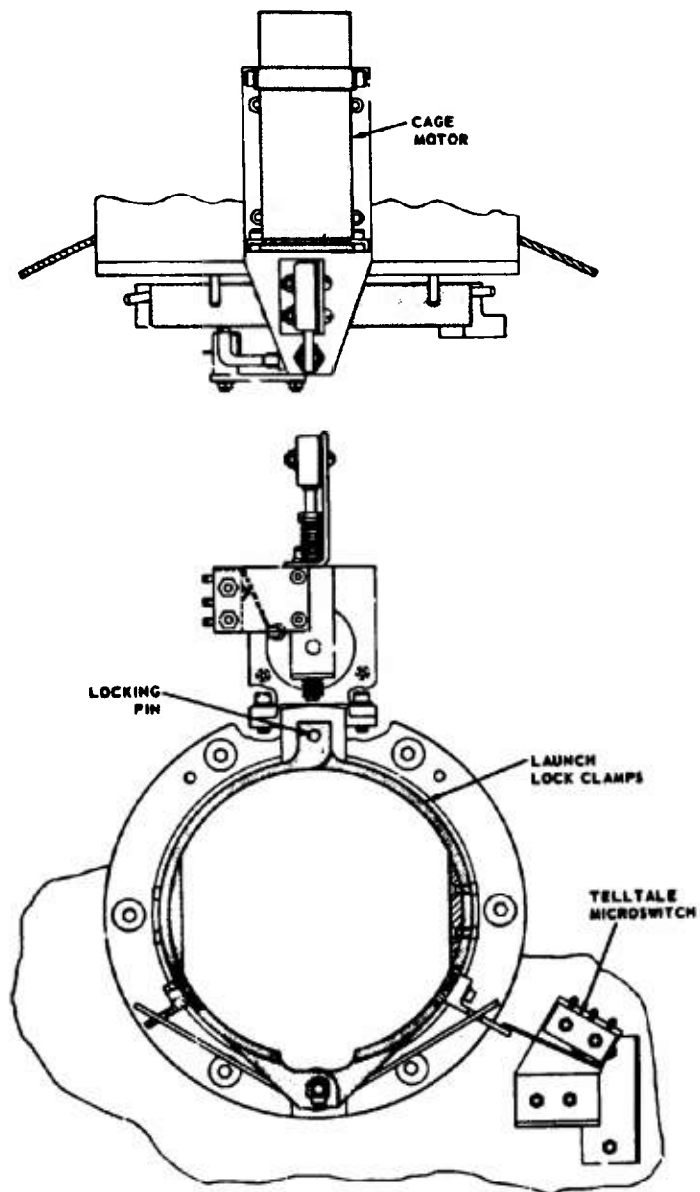


Fig. 2-26 LAUNCH LOCK CLAMPING SYSTEM

2.2.4.4 Electrical System

Hysteresis synchronous motors receiving power from a 31-volt 400 Hz square wave inverter are used to operate all of the boom and caging mechanisms. Proper functioning of the extended damper booms is possible only if they can oscillate about the torsion wire axis with not other restraint than that attributable to the torsion wire itself. For this reason the damper booms are powered inductively through transformers. The transformer cores and primary windings are attached rigidly to the satellite structure whereas the secondary windings are fixed to the oscillating elements suspended on the torsion wire. The telemetry signal for monitoring boom length also uses this method to bridge the gap between the suspension system and fixed structure.

2.2.4.5 Angle Sensor

The angle of the damper booms relative to the satellite body axes is monitored by continuously reading a discrete angle-sensing device. It consists of a thin fan-shaped element with slots etched into it and a digital device made up of a row of six photo-emitters and phototransistor detectors. The fan shaped element oscillates with the booms while light from the photoemitters passes through the slots (a binary gray code) and impinges on the phototransistors. Detector outputs provide angular position data with a 1.2 degree resolution.

2.2.4.6 Eddy-Current Damper

The eddy-current damper is designed to damp the libration motion of the satellite by dissipating the energy of the damping boom. This boom moves a copper vane through the gap of a chargeable magnet. The motion of the boom is damped by eddy currents generated in the vane, providing torques proportional to their relative angular rates of motion. Fig. 2-27 shows the van and the magnet.

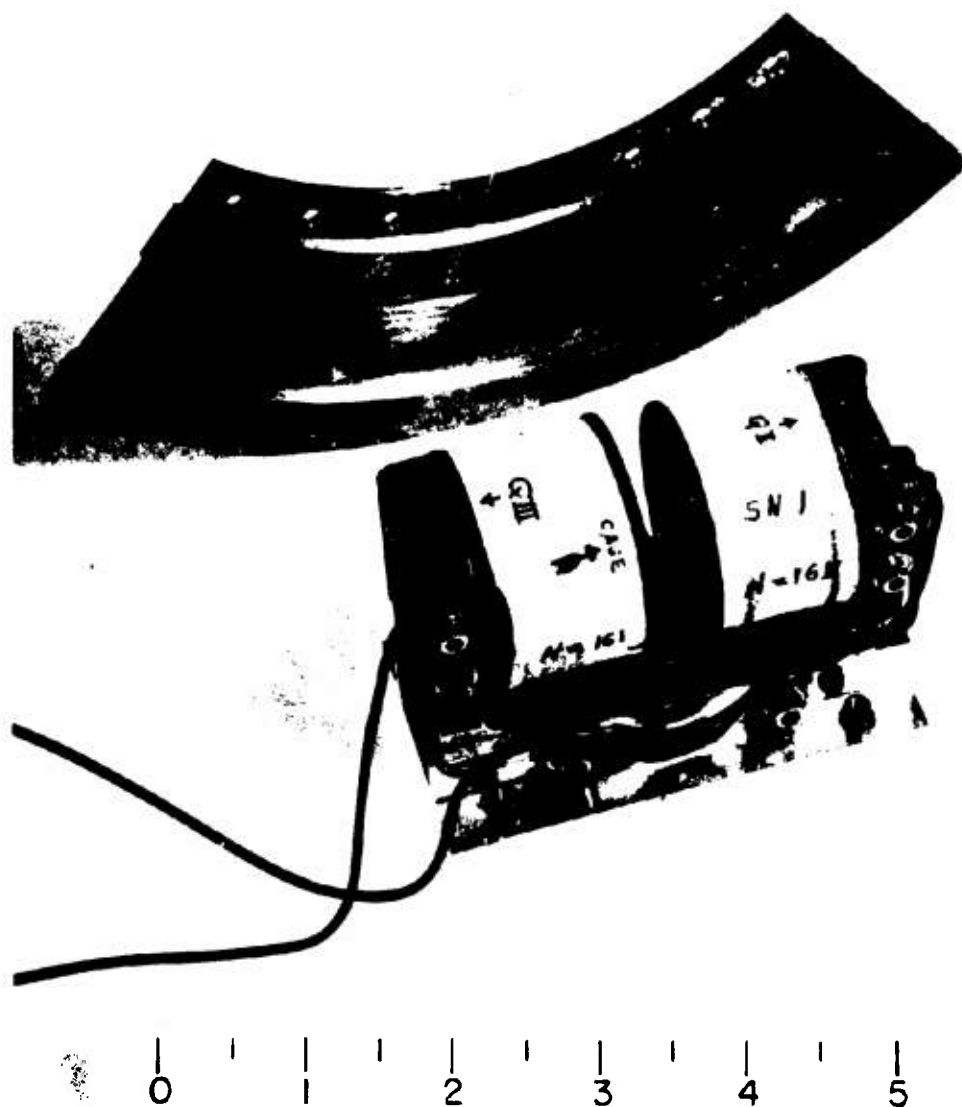


Fig. 2-27 VANE AND MAGNET

During damping experiments, the chargeable magnet is magnetized to provide 2.3 kilogauss in the gap. This magnetic field causes the optimum damping constant of 230,000 dyne-cm-sec for a 60 foot damping boom. Damping constants to 480,000 dyne-cm-sec may be set. To eliminate eddy-current damping effects, the magnet is demagnetized. A Hall effect detector is used to monitor the field in the gap.

In-flight checks have confirmed satisfactory operation of the eddy-current damper. Telemetry data from the Hall detector have been found to be consistent with ground calibration data. Tests with the damping boom at minimum length have confirmed damping action when the magnet is magnetized. The boom moves freely when the magnet is demagnetized.

In use, the eddy-current damper seems to have no effect on satellite libration. The system was first used on Days 206 through 214 of 1967. During these tests, roll and pitch peaks of 20 degrees, and yaw angles of 40 to 60 degrees were observed. During later tests started on Day 329 of 1967, the libration amplitude seemed to build up.

The trouble seems to be in the boom suspension structure. The torsion wire suspension was designed to permit ± 30 -degree excursions about the zero equilibrium position. During a test in orbit, the boom equilibrium position was found to be offset 28 degrees. This bias is believed to be caused by a torque from the main structure on the suspension system. Additional data indicate that this torque varies; thus, the damping effects of the eddy-current system may be lost in the random effects of the suspension system.

2.2.4.7 Magnetic Hysteresis Damper

As part of the DODGE experiment in gravity-gradient stabilization the suspended-boom assembly includes two dampers -- an eddy-current damper and a magnetic hysteresis damper. The distinction between the two is that the eddy-current damper produces torques proportional to the relative

angular rate, whereas the hysteresis damper generates a torque of constant strength opposing the relative motion.

The hysteresis damper operates from DC power and provides four levels of damping torque that can be selected by command. When not energized, the unit generates zero torque. The damper unit weights 1.10 pounds, and provides the following constant torque levels:

State	Coils Energized	Torque (dyne-cm)	Power Dissipation (watts)
1	A, B, and C	250	3.52
2	B and C	130	0.88
3	C	65	0.44
4	C at lower current	20	0.08

The DODGE hysteresis damper is shown in Fig. 2-28. It consists of three elements: a hysteresis ring, flux generating solenoids, and a magnetic shield. The hysteresis element is a closed toroid of AEM 4750; it is attached via the three spoke support to the oscillating boom unit. The axis of the toroid coincides with the axis of rotation of the boom unit. Three solenoids enclosed within a magnetic shield are mounted to a stationary hub. When the boom oscillates, the toroid slides through the solenoids without contact. The shield that surrounds the solenoids is a closed torus of Mu-metal (top half not shown in Fig. 2-28). It has the dual function of preventing solenoid generated fields from biasing the magnetometer sensors and shielding the hysteresis element from external fields. The solenoids are referred to as reversing solenoids because in each solenoid the field produced in one section is reversed in the adjacent section. Of the three solenoids, two have a single reversal (Coils B and C) while one (Coil A) has a double reversal.

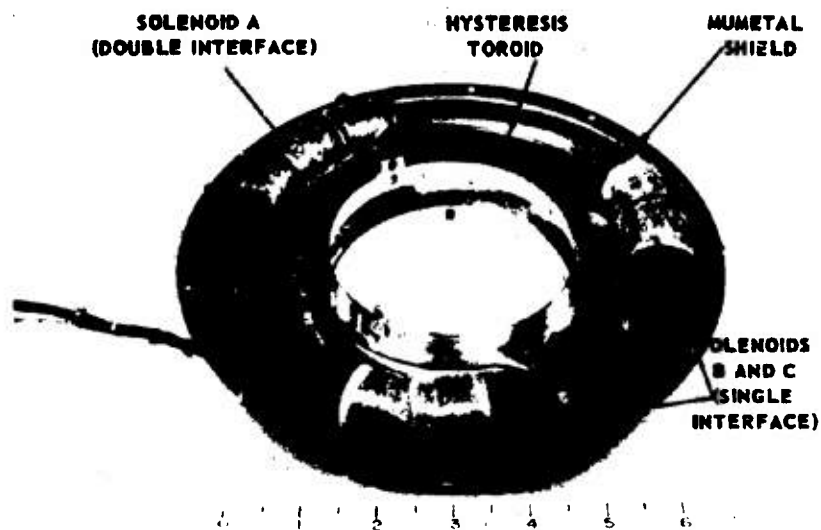


Fig. 2-28 MAGNETIC HYSTERESIS DAMPER

The principle of operation is that as the suspended-boom rotates the toroid slides through the solenoids while the magnetic reversals stay fixed relative to the solenoids. Thus as the system rotates, some of the magnetic material has its direction of magnetization reversed. Since this material exhibits magnetic hysteresis, energy is dissipated, and the gimballed boom experiences a retarding torque. This torque is of constant strength, and changes sense as the rotation reverses.

Damper torque performance of States 2, 3, and 4 is shown in Fig. 2-29. Torque levels are constant over the full range of rotation, but as noted the torque does not reverse abruptly with a change in the sense of rotation. Typically 15 degrees of rotation is required before full torque reversal is achieved, primarily because the solenoids do not completely saturate the hysteresis toroid. Thus only a minor hysteresis loop, producing lower torque, is established at the end of each swing.

The torsion wire hysteresis damper has been used in an attempt to achieve inertial damping or at least to reduce the bias angle on the torsion wire suspension. The torsion wire hysteresis damper was energized for short periods of time during Passes #23 and 25 and demonstrated its performance in damping motions of the damper booms.

On Pass #26 the torsion wire hysteresis damper was used with the "X" booms at 80 feet and damper booms at 36 feet. The hysteresis damper torque was 130 dyne-cm. Pitch remained at about ± 30 degrees and roll reduced slightly to ± 10 degrees, but the yaw angle was uncontrolled. The hysteresis damper was energized in the 250 dyne-cm torque state at the set of Pass #26. At the rise of Pass #27 pitch and roll were within ± 20 degrees but satellite motion remained uncontrolled in yaw.

2.2.4.8 In-Orbit Performance

The launch caging system which was to protect the torsion wire damping system from damage during launch performed satisfactorily. Shortly

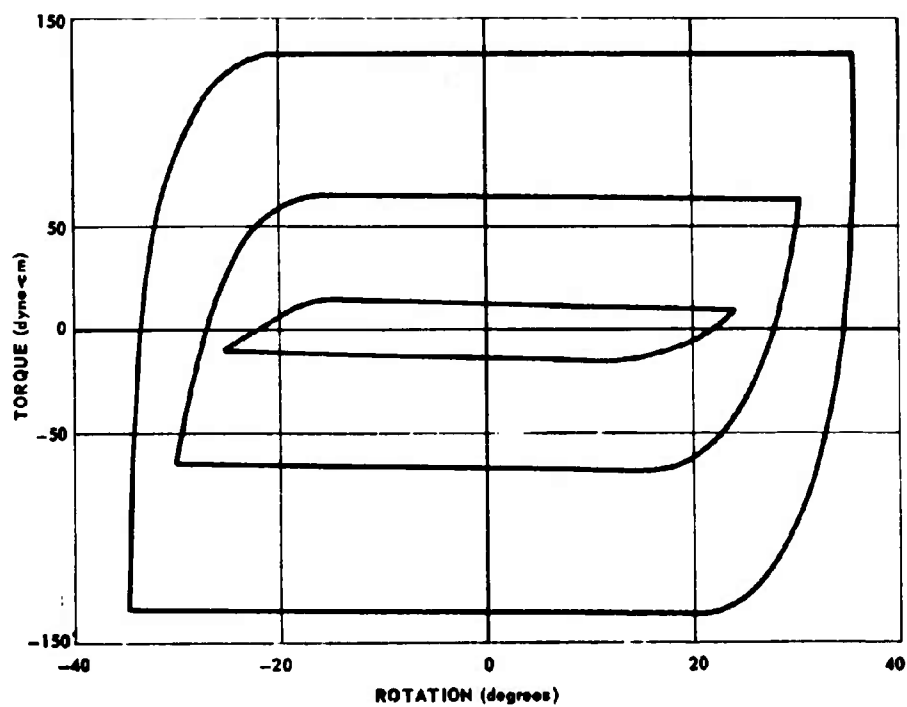


Fig. 2-29 HYSTERESIS DAMPER PERFORMANCE

after the command to uncage was transmitted to the satellite, the angle sensor picked up a boom oscillation which indicated that the sensor was operating and the torsion wire was intact.

The orbit caging system was exercised numerous times and worked faultlessly as did the damper booms during a dozen extensions and retractions.

A satisfactory explanation of an off-center bias that exists in the equilibrium position of the suspension system is still awaiting formulation. Magnetic interaction and some mechanical misalignment are the main suspects so far.

2.2.5 Manual Damping Using the Angular Momentum Flywheel

A new technique of damping the librations of a satellite has been demonstrated with the DODGE spacecraft. This is illustrated in Fig. 2-30. At time zero the satellite pitch angle was -30° degrees. Under normal conditions it would require $1/4$ of a libration period to reach zero degrees; i.e., for the satellite to be aligned exactly along the local vertical. For this configuration, the DODGE satellite had a $1/4$ libration period of 3.2 hours. At the peak libration angle of -30 degrees the satellite has the correct angular rate in pitch of 1.0 rpo. During the 3.2 hours of a quarter libration period, gravity-gradient torque produces a torsional impulse with the result that when the satellite crosses the local vertical the angular rate is much higher than 1 rpo. This torsional impulse, I_t , is given by the equation

$$I_t = \int_0^{T/4} \tau_p dt = \int_0^{3.2 \text{ hrs.}} \tau_p dt \quad 2.2 (1)$$

where

τ_p = pitch angular rate

and

T = orbit period

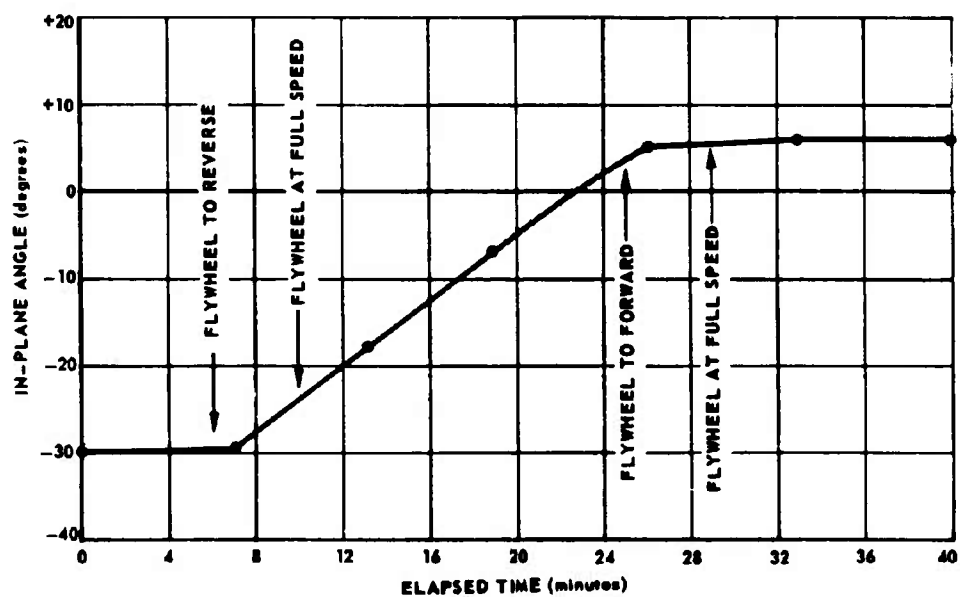


Fig. 2-30 MANUAL DAMPING BY FLYWHEEL REVERSAL

If the flywheel is reversed at or near the peak of the satellite libration, the time during which the gravity torque acts to increase the angular rate of the spacecraft is distinctly shortened. In Fig. 2-30 the flywheel reversal reduces the time during which the gravity torque acted from 3.2 hours to slightly less than 16 minutes. In this case the torsional impulse is given by

$$I_t = \int_0^{0.27 \text{ hrs.}} \tau_p dt$$

The net result is that the libration angle is immediately and dramatically reduced to a lower level. In the case of Fig. 2-30 the angle was reduced from 30 degrees to only 6 degrees in a matter of 19 minutes. This figure illustrates the first attempt using this damping procedure. Later attempts, starting from smaller angles, resulted in manual damping of the angle to a final angle of less than 2 degrees.

2.3 Prelaunch Computer Simulation of Time-Lag Magnetic Damping and Torsion Wire Gimbal Damping, Neglecting External Effects

2.3.1 Simulation Objectives

There are two distinct simulations of attitude dynamics, one developed for prelaunch hardware design, and one for post-launch system performance; they are referred to as the S2P Group (prelaunch) and DAS (post-launch) programs. The computer simulations of the satellite attitude dynamics developed by the S2P Group were used extensively during the early phases of the DODGE preliminary design. The purpose of these simulations was (a) to optimize system design parameters, (b) to provide an independent verification of the gimballed torsion wire damping system simulation completed earlier at the Ames Research Center, of NASA, and (c) to provide a basis for comparison of the theoretical and experimental post-launch attitude data.

Because these simulations were to be employed in the early preliminary design phases in which parametric studies would necessitate many computer runs, they were developed to consider a specific physical model, and did not include such effects as solar radiation pressure, thermal bending, etc. As a consequence, it is relatively easy to provide input data for the resulting simulations, and they do not require the long computer running time characteristic of the more general DAS program. The S2P programs are effective in analyzing transient response properties and in particular in comparing the relative performance of the various damping systems for a wide range of physical parameters. On the other hand, a complete simulation of the absolute performance of any system in the presence of various external perturbations would require the use of the DAS program.

The S2P simulation effort resulted in two different computer programs each of which was designed to analyze a distinct method of damping the DODGE satellite motions relative to the equilibrium earth-pointing orientation. The first simulation considers the energy dissipation as provided by the relative motion between the satellite and an asymmetrically connected auxiliary body as originally proposed by Tinling and Merrick in 1963 (Ref. 2-1). The second computer program simulates the no-moving-parts magnetic damping system which utilizes the interaction of the earth's magnetic field with a time dependent magnetic dipole generated on-board the satellite (Ref. 2-2).

2.3.2 Simulation of the Torsion Wire Gimbal Damping System

The use of a single degree of freedom, inertially coupled damper for damping the motions of a gravity stabilized spacecraft was first discussed by Tinling and Merrick in 1963 (Ref. 2-1). Although it is possible to improve the rapidity of damping by using several activated booms as in the "Vertistat" concept (Ref. 2-3), a single asymmetrically connected member has been shown by Tinling and Merrick to provide completely adequate

damping response while providing considerable advantages in the simplicity of the engineering design.

The primary satellite configuration consisting of the main satellite and a single movable damper boom is shown in Fig. 2-31. As noted in previous sections the damper boom is mounted on a delicate torsion wire which provides an essentially frictionless support as well as a restoring spring torque that causes the damper boom to seek a horizontal position when the satellite is at rest under gravity-gradient stabilization. When in equilibrium the damper boom is oriented at an offset angle, β , with the main body principal axis that is closest to the nominal flight path direction. The torsion wire damper assembly incorporates a vane of electrically conducting material which moves with the gimbaled damper through a gap in a chargeable permanent magnet. This horseshoe magnet can be magnetized anywhere between zero and full magnetization by discharging a condenser through an electric winding about the magnet (Ref. 2-4). The maximum eddy-current damping constant achieved with this device is approximately five times the optimum that has been theoretically determined. The minimum damping is zero since the magnet can be readily demagnetized in orbit (Ref. 2-4).

2.3.2.1 Development of Rotational Equations of Motion

The development of the rotational equations of motion for this system has been presented previously (Refs. 2-5, 2-6, and 2-7), with a complete unabridged version given in Ref. 2.5; only a brief outline of this development will be given here. The Lagrangian form of derivation was selected in order to provide an independent check with the results of Tinling and Merrick which are based on the simulation of an Eulerian (Newtonian) development. The assumptions made during this development are:

- a. The relative motion of the damper boom with respect to the main satellite is restricted to a single degree

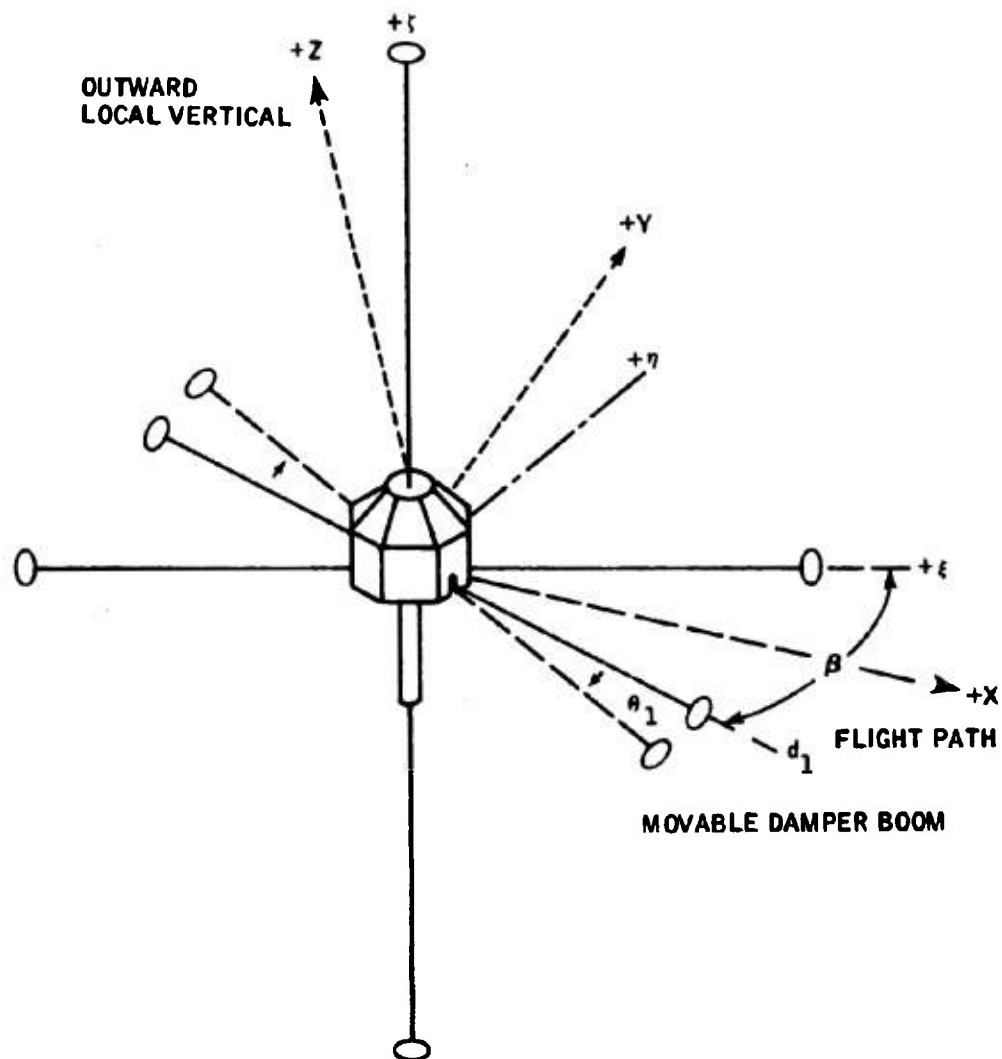


Fig. 2-31 PRIMARY CONFIGURATION WITH TORSION WIRE DAMPER.

of freedom; it is assumed the connection point is at, or very near, the center of mass of the system.

- b. The moment of inertia of the damper boom about its longitudinal axis is negligible when compared with the transverse moments of inertia.
- c. The rotational and orbital translational motions of the configuration are uncoupled.
- d. The center of mass of the system is assumed to move in a circular orbit about a spherical, homogeneous earth.
- e. The external torques caused by solar radiation pressure and thermal bending are not included here.

(The last three assumptions will also be made for the analysis of the time-lag magnetic system, thereby providing a valid basis for comparison between the performance of the two systems.)

The three axis systems employed to describe the orientation of the two bodies relative to each other and to the local vertical reference are:

- ξ, η, ζ - main body principal axes
having unit vectors $\bar{b}_1, \bar{b}_2, \bar{b}_3$
- d_1, d_2, d_3 - damper boom axes having unit vectors $\bar{d}_1, \bar{d}_2, \bar{d}_3$ where \bar{d}_1 is along the longitudinal damper axis, \bar{d}_2 is along the axes of relative rotation.

X, Y, Z - local vertical axes system
having unit vectors $\bar{o}_1, \bar{o}_2, \bar{o}_3$ where \bar{o}_1 points along the
local horizontal, \bar{o}_3 along
the outward local vertical.

When in equilibrium \bar{b}_3 is aligned with \bar{o}_3 , $\bar{b}_1 \cdot \bar{o}_1 = \bar{b}_2 \cdot \bar{o}_2 = \cos \Psi_0$ where Ψ_0 is a small equilibrium yaw angle attributed to the asymmetrical mounting of the damper boom.

An Euler angle sequence of: (a) pitch (ϕ), (b) roll (θ), and (c) yaw (Ψ)--taken in that order--describes the orientation of the main body perturbed relative to the local vertical system. The transformation from the local vertical system to the principal body axes system becomes, after combining the three rotational matrices:

$$\begin{bmatrix} \bar{b}_1 \\ \bar{b}_2 \\ \bar{b}_3 \end{bmatrix} = \begin{bmatrix} C\psi C\phi + S\psi S\phi S\theta & S\psi C\phi & -S\phi C\psi + S\psi S\phi C\theta \\ -S\psi C\phi + C\psi S\phi S\theta & C\psi C\phi & S\phi S\psi + C\psi S\phi C\theta \\ C\theta S\phi & -S\theta & C\theta C\phi \end{bmatrix} \begin{bmatrix} \bar{o}_1 \\ \bar{o}_2 \\ \bar{o}_3 \end{bmatrix} \quad 2.3 (1)$$

where positive angles correspond to rotations in the positive right-hand sense, S represents sine function and C represents cosine function. The velocity transformation between Euler angular rates and inertial angular velocities about the principal axes can be similarly written as:

$$\begin{aligned} \Omega_\xi &= \dot{\theta} C\psi + (\omega + \dot{\phi}) C\theta S\psi \\ \Omega_\eta &= -\dot{\theta} S\psi + (\omega + \dot{\phi}) C\theta C\psi \\ \Omega_\zeta &= \dot{\Psi} - (\omega + \dot{\phi}) S\theta \end{aligned} \quad 2.3 (2)$$

where ω is the orbital angular velocity. Finally, the damper rod axes can be related to the body axes by:

$$\begin{bmatrix} \bar{d}_1 \\ \bar{d}_2 \\ \bar{d}_3 \end{bmatrix} = \begin{bmatrix} C\theta_1 C\beta & -C\theta_1 S\beta & -S\theta_1 \\ S\beta & C\beta & 0 \\ S\theta_1 C\beta & -S\theta_1 S\beta & C\theta_1 \end{bmatrix} \begin{bmatrix} \bar{b}_1 \\ \bar{b}_2 \\ \bar{b}_3 \end{bmatrix} \quad 2.3 (3)$$

where β is the damper rod offset angle when in the ξ, η plane and θ_1 is the elevation angle of the damper from this plane.

The equations given below are for (a) the rotational kinetic energy for the main body and damper rod, (b) the potential energy for the main body, damper boom, and the torsion boom linear extension, (c) the Raleigh dissipation function, and (d) Lagrange's general equations of motion.

a. Rotational Kinetic Energy

The rotational kinetic energy for the main body can be written:

$$T_b = \frac{1}{2} \left[I_\xi \Omega_\xi^2 + I_\eta \Omega_\eta^2 + I_\zeta \Omega_\zeta^2 \right] \quad 2.3 (4)$$

and after substituting equation (2) into (4),

$$\begin{aligned} 2T_b = I_\xi & \left[\dot{\theta}^2 C^2 \gamma + 2\dot{\theta}(\omega + \dot{\phi}) C\theta S\gamma C\gamma + (\omega + \dot{\phi})^2 C^2 \theta S^2 \gamma \right] \\ & + I_\eta \left[\dot{\theta}^2 S^2 \gamma - 2\dot{\theta}(\omega + \dot{\phi}) C\theta S\gamma C\gamma + (\omega + \dot{\phi})^2 C^2 \theta C^2 \gamma \right] \\ & + I_\zeta \left[(\omega + \dot{\phi})^2 S^2 \theta - 2\dot{\gamma}(\omega + \dot{\phi}) S\theta + \dot{\gamma}^2 \right] \end{aligned} \quad 2.3 (5)$$

The rotational kinetic energy for the movable damper rod can be written:

$$T_d = \left[\frac{1}{2} \left(I_1 \Omega_{d1}^2 + I_2 \Omega_{d2}^2 + I_3 \Omega_{d3}^2 \right) \right] \quad 2.3 (6)$$

where I_1, I_2, I_3 are the moments of inertia about the damper rod principal axes, and

$$\bar{\Omega}_d = \Omega_{d_1} \bar{d}_1 + \Omega_{d_2} \bar{d}_2 + \Omega_{d_3} \bar{d}_3 \quad 2.3 (7)$$

is the absolute (inertial) angular velocity of the damper rod projected along the damper rod axes.

The angular velocity of the damper rod is expressed as the vector sum of the relative angular velocity of the damper rod with respect to the main body and the angular velocity of the main body relative to an inertial reference. Thus, in equation form:

$$\bar{\Omega}_d = \bar{\Omega}_{d/b} + \bar{\Omega}_b \quad 2.3 (8)$$

and expanding,

$$\bar{\Omega}_d = \dot{\theta}_1 \bar{d}_2 + \Omega_{\xi} \bar{b}_1 + \Omega_{\eta} \bar{b}_2 + \Omega_{\zeta} \bar{b}_3 \quad 2.3 (9)$$

In order to transform $\bar{\Omega}_b$ from the body frame to the damper frame, the inverse transformation of 2.3 (3) is used noting that $\beta = \gamma - \gamma_1$. The components of 2.3 (9) may be substituted into 2.3 (6), assuming that $I_0 = I_2 = I_3$ and $I_0 \gg I_1$ to yield,

$$\begin{aligned} 2T_d = I_0 & \left[\dot{\theta}^2 (S^2 \gamma_1 + C^2 \gamma_1 S^2 \theta_1) \right. \\ & + (\omega + \dot{\varphi})^2 (C^2 \theta C^2 \gamma_1 + C^2 \theta S^2 \gamma_1 S^2 \theta_1 - C \theta S \theta S \gamma_1 S^2 \theta_1 + S^2 \theta C^2 \theta_1) + \dot{\gamma}^2 C^2 \theta_1 \\ & + \dot{\theta}_1^2 + (\omega + \dot{\varphi}) (-2 \dot{\theta} C \theta C \gamma_1 S \gamma_1 + 2 \dot{\theta} C \theta C \gamma_1 S \gamma_1 S^2 \theta_1 + 2 \dot{\theta}_1 C \theta C \gamma_1 \\ & + \dot{\gamma} 2 S \theta_1 C \theta_1 C \theta S \gamma_1 - \dot{\theta} C \gamma_1 S \theta S^2 \theta_1 - 2 \dot{\gamma} S \theta C^2 \theta_1) \\ & \left. + \dot{\theta} (-2 \dot{\theta}_1 S \gamma_1 + 2 \dot{\gamma} S \theta_1 C \theta_1 C \gamma_1) \right] \quad 2.3 (10) \end{aligned}$$

b. Potential Energy

The gravitational potential energy for the main body will be derived using the method presented in Ref. 2-5. Let $dm = \rho_m dV = \rho_m dx dy dz$ be an element of mass at point (x, y, z) .

Then its gravitational potential energy is given by:

$$DV_b = \frac{-GM_E dm}{|\vec{r}|} \quad 2.3 (11)$$

where GM_E is the earth's gravitational constant, and $|\vec{r}|$ is the distance of dm from the center of the spherical earth. If x, y, z are the coordinates of dm in the local vertical system (XYZ) with origin at the system center of mass, and recalling that $GM_E = R^3 \omega^2$, where R is the magnitude of the geocentric radius vector, then 2.3 (11) may be written as:

$$dV_b = -R^2 \omega^2 \left[1 + \frac{2z}{R} + \frac{(x^2 + y^2 + z^2)}{R^2} \right]^{-1/2} \rho_m dx dy dz \quad 2.3 (12)$$

The term contained within the brackets may be expanded using the binomial expansion since $z \ll R$ and $(x^2 + y^2 + z^2) \ll R^2$. Performing this expansion and deleting all terms of order $1/R$ and higher yields:

$$dV_b = -\omega^2 \left[R^2 - Rz - \frac{(x^2 + y^2 + z^2)}{2} + \frac{3}{2} z^2 \right] \rho_m dV \quad 2.3 (13)$$

Equation 2.3 (13) must now be integrated over the total volume of the main satellite. It is assumed that the center of mass of the primary body and that of the damper boom are coincident. Thus, the origin of the local vertical coordinate system is also coincident with the individual centers of mass; without any loss of generality and, neglecting integration constants, it is seen that the first three terms of 2.3 (13) do not contribute to V_b .

The fourth term may be evaluated by transforming the z coordinate of dm from the local vertical system into the body system with the aid

of 2.3 (1). The integration of this term may be facilitated by noting that the origin of the (ξ, η, ζ) system is at the center of mass of the main body and that since ξ, η, ζ are principal axes the corresponding cross product of inertia terms vanish. The result of this integration yields the potential energy of the main body attributed to the earth's gravitational field as:

$$\begin{aligned} V_b = & \frac{3}{4}\omega^2 \left\{ I_\xi \left[(C^2\varphi S^2\theta - S^2\varphi)C2\gamma + S2\varphi S2\gamma S\theta + C^2\varphi C^2\theta \right] \right. \\ & + I_\eta \left[-(C^2\varphi S^2\theta - S^2\varphi)C2\gamma - S2\varphi S2\gamma S\theta + C^2\varphi C^2\theta \right] \\ & \left. + I_\zeta \left[-2C^2\varphi C^2\theta \right] \right\} \end{aligned} \quad 2.3 (14)$$

The development of the damper boom gravitational potential energy follows that given above until

$$dV_d \approx \frac{-3\omega^2}{2} \int z^2 dm \quad 2.3 (15)$$

In order to express z^2 in terms of coordinates in the damper rod reference system, the transformation from the local vertical system to the damper rod principal axes system will be used. The resulting expression for V_d is given in 2.3 (16) as:

$$V_d = -\frac{3}{2}\omega^2 I_o \left[C\theta_1 (-S\varphi C\gamma_1 + S\gamma_1 S\theta C\varphi) - S\theta_1 C\theta C\varphi \right]^2 \quad 2.3 (16)$$

If it is assumed that the torque due to the angular displacement (θ_1) of the damper boom is linearly related to this displacement, then the torque may be derivable from the potential given by:

$$V_{\theta_1} = \frac{1}{2} (K_m \omega^2 L^2) \theta_1^2 \quad 2.3 (17)$$

such that $\frac{\partial V}{\partial \theta_1} = (Kmw^2L^2)\theta_1$ is the generalized torque tending to change the angle, θ_1 . In this case K is the dimensionless torsion constant of the gimbals, and mL^2 has units of moment of inertia. It is this torque which maintains the equilibrium position of the damper rod in the horizontal plane under the presence of the gravitational torques. Without this restoring effect, the damper rod would tend to seek a local vertical equilibrium orientation.

c. Rayleigh Dissipation Function

The damping is assumed to be proportional to the relative angular motion, $\dot{\theta}_1$, between the satellite main body and the damper boom. The Rayleigh dissipation function may be used for non-conservative systems involving only equivalent linear viscous damping (Ref. 2-8).

The Rayleigh function is explicitly a function of the generalized velocities, \dot{q}_j , such that the resulting dissipative forces are derivable treating \mathcal{F} as a "potential type" term:

$$Q_j = - \frac{\partial \mathcal{F}}{\partial \dot{q}_j} \quad 2.3 (18)$$

For this application,

$$\mathcal{F} = \frac{1}{2} \omega k \dot{\theta}_1^2 \quad 2.3 (19)$$

yielding,

$$Q_{\theta_1} = -k\omega \dot{\theta}_1 \quad 2.3 (20)$$

as the dissipative damping force, where k is the dimensionless torsional (equivalent viscous) damping constant.

d. Lagrange's General Equations of Motion

Lagrange's general equations of motion as applicable to a nonconservative system with linear viscous damping may be written (Ref. 2-8):

$$\frac{d}{dt} \left(\frac{\partial T}{\partial \dot{q}_i} \right) - \frac{\partial (T - V)}{\partial q_i} = - \frac{\partial \mathcal{F}}{\partial \dot{q}_i}, \quad i = 1, \dots, N$$

2.3 (21)

where T and V represent the total (complete) rotational kinetic and potential energies of the system and $L = T - V$.

The generalized coordinates selected here are

- $q_1 = \varphi$ - pitch degree of freedom
- $q_2 = \theta$ - roll degree of freedom
- $q_3 = \psi$ - yaw degree of freedom
- $q_4 = \theta_1$ - damper boom rotational degree of freedom

Lagrange's general equations of motion may then be expanded and linearized to obtain the following set of coupled equations with constant coefficients:

$$\begin{aligned} & [I_\xi s^2 \gamma_o + I_\eta c^2 \gamma_o + I_o c^2 \gamma_{1o}] \ddot{\varphi} + 3\omega^2 [I_\xi c^2 \gamma_o + I_\eta s^2 \gamma_o - I_c - I_o c^2 \gamma_{1o}] \varphi \\ & + I_o c \gamma_{1o} (\ddot{\theta}_1 - 3\omega^2 \theta_1) = 0 \end{aligned}$$

2.3 (22)

$$\begin{aligned} & [I_\xi c^2 \gamma_o + I_\eta s^2 \gamma_o + I_o s^2 \gamma_{1o}] \ddot{\theta} + 4\omega^2 [I_\xi s^2 \gamma_o + I_\eta c^2 \gamma_o - I_c - I_o s^2 \gamma_{1o}] \theta \\ & - I_o s \gamma_{1o} (\ddot{\theta}_1 - 4\omega^2 \theta_1) + \omega [(I_\xi - I_\eta) c 2 \gamma_o + I_c + 2 I_o s^2 \gamma_{1o}] \dot{\varphi} = 0 \end{aligned}$$

2.3 (23)

$$\begin{aligned} & [I_\zeta + I_o] \ddot{\gamma} + \omega^2 [(I_\eta - I_\xi) C 2\gamma_o + I_o C 2\gamma_{1o}] \gamma' + 2I_o \omega S \gamma_{1o} \dot{\theta}_1 \\ & - \omega [(I_\xi - I_\eta) C 2\gamma_o + I_\zeta + 2I_o S^2 \gamma_{1o}] \dot{\theta} = 0 \end{aligned} \quad 2.3 (24)$$

$$\begin{aligned} & \ddot{\theta}_1 + (k\omega) \dot{\theta}_1 + [K - 3S^2 \gamma_{1o}] \omega^2 \theta_1 - S \gamma_{1o} (\ddot{\theta} - 4\omega^2 \theta) \\ & + C \gamma_{1o} (\ddot{\phi} - 3\omega^2 \phi) - 2\omega S \gamma_{1o} \dot{\gamma} = 0 \end{aligned} \quad 2.3 (25)$$

where the equilibrium yaw angle, γ_o , is related to the system parameters by (Ref. 2-5)

$$\tan 2\gamma_o = \frac{I_o S 2\beta}{I_\eta - I_\xi + I_o C 2\beta} \quad 2.3 (26)$$

$$\text{and } \gamma' = \gamma - \gamma_o ; \quad \gamma_{1o} = \gamma_o - \beta$$

Equations 2.3 (22) - 2.3 (25) are the variational or perturbation equations for the system since nonzero values of the ϕ , θ , γ' , and θ_1 coordinates represent departures from the equilibrium position or zero-solution. In the absence of the damper boom, $I_o = 0$, and equations 2.3 (22) - 2.3 (24) are immediately identified with the linearized rotational equations of motion for a rigid satellite, noting that the equilibrium yaw angle, γ_o , is obviously also zero.

2.3.2.2 Stability Analysis--Application of Lyapunov's Second Method

In addition to the classical linearization methods involving the characteristic equation of a system of constant coefficient equations, it is found that Lyapunov's direct or second method may often be used to facilitate stability analysis. The main difficulty in the application of Lyapunov techniques has been in finding a relatively simple

Lyapunov function which still has physical meaning. For a mechanical system, where the coordinate constraints are scleronomic, (free from explicit time dependence), this difficulty can be avoided by selecting the Hamiltonian as the Lyapunov function (Ref. 2-9). The Hamiltonian approach is particularly well adapted for use in connection with the Lagrangian formulation which was used in deriving the system rotational equations of motion.

Certain basic definitions of stability and the main theorems of Lyapunov are stated and, in some cases, proven in several contemporary references (2-9, 2-10, 2-11, 2-12, 2-13, and 2-14). For the purposes of this paper, it will suffice to paraphrase some of the more salient ideas. Stability in the Lyapunov sense implies that the state variables will always remain in a sufficiently small neighborhood of the equilibrium point when given an initial small perturbation. For an asymptotically stable system the state variables will always remain in a neighborhood of equilibrium and will eventually return to the equilibrium state. As contrasted with this, stability in the Lagrange sense may be interpreted to mean: that given a sufficiently small initial perturbation in the state variables from the equilibrium point, the norm of the difference between the state variable components and their equilibrium value will always have a finite (geometrical) bound. It is apparent that it is Lyapunov stability that is the more applicable for passive gravity-gradient attitude stabilization with the requirement of alignment to the local vertical to within a few degrees in roll, pitch, and yaw.

Theorems as developed in the references mentioned above state that if there exists a scalar function of the state variables that is positive definite in some subregion of the equilibrium point whose total time derivative is negative definite (semi-definite) in this same subregion, then the motion about the equilibrium point is asymptotically stable (Lyapunov stable).

Lagrange's general equations of motion, 2.3 (21), a system of N second order differential equations, may also be written in the form of Hamilton's canonical equations,

$$\left. \begin{aligned} \dot{p}_i &= -\frac{\partial H}{\partial q_i} + Q_i \\ \dot{q}_i &= \frac{\partial H}{\partial p_i} \end{aligned} \right\} \quad 2.3 (27)$$

where $H = H(p, q, t)$ as the Hamiltonian function and $Q_i = -\frac{\partial \mathcal{F}}{\partial q_i}$. Equation 2.3 (27) thus represents a system of $2N$ first order differential equations, where the Hamiltonian is related to the Lagrangian by,

$$H = \sum_{i=1}^N (p_i \dot{q}_i - L) \quad 2.3 (28)$$

with $L = T - V$ and $p_i = \frac{\partial L}{\partial \dot{q}_i}$ $i = 1 \rightarrow N$

The total time derivative of the Hamiltonian is given by:

$$\frac{dH}{dt} = \frac{\partial H}{\partial t} + \sum_{i=1}^N \left[\frac{\partial H}{\partial q_i} \dot{q}_i + \frac{\partial H}{\partial p_i} \dot{p}_i \right] \quad 2.3 (29)$$

Equation 2.3 (27) may be substituted into the above yield:

$$\frac{dH}{dt} = \bar{Q} = \sum_{i=1}^N Q_i \dot{q}_i \quad 2.3 (30)$$

if H is not explicitly time dependent, as in the case of scleronomic coordinate constraints.

In general, the kinetic energy may be expressed as (Refs. 2-9, 2-13)

$$T = T_0 + T_1 + T_2 \quad 2.3 \quad (31)$$

with T_2 a quadratic form in the generalized velocities, T_1 a linear form in these derivatives and T_0 independent of them. After substitution of $T = V$ for L and $T_0 + T_1 + T_2$ for T into equation 2.3 (28), the Hamiltonian becomes:

$$H = T_2 + V - T_0 \quad 2.3 \quad (32)$$

Both V and T_0 are independent of the generalized velocities, and when T_0 does not involve time explicitly, then the quantity $V - T_0$ may be grouped together as a scalar potential function of the coordinates (Refs. 2-9, 2-13),

$$P = V - T_0 \quad 2.3 \quad (33)$$

where P is called the dynamic potential.

For this application, the total time derivative of the Hamiltonian is expressed as:

$$\bar{Q} = Q_{\theta_1} \dot{\theta}_1 = -\omega I_0 k \dot{\theta}_1^2 \quad 2.3 \quad (34)$$

where k , the dimensionless damping constant, is always positive. For this completely damped mechanical system (Ref. 2-14) dH/dt is identically zero for all-time if and only if the variational coordinates are all zero simultaneously (i.e., the system is in equilibrium). Thus the motion "passes through" the instantaneous time points where $\dot{\theta}_1$ is zero, and H decreases over a finite interval of time surrounding this point.

The Hamiltonian is given by 2.3 (32) as $H = T_2 + P$ where the T_2 function is always positive definite in a neighborhood of the zero solution. Thus, the sufficient condition for stability is the positive definiteness of the dynamic potential.

$$P = V - T_0 = V_b + V_d + V_{\theta_1} - T \quad 2.3 (35)$$

If P is examined at near equilibrium conditions where ϕ, θ, θ_1 are small and where $\psi \rightarrow \psi_0$, and $\psi_1 \rightarrow \psi_{10}$, then $2P$ becomes a homogeneous, quadratic

form in the generalized coordinates and may be tested for positive definiteness using Sylvester's criterion (Ref. 2-16). Applying Sylvester's criterion it is seen that the principal non-trivial condition for stability is the positive-ness of the corresponding fourth order determinant whose elements are composed of the second order partial derivatives of $2P$ with respect to the generalized coordinates. After much algebra and rearranging of terms, the following inequality results (Refs. 2-5, 2-6):

$$\begin{aligned} \frac{k-3-s^2\psi_{10}}{I_0} &> \frac{4s^2\psi_{10}}{I_\xi s^2\psi_0 + I_\eta c^2\psi_0 - I_\zeta - I_0 s^2\psi_{10}} \\ &+ \frac{3c^2\psi_{10}}{I_\xi c^2\psi_0 + I_\eta s^2\psi_0 - I_0 c^2\psi_{10} - I_\zeta} \quad 2.3 (36) \end{aligned}$$

as the principal (nontrivial) sufficient condition for the positive definiteness of the dynamic potential and, thus, the Hamiltonian.

The asymptotic stability of the system is dependent upon the satisfaction of inequality 2.3 (36) and also upon the presence of damping, but not on the amount of damping (there is no restriction on the size of $\bar{Q} = \omega I_0 k \dot{\theta}_1^2$).

2.3.2.3 Numerical Results

The linear and nonlinear Lagrangian equations of rotational motion for the two-body satellite were programmed for numerical integration on the IBM 7094 digital computer using the Adams-Moulton method of numerical integration. As a starting point, some of the parameters suggested by Tingling and Merrick (Ref. 2-1) which yield the optimum torque-free response to initial displacements were used. Figs. 2-32 through 2-36 show the result of this numerical study for the torque-free system in a circular orbit. A typical machine running time for a ten orbit transient response was 0.02 hour using 200 integration steps per orbital period.

Fig. 2-32 illustrates the transient response to an initial 10 degree pitch displacement; similar type responses were observed with initial 10 degree displacements in roll and yaw respectively and the same physical constants. The yaw angle appearing in this figure is the variational coordinate, Ψ' . The asymptotic stability of the zero solution is clearly demonstrated since the amplitude of all coordinates is eventually damped and reduced to zero within ten orbits.

It was indicated that system stability is dependent on the presence of damping but not on the amount of damping. The results of a study to optimize the dimensionless damping constant, k , are shown in Fig. 2-33 by comparing the damping time constants (i.e., time to reach $1/e$ of the initial amplitude) for initial 10 degree displacements in pitch, roll, and yaw respectively. It is seen that the optimum value is between 1.0 and 1.1; a value of 1.06 was selected for further studies.

The effect of the ratio of I_o/I_ξ (or I_d/I_ξ) on the time constant is examined in Fig. 2-34. It is seen that the time constants can not be significantly reduced by increasing the damper rod transverse moments of inertia much beyond $I_o/I_\xi = 0.04$. This result has also been obtained independently by Tingling and Merrick (Ref. 2-1) who have numerically analyzed the roots of the system

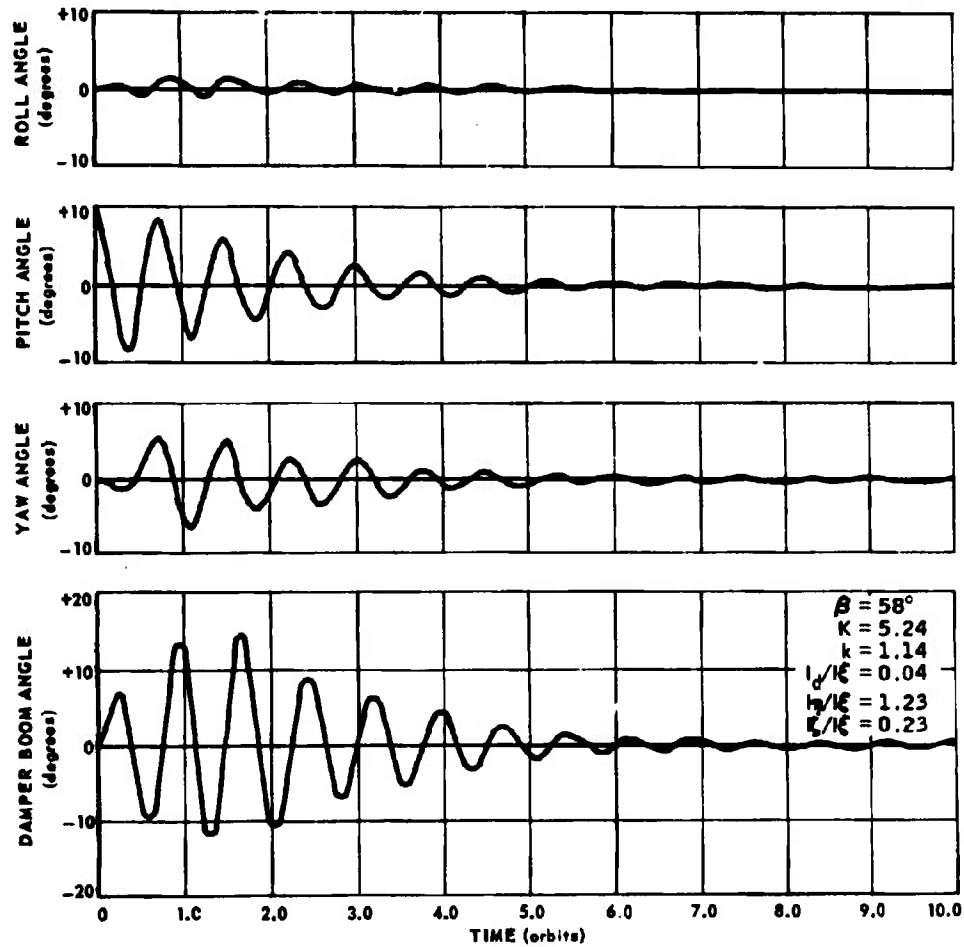


Fig. 2-32 TRANSIENT RESPONSE TO INITIAL 10° PITCH DISPLACEMENT

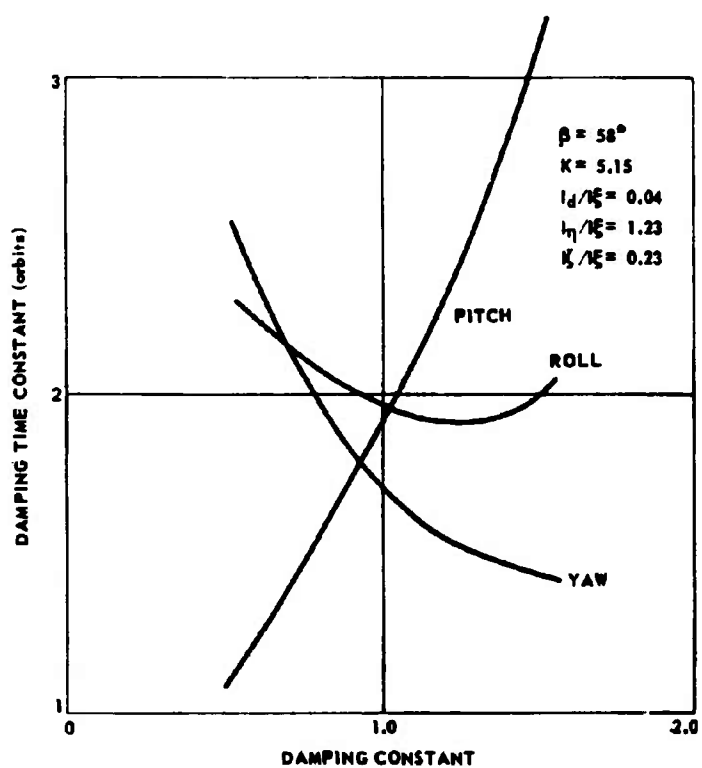


Fig. 2-33 STUDY TO OPTIMIZE DAMPING CONSTANT, k

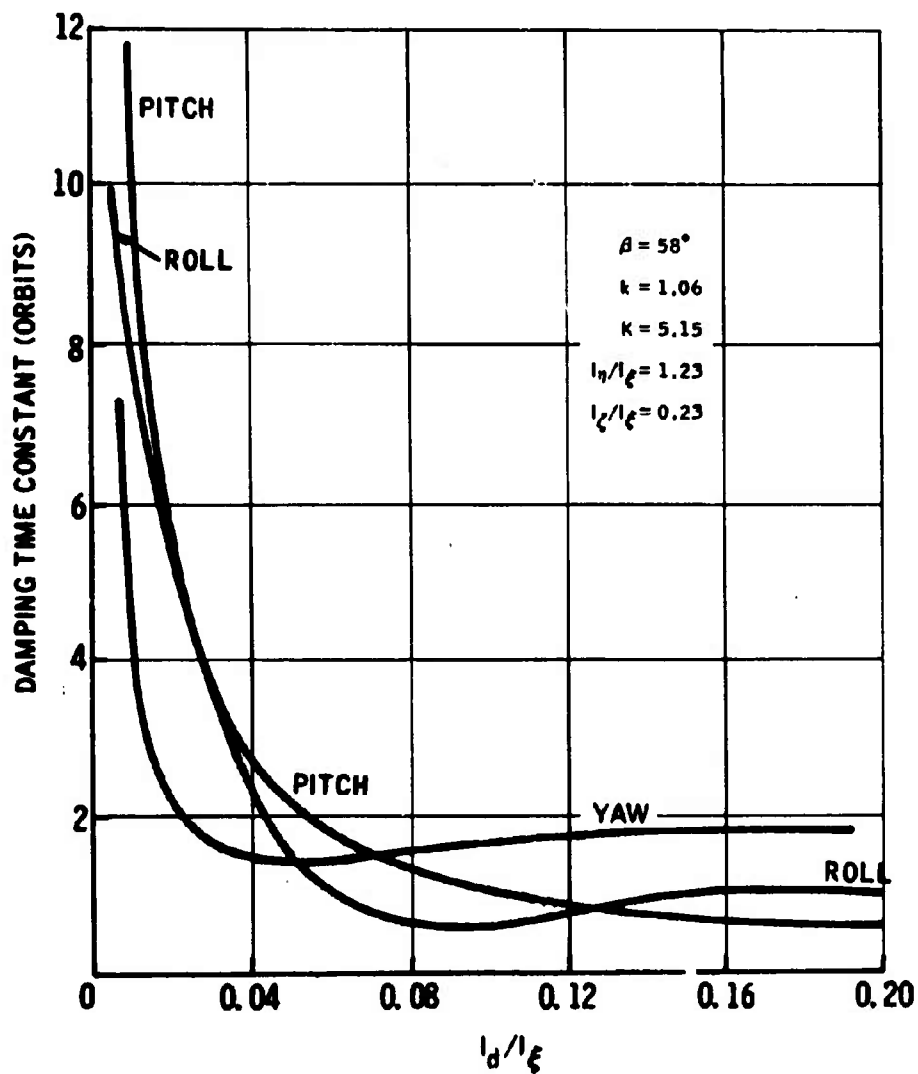


Fig. 2-34 EFFECT OF RATIO I_d/I_ξ ON DAMPING TIME

characteristic equation with an application of the method of steepest descent to determine the parameters that maximize the damping in the least damped normal mode of oscillation. Throughout these studies the "four percent" damper has been considered as optimum.

The next investigation considers the effect of varying the torsion wire constant, K , on the damping time constant (Fig. 2-35). For the damper offset angle indicated and for

$$\begin{aligned} I_{\xi} &= 0.22329 \times 10^{11} \text{ g-cm}^2 \\ I_{\eta} &= 0.29474 \times 10^{11} \text{ g-cm}^2 \\ I_{\zeta} &= 0.71453 \times 10^{10} \text{ g-cm}^2 \\ I_0 &= 0.89315 \times 10^9 \text{ g-cm}^2 \end{aligned}$$

corresponding to the optimum inertia ratio of $I_0/I_{\xi} = 0.04$, inequality 2.3 (36) yields $K > 3.83$ as the necessary stability criterion in the presence of damping. For $K < 3.83$, there is insufficient torsional restoring torque to offset the gravitational torques which tend to align the damper boom with the local vertical. In actual practice the damper boom would reach the end stops at a nominal value of ± 35 degrees from the satellite horizontal (ξ, η) plane where the stability criterion would no longer be valid. A large amplitude oscillation would result as momentum is continuously exchanged between the damper motion and the stops. An optimum value for K of 5.15 was selected as a result of this investigation. Using DODGE satellite parameters, this corresponds to a dimensional torsion wire constant of 85 dyne-cm/radian.

The final optimization study examines the effect of changing the damper boom offset angle. It is noted in Fig. 2-36 that pitch damping improves greatly as β approaches zero and roll damping is increased as β approaches 90 degrees, while the yaw damping at intermediate angles

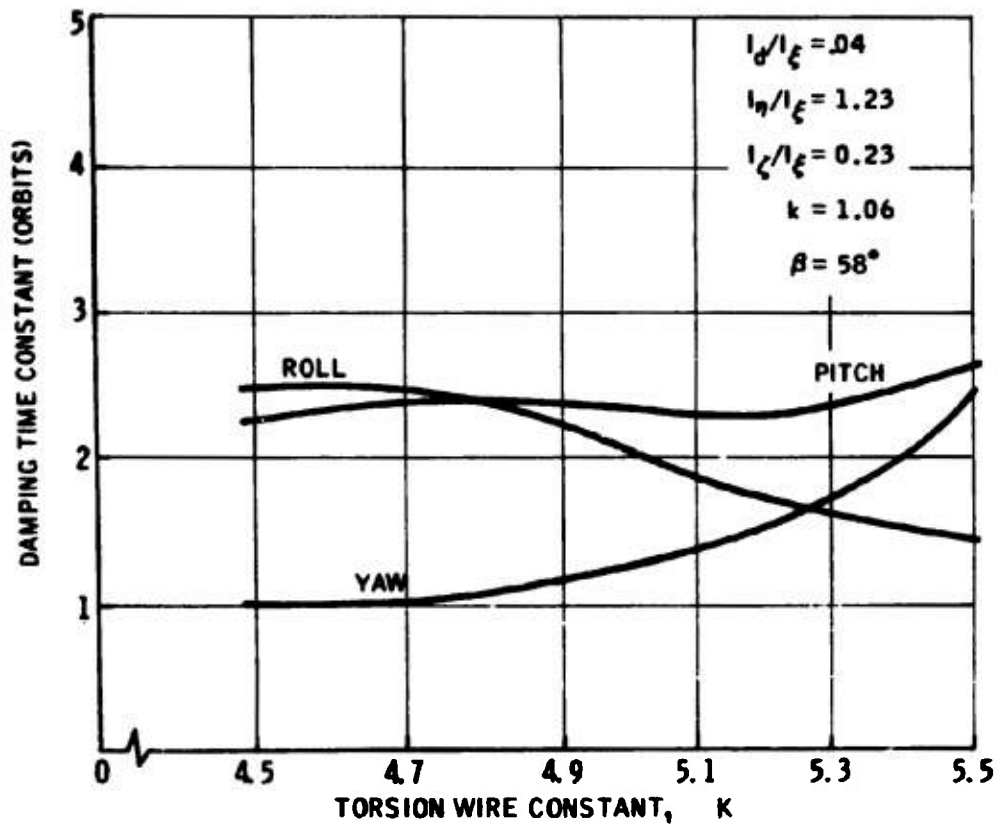


Fig. 2-35 EFFECT OF TORSION WIRE CONSTANT

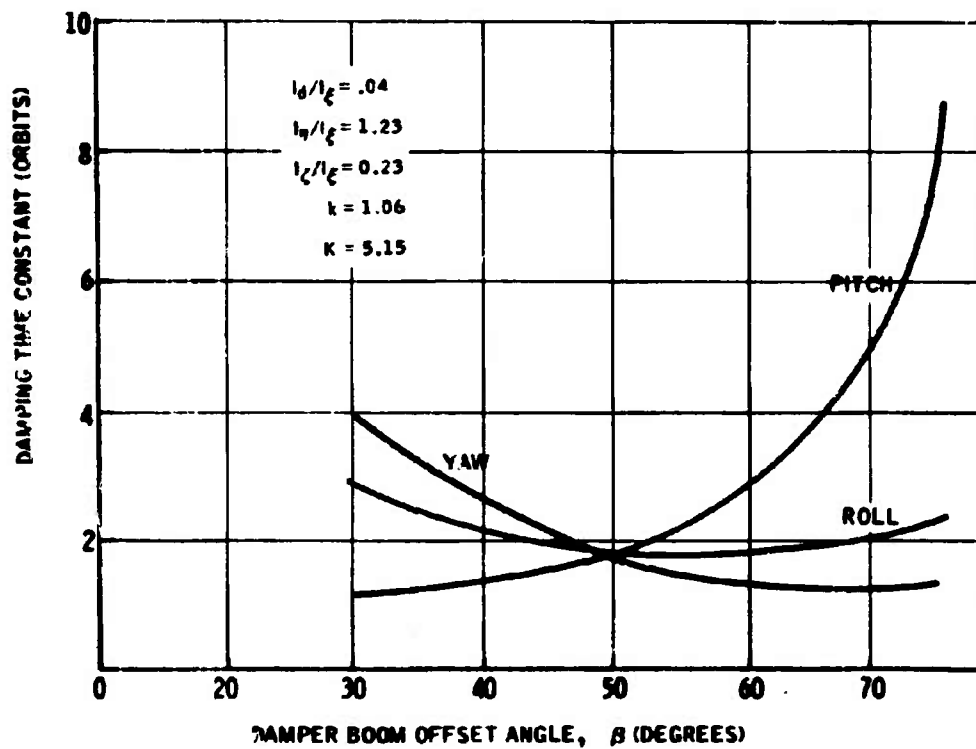


Fig. 2-36 EFFECT OF DAMPER BOOM OFFSET ANGLE

results largely from the inertial coupling. The figure verifies that $\beta = 58$ is an optimum value for the constants and inertia ratios listed.

2.3.3 Simulation of Time-Lag Magnetic Damping

Time lag, or "sample and hold," magnetic damping provides a method of using the earth's magnetic field for rapid libration damping when the ambient field strength is insufficient to dissipate energy with magnetic hysteresis material (Ref. 2-2). This system for magnetically damping gravity librations is illustrated in Fig. 3-37 where only one axis of a three-axis system is shown. As noted in previous sections the magnetometer output is fed into a memory device which stores for a preset period of time a particular reading of the magnetometer. This constant voltage signal is then fed into an amplifier which creates by means of an electromagnet a dipole moment which is proportional to the magnetic field measured by the magnetometer sensor. The dipole moment level is retained for a prescribed time interval, after which the memory again samples the magnetometer output and drives the amplifier to this new value for the next time interval.

By having a three-axis system operate in this manner the satellite produces a magnetic dipole moment which at the start of the interval is proportional to and along the direction of the local magnetic field. Since this magnetic moment is held for the time interval, a restoring torque relative to the stationary magnetic field is generated and tends to damp the satellite librations about the local vertical.

For a fixed spacecraft geometry and level of the dipole moment, the rate at which energy may be removed is a function of the length of time the dipole is held and of the relative phasing between the libration of the satellite with respect to its mechanical equilibrium attitude and its libration with respect to a necessarily time dependent magnetic equilibrium attitude. A mathematical model has been developed relating each of these variables for the case of a spacecraft in a near-synchronous

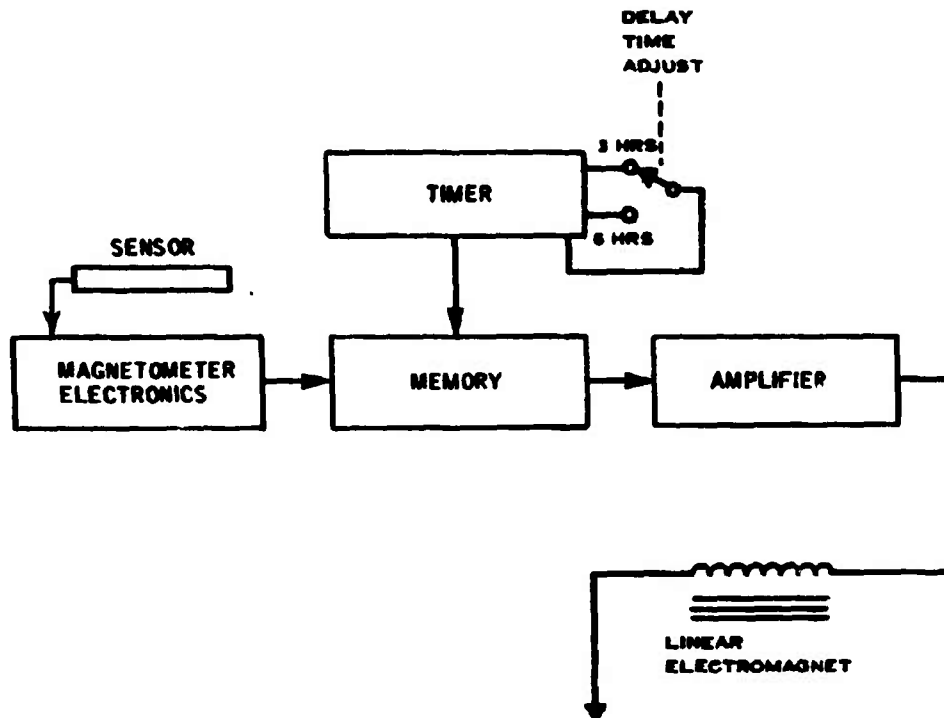


Fig. 2-37 TIME LAG MAGNETIC DAMPING SYSTEM (SINGLE-AXIS)

equatorial orbit (Ref. 2-17). Comparisons are made between the damping time constants predicted analytically and those obtained from numerical integration of the differential equations of motion. A brief summary of this treatment will be presented in this section.

2.3.3.1 Equations of Motion

The differential equations of attitude motion for a gravity stabilized satellite may be derived with an application of Newton's second law and are written in matrix form:

$$\frac{d}{dt} [\mathbb{I}\dot{\Omega}] = L \quad 2.3 (37)$$

where \mathbb{I} is the matrix of the inertia tensor, $\dot{\Omega}$ is the matrix form of the inertial angular velocity vector. For this problem, L consists of terms due to the gravity gradient:

$$L_g = 3\omega^2 \tilde{\alpha}_3 \mathbb{I} o_3 \quad 2.3 (38)$$

and a term attributed to the magnetic effects,

$$L_m = \tilde{P}B \quad 2.3 (39)$$

where P is the magnetic dipole moment, and B the earth's magnetic field intensity. (Note that \tilde{A} is an asymmetric matrix associated with the vector \tilde{A} such that

$$(\tilde{A})_{ik} = \epsilon_{ijk} A_j$$

After carrying out the differentiation indicated in 2.3 (37), Euler's equations of rotational motion may be written as:

$$\mathbb{I}\dot{\dot{\Omega}} + \tilde{\Omega}\mathbb{I}\dot{\Omega} = 3\omega^2 \tilde{\alpha}_3 \mathbb{I} o_3 + \tilde{P}B \quad 2.3 (40)$$

The first three terms in equation 2.3 (40) may be expressed in terms of the three Euler angles, ϕ , θ , ψ which relate the coordinates in the satellite

principal axes system to those in the local vertical system according to the transformation given by equation 2.3 (1). Our attention here will be concentrated on the development of the magnetic torque expression,

$$\mathbf{L}_m = \tilde{\mathbf{P}}\mathbf{B} = \begin{bmatrix} -P_3B_2 + P_2B_3 \\ P_3B_1 - P_1B_3 \\ -P_2B_1 + P_1B_2 \end{bmatrix} \quad 2.3 (41)$$

as expressed in the principal axes system of the rigid satellite.

For this analysis, only the dipole moment contribution of the earth's magnetic field will be considered. It can be shown that with suitable small angle assumptions, the magnetic field intensity may be expressed as (Refs. 2-17, 2-18):

$$\bar{\mathbf{B}} = \frac{p}{r^3} \left\{ \begin{bmatrix} 1 & \gamma & -\phi \\ -\gamma & 1 & 0 \\ \phi & -\theta & 1 \end{bmatrix} \begin{bmatrix} (3\phi - \gamma_m) \sin(\omega_E - \omega)t \\ 2\phi(\phi - \gamma_m) - 1 \\ (3\phi - \gamma_m) \cos(\omega_E - \omega)t \end{bmatrix} \right\} \quad 2.3 (42)$$

where ω_E is the earth's rotational rate about its polar axis, ϕ is the satellite's magnetic latitude angle, γ_m is the colatitude of the earth's dipole axis, r is the radial distance from the geocenter and p is the dipole moment of the earth. For the case of a synchronous orbit, $\omega_E = \omega$, and $\bar{\mathbf{B}}$ can be written:

$$\bar{\mathbf{B}} = \begin{bmatrix} B_E + \gamma B_N - \phi B_V \\ -\gamma B_E + B_N + \theta B_V \\ \phi B_E - \theta B_N + B_V \end{bmatrix} \quad 2.3 (43)$$

where B_E , B_N , and B_V are the east, north, and vertical components of the earth's magnetic field

respectively. For a near-synchronous orbit and for time intervals that are small compared with the period of motion of the local vertical relative to the magnetic field, and product $(\omega_E - \omega)t \ll 1$. Under these conditions 2.3 (43) is an adequate representation of the earth's magnetic field for the case of near-synchronous orbits.

The differential equations of motion for small amplitude motion about the equilibrium point may be obtained under the same assumptions, (c), (d), (e), of Section 2.3.2.1; if, in addition, planar mass distribution ($I_2 = I_1 + I_3$) is assumed, which is typical of the DODGE satellite (Ref. 2-2) configuration, the following equations result:

$$\begin{aligned} I_1 \ddot{\theta} &= 4\omega^2 \theta (I_2 - I_3) + (P_2 B_3 - P_3 B_2) \\ I_2 \ddot{\phi} &= 3\omega^2 \phi (I_1 - I_3) + (P_3 B_1 - P_1 B_3) \\ I_3 \ddot{\gamma} &= \omega^2 \gamma (I_2 - I_1) + (P_1 B_2 - P_2 B_1) \end{aligned} \quad 2.3 (44)$$

To evaluate the magnetic torque terms in 2.3 (44), recall that according to the time lag (sample and hold) concept the dipole moment components may be expressed as:

$$\begin{aligned} P_i(t) &= 0, & t < t_0 \\ &= KB_i(t_0), & t_0 < t < t_0 + \tau \end{aligned} \quad 2.3 (45)$$

where τ is the length of the magnetic dipole holding period and K is a proportionality constant. With the additional assumption of an equatorial orbit it is seen that the northward component of the magnetic field is much larger than the other two components and, to the first order,

$$L_{m1} = -KB_N^2 [\theta(t) - \theta(t_0)] ; \quad t_0 < t < t_0 + \tau \quad 2.3 (46)$$

The second component contains no first order terms, i.e., there is no first order magnetic damping about the pitch axis. Similarly, the torque about the yaw axis can be obtained:

$$L_{m3} = -KB_N^2 [\psi(t) - \psi(t_0)] ; \quad t_0 < t < t_0 + \tau \quad 2.3 (47)$$

For small amplitude motions and the assumed planar mass distribution there is no coupling between the individual modes corresponding to roll and yaw motions and they may be treated commonly:

$$\ddot{q}_1 + \Omega_1 q_1 = -\frac{KB_N^2}{I_1} q_1(t_0); \quad t_0 < t < t_0 + \tau, \quad 2.3 (48)$$

2.3.3.2 Analysis of the Damping

Two questions of immediate concern relative to 2.3 (44) and 2.3 (48) are:

- What length holding period, τ , will provide the maximum rate of energy dissipation?
- Of what damping rates is this system capable?

Consider the magnetic potential energy associated with each mode, e.g., the θ mode:

$$P_m = -\int_{\theta_0}^{\theta} -KB_N^2 [\theta(t) - \theta(t_0)] d\theta \quad 2.3 (49)$$

For convenience let t_0 be zero, then:

$$P_m = -\frac{KB_N^2}{2} [\theta(t) - \theta_0]^2 - \frac{\Omega_m^2}{2} I_1 [\theta(t) - \theta_0]^2 \quad 2.3 (50)$$

Equation 2.3 (48) may be solved using Laplace transform techniques to yield:

$$q(t) = q_0 \cos \Omega t + \frac{\dot{q}_0}{\Omega} \sin \Omega t - q_0 \frac{\Omega_m^2}{\Omega^2} [\cos \Omega t - 1];$$

$$0 \leq t \leq \tau$$

2.3 (51)

where the combined modal natural frequency, Ω , is given by:

$$\Omega = (\Omega_m^2 + \Omega_g^2)^{1/2}$$

2.3 (52)

and the initial conditions are denoted by the zero subscript. Then, for the θ (roll) mode:

$$\Omega_\theta = \left[\frac{K \theta_N^2 + 4\omega^2 (I_2 - I_3)}{I_1} \right]^{1/2}$$

2.3 (53)

Upon substitution of 2.3 (51) for $\theta(t)$ into 2.3 (50), the magnetic potential energy associated with the roll motion becomes:

$$P_m = \frac{\Omega_m^2}{2} I_1 \left[\sqrt{\left(\frac{\dot{\theta}_0}{\Omega_\theta} \right)^2 + \left(1 - \frac{\Omega_m^2}{\Omega_\theta^2} \right)^2} \theta_0^2 \sin(\Omega_\theta t + \alpha) - \theta_0 \left(1 - \frac{\Omega_m^2}{\Omega_\theta^2} \right) \right]^2$$

2.3 (54)

The total energy of this mode relative to its equilibrium position can be written (Ref. 2-8):

$$E = \frac{I_1}{2} [\theta_0^2 \Omega_\theta^2 + (\dot{\theta}_0)^2]$$

2.3 (55)

An order of magnitude calculation based on typical DODGE satellite parameters reveals that:

$$\frac{\Omega_m^2}{\Omega_1^2} \ll \ll 1$$

for both the roll and yaw motions. Thus, 2.3 (54) may be approximated by:

$$P_m \approx \frac{\Omega_m^2}{\Omega_\theta^2} E \left[\sin(\Omega_\theta t + \alpha) - \sin \alpha \right]^2 \quad 2.3 (56)$$

where α is a phase angle dependent on the initial conditions and expressed as:

$$\alpha \approx \arcsin \left\{ \frac{\dot{\theta}_0}{\left[\left(\frac{\dot{\theta}_0}{\Omega_\theta} \right)^2 + \theta_0^2 \right]^{1/2}} \right\} \quad 2.3 (57)$$

P_m , as given by 2.3 (56) is then the amount of libration energy that is removed from the mode when the satellite dipole is turned off at some time, t . The energy removed is proportional to the energy present in the mode at that time; i.e., the energy (and hence, the coordinate) is exponentially damped.

The answer to both questions posed above, can be found by consideration of equation 2.3 (56). The optimum holding time for each mode is that time for which P is a maximum. Since the energy decay is exponential, damping time constants may be readily calculated.

From 2.3 (56), the energy present in the θ mode after N cycles, each of length τ , can be written:

$$E_N = E_0 \prod_{i=1}^N \left\{ 1 - \frac{\Omega_m^2}{\Omega_\theta^2} \left[\sin(i\Omega_\theta \tau + \alpha) - \sin[(i-1)\Omega_\theta \tau + \alpha] \right]^2 \right\} \quad 2.3 (58)$$

where E_0 is the initial value of the energy. This expression may be easily evaluated only for certain values of α and τ .

For example:

α	τ	E_N
0	$\frac{T_0}{4}$	$E_0 \left[1 - \frac{\Omega_m^2}{\Omega_0^2} \right]^N$
$\frac{\pi}{2}$	$\frac{T_0}{2}$	$E_0 \left[1 - 4 \frac{\Omega_m^2}{\Omega_0^2} \right]^N$
0	$\frac{T_0}{2}$	E_0
$\frac{\pi}{4}$	$\frac{T_0}{4}$	$E_0 \left[1 - 2 \frac{\Omega_m^2}{\Omega_0^2} \right]^N$

In practice the holding time, τ , may not be a simple fraction of the natural period of the mode, T_0 . Also, the parameter α is dependent upon the initial conditions of the mode at the onset of magnetic damping. One might choose then to select a value of τ which provides reasonable damping rates of both the roll and yaw modes, regardless of the value of α for each mode.

For the case of a satellite with non-planar mass distribution, the coefficient $(I_1 - I_2 + I_3)$ does not vanish and the roll and yaw motions remain coupled. Each of the natural frequencies corresponding to these two normal modes of oscillation are complex functions of the two combined natural frequencies Ω_0 and Ω_y given by 2.3 (52) and 2.3 (53). To extend the present analysis to this case, the energy expression, 2.3 (58), should then be related to each of the three normal modes and the damping of each of these modes considered.

2.3.3.3 Numerical Analysis

Computer studies for this analysis were accomplished in two phases: (a) numerical integration of the complete nonlinear equations of attitude motion, 2.3 (40), and (b) parametric studies using the small angle energy solutions to 2.3 (40), equation 2.3 (58). The satellite configuration considered was the rigid DODGE primary configuration (Fig. 2-31, without the movable torsion wire damper). The use of the energy solution allowed economical mapping of the damping time constant surface in a three dimensional Euclidean space whose coordinates are α , τ , and $T_{1/e}$. ($T_{1/e}$ is the energy damping time constant; in order to convert to the damping time constant associated with the amplitude of the coordinates, this value should be multiplied by two.) Figs. 2-38 and 2-39 show these surfaces for the yaw mode and the roll mode respectively. As is evident from the topography, there is no unique value of τ which provides optimum damping. Instead, a value of τ must be chosen which provides good, if not optimum, damping for all values of α and for both the roll and yaw modes.

To demonstrate the validity of the energy solution, numerical integrations were performed for $\alpha = 0$ and for holding times (τ) varying from one hour to ten hours in roll, and from one hour to sixteen hours in yaw. The same parameters were used with the energy solution and the two sets of results compared (Figs. 2-40 and 2-41). All further numerical evaluations were then made with the energy solution as this method requires about 1/100 of the machine time necessary for numerical integration of the nonlinear equations. The physical parameters used in these studies were:

$$\begin{aligned}I_1 &= 6.7421 \times 10^{10} \text{ g-cm}^2 \\I_2 &= 8.192 \times 10^{10} \text{ g-cm}^2 \\I_3 &= 1.4572 \times 10^{10} \text{ g-cm}^2\end{aligned}$$

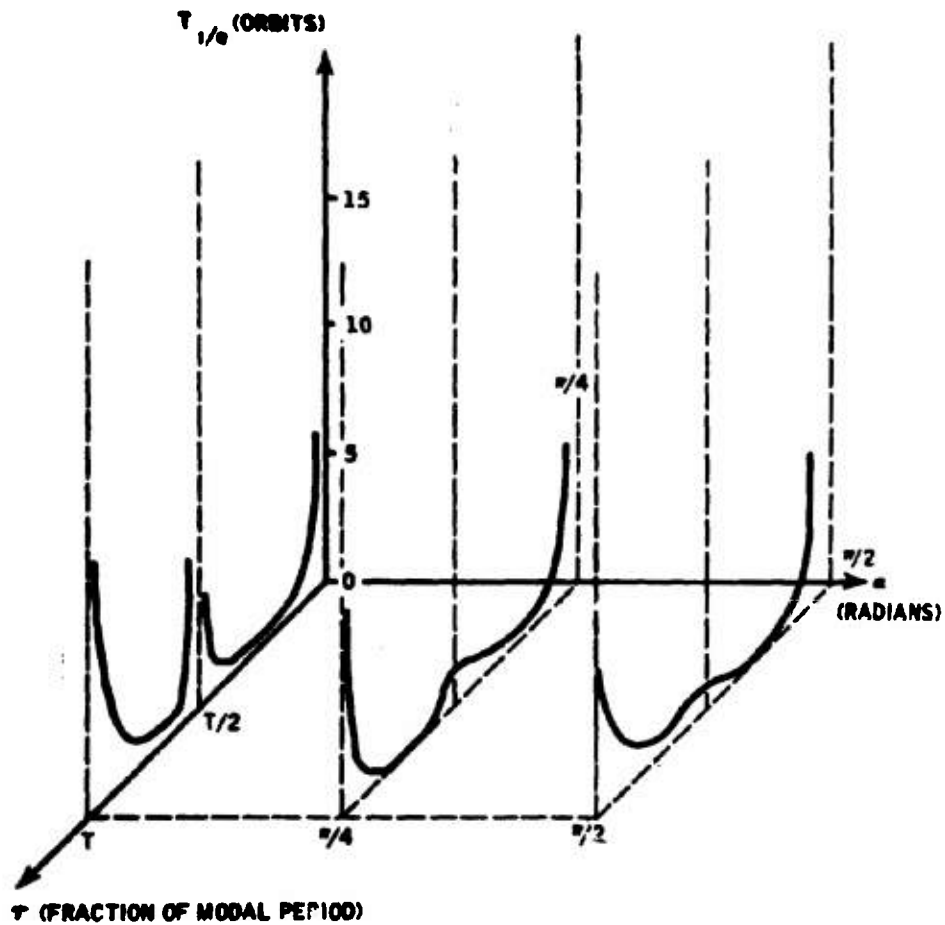


Fig. 2-38 ENERGY DAMPING TIME CONSTANT AS A FUNCTION OF HOLDING TIME AND INITIAL PHASING (INITIAL YAW PERTURBATION)

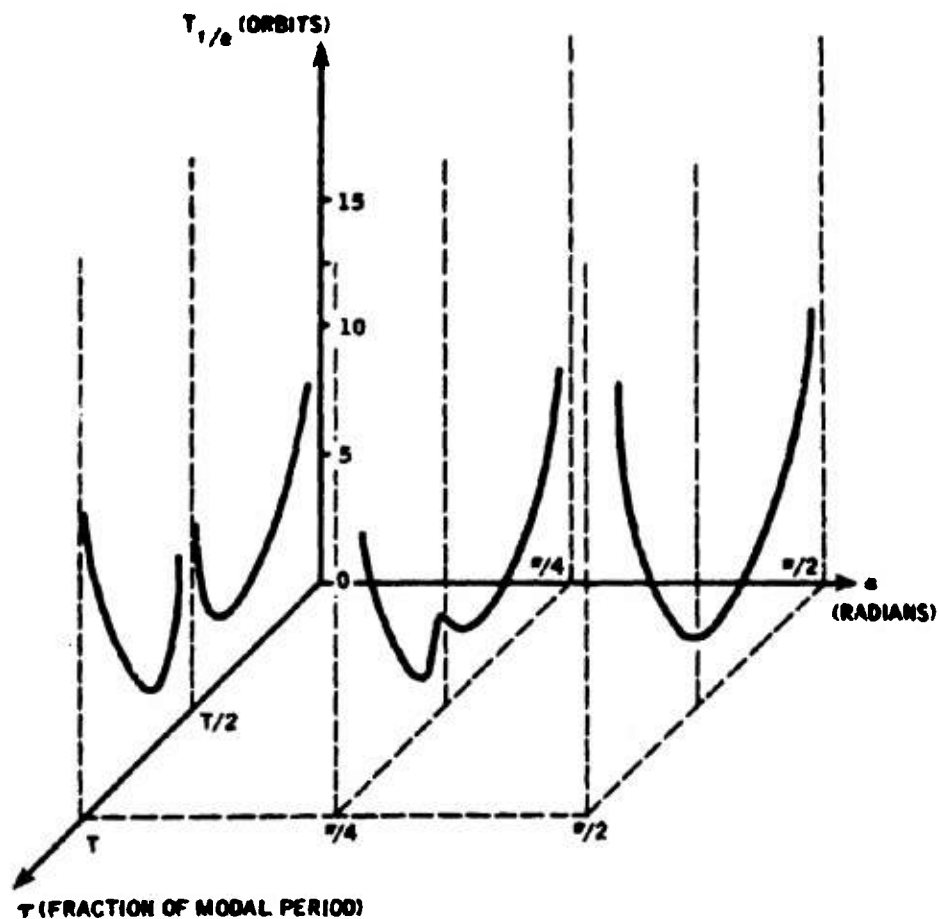


Fig. 2-39 ENERGY DAMPING TIME CONSTANT AS A FUNCTION OF HOLDING TIME AND INITIAL PHASING (INITIAL ROLL PERTURBATION)

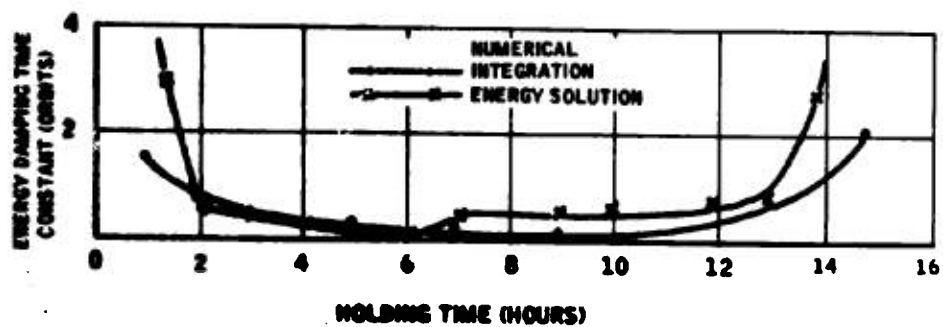


Fig. 2-40 ENERGY DAMPING TIME CONSTANT AS A FUNCTION OF HOLDING TIME (YAW PERTURBATION OF MAXIMUM AMPLITUDE, $\alpha = \pi/2$)

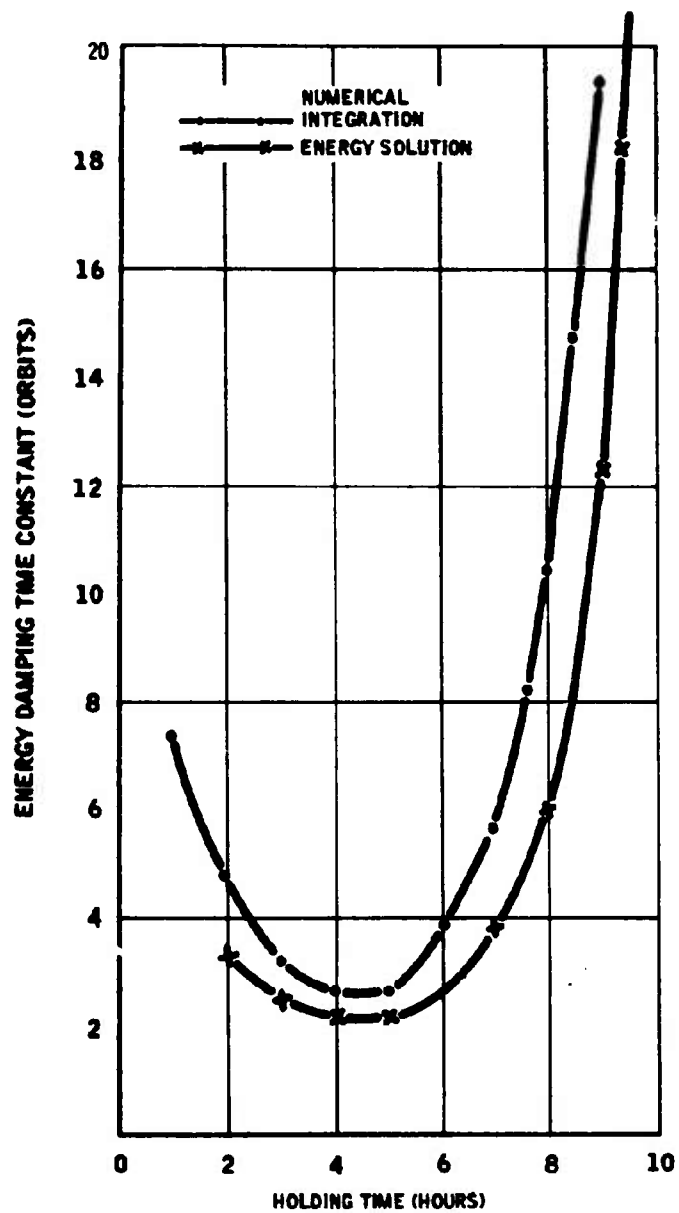


Fig. 2-41 ENERGY DAMPING TIME CONSTANT AS A FUNCTION OF HOLDING TIME (ROLL PERTURBATION OF MAXIMUM AMPLITUDE, $\alpha = \pi/2$)

Orbital period 22.26 hours
Orbital eccentricity 0.0
Orbital inclination 0.0
Time-lag gain 4.69×10^7
pole-cm/oersted
Limit on dipole strength generated:

$$|P_1|_{\max} = |P_2|_{\max} = 7.5 \times 10^4 \text{ pole-cm}$$

$$|P_3|_{\max} = 9.0 \times 10^4 \text{ pole-cm}$$

and the combined modal frequencies,
2.3 (52), calculated as:

$$\Omega_\theta = 1.629 \times 10^{-5} \text{ rad./sec}$$

$$\Omega_\psi = 1.008 \times 10^{-5} \text{ rad./sec}$$

with the periods:

$$T_\theta = 10.72 \text{ hrs.}; \quad T_\psi = 17.35 \text{ hrs.}$$

A superposition of the sections of the damping surface for the roll mode (Fig. 2-39) for $\alpha = 0$, $\alpha = \pi/4$, and $\alpha = \pi/2$ is shown in Fig. 2-42. From this diagram the obvious choices for τ for the roll mode would appear to be about six hours or four hours. The damping for a three hour holding period is only slightly less than that for $\tau = 4$ hours. The surface for the yaw mode while having valleys at about $\tau = 4$ hours and $\tau = 11$ hours are relatively flat in the region of the minima. This very effective yaw damping (Fig. 2-38) can be explained by considering the larger value of $(\Omega_m^2/\Omega_\psi^2)$ occurring in equation 2.3 (56), reflecting the smaller yaw axis moment of inertia; thus a greater fraction of the libration energy is removed per damping cycle from the yaw mode than from the roll mode. Values of τ which provide good damping for roll (three or six hours), should also provide near optimum damping for yaw libration.

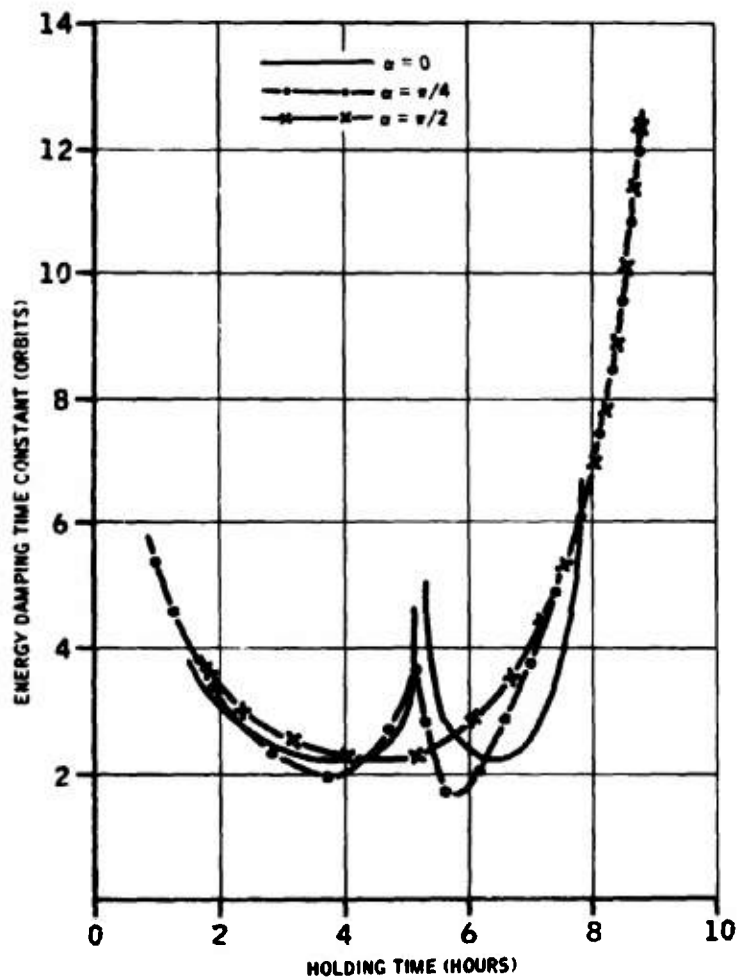


Fig. 2-42 STUDY TO OPTIMIZE HOLDING TIME
FOR INITIAL ROLL PERTURBATIONS

For values of τ which are large some forced attitude motion results at the frequency of the motion of the local vertical with respect to the magnetic field. For example, Fig. 2-43 illustrates the time response to an initial yaw perturbation of 10 degrees with a holding time of 15 hours. This corresponds nearly to the case of a satellite with constant dipole moment subjected to a forced motion with frequency, $\omega = \omega_E$.

2.3.4 Conclusions

The torsion wire gimballed damper is an effective means of damping three axis small amplitude librations of a satellite in synchronous or near-synchronous altitude orbit at any orbital inclination. By optimizing the DODGE satellite system design parameters, damping time constants of under three orbits are certainly realizable. An application of Lyapunov's second method yields a constraining relationship of the main body and movable damper, and damper boom offset angle. In the presence of damping, and for a given set of inertia parameters and offset angle, this places a restriction on the minimum size of the torsion wire constant, below which there would be insufficient (torsional) restoring torque to counteract the gravitational torques tending to align the damper boom with the local vertical.

The time-lag magnetic damping scheme, with the inherent engineering simplicity of having no moving parts, is an efficient method of dissipating roll and yaw librational energy in near-synchronous equatorial orbits. With the physical parameters chosen for the DODGE satellite, the optimum damping time constants are of the same order of magnitude (but slightly longer) as those obtained with the Tinling-Merrick torsion wire damper. There is no appreciable forced motion in near-synchronous orbits, provided that the holding period, τ , is near an optimum value. The pitch motion of the spacecraft remains undamped to the first order, but higher order damping (time constants in weeks) does occur through coupling with the roll and yaw modes.

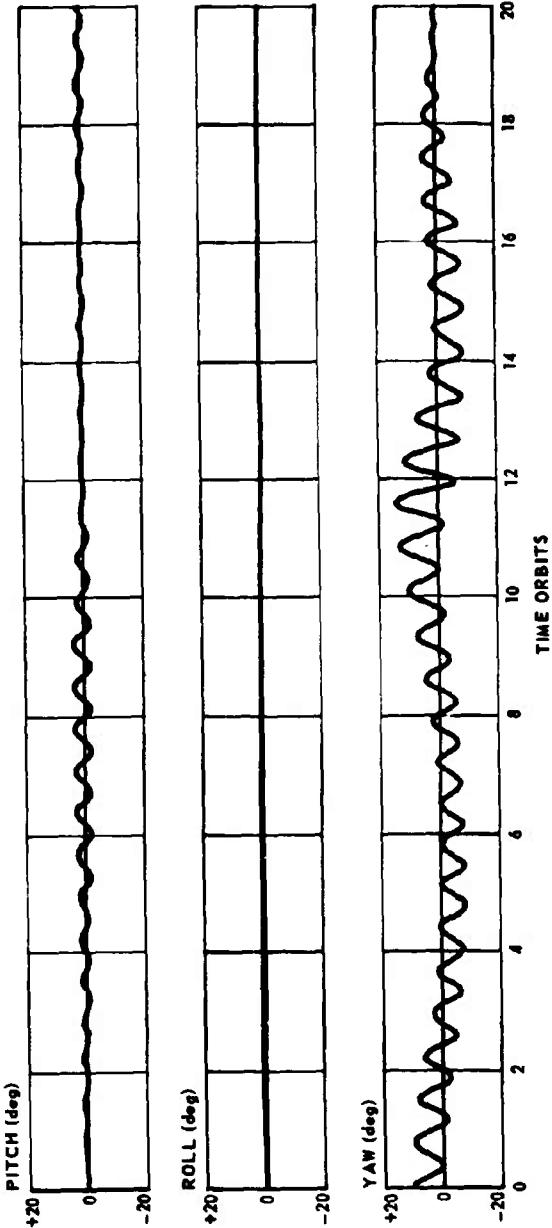


Fig. 2-43 TRANSIENT RESPONSE TO AN INITIAL 10° YAW ANGLE WITH 15 HOUR TIME LAG HOLDING PERIOD

2.4 Comparison of Theoretical and Experimental Data for Time-Lag Damping Systems in the Presence of an Apparent Time Dependent Magnetic Field

It was stated in Section 2.3 that one of the main objectives of the computer simulations of satellite attitude dynamics was to provide a basis for comparison of the theoretical and experimental post-launch attitude data. Because of the apparent failure of the gimbaled torsion wire damper to remove a significant amount of librational energy and the relative scarcity of data points when this system alone was operational, it has not been possible to draw a meaningful correlation between theoretical and orbital results with this experiment. No theoretical explanation of the observed anomalous behavior of the gimbaled damping system can be inferred to date, however, speculation as to possible causes of mechanical failure are presented in Section 2.2.4.8.

Successful correlation between theoretical and orbital experimental results has been completed using the S2P time-lag magnetic damping digital computer program. A comparison has been made between the theoretical motion in a time varying magnetic field and the motion of the DODGE satellite during the early passes of the spacecraft over the Western Hemisphere during the last quarter of 1967.

Fig. 2-44 shows the correlation between the average predicted attitude energy relative to the local vertical with actual energy values based on observed attitude data during the eighth pass of the DODGE satellite over APL. The predicted energy values are results from the S2P time delay magnetic damping digital computer program using a time-varying earth's magnetic field with a three-hour, low gain sample and hold damping mode. Initial conditions were taken from attitude data near the end of the seventh APL pass. It should be mentioned that the predicted attitude energy varies sinusoidally about some mean or average value, shown here by the solid curve.

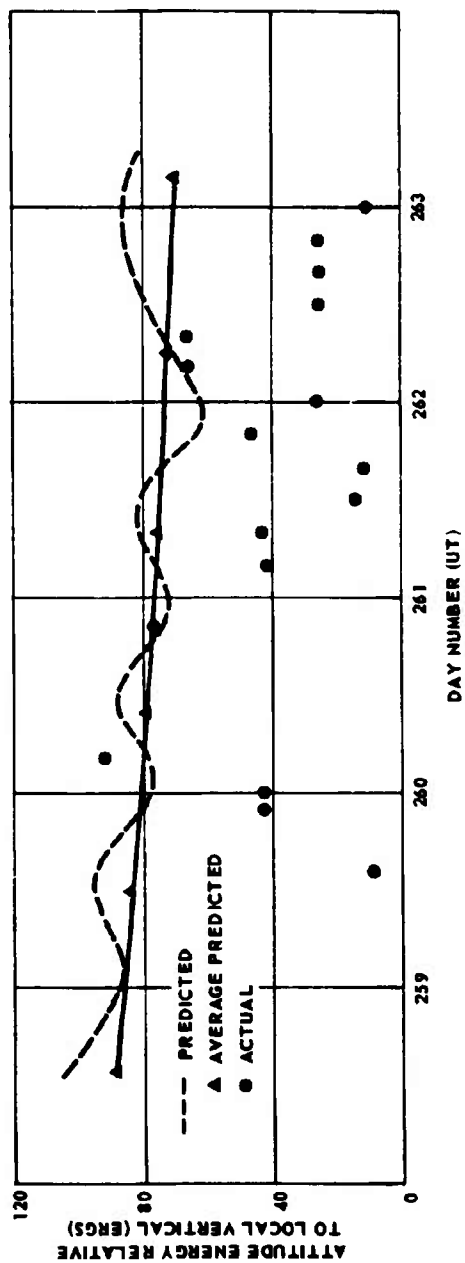


Fig. 2-44 DODGE ATTITUDE ANALYSIS-EIGHTH PASS-CORRELATION OF
AVERAGE PREDICTED ATTITUDE ENERGY WITH ACTUAL ATTITUDE ENERGY

The attitude energy function is the Hamiltonian function (Refs. 2-5, 2-7) modified in such a way as to yield a zero value when the satellite is aligned along the local vertical equilibrium position and rotating with an inertial angular velocity of 1 rpo. The large initial actual energy is indicative of the large amplitude motion observed at the beginning of the eighth APL pass.

The eighth DODGE pass over APL was one of the few quiescent periods of attitude motion for the spacecraft during its early history. During the ninth pass, in contrast, the attitude angles grew quite large. A question remains, then, as to what the "steady state" attitude motion of the satellite is when the sample and hold damping system is operational.

Fig. 2-45 shows the correlation between the predicted attitude energy during the ninth pass, and the energy determined from measured attitude angles and rates. The computer simulation used for this calculation includes an exterior model for the earth's magnetic field, which is based on five orbits of magnetometer readings during the fifth pass of DODGE over APL.

Although there is some time variation between the simulation and the actual data, the results are qualitatively the same. Possible time variations between the simulation and the actual attitude data may be attributed to the fact that the simulation does not include the effects of thermal bending and solar radiation pressure.

The results indicate that time lag damping in time-dependent fields can cause large attitude motions due to the dipole-magnetic field interaction which can be at or near resonance with the normal modal frequencies of the attitude motion. In other words, even though the optimum holding time can be selected so as to avoid resonance problems and provide adequate damping for the case of a non-time varying field,

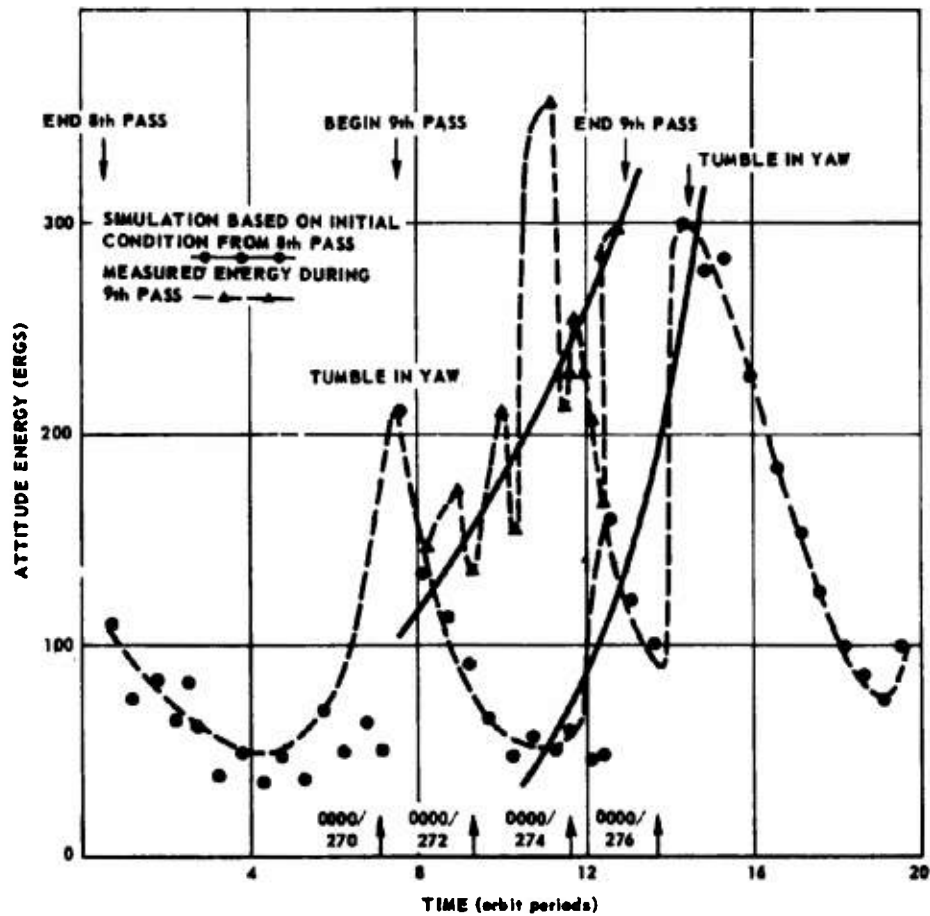


Fig. 2-45 DODGE ATTITUDE ANALYSIS-NINTH PASS-CORRELATION OF PREDICTED ATTITUDE ENERGY WITH MEASURED VALUES

there is no guarantee that such problems can be avoided in the case of a time dependent field with an open-loop control system.

2.4.1 Conclusion

A comparison of the predicted (simulated) theoretical motion of the DODGE satellite in a time varying magnetic field with the actual observed motion when the sample and hold damping system is operating indicates the results are qualitatively the same. The results indicate that the principal cause of the large attitude motion of DODGE during the ninth pass over APL was the dipole-magnetic field interaction, which was at near resonance with normal modes of the attitude motion.

2.5 Prelaunch Computer Simulation of Time-Lag Magnetic Damping, Including External Effects

A number of papers have been written describing the DODGE experiment (Refs. 2-6, 2-2, 2-19, 2-7, 2-17). However the published results relating to the performance of the time lag magnetic damping system consider only rigid body configurations in the absence of solar and orbit induced perturbations. The solar effect, which consists of both a change in mass properties because of thermal distortion of the stabilizing booms and a radiation pressure torque on the deformed spacecraft, constitutes the dominant attitude perturbation for the DODGE orbit. Using multiple booms in symmetrical configurations will minimize the solar effects. However thermal bending destroys the symmetry so that the change in mass properties and the shift of both the center of mass and center of pressure induce attitude perturbations.

The use of a constant-speed rotor to augment gravity-gradient stabilization is well known (Refs. 2-20, 2-21). This technique is especially attractive because with a passive mass distribution the yaw stabilizing torque is obtained at the expense of the pitch restoring torque and the introduction of disturbing torques that are boom length dependent. The rotor also provides a method by which

to introduce controlled perturbations so that the transient response of the various stabilization systems can be studied. The rotor is situated such that its spin angular momentum vector is normal to the dumbbell axis so that gyroscopic coupling will align it with the orbital angular momentum vector. This establishes preferred yaw stabilization as contrasted to the bistable yaw equilibrium for a passive mass distribution.

In this study the digital attitude simulation (Ref. 2-22) constructed for the DODGE experiment is used to perform a system evaluation. The equations of motion are presented and simplifying assumptions consistent with the DODGE orbit are discussed. Of particular interest is the discussion of the time-lag magnetic damper and the modeling of the thermal deformation and radiation pressure torque on extendible gravity-gradient booms.

The following defines some of the symbols used throughout this section:

$F_{a\mu}$	\equiv generalized force conjugate to a_μ
$\ddot{\theta}_{akj}$	\equiv j^{th} partial acceleration of the Euler angles
\vec{H}	\equiv column matrix representing the geomagnetic field in $0_s(x_{si})$
$0_e(x_{ei})$	\equiv cartesian frame of reference fixed in inertial space and located at the center of mass of the principal gravitating body ($i = 1$ to 3)
$0_s(x_{si})$	\equiv cartesian frame of reference fixed in the spacecraft ($i = 1$ to 3)
$0_t(x_{ti})$	\equiv cartesian frame of reference whose origin and orientation can be arbitrarily specified as a function of time ($i = 1$ to 3)
\vec{r}	\equiv column matrix of components in $0_s(x_{si})$ representing the position of an element of mass from the origin of $0_s(x_{si})$

- \bar{r}_t ■ column matrix of components in $O_e(x_{ei})$ representing the position of the origin of $O_t(x_{ti})$ with respect to the origin of $O_e(x_{ei})$
- t ■ time
- \bar{T} ■ a three by three matrix which transforms a torque vector in $O_s(x_{si})$ to generalized forces conjugate to the α_μ
- α_i ■ generalized set of Euler angles used to define orientation of $O_s(x_{si})$ with respect to $O_t(x_{ti})$ ($i = 1$ to 3)
- $\varphi_1, \varphi_2, \varphi_3$ ■ Eulerian angles used to define orientation of $O_t(x_{ti})$ with respect to $O_e(x_{ei})$ for a Keplerian elliptical trajectory

2.5.1 Equations of Motion

The nonlinear differential equations governing the large-angle motion of the spacecraft must in general be integrated numerically. Thus it is important to generate the equations in a form that is suitable for solution on a high-speed digital computer. With this in mind, the dynamical theory for the trajectory and attitude motion of a spacecraft in the vicinity of a gravitating mass was developed as part of the DODGE effort (Ref. 2-23). In this development, the spacecraft is considered to have a completely general configuration with mass an explicit function of time and the mass distribution a function of time and the generalized coordinates and velocities. The oblateness of the principal gravitating mass and the coupling between the attitude and trajectory motions which result from the nonlinearity of the Newtonian potential are included. The orbital motion is specified in terms of a perturbation from an arbitrary reference trajectory. The attitude is specified in

terms of a general set of Euler angles which relate the orientation of a reference frame fixed in the spacecraft to a reference frame whose orientation can be specified in inertial space as an arbitrary function of time. The introduction of the general set of Euler angles provides for convenient use of a dual set of angles to avoid singularities in the differential equations or the selection of a natural set for any specific application.

For the DODGE spacecraft and orbit, it is possible to impose some restrictions and make some approximations in order to simplify the equations of motion. For time lag magnetic damping it is appropriate to restrict the equations to a system in which the mass is conserved and the motion of the stabilizing rotor is specified a priori. The effect of the oblateness of the principal gravitating mass on the attitude motion follows from Eq. (62) of Ref. 2-23 to be small and ignorable. The coupling between the attitude and trajectory motions, which result from the nonlinearity of the Newtonian potential, follows from Eq. (66) of Ref. 2-23 to also be ignorable. The additional assumption that the external forces - due to radiation pressure - are a weak function of the attitude of the spacecraft results in the decoupling of the trajectory equations of motion from the attitude equations. Consequently the trajectory motion can be specified a priori. Tracking of satellites at the Applied Physics Laboratory has indicated that a good approximation to the orbital motion can be obtained from least squares fitting a Keplerian orbit whose right-ascension of the ascending node and argument of perigee are linear functions of time. The validity of this approximation for attitude simulation has been demonstrated (Ref. 2-24).

For gravity-gradient stabilization, it is natural to choose the reference frame from which the orientation of the spacecraft is measured to be the local vertical reference frame illustrated in Figs. 2-46 and 2-47 and specified by O_t . The choice of the Euler angle set is more subjective; here the yaw, roll, and pitch set is used. These

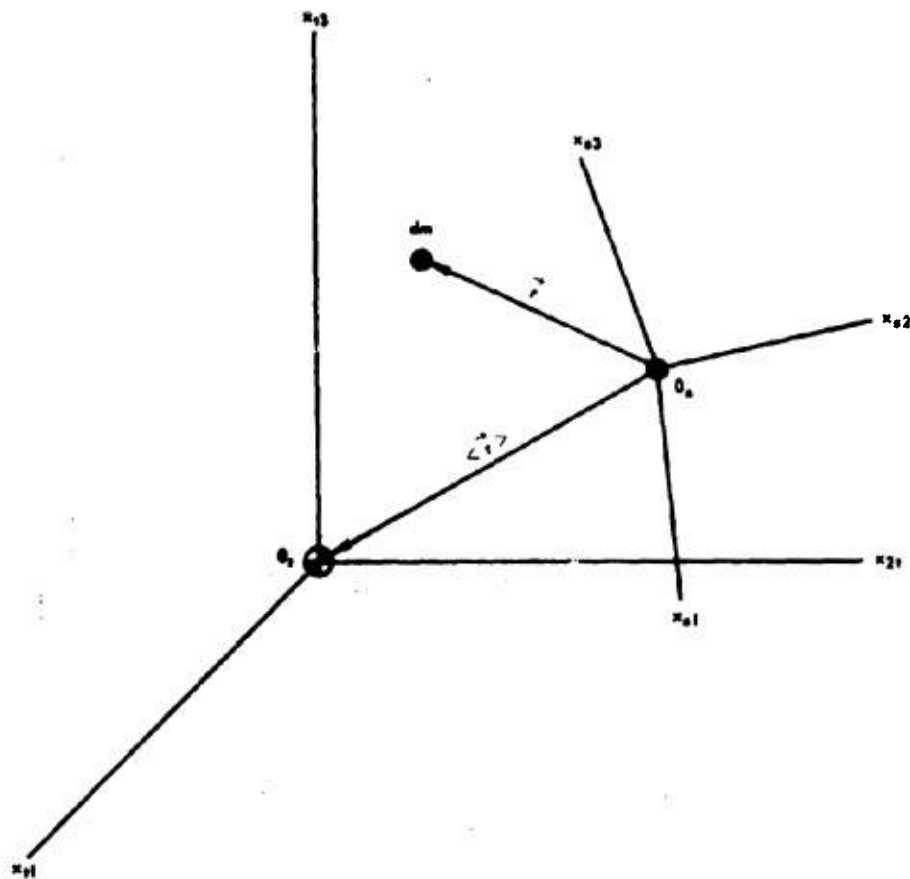


Fig. 2-46 REFERENCE FRAMES USED TO DEFINE ORIENTATION OF SPACECRAFT

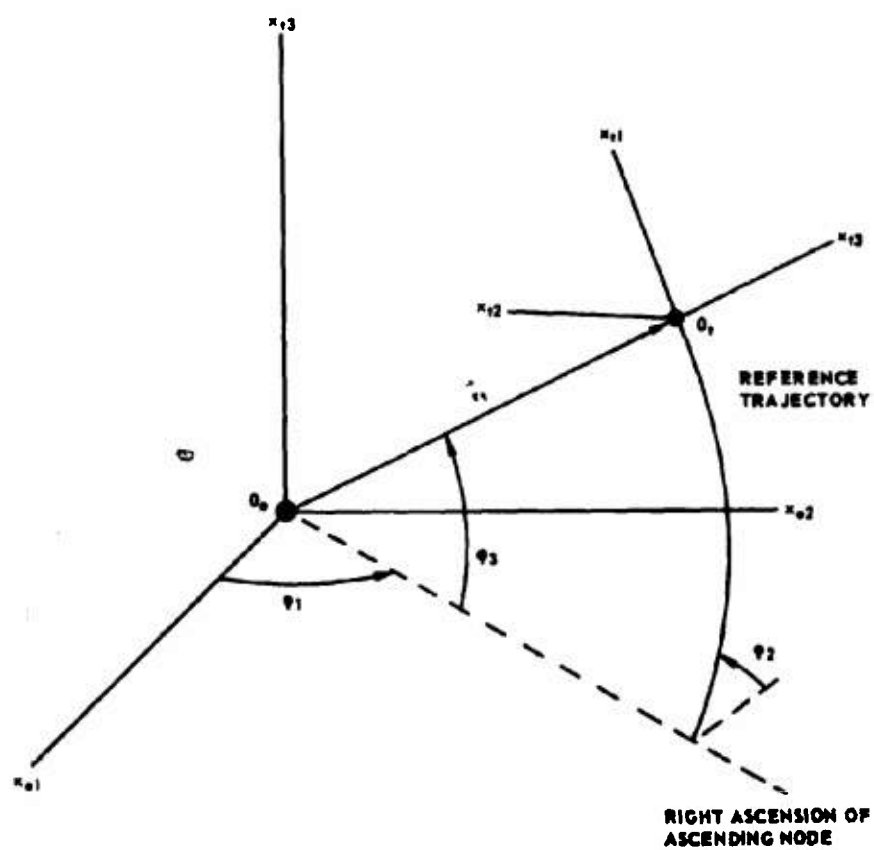


Fig. 2-47 LOCAL VERTICAL REFERENCE FRAME

angles are defined as rotations about the successively carried positions of the x_{t3} , x_{t1} , and x_{t2} axes.

With these restrictions, Eqs. (26) and (27) of Ref. 2-23 which are the nonlinear differential equations for the attitude motion, are:

$$\ddot{\alpha}_k = \sum_{j=1}^8 \mathcal{F}_{\alpha kj}, \quad (k = 1 \text{ to } 3) \quad 2.5 (1)$$

where the $\mathcal{F}_{\alpha kj}$ are defined in Ref. 2-23.

Eq. 2-5 (1) has been partitioned in a form that permits convenient simplification and modification. Each $\mathcal{F}_{\alpha kj}$ represents a particular separable effect:

- $j = 1$ represents the generalized external forces
- $j = 2$ represents the effect of variable mass
- $j = 3$ represents the disturbing effect of the effect of the principal and secondary bodies
- $j = 4$ represents the effect of the elastic potential
- $j = 5$ represents the effect of the higher-order terms of the Newtonian potential of the principal gravitating body
- $j = 6$ represents the effect of the mass distribution of the spacecraft
- $j = 7$ represents the effect of the first time derivative of the mass distribution
- $j = 8$ represents the effect of the first and second time derivatives of the mass distribution.

Partitioning of the equations of motion in this manner allows for efficient use of the digital computer program for any particular spacecraft

configuration by including only the appropriate acceleration terms. For changes in configuration only the mass parameters need be modified.

2.5.2 Magnetic Torques

The magnetic torques which act on a spacecraft at synchronous altitudes arise principally from the interaction of the time lag magnetic damper with the geomagnetic field. Tests indicate that the residual magnetization of the DODGE spacecraft is less than 50 pole-cm which yields a maximum disturbing torque of less than .06 dyne-cm. A schematic of the time lag magnetic damping system is shown in Fig. 2-37. This system consists of a sensor that is a vector magnetometer, a memory device, a timer, an amplifier, and a linear electromagnet. The principle of the damper is the electronic emulation of magnetic hysteresis damping. It has been demonstrated in Ref. 2-25 to be very effective in damping librational motion of earth satellites at altitudes below the magnetosphere.

The operation of the time lag magnetic damping system is illustrated in Fig. 2-48. At some instant time, t_0 , the output of the vector magnetometer is used to generate a magnetic dipole in the spacecraft, \vec{M}_0 , which is proportional and parallel to the geomagnetic field, \vec{H}_0 . The dipole is held fixed with respect to the spacecraft for an interval of time, τ , during which the relative motion of the geomagnetic field and the spacecraft causes an angular displacement between the two vectors which generates a torque equal to their cross-product. Qualitatively the damper torques can be partitioned into actual damping torques which result from the attitude motion of the spacecraft relative to the local vertical reference frame and attitude perturbing torques which result from motion of the geomagnetic field relative to the local vertical reference frame. Obviously the selection of system parameters is essentially an attempt to balance these two effects. In a near synchronous orbit, where there is very little relative motion of the geomagnetic field, the

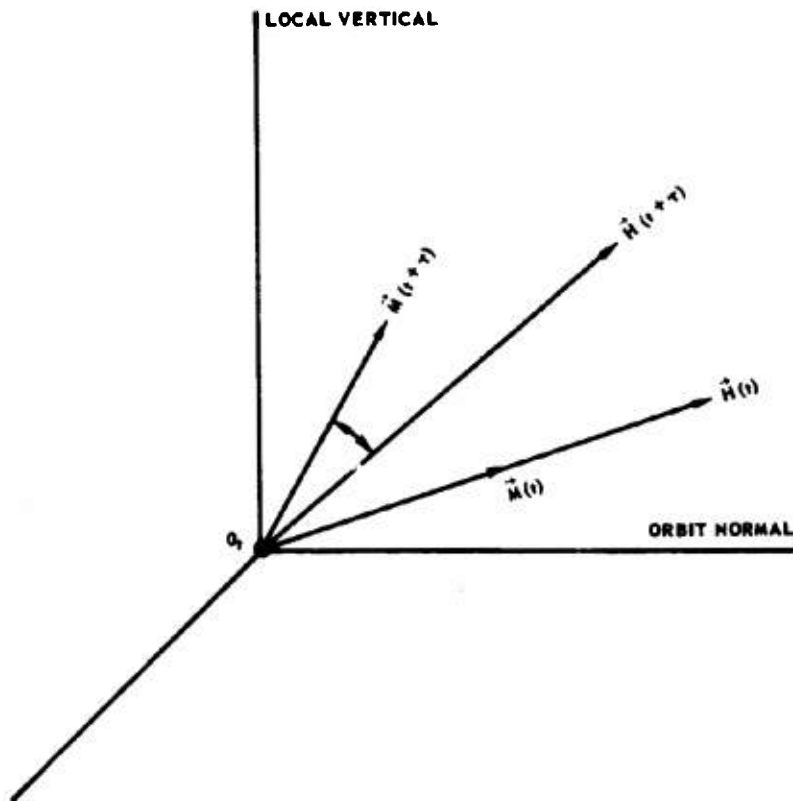


Fig. 2-48 TIME LAG MAGNETIC DAMPING

perturbing effect of the damper is a minimum so that both large damping torques and small perturbing torques can be obtained.

The generalized torque induced by the damper can be represented by

$$F_{\alpha\mu} = \sum_{v=1}^3 \bar{k}_{p,v} \bar{T}_{\mu v} \sum_{\gamma,\delta=1}^3 \left[\sum_{\alpha=1}^3 \bar{H}_{\alpha}(t_1) \bar{\epsilon}_{\alpha,\gamma\delta} \right] \bar{H}_{\gamma}(t) \quad 2.5 (2)$$

$$t_1 \leq t \leq t_1 + \tau$$

where the $\bar{\epsilon}_{\alpha,\gamma\delta}$ are rotation matrices. The proportionality constant, $K_{p,v}$, between the geomagnetic field and the magnetic dipole and the sample rate or time lag interval, τ , are the basic parameters of the damper. Internal geomagnetic field models yield values of approximately 125 gamma for the DODGE orbit. Measurements of the distant field have been performed by a number of satellites and space probes. Mead and Cahil (Ref. 2-26) have compared results from Explorer 12 with a model consisting of only internal sources and also a model consisting of the same internal field but distorted by external sources. This comparison indicates that both models yield values that are within 10 gamma of the measured field for the DODGE orbit. Consequently, the geomagnetic model proposed by Cain et al. (Ref. 2-27), which represents only internal sources is used in the simulation. This geomagnetic model which is described in terms of spherical harmonics and has a maximum order of eight is truncated to order two for the DODGE orbit because of the large radial distance to the spacecraft. Order two results in an eight-term Legendre polynomial expansion for the geomagnetic field.

The frequency and magnitude of magnetic storms are very important considerations for geomagnetic damping systems. An estimate of the number of 100 gamma or higher storms at near

synchronous altitudes from mid-1967 to mid-1968 is given by Weygant (Ref. 2-28) to be from two to five. Storms of lesser magnitude occur at more frequent intervals. The effect of the storm is to alter the magnitude and direction of the geomagnetic field in the local vertical frame of reference which, as discussed earlier, will introduce attitude perturbations. Since it is only the change in geomagnetic field during a time-lag interval on which perturbation is dependent a small time-lag interval will minimize this effect.

2.5.3 Thermal Bending of Stabilizing Booms

Extendible booms of the deHavilland type have been accepted as efficient devices with which to achieve the large spacecraft inertia that is necessary for gravity-gradient stabilization. This type of boom is formed in orbit from a pre-stressed tape stored on a cylindrical spool. When deployed, the tape forms a long slender cylinder with an overlapped seam of near uniform spiral. As described previously, the tape is made from beryllium copper and the exterior surface is silver plated to reduce the thermal absorptivity. Exposure of the boom to anisotropic thermal radiation causes a temperature gradient around the circumference of the tape which results in boom bending. The effect of the tape overlap is to give an asymmetrical temperature distribution and consequently both in-plane and out-of-plane bending. In-plane bending refers to the component of deflection which occurs in the plane of the undeformed boom's longitudinal axis and the principal source of heat. Out-of-plane bending is the component of deflection normal to the plane described above.

The temperature distribution problem has not been solved for a spiraled overlapped boom. However for a small turn to length ratio, the

bending problem can be solved to a good approximation by assuming that the equilibrium temperature distribution at a cross section is independent of the temperature at adjacent cross sections. Additional assumptions that need to be made are that thermal equilibrium conditions exist at each point in time, that the curvatures are small at all points along the boom, that the boom is straight prior to thermal bending and that the surface properties, amount of overlap and contact between layers, and the spiral of the overlapped seam are constant over the length of the boom. To allow for generality the in-plane and out-of-plane curvature at each cross section is expressed as a Fourier series

$$C_i = a_{i0} + \sum_{m=1}^{\infty} [a_{im} \cos m \xi + b_{im} \sin m \xi] \quad \text{for } i = N, T \quad 2.5 (3)$$

where N and T refer to in-plane and out-of-plane respectively and ξ is the included angle in a cross section between the seam and the plane containing the boom and sun. At DODGE altitudes, the thermal inputs to the boom from earth emitted and reflected radiation are negligible. The components of the deflection at any point z_0 along the boom illustrated in Fig. 2-49 are given by

$$\delta_i(z_0) = \int_0^{z_0} C_i(z_0 - z) dz \quad (i = N, T) \quad 2.5 (4)$$

For small deflections, it is reasonable to approximate the boom deflections by constant radii of curvature obtained by a least squares

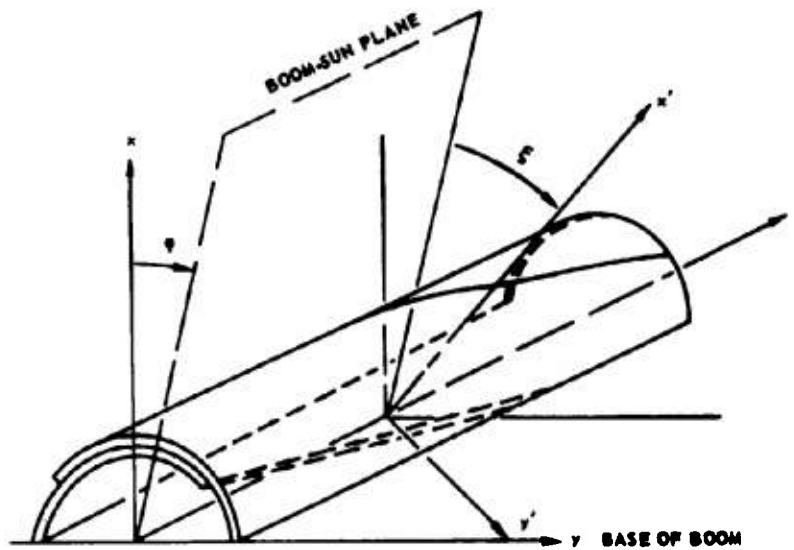


Fig. 2-49 THERMAL BENDING REFERENCE SYSTEMS

fit to Eq. 2.5 (4). If this is done, the deflections are represented by

$$\delta_{Li}(z_0) = C_{Li} \frac{z_0^2}{2} \quad (i = N, T) \quad 2.5 (5)$$

Where C_{Li} is determined from the least square fit. The rationale for the fitting of the constant radii of curvature is the enormous simplification it affords in the computation of the mass properties and radiation pressure torque on the deformed booms.

Necessary ingredients in this analysis are the coefficients of the Fourier series (a_{im} , b_{im}) which expresses the curvature at a cross-section as a function of the orientation of the sun with respect to the seam. Experimentally determined coefficients would be ideal but a comparison of existing test data indicated that unacceptable discrepancies existed. This approach was then abandoned in favor of the results of a theoretical analysis by Whisnant and Anand (Ref. 2-29). This paper shows that it is sufficient to represent the in-plane curvature by a_{N0} , a_{N1} , and a_{N2} and the out-of-plane curvature by b_{T1} and b_{T2} . In Fig. 2-50 the deflections and their least squares fits are plotted as a function of boom length for a spiral overlap of 98.6° , spiral rate of 2π rad/150 ft. and for an angle of the sun to the seam at the base of the boom, ϕ , of zero.

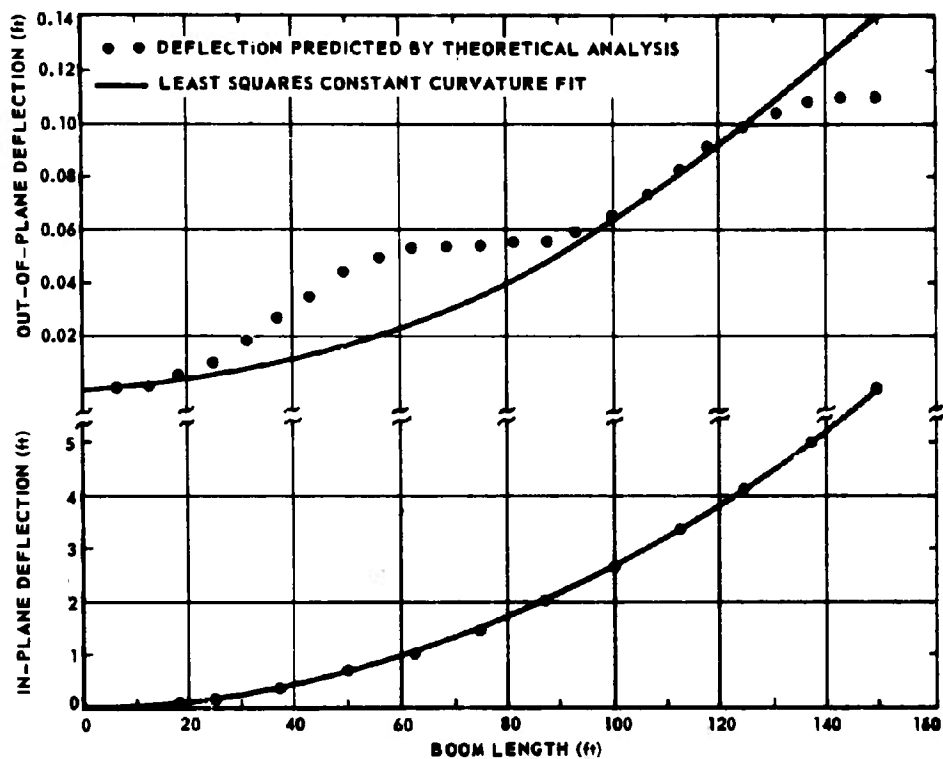


Fig. 2-50 LEAST SQUARES CONSTANT CURVATURE FIT OF A THERMALLY DEFORMED BOOM
($p = 2 \pi \text{ RAD./150 FT.}$, $\phi = 0$, OVERLAP = 98.6°)

2.5.4 Radiation Pressure Torques

Direct solar pressure induced torques which have a weak dependence on altitude increase in significance at high altitudes because of the large decrease in gravity-gradient restoring torque. This essentially precludes the use of configurations with large center-of-mass center-of-pressure offsets at the high altitudes; balanced or symmetrical configurations are required. However the thermal deformation of the stabilizing booms, discussed in the previous section, destroys the balance and introduces radiation pressure torques. It follows that this effect will impose an upper limit on the lengths of stabilizing booms that can be utilized to achieve the required mass distribution.

Simulated radiation forces on the thermally bent booms, end masses, and spacecraft main body are combined so as to produce the total radiation torque about the instantaneous center of mass of the spacecraft. Analytical expressions are obtained for the contribution of each member of the spacecraft by summing three fundamental force components: forces due to incident radiation, specularly reflected radiation, and diffusely reflected radiation obeying Lambert's cosine law (Ref. 2-30). Derivation of these expressions follows from the added assumptions that no structural shadowing occurs for any member of the spacecraft, that the surface radiation properties of any member of the spacecraft are homogenous and isotropic but differ from one member to another, that all stabilization booms are composed of right circular cylindrical elements, that all stabilization booms contain spherical end masses and that the main body of the spacecraft is equivalent to a closed right circular cylinder. The equivalent force system for the radiation pressure on the closed right circular cylinder about its geometrical center is a force. The magnitude of the associated couple is zero.

2.5.5 Prelaunch Performance Evaluation

The mission objective was to obtain steady-state libration amplitudes of less than two degrees rms in pitch and roll and less than four degrees rms in yaw. The spacecraft parameters were selected on the basis of an equatorial orbit. However when the spacecraft was astride the launch vehicle problems with the booster dictated a change in orbit inclination to seven degrees. The qualitative effect of this change on the attitude performance can be determined by examining both satellite subtracks over one orbital revolution. For the equatorial orbit, there is little motion of the geomagnetic field relative to the local vertical reference frame so that high gains and long time-lag intervals can be effectively used to give good damping characteristics with a minimum of disturbing effects. For the inclined orbit, the situation is changed. The satellite subtrack oscillates about the equator with an amplitude equal to the inclination, period equal to the orbital period and a wavelength in hour angle that is the difference between 24 hours and the orbital period. The local vertical reference frame oscillates relative to the equator about the local vertical with an amplitude equal to the inclination of the orbit. The increased motion of the geomagnetic field in the local vertical reference frame will give rise to perturbing torques that are greater than those associated with the equatorial orbit. The simulation indicated that for the equatorial orbit it should be possible to achieve the steady-state performance objectives with a wide range of spacecraft and damper parameters. Consequently they were selected on the basis of the transient attitude performance; the important parameters, given previously, are repeated in Table 2-4.

Results of the digital simulation study of the steady-state performance of the DODGE spacecraft in the inclined orbit are given in Figs. 2-51, 2-52, and 2-53. The angles represent the peak amplitude noted over a twenty day simulation; in general the maximum angles do not occur simultaneously. To effect a comparison of the

TABLE 2-4
SPACECRAFT CHARACTERISTICS

A. Mass Properties

Total payload mass	429.5	lbs
Vertical boom end masses	8.25	lbs
Horizontal boom end masses	4.94	lbs
Times boom end masses	4.94	lbs
Boom tape	.015	lbs /ft

B. Maximum Boom Lengths

Vertical booms	150.	ft
Horizontal booms	100.	ft
Times booms	150.	ft

C. Flywheel Characteristics

Moment of inertia	2.84×10^{-4}	slug-ft ²
Speed	8400.	RPM

D. Time Lag Damper Characteristics

High gain	600.	pole-cm/gamma
Low gain	150.	pole-cm/gamma
High time lag interval	6.	hours
Low time lag interval	3.	hours

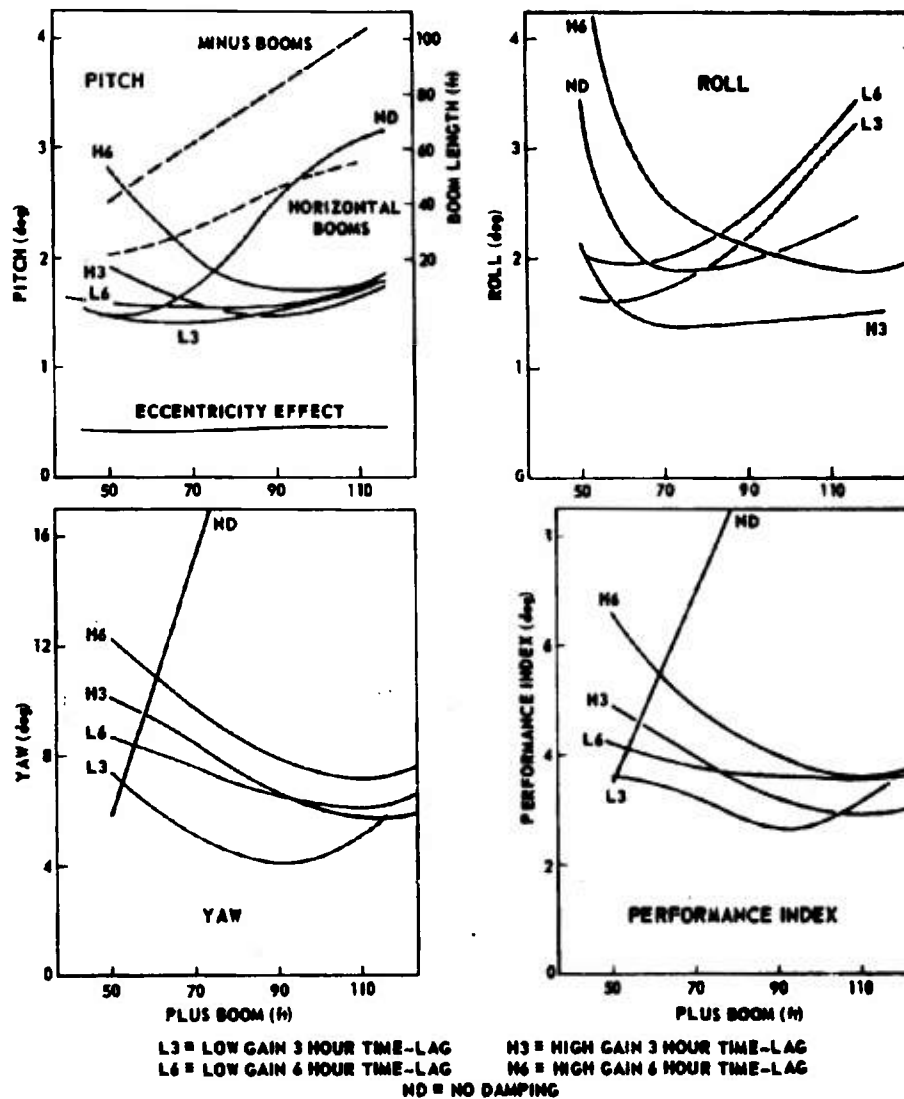


Fig. 2-51 SIMULATION RESULTS FOR PLUS CONFIGURATION
OF DODGE SPACECRAFT IN INCLINED ORBIT

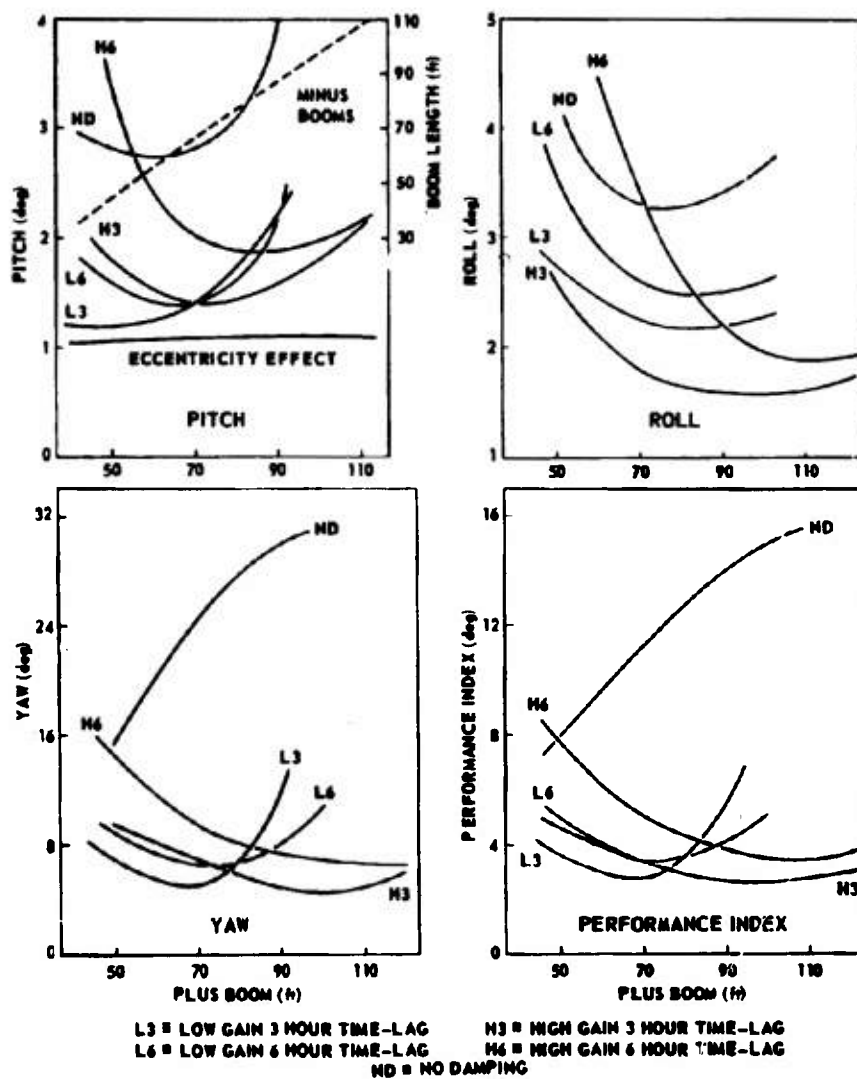


Fig. 2-52 SIMULATION RESULTS FOR TIMES CONFIGURATION OF DODGE SPACECRAFT IN INCLINED ORBIT

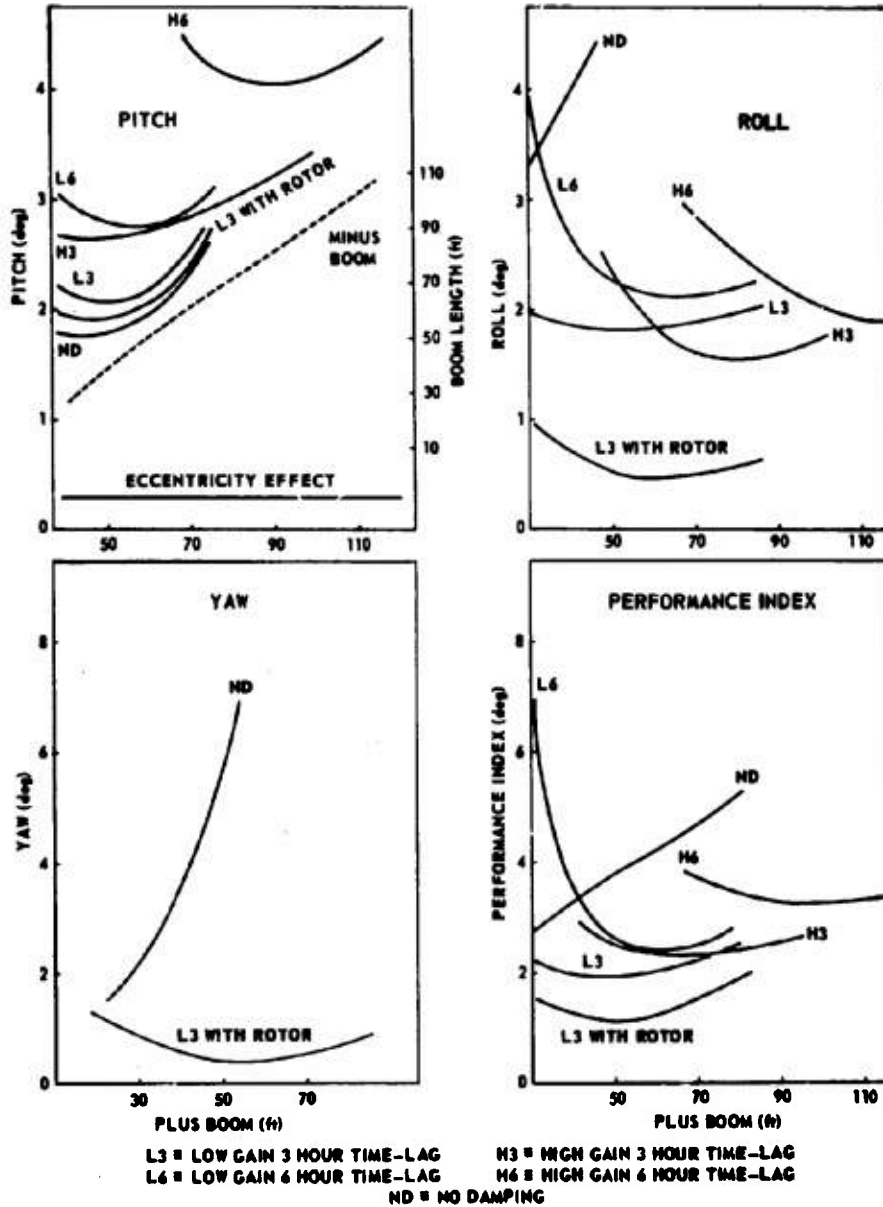


Fig. 2-53 SIMULATION RESULTS FOR DUMBELL CONFIGURATION OF DODGE SPACECRAFT IN INCLINED ORBIT

results, a performance indicator defined as the root mean square of the peak libration amplitudes is plotted. For each run, the initial state vector was chosen such that the spacecraft would have remained stabilized if there were no perturbations. The magnitudes of the solar induced roll and yaw perturbations depend on the orientation of the sun with respect to the orbit plane. When the sun is in the orbit plane the disturbing torque is primarily in pitch. The 20 - day simulations were centered about a day during which the sun reached a local maximum deviation of 22.2 degrees from the orbit plane. During this interval the roll and yaw disturbances are near their maximum value.

To balance the radiation pressure torque induced by the asymmetrical main body, unequal vertical boom lengths are used. Since a balance cannot be effected for all orientations with respect to the sun, the desired ratio of lengths is computed for normal incidence when the disturbance would be a maximum. The performance of each configuration was first studied in the absence of the time lag magnetic damper; at this time the horizontal boom lengths of the plus configuration were selected to minimize the performance indicator. Increased libration amplitudes at the shorter boom lengths result from the radiation pressure unbalance at other than normal incidence. At the longer boom lengths, the increased libration amplitudes are a result of the thermal distortion of the booms. The performance indicator shows that when the damper was added the overall performance improved significantly. As anticipated, the addition of the stabilizing rotor to the dumbbell configuration improved the roll performance and induced very good yaw stabilization.

The study indicates that the mission objectives can still be obtained for the spacecraft in the inclined orbit. Radiation pressure torques induced by the thermally bent booms occur at a frequency near the natural frequency of the

yaw mode of motion so that some form of damping is required to obtain acceptable libration amplitudes. The dumbbell configuration with the stabilizing rotor gives the best pointing accuracy of all the systems. There is little difference in the overall performance of the plus and times configurations.

2.6 Comparison of Theoretical Experimental DODGE Attitude Data with DAS Program

This section discusses the comparison between DODGE theoretical and experimental attitude data. The attitude of the spacecraft at some epoch was determined by the TV cameras and used to provide initial conditions for the digital attitude simulation (DAS). The simulation results were then compared with the experimental data obtained over the next 10 to 20 days.

In the digital attitude simulation a system of non-linear, coupled differential equations is solved to describe the attitude of the spacecraft while in orbit. External forces and perturbations due to the orbital environment are included, and there are no assumptions as to small angles. The simulation is described in more detail in section 2.4 on the prelaunch simulation of time lag damping.

After capture of the satellite with the booms in the times configuration, the time lag magnetic damping system was turned on. The prelaunch analysis had shown that this system should damp the librational motions to within the mission requirements. However, the librational motion did not damp as well as expected; in fact increased at times. The problem was determined to be fictitious magnetometer readings of an unknown origin. This caused poor agreement between the actual flight attitude data and simulation results.

To simulate the DODGE motions better, the DAS program was modified to include the effects of both an actual external magnetic field and also anomalies in the magnetometer readings. For the DODGE simulation runs the following model was used

$$\overline{H}_{\text{sensed by magnetometer}} = \overline{H}_{\text{actual}} + \overline{H}_{\text{fictitious}} \quad 2.6 (1)$$

$\overline{H}_{\text{fictitious}}$ is of the following form

$$\overline{H}_{\text{fictitious}} = \begin{pmatrix} \overline{H}_{\text{north}} \\ \overline{H}_{\text{east}} \\ \overline{H}_{\text{down}} \end{pmatrix}_{\text{fictitious}} = \begin{pmatrix} A = B \sin(\lambda - \lambda_s + \varphi) \\ 0 \\ 0 \end{pmatrix} \quad 2.6 (2)$$

where A, B, and φ are constants, λ is the longitude of the spacecraft, and λ_s is the longitude of the sun.

Figs. 2-54, 2-55, 2-56, and 2-57 compare the actual and theoretical DODGE attitude results. The attitude motion is specified by a sequence of three rotational angles α_1 , α_2 , and α_3 taken in that order. Starting with the spacecraft in its equilibrium position with the spacecraft coordinate system parallel to the local vertical coordinate system, α_1 or yaw is a rotation about the spacecraft Z axis. Roll or α_2 is a rotation about the carried X axis and pitch or α_3 is a rotation about the carried Y axis. For small angles α_3 and α_2 correspond to in-plane and cross-plane motion respectively.

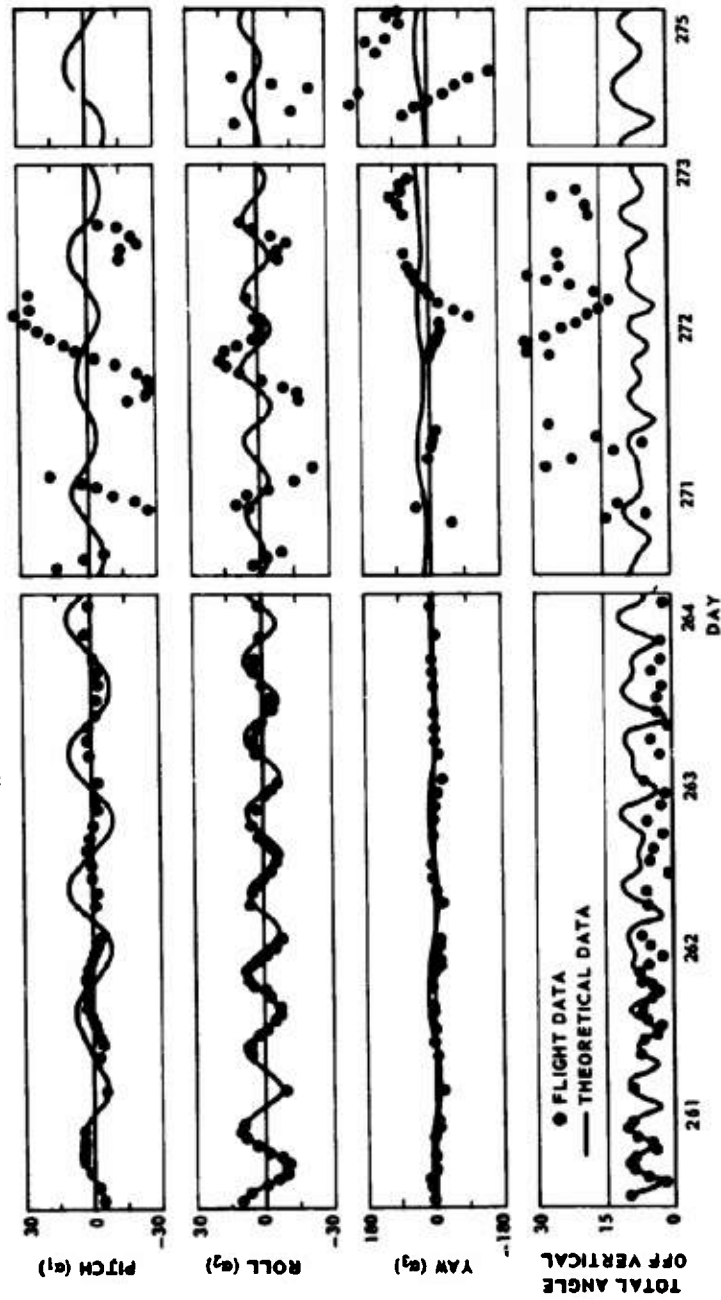


Fig. 2-54 COMPARISON OF FLIGHT AND THEORETICAL DATA FOR
DAYS 260-275, 1967

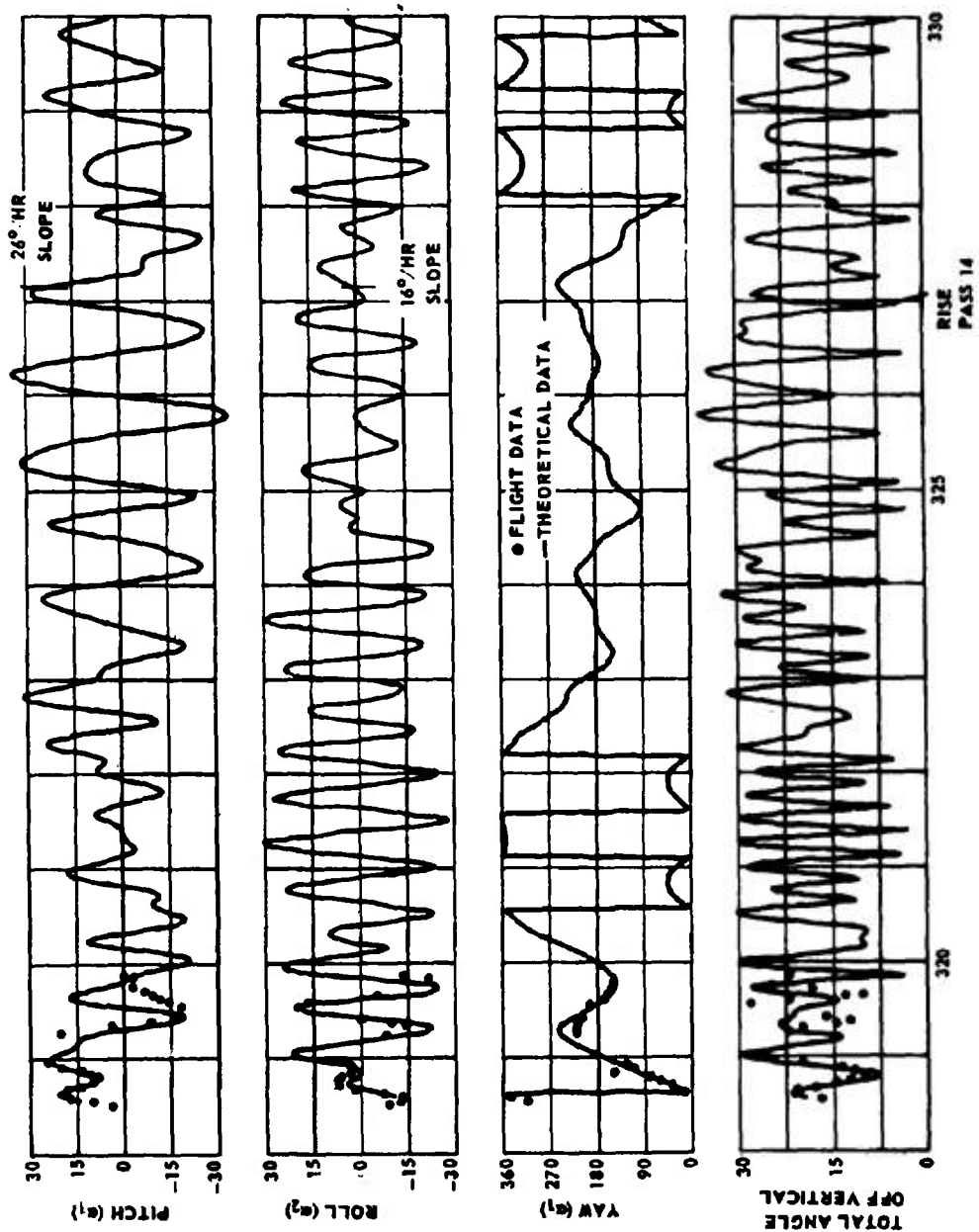


Fig. 2-55 COMPARISON OF FLIGHT AND THEORETICAL DATA FOR
DAYS 318-330, 1967

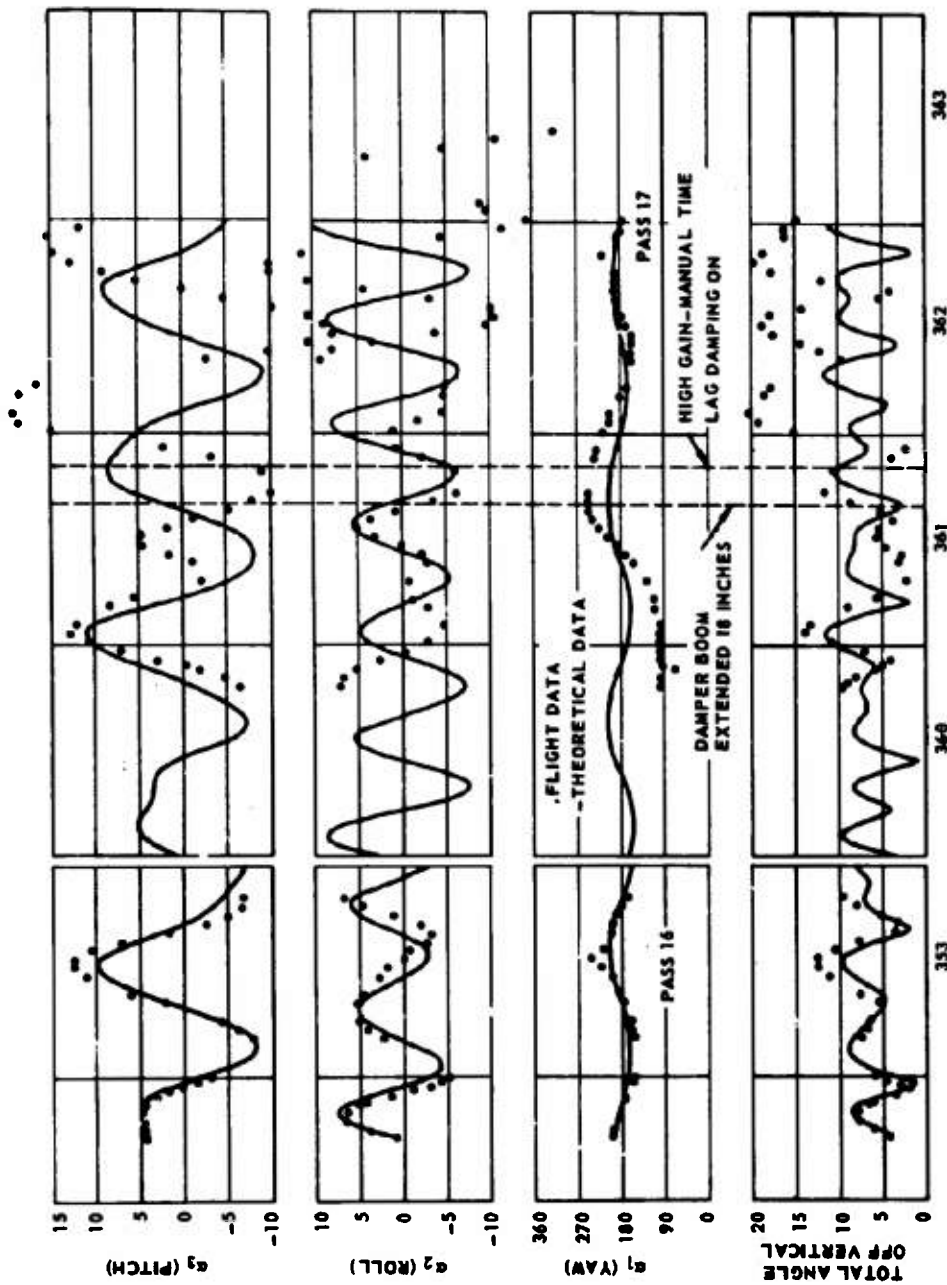


Fig. 2-56 COMPARISON OF FLIGHT AND THEORETICAL DATA
FOR DAYS 352-363, 1967

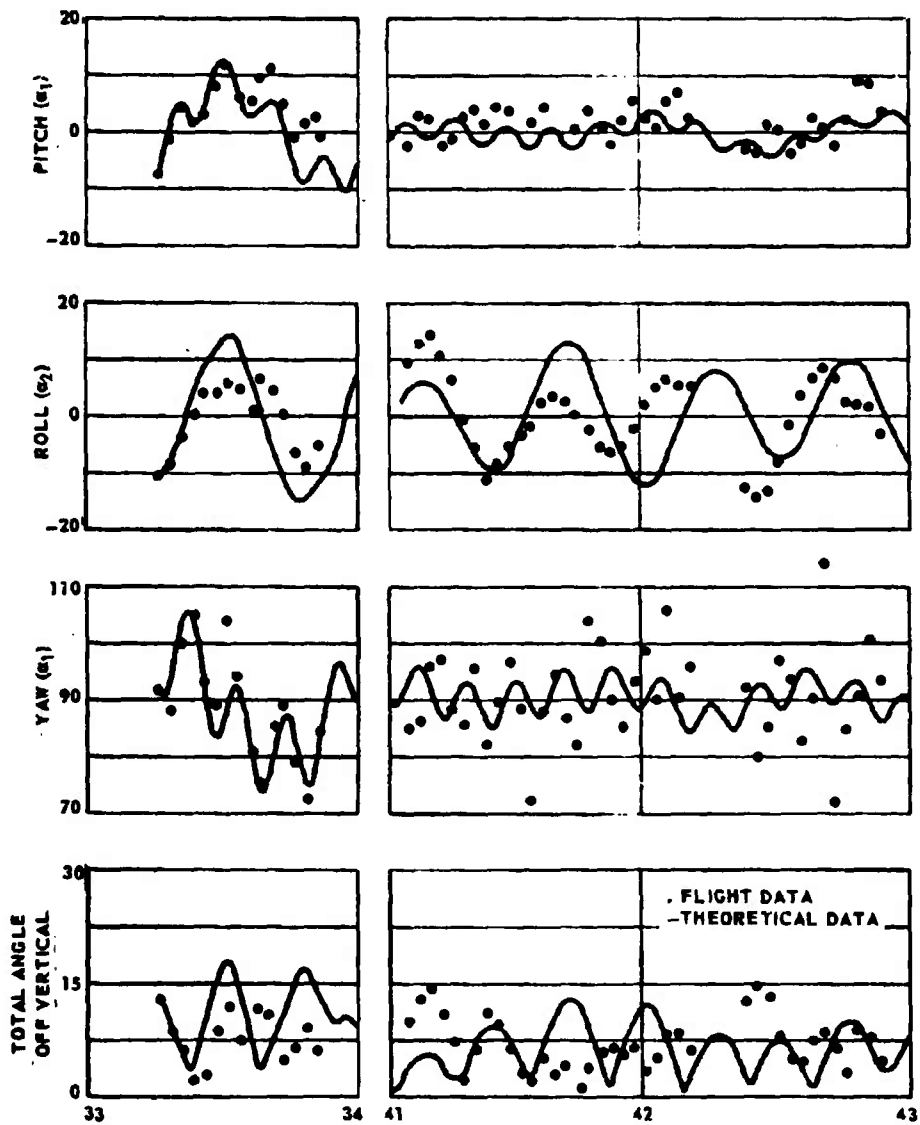


Fig. 2-57 COMPARISON OF FLIGHT AND THEORETICAL DATA FOR
DAYS 033-048, 1968

2.6.1 Simulation for Days 260-275, 1967

This simulation run was made using initial conditions determined from the 8th APL pass. The time lag magnetic damping system was in the low gain, 3-hour mode. The boom lengths were approximately 99 feet. $\bar{H}_{\text{fictitious}}$ was determined from the magnetometer readings and the following values were used:

$$\bar{H}_{\text{fictitious}} = \begin{pmatrix} -20 + 80 \sin(\lambda - \lambda_s + 30^\circ) \\ 0 \\ 0 \end{pmatrix} \quad 2.6 (3)$$

where the magnetic field units are gamma.

For the remainder of APL pass No. 8, damping seems to be apparent from both the actual flight and the simulation results. The overall agreement is good; however the flight data show slightly better damping than the simulation predicts, especially in the α_3 motion.

For days 264-275, the DAS program predicted continued damping, even with the fictitious magnetometer readings. However when the satellite rose on day 270 at the beginning of APL pass No. 9, large libration amplitudes were observed. During this pass, α_2 and α_3 reached amplitudes of 30 degrees-45 degrees. The satellite appeared to have tumbled at least once in α_1 (yaw). The poor comparison evident during pass No. 9 is attributed to either an unknown perturbation or to the unpredictability of the fictitious magnetometer readings.

2.6.2 Simulation for Days 318-338, 1967

This simulation run was made using initial conditions determined from the 13th APL pass. All damping systems were turned off thus eliminating the effect of the fictitious magnetometer readings. The boom lengths were approximately 83 feet.

For the remainder of APL pass No. 13 there is good agreement between the simulation and flight results.

For days 320-328, the DAS program predicted little change in the amplitudes of the librational motion. However, when the satellite rose at the beginning of APL pass No. 14, the attitude motion was unstable. The satellite appeared to be tumbling in all motions and the rates are given in Fig. 2-55. Due to the unexplained tumbling, there is no comparison between two results for the remainder of this pass.

2.6.3 Simulation for Days 352-363, 1967

This simulation run was made using initial conditions determined from the 16th APL pass. Again all damping systems were turned off. The boom lengths were approximately 99 feet.

For the remainder of APL pass No. 16, there is good agreement between the simulation and flight results.

Seven days later, the satellite rose to begin APL pass No. 17. This time there was still good agreement between the two results in the amplitudes of α_3 and α_2 . Agreement in α_1 was poor. On day 361, manual damping with the time lag system in the high gain mode was initiated. Almost immediately, the libration amplitudes increased and the two results no longer agreed.

2.6.4 Simulation for Days 033-048, 1968

This simulation run was made using initial conditions determined from the 20th APL pass. The time lag magnetic damping system was in the low gain, 3-hour mode. The boom lengths were approximately 42 feet. Again, the fictitious model was used. During this time the constant speed rotor was being used which caused $\alpha_1 = 90^\circ$ to be the equilibrium yaw angle. This also made α_2 represent in-plane motion and α_3 the cross-

plane motion. Previous studies have shown that the cross plane motion will have a high frequency component when the rotor is turned on.

For the remainder of APL pass No. 20, there was general agreement between the simulation and flight results.

For days 033-048, the DAS program predicted damping which is most evident in the cross-plane and yaw modes. This damping occurs even with the time dependent magnetic effects. When the satellite rose at the beginning of the 21st APL pass, the cross plane motion had damped, but the yaw appeared to be increasing. There was good agreement between the amplitudes of the in-plane motion for the two results.

2.6.5 Conclusion

During APL passes Nos. 20 and 21, the differences between the theoretical and flight results can be attributed to the unpredictable magnetometer readings. APL passes Nos. 16 and 17 show good agreement when the magnetic damping system was turned off and the magnetometer readings were not used. Again, good agreement was obtained during APL pass No. 13 when no damping was present. The overall comparison between the two results supports the validity of using the computer simulation (DAS) to perform a system analysis.

2.7 References

- 2-1. Tinling, B. E., and V. K. Merrick, "The Exploitation of Inertial Coupling in Passive Gravity-Gradient Stabilized Satellites," AIAA Guidance and Control Conference, MIT, August 1963; also, Journal of Spacecraft and Rockets, Vol. 1, No. 4, July-August 1964, pp. 381-387.
- 2-2. Fischell, R. E., "The DODGE Satellite," AIAA/JACC Guidance and Control Conference, Seattle, Washington, August 15-17, 1966.
- 2-3. Kamm, Lawrence J., "'Vertistat': An Improved Satellite Orientation Device," ARS Journal, Vol. 32, No. 6, June 1962, pp. 911-913.
- 2-4. Fischell, R. E., "Spin Control of Earth Satellites," Applied Physics Laboratory Technical Digest, September-October 1965, pp. 8-14.
- 2-5. Bainum, P. M., "On the Motion and Stability of a Multiple Connected Gravity-Gradient Satellite with Passive Damping," Ph.D. dissertation, The Catholic University of America, December 1966; also, Applied Physics Laboratory Technical Report TG-872, January 1967.
- 2-6. Bainum, P. M., D. K. Anand, and D. L. Mackison, "Perturbations and Lyapunov Stability of a Multiple Connected Gravity-Gradient Satellite at Synchronous Altitude," Fifth U. S. National Congress of Applied Mechanics, Minneapolis, Minnesota, June 1966.
- 2-7. Bainum, Peter M. and Mackison, Donald L., "Gravity-Gradient Stabilization of Synchronous Orbiting Satellites." The British Interplanetary Society Spring Meeting, Loughborough, England, April 1967; also to appear JBIS, December 1968.

- 2-8. Goldstein, Herbert, Classical Mechanics, Addison-Wesley Publishing Company, 1959.
- 2-9. Pringle, Ralph, Jr., "On the Capture, Stability, and Passive Damping of Artificial Satellites," Ph.D. dissertation, Stanford University; also, NASA Report No. CR-139, December 1964.
- 2-10. Likins, P. W., "Stability of a Symmetrical Satellite in Attitudes Fixed in an Orbiting Reference Frame," The Journal of the Astronautical Sciences, Vol. XII, No. 1, Spring 1965, pp. 18-24.
- 2-11. LaSalle, Joseph, and Solomon Lefschetz, Stability by Lyapunov's Direct Method with Applications, Academic Press, New York, 1961.
- 2-12. Malkin, I. G., Theory of Stability of Motion, Atomic Energy Commission TR-3352, translation from a publication of the State Publishing House of Technical Theoretical Literature, Leningrad, 1952.
- 2-13. Likins, Peter W., and Robert E. Roberson, "Attitude Stability of Space Vehicles," University of California, Los Angeles, Short Course, April 4-15, 1966.
- 2-14. Cesari, Lamberto, Asymptotic Behavior and Stability Problems in Ordinary Differential Equations, Academic Press, New York, 1963, Second Edition.
- 2-15. Pringle, Ralph, Jr., "On the Stability of a Body with Connected Moving Parts," AIAA Third Aerospace Sciences Meeting, New York, January 24-26, 1966; also, AIAA Journal, Vol. 4, No. 8, August 1966, pp. 1395-1404.
- 2-16. Hildebrand, F. B., Methods of Applied Mathematics, Prentice Hall, 1952, Sec. 1.18.

- 2-17. Mackison, D. L., "Analysis of Time Delay Magnetic Damping of Spacecraft Librations in Near-Synchronous Equatorial Orbits," Applied Physics Laboratory TG 916 June 1967.
- 2-18. Jackson, John David, Classical Electrodynamics, John Wiley and Sons, 1962.
- 2-19. Fischell, R. E. and Kershner, R. B., "Attitude Stabilization Experiments with the DODGE Spacecraft," Proc. XVII Cong. Int. Astronau. Fed., Madrid (Oct. 1966).
- 2-20. Burt, E. G. C., "On the Attitude Control of Earth Satellites," Royal Aircraft Establishment, T. N. Space 3 (Jan. 1962).
- 2-21. Piscane, V. L., "Three-Axis Stabilization of a Dumbbell Satellite by a Small Constant-Speed Rotor," APL/JHU, TG-855 (Oct. 1966).
- 2-22. Pardoe, P. P., "A Description of the Digital Attitude Simulation", APL/JHU TG-964 (February 1968).
- 2-23. Pisacane, V. L., Guier, W. H., and Pardoe, P.P., "Dynamical Equations for the Position and Attitude of a Spacecraft with Time Dependent Mass and Mass Properties," APL/JHU, TG-919 (June 1967).
- 2-24. Pisacane, V. L., Pardoe, P. P., and Hook, B. J., "Stabilization System Analyses and Performance of the GEOS-A Gravity-Gradient Satellite," AIAA/JACC Guidance and Control Conf., Seattle (Aug. 1966); also Journal of Spacecraft and Rockets, 4 (12), 1623-1630, (1967).
- 2-25. Pisacane, V. L. and Stuart, J. D., "Digital Computer Simulation of a Time-Lag Magnet Damping Device," APL/JHU, Internal Memo. (Oct. 1965).

- 2-26 Mead, G. D. and Cahill, L. J., Jr.,
"Explorer 12 Measurements of the
Distortion of the Geomagnetic Field by
the Solar Wind," J. Geophys. Res.,
72 (11), 2737-2748 (1967).
- 2-27. Cain, J. C., Daniels, W. E., Hendricks, S. J.,
and Jensen, D. C., "An Evaluation of the
Main Geomagnetic Field," J. Geophys. Res.,
70 (15), 1940-1962 (1965).
- 2-28 Weygant, P. and Moyer, R., "Attitude Control
for the Gravity-Gradient Test Satellite,"
AIAA/JACC Guidance and Control Conf.,
Seattle (Aug. 1966).
- 2-29. Whisnant, J. M. and Anand, D. K., "Thermal
Bending of Gravity-Gradient Stabilization
Booms," (in preparation).
- 2-30 Wiggins, L. E., "Theory and Application
of Radiation Forces," Lockheed Missile
and Space Company, LMSC A-384055 (Sept. 1963).

3. ATTITUDE DETECTION SYSTEM

3.1 Dual Television Camera System

Attitude determination is accomplished with the DODGE television cameras by measuring the displacement of the Earth's image from the center of the received TV picture. Earth edge measurement is sufficient for satellite pitch and roll determination. A rough yaw measurement is obtainable from a picture whenever the terminator (line of separation of day and night) is visible. More accurate yaw measurement is possible when identifiable land mass areas are visible within a picture. The method routinely employed for yaw determination couples the data from the solar attitude detectors with the pitch and roll measurement from the camera system.

While other Earth edge detectors were considered for use on the DODGE satellite, the TV system was selected because it would also allow measurement of solar induced bending of the downward pointing stabilization boom. Attitude determination and boom bending measurements were the principle objectives for the DODGE TV System. A secondary objective of the DODGE camera system was to provide multispectral picture data of the Earth, as seen from the near synchronous altitude region, for study of the possible uses of such data. All the objectives of the system have been met.

3.1.1 TV System Configuration

A wide and narrow angle camera system was used to provide high accuracy attitude data in the near stabilized condition without sacrificing coverage for wide angle librations. Use of a dual camera system also has the advantage of providing redundancy for critical functions of the system. The selected formats for the two cameras were: for the wide angle, a $60^\circ \times 60^\circ$ field (the 60° camera), and for the narrow angle a $22^\circ \times 22^\circ$ field (the 22° camera). Fig. 3-1 is an artist's concept of the DODGE Satellite showing the two cameras and their picture characteristics. As the orientation of the satellite changes, the relative position of the Earth as seen in the picture also changes, thus

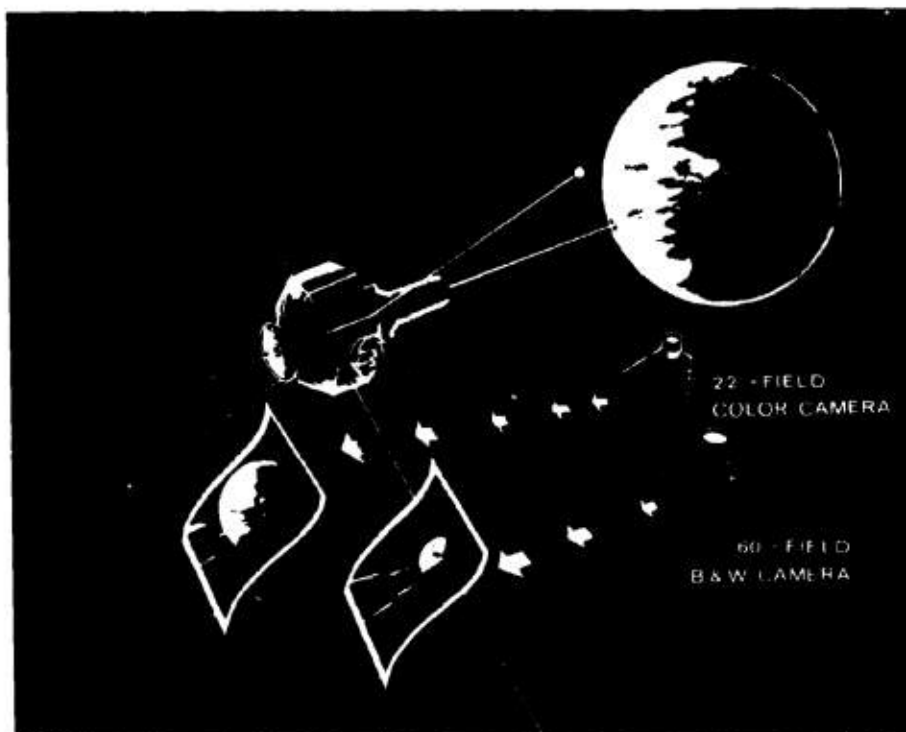


Fig. 3-1 ARTIST'S CONCEPTION OF DODGE, SHOWING ITS TWO CAMERAS AND THEIR PICTURE CHARACTERISTICS

providing a measure of satellite attitude. The cameras are mounted with their optical axes aligned with the satellite Z-axis. The attitude is measured relative to a fixed mechanical reference provided by a reticle pattern fixed on the face plate of the vidicon. This method of measurement is independent of electronic scan stability. The vidicon sensor was selected to provide storage of the picture data for the 200-second transmission time set by the system data link. The actual exposure time for each camera is provided by a mechanical shutter and is set at approximately one second.

A basic block diagram of the television system is shown in Fig. 3-2. The normal sequence consists of a 200-second charge cycle, followed by exposure of the 60° camera and a 200-second read cycle, and finally, exposure and a 200-second read cycle of the 22° camera. In continuous operation, a 60° camera exposure and read cycle will follow immediately. The initial charge cycle is required only at turn-on. In the programmed mode of operation the satellite programmer turns the system on every hour for 10 minutes, thus providing one picture from each camera every hour. For more specialized camera operations, the programmer can be bypassed and the system can be controlled by ground command.

The complete camera system is shown in Fig. 3-3. The electronics packages on the left are the DC/DC converter (bottom) and the TV sequencer (top). The 22° camera head is in the center and the 60° camera head is at the right. Table 3-1 is a summary of the DODGE camera system characteristics. A more complete description of the system characteristics can be found in Ref. 3.1.

3.1.2 Camera Design

The design of both cameras is identical with the exception of the optics and shutter details. The heart of the DODGE cameras is a one-inch diameter vidicon tube whose photosensitive "target" is capable of storing a charge pattern corresponding to an optical image for very long times. An electron gun is used to focus an electron beam

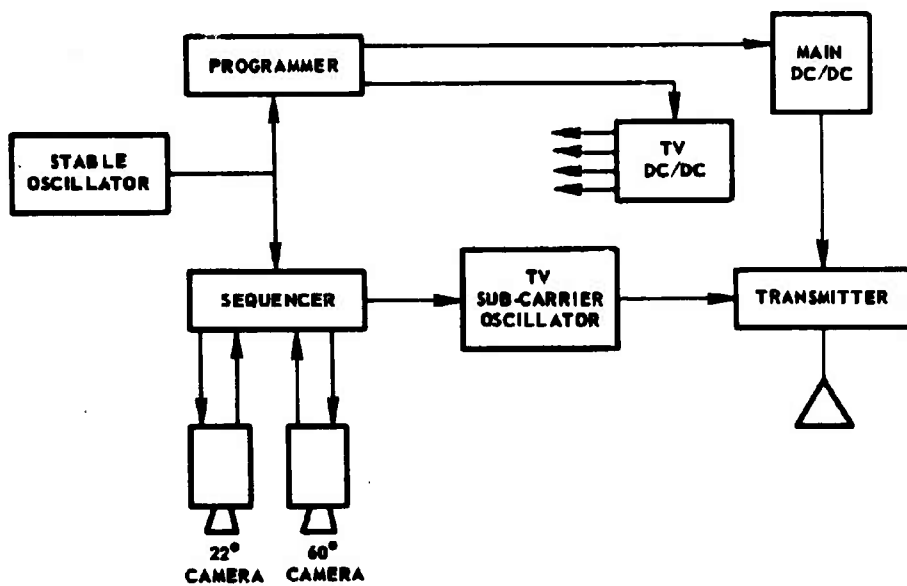


Fig. 3-2 TV SYSTEM BLOCK DIAGRAM

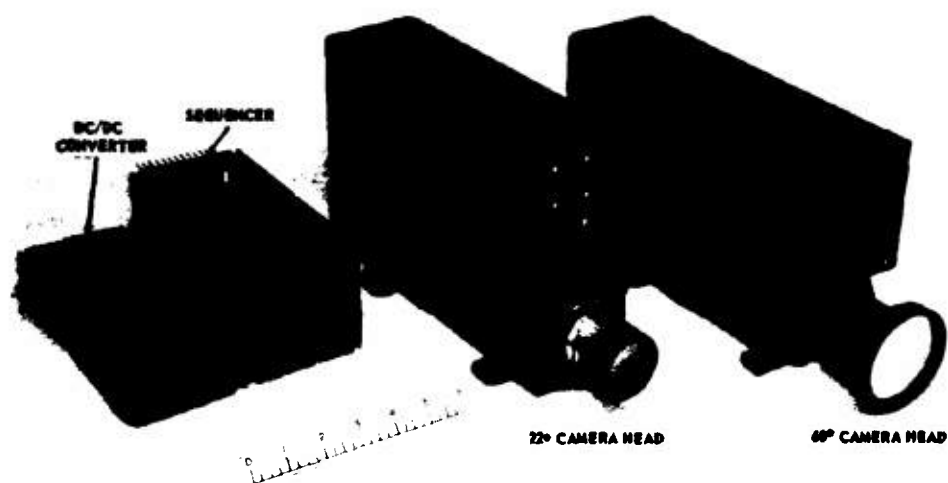


Fig. 3-3 DODGE CAMERA SYSTEM

TABLE 3-1

SUMMARY OF DODGE CAMERA SYSTEM CHARACTERISTICS

Number of Cameras	Two
Prime Sensor	GEC 1" Vidicon 1339-023
Fields of View	22° and 60°
Resolution of Sensor	700 lines limiting
Sampling	512 x 512 per frame
Exposure Time	1.18 seconds
Read-out Time	201.3 seconds
Line Rate	0.393 seconds
Video Bandwidth	651 Hz
Highlight Brightness	10 ⁴ Foot Lamberts
Dynamic Range (Brightness)	— 250:1
22° Lens	Kodak 25 mm Focal Length
60° Lens	Argus 8.1 mm Focal Length
Weight (total)	18.8 pounds
Camera Heads (2)	15.0 pounds
Sequencer	1.1 pounds
DC/DC Converter	2.7 pounds
Power Requirement	8 watts

onto the target area. Deflection of the beam is accomplished electromagnetically. A thin transparent conductive film is used on the glass side (light input side) of the target to act as a signal electrode. A positive voltage is applied at this electrode through a load resistor. In the absence of light, the target will act as a capacitor and the scan beam will charge it to the target potential, the cathode being at ground potential (charge cycle). When a light pattern is imaged on the target, it will selectively discharge. After an appropriate exposure interval, the shutter is closed and the image is stored in the form of a charge pattern. When the target is scanned, a signal output results from the recharging of each picture element (read cycle). The signal output is dependent on the degree of discharge, and hence related to the illumination level. The design can be considered in three main sections: (a) electronic design, (b) optical design, and (c) mechanical design. Although there are obviously very strong interactions among the design efforts, this breakdown will be used for the following discussion. Refs. 3.2 and 3.3 have much additional information on design considerations for the DODGE camera.

3.1.2.1 Electronic Design

The electronic design is fundamentally concerned with operation of the image tube and with extracting and arranging the image information in a form suitable for transmission. A functional block diagram of the camera electronics is shown in Fig. 3-4. All timing information is derived from the 5 MHz satellite oscillator, including shutter pulses, sweeps, beam modulation synchronization, and camera sequencing. The first two stages of frequency division reduce the clock to 1/3 MHz; all further division is binary. The resulting frame time (read time for one picture) is approximately 201.3 seconds and the image is sampled 512 times in each direction during this interval. Neglecting the satellite oscillator offset, the element dwell time (time per picture element) is 768 μ seconds. The time

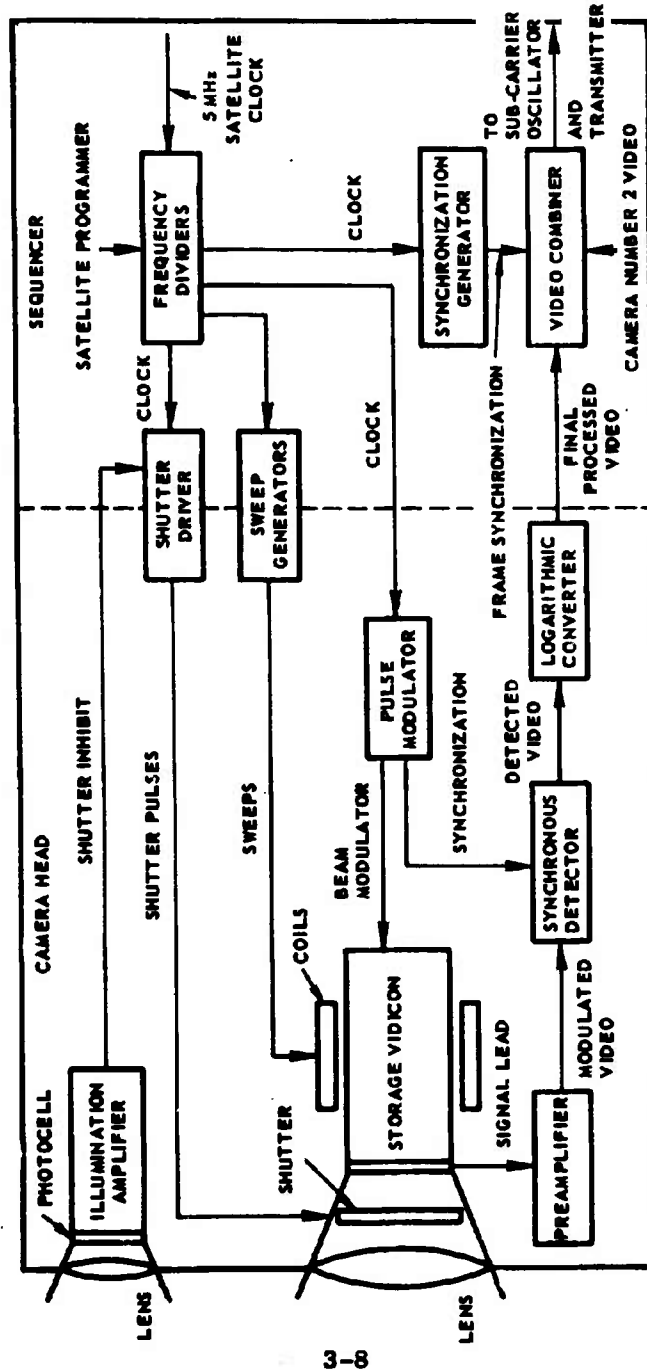


Fig. 4 FUNCTIONAL BLOCK DIAGRAM OF CAMERA ELECTRONICS

per line is 512 times the element dwell time and the frame time is 512 times the line time. The shutter interval is equal to the time of three lines (about 1.18 sec.).

The sweep generators provide the drive currents for the horizontal and vertical deflection coils for the vidicon. The horizontal current driver is a linear ramp generator with the retrace time controlled by the digital logic in the sequencer. The vertical sweep generator provides a staircase output, generated by feeding a resistive ladder chain with binary inputs generated from a counter within the sequencer. As shown in the diagram, the sweep generator function is split between the sequencer and the camera head. The desired waveforms are generated by the sequencer, and a module within the camera head converts the input voltage waveforms into the currents required by the coils. A high degree of feedback is employed to retain the system linearity.

The shutter driver function is similarly split between the sequencer and camera heads. The pulses are generated by the sequencer, and the solenoid drivers are mounted within the camera head. A capacitive discharge is used for driving the shutters. This method has the advantage of providing isolation from the satellite power supply, allows a high voltage solenoid drive for more rapid "pull-in", and provides a simple means for adding a low power holding current for the 60° shutter. Basically the driver circuit consists of a transistor switch which connects a capacitor bank to the solenoid winding when pulsed by the sequencer. The actual operation of the shutters will be discussed below with a description of the shutter mechanisms in the mechanical design section.

The synchronization generator provides the frame synchronization word. The first two lines of each frame are used for synchronization and for camera and filter identification. Each line is divided into four equal segments. The first two segments of each line are used for synchronization, and the remaining segments identify the camera and

filter wheel position. The video combiner commutates between the synchronization words and the video of the two camera heads.

Protection from accidental exposure to the sun is provided by a small lens, a photocell, and an illumination amplifier. The field of view of the protection system lens is slightly larger than the camera field of view. When the sun enters the field of the protection sensor, the high output of the illumination amplifier provides a trigger for a comparator circuit that sets an inhibit for the shutter logic circuitry which in turn prevents the shutter from opening.

The remainder of the circuitry is concerned with the processing of the video from the vidicon. A 768 μsec clock from the sequencer provides synchronization for the pulse modulator to generate both the beam modulation pulse and a set of demodulation pulses. Beam modulation provides a means of capacitively coupling a high gain preamplifier to the vidicon, and reduces the effect of noise components which are independent of the beam current. Fig. 3-5 shows the modulation scheme used in DODGE. As the beam is linearly deflected (a) across the image (b), at the rate of one beam width per dwell time, the beam is pulsed on (c) for 40 μsec , and the corresponding signal current (d) flows through the load resistor. The image is thus sampled by the beam signal function (e) at a series of discrete points. A capacitively coupled amplifier is now used to raise the signal level to a point where it can be conveniently detected. A synchronous detector that couples the output voltage during a 4 μsec interval at the last portion of the beam pulse is used. This sampled voltage is held by a hold circuit for the dwell time of 768 μsec at which point the next sample is taken. The resulting demodulated video is filtered to remove sampling frequency components with a third-order Butterworth filter and then passed through a logarithmic amplifier whose purpose is to distribute the video information uniformly throughout the total dynamic range of the camera. Such an output tends to be equally immune to transmission noise at all levels of illumination.

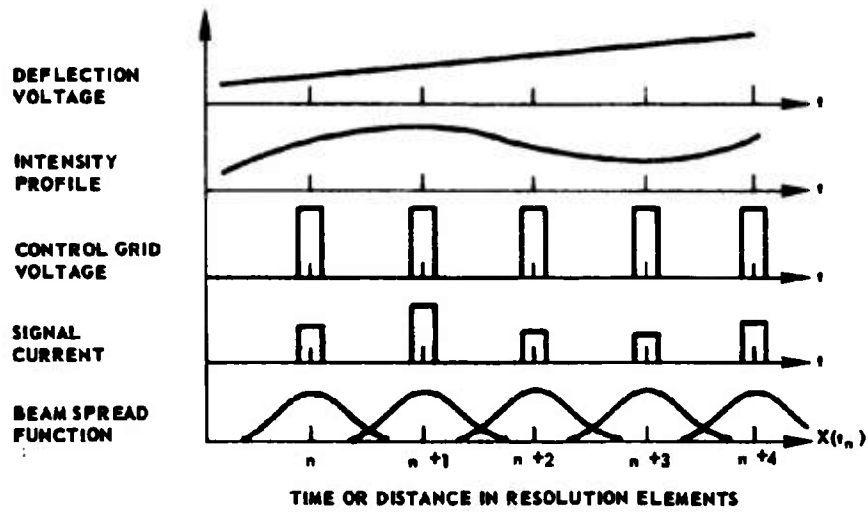


Fig. 3-5 BEAM MODULATION IN THE DODGE CAMERAS

To provide independence from any DC shifts in the preamplifier output, the detector circuit uses two identical sample and hold circuits. One samples during the on time of the beam, as described above, and the other samples while the beam is off. The temporal relationship of sampling for one video sample pulse is shown in Fig. 3-6. The instantaneous difference between these signals represents the demodulated video. The positions of the "on" and "off" sampling points are somewhat critical in eliminating certain types of noise. Sampling near any signal transition must be carefully avoided to eliminate errors caused by capacitively coupled "spikes" originating from the pulses on the vidicon control grid.

A balanced circuit configuration provides temperature compensation for the logarithmic amplifier. In its simplest form, a logarithmic amplifier consists of a semiconductor junction in which the output voltage is proportional to the logarithm of input current. Additional dynamic range can be obtained by substituting a grounded base transistor for the diode (commonly referred to as a Patterson diode), and favorable impedance interfaces are obtained by using the logarithmic element in the feedback loop of an operational amplifier. Temperature variations are greatly reduced by comparing the logarithmic output of one amplifier whose input is the video with that of a similar logarithmic amplifier whose input is a standard reference voltage. Temperature variations of each amplifier remains nearly equal because a good thermal coupling is maintained between the logarithmic elements. The output signal is the difference between the two logarithmic amplifiers.

Filament regulators are used to provide a constant current for the vidicon filaments. Since the vidicons are turned on and off many times, this form of regulation prevents turn-on current surges to the cold filaments which might adversely affect lifetime. In addition, the 60[°] filament regulator provides a means of initial filament warm-up by responding to a signal pulse from the satellite programmer occurring one minute before camera system turn-on.

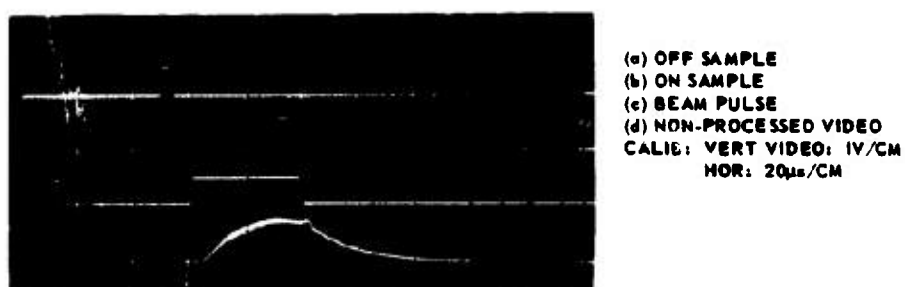


Fig. 3-6 TEMPORAL RELATIONSHIP OF SAMPLING

The camera head electronics is constructed in modular fashion. There are six modules in each camera head, and their functions in terms of Fig. 3-4 are as follows:

- (a) PREAMPLIFIER - corresponds to pre-amplifier and illumination amplifier.
- (b) VIDEO PROCESSOR - contains the low-level-portion of the pulse modulator, sample and hold circuits, differential amplifier, filter, and logarithmic amplifier.
- (c) BIAS AND BEAM MODULATION AMPLIFIER - corresponds to DC biases and high level amplifier portion of the pulse amplifier.
- (d) DEFLECTION AMPLIFIERS - corresponds to the deflection amplifiers (camera head part of the sweep generators).
- (e) FILAMENT REGULATOR - corresponds to filament regulator (not shown in the block diagram).
- (f) SHUTTER DRIVERS - corresponds to the camera head portion of the shutter driver.

A detailed description of the camera head electronics with complete module schematics is contained in Ref. 3.4.

3.1.2.2 Mechanical Design

The mechanical design was primarily concerned with the reliability of the shutter mechanisms, with maintaining alignment of the optical components, and with providing a precision mounting which would maintain the alignment of the cameras within the satellite. Photographs of the shutters for the DODGE cameras are shown in Figs. 3-7 and 3-8. The 60° shutter is similar in design to that flown on NIMBUS except that it has been greatly reduced in

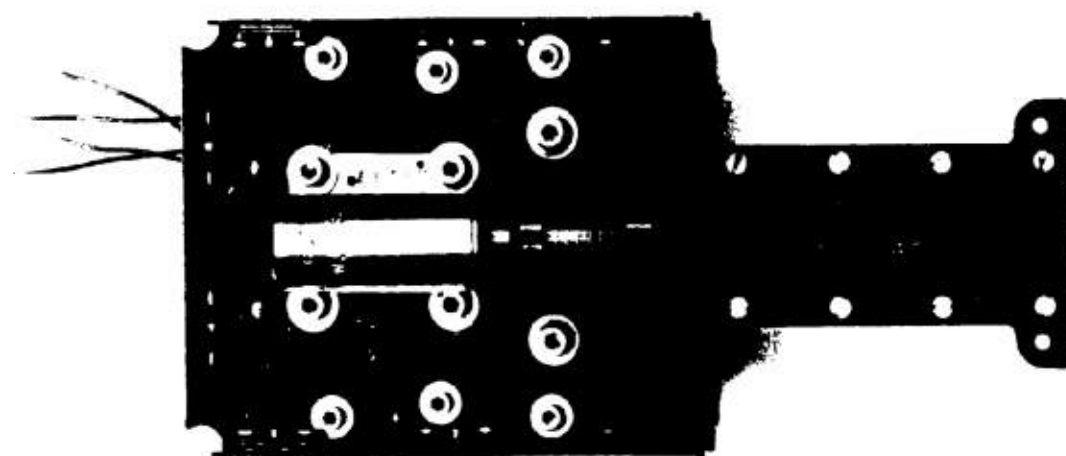


Fig. 3-7 60° SHUTTER ASSEMBLY

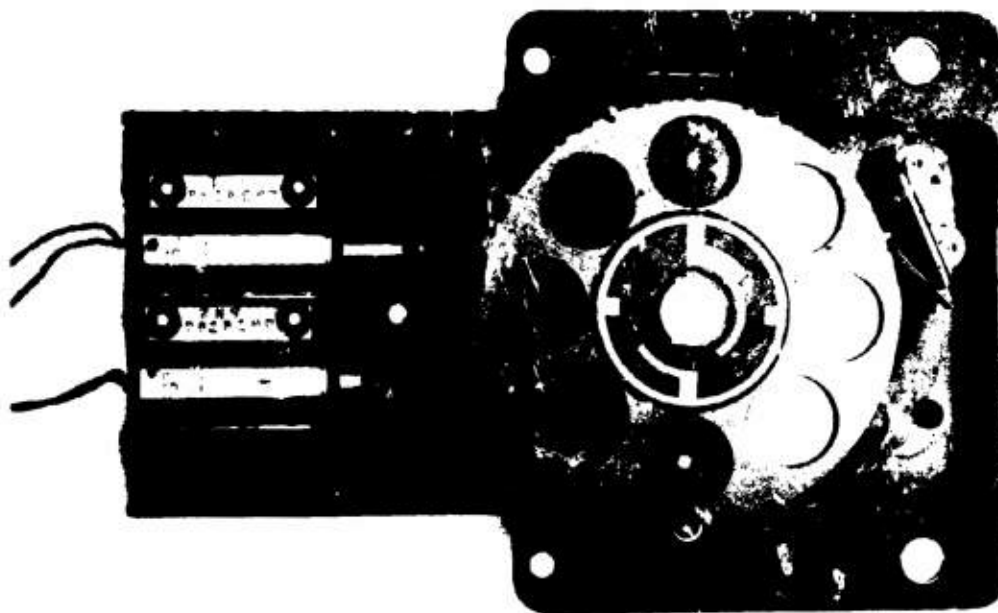


Fig. 3-8 22° SHUTTER ASSEMBLY

size, weight, and power requirements. This shutter consists of two blades, with appropriate apertures, operated by linear solenoids. The blades located between the lens and the vidicon operate in essentially the same manner as the curtains of a conventional focal plane shutter. The aluminum sliding surfaces are hard coated and sealed with Teflon (TUFRAM) for lubricity and long wear. The open blade has its aperture in line with the optical path when its solenoid is activated. The closed blade has its aperture in line with the optical path when its solenoid is not activated. The shutter is opened by activating the open blade solenoid and closed by activating the closed blade solenoid. After the closed solenoid is activated, the open solenoid is released then the closed solenoid is released.

Both blades are returned by the coil springs seen in the figure. The dual slide technique has the advantage of providing symmetrical open and closing characteristics, and with the high voltage capacitive discharge employed, a very rapid "pull-in" is provided. The measured rise and fall times for this shutter are less than one millisecond. A low power holding current is provided by supplying a low voltage line to the solenoid through a diode "or" that supplies sufficient current to hold the solenoid after the capacitor bank is discharged.

In addition to the normal exposure function, the 22° camera shutter must change filters for color work. Accordingly, the design of this shutter is radically different from that of the 60° shutter. The main components are the shutter disc and filter disc, both mounted on the same shaft. The shutter disc is rotated through an arc of 45° by a pair of linear solenoids with a timing belt and sprocket arrangement. Fig. 3-7 shows the filter disc with its position cogs and the filter position encoder. Blank glass was installed in the filter positions at the time this picture was taken. Two edges of the shutter disc which hold the filter wheel drive springs can be seen in the upper right and lower left of the wheel. The shutter is shown in its closed position. When the left solenoid pulls-in, the shutter disc will rotate counter-clockwise 45° such that its aperture becomes aligned with the

optical axis and the upper position of the filter wheel. The spring on the upper right of the shutter disc clears the near cog and when in position, depresses the upper spring to release the wheel for rotation during the close stroke. At the same time the spring at the lower left rotates into position behind the next cog on the filter wheel. When the right solenoid is energized the shutter returns to its closed position and the spring in the lower left drives the filter wheel to the next position. The U-shaped spring in the upper left is held back by the other spring on the shutter disc while the cog previously held by this spring advances. This U-shaped spring then returns to its original position to stop the filter wheel at the next cog. An over-the-center spring is also employed; it prevents the shutter from stopping between the open and closed positions. The filter wheel is hard coated with TUFRAM, and Nylontron bearings are used for the filter wheel and shutter disc. The shutter action is such that the filter wheel advances one position each exposure.

Mounting of the vidicon tube, deflection coils, and magnetic shield for precise alignment within the camera head is accomplished with the items shown in Fig. 3-9. The precision cylinder at the left has accurate bearing surfaces at each end which mate with a precision bore in the main camera mounting frame. The shield, coil assembly, and vidicon shown in the figure are mounted in the precision cylinder with the various spacers shown. The design is such that each internal component carries its load to the outer cylinder through the spacer arrangement. Fig. 3-10 is a drawing of the vidicon tube assembly. It shows more clearly the relationship between the various parts. Note how the front and rear retainers separately position the vidicon, deflection coil, and magnetic shield. The method of connecting to the vidicon target ring is also shown. The spring fingers, which fit into the front retainer, contact the target ring on the tube and are held in position laterally by the spring retainer. A lead is attached to the spring finger ring and brought

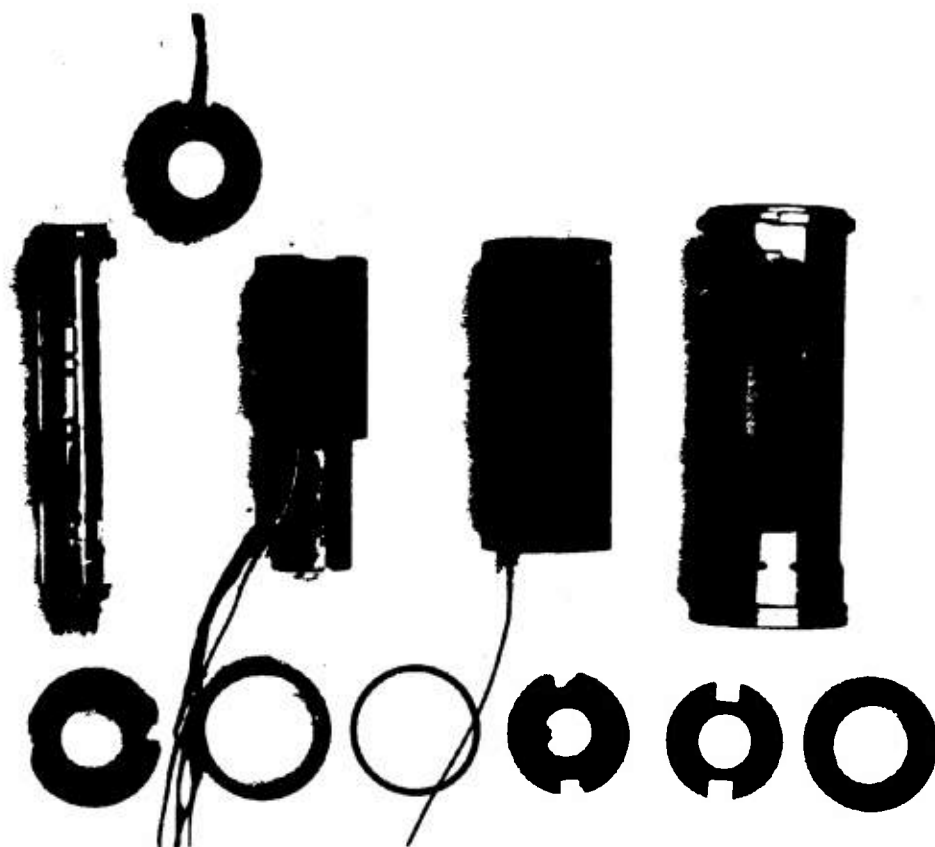


Fig. 3-9 VIDICON MOUNTING HARDWARE

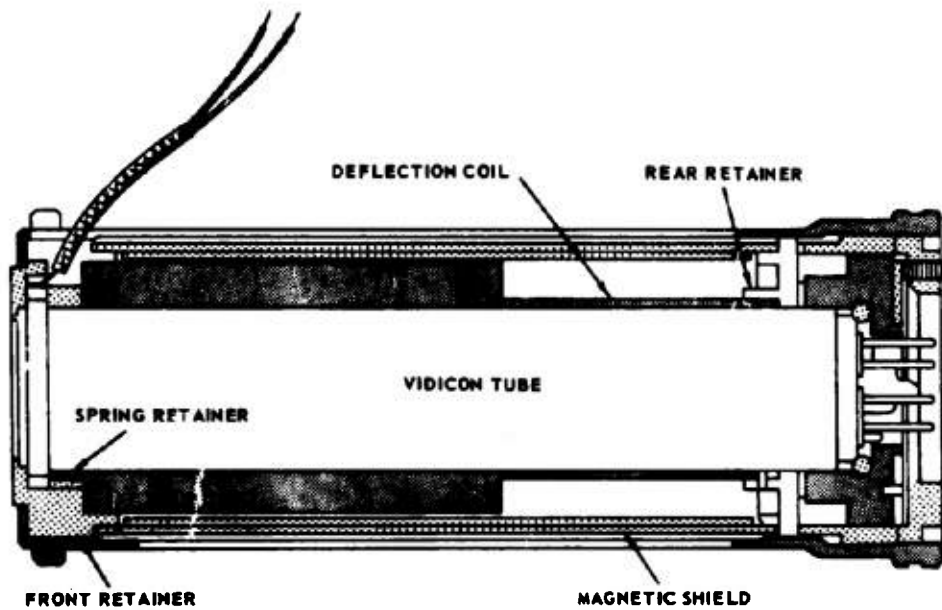


Fig. 3-10 VIDICON TUBE ASSEMBLY, 22° AND 60° CAMERA

through a slot in the front retainer and precision cylinder.

Fig. 3-11 shows the 22° camera head with the cover removed, identifies three of the electronic modules, and shows the wire wrap interconnections. The positions of the inner housing, magnetic shield, and vidicon target lead (input signal lead) are also shown. Two of the four precision mounting feet can be seen behind the reference scale. The mounting feet are machined for a precision surface mount. The mounting positions within the satellite were adjusted to the proper relationship with the attached flange reference plane by adjusting the camera support with Shims as required.

3.1.2.3 Optical Design

The optical design is concerned primarily with lens and filter selections and with the mounting and alignment of the optical components.

The lens selection was governed by the vidicon format, the desired field of view, resolution requirement, weight, ruggedization requirement, and availability. The lenses that best suited the DODGE requirements were a 16 mm camera lens manufactured by Kodak and a special wide angle lens that was designed by Argus for another space program. In the case of the Kodak lens several units were selected from the regular manufacturing line and were reassembled with appropriate cements to be more suitable for the DODGE application.

Filter selection was based on standard color separations for the blue, green, and red filters. However, the standard Wratten filters were not used due to their potential degradation in a radiation environment. The filters are all thin films formed on quartz substrates. The four haze cutoff filters were selected to give a good range of experimental data. The eight positions of the filter wheel contain the four haze cutoff filters, the color separation filters, and a blank position. The seven color positions have all been equalized for equivalent energy response by using

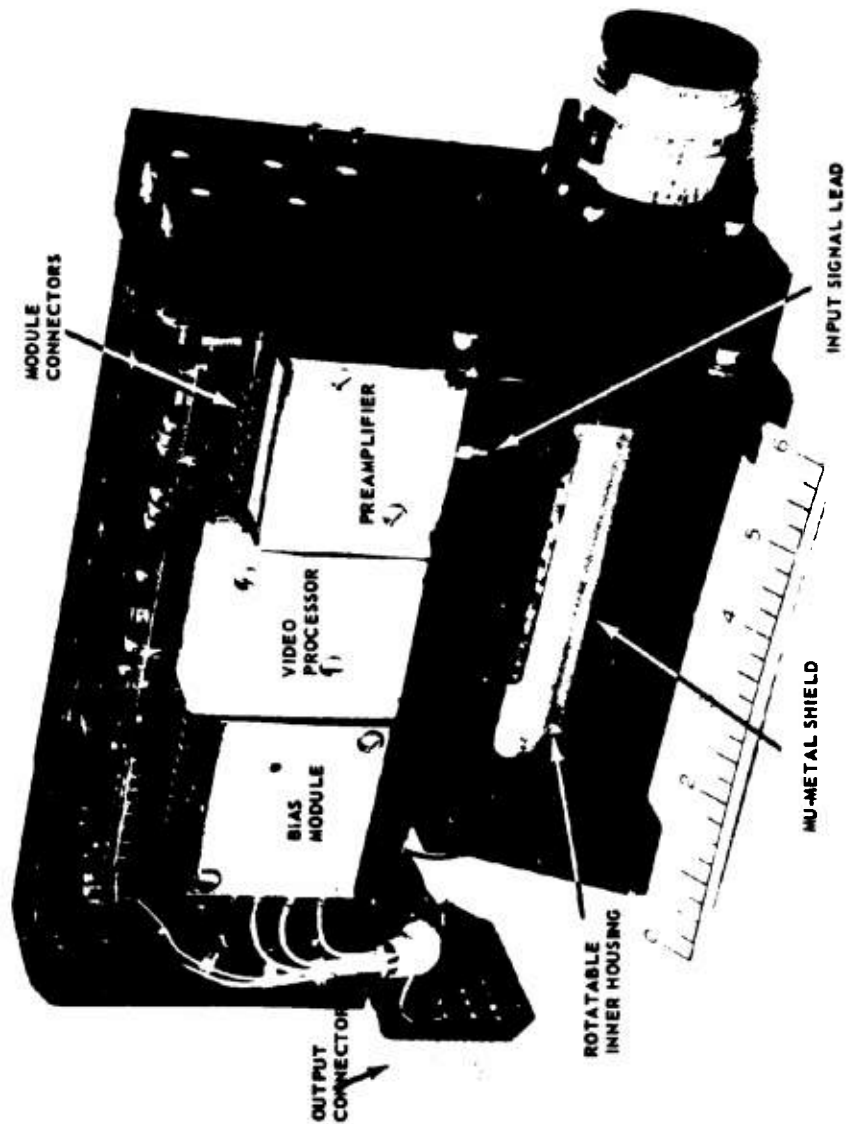


Fig. 3-11 22° CAMERA HEAD ASSEMBLY WITH COVER REMOVED

neutral density filters. Fig. 3-12 shows the measured response of the DODGE primary color filters, before normalization, and Fig. 3-13 shows the measured response of the haze filters. The blank position was not equalized to the other filters and therefore has a greater sensitivity, by a factor of ten, than the other positions.

After the optical components were mounted and aligned, a geometrical calibration was carried out to establish a precise angular displacement to each of the reticle markings on the face of the vidicon. Fig. 3-14 shows the optical arrangement used to perform the alignment and calibration. The alignment telescope-autocollimator and optical rotary table shown have a direct readout capability of one second of arc. The cameras were calibrated to an optical axis that is perpendicular to the lens mounting plane and parallel to the plane of the mounting feet. The reticle positions of the 22° camera are calibrated to an accuracy of 0.05° relative to the reference axis and those of the 60° camera are calibrated to 0.1°.

3.1.3 In-Orbit Performance

The DODGE TV cameras have proved to be effective attitude sensors. Attitude determination is accomplished routinely, giving values for satellite pitch and roll angles within minutes after a picture is received. The filter wheel mechanism on the 22° camera has performed properly, providing the first color pictures of the full earth as seen from deep space. Data have also been gathered on the haze filter experiment included in the filter wheel. The ability to see parts of the satellite within the camera field of view has aided both attitude measurement and picture reproduction. Of particular note, the color pattern on the -Z boom end mass has made it possible to color balance the color photographs. The shutter-inhibit circuit, which prevents accidental exposure of the cameras when the sun is in the field of view, has performed well. All telemetry readouts have been normal.

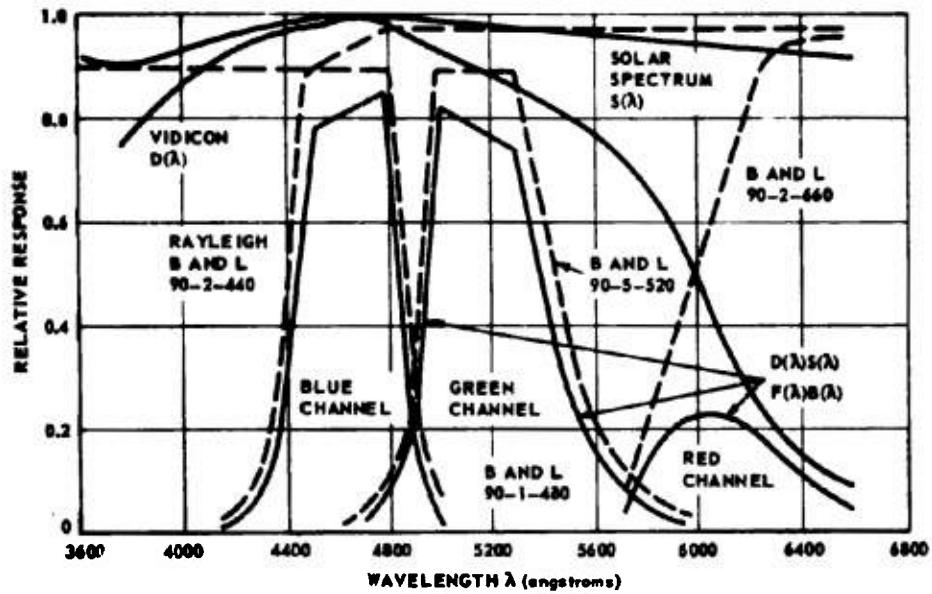


Fig. 3-12 COLOR CHANNEL SPECTRAL CHARACTERISTICS

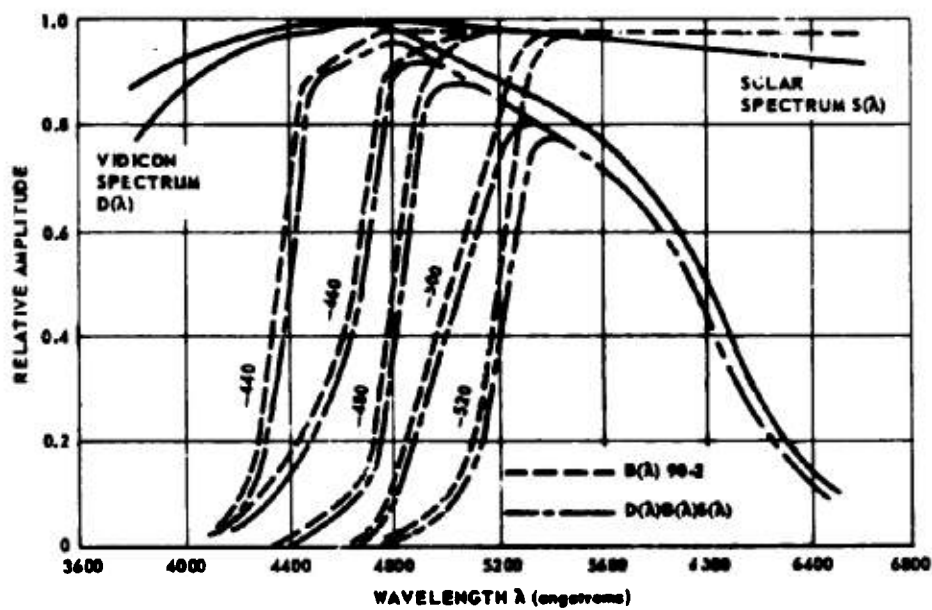


Fig. 3-13 HAZE FILTER CHARACTERISTICS

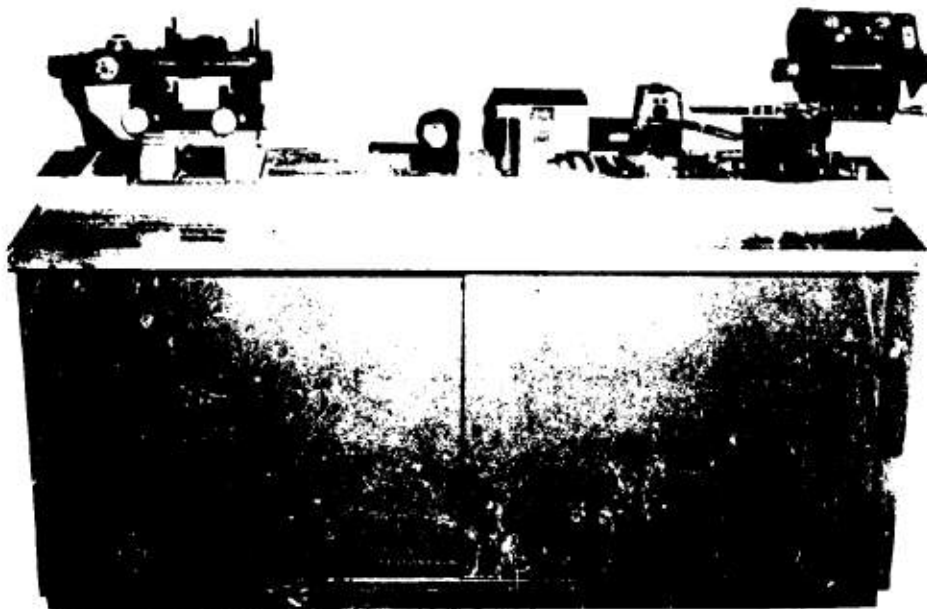


Fig. 3-14 OPTICAL CALIBRATION SETUP

3.1.3.1 Attitude Measurement

Satellite pitch and roll are obtained from the location of the earth's horizon in either the 60° or 22° picture. With reasonable picture illumination, these angles can be determined with an accuracy better than 0.25° from the 22° picture and 1.0° from the 60° picture. Pitch and roll can be obtained immediately from a table or, when combined with solar aspect data in a computer program, complete attitude data can be available within 10 or 15 minutes after receipt of the pictures. The computer calculation is performed on the CDC-3200 at the APL Command and Telemetry station. A data card is punched on the card punch at the Command and Telemetry station immediately after the picture measurements are completed, and the attitude program can usually be run as soon as the cards are prepared. The CDC-3200 program computes pitch and roll to the accuracy indicated above, and computes yaw to an accuracy of approximately 2° . In the smoothing process of plotting the attitude data, the above accuracies can usually be improved by about a factor of two. The normal data processing routine for attitude determination is discussed more fully in Section 3.4.

Figs. 3-15 to 3-17 are pictures taken with the DODGE cameras. The first was taken with 60° camera. The satellite mast structure, two of the antenna elements, and the -Z end mass are seen clearly. Also visible on the mast is a shadow of one of the stabilization booms and several of the reticle marks used for precise attitude determination. The center reticle mark (camera axis mark) can be seen on the earth just above the terminator directly over the end mass. The west coast of South America can be seen to the right of the center reticle mark, and hurricane Beulah directly above it. These earth features are more clearly seen on the 22° picture taken at the same time, shown as Fig. 3-16. Fig. 3-17 is a picture taken through the blank position of the filter wheel. This filter position has the effect of increasing the camera sensitivity by a factor of ten, causing most of the earth to appear white

THE JOHNS HOPKINS UNIVERSITY
APPLIED PHYSICS LABORATORY
SILVER SPRING MARYLAND

NOT REPRODUCIBLE

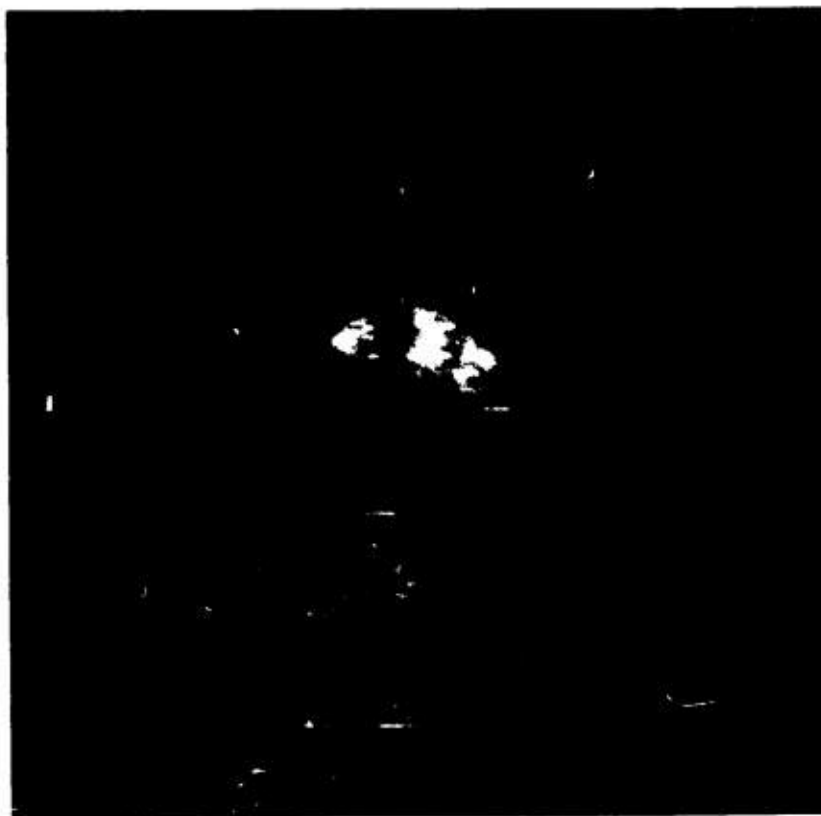


Fig. 3-15 EARTH FROM THE 60° DODGE CAMERA

NOT REPRODUCIBLE



Fig. 3-16 EARTH FROM THE 22° DODGE CAMERA

NOT REPRODUCIBLE

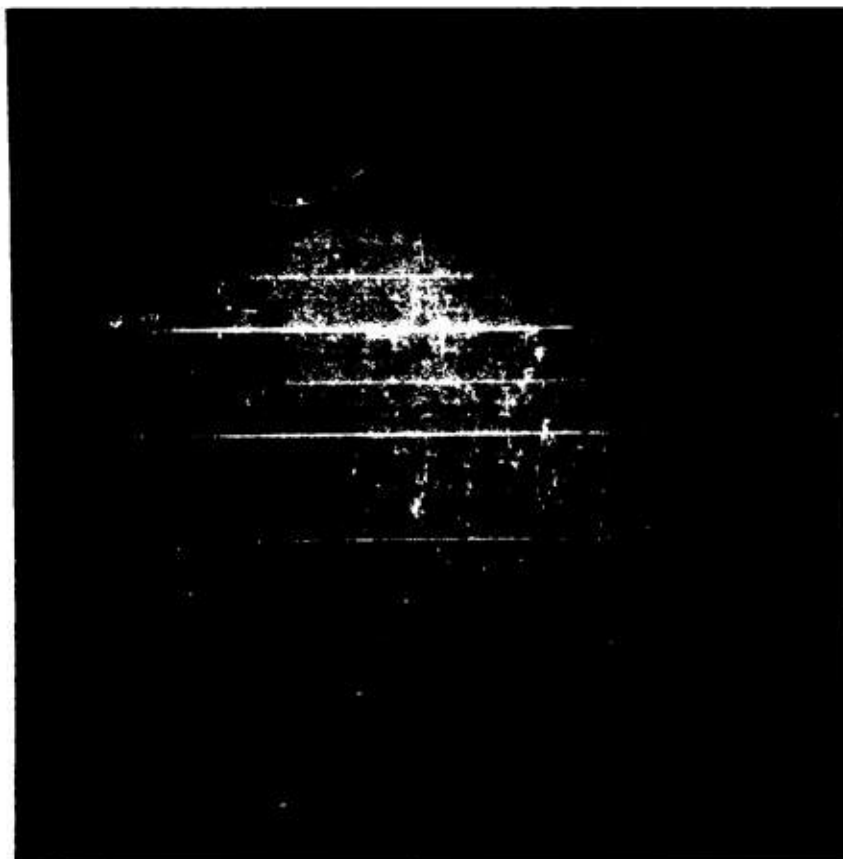


Fig. 3-17 EARTH THROUGH THE BLANK POSITION OF THE 22° DODGE CAMERA

in the picture. An interesting feature of this picture is the presence of the moon. The moon can be seen due east of the terminator toward the upper right corner of the picture. The camera reticle pattern is also more clearly seen against this light background. None of these pictures has been processed in any way except to alter the range of the video information to insure maximum utilization of the dynamic range of the cathode-ray tube and film combination of the TV reproducer.

3.1.3.2 Multispectral Experiment

As indicated above, a secondary objective of the DODGE camera was to provide multispectral picture data of the earth as seen from the near synchronous altitude region. It should be recalled that the 22° shutter automatically advances the filter wheel one position each exposure. Therefore, each sequential set of eight pictures contains a full data set. However, when the camera is operating on a once per hour basis the variations in scene content frequently restrict comparisons to adjacent filter positions. The best data gathered for this experiment were obtained from continuous data runs wherein pictures were taken with the 22° camera every six minutes. Many short continuous sequences have been run, but the most complete data for this experiment were obtained during two long term continuous runs on Days 206-207 and Day 263 of 1967. These two runs have provided several hundred pictures for analysis.

3.1.3.3 Engineering Performance

From an engineering standpoint, the camera performance has been exceptional. While the raw received pictures have several undesirable characteristics in a photographic sense, the performance of the cameras has been nominal in every sense and totally suitable to the planned mission objectives. Fig. 3-18 is a plot of the temperatures at each camera head and at the control electronics during a recent pass. The 22° focus voltage is also plotted as a representative

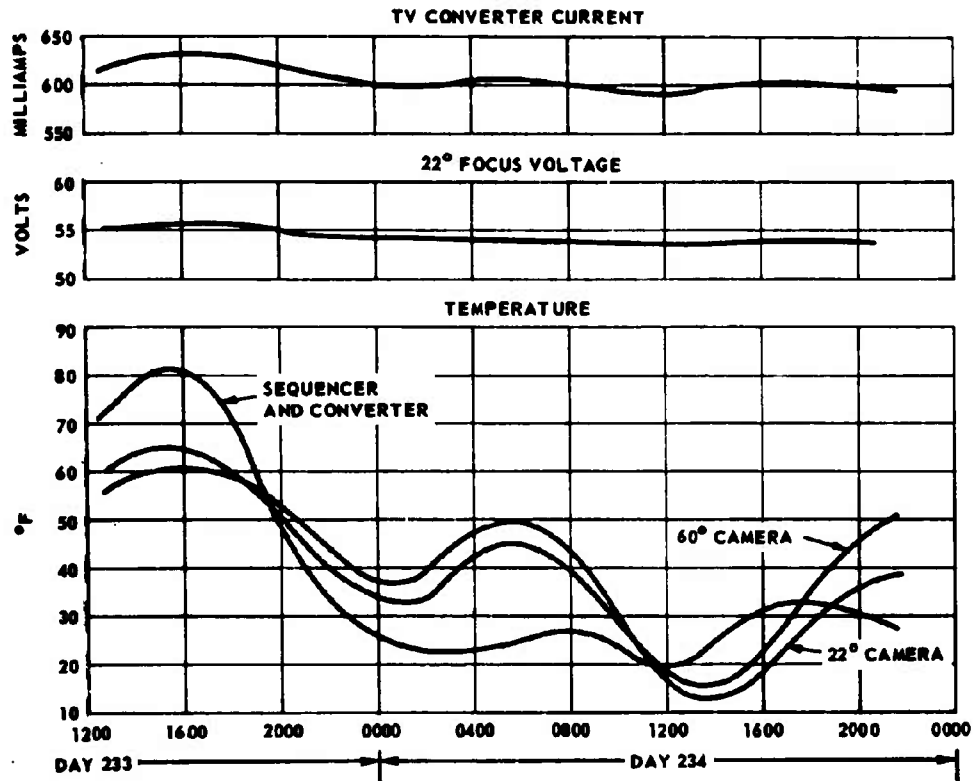


Fig. 3-18 DODGE CAMERA PERFORMANCE DATA-DAYS 233 AND 234, 1968

output of the regulated TV DC/DC converter, and the converter input current is shown. The lowest temperature at which the cameras have had to perform has been about -5°F ; the highest temperature has been about 90°F . The maximal daily thermal variation has been about 85°F ; the typical daily variance is about 45°F . The output voltages of the converter have been maintained generally to within 1%. The largest noted voltage variation over a full year has been less than 5%. The converter input current tends to vary slightly with temperature as can be noted in the figure.

3.2 Solar Attitude Detectors

3.2.1 Cosine Detectors

Analog solar attitude detectors are mounted on each of the satellite axes in order to permit the unique determination of the orientation of the spacecraft relative to the sun with an accuracy of $\pm 1^{\circ}$. Typically, two types of detectors are employed. The first, termed a "cosine" detector consists of a pair of N/P silicon solar cells, with protective sapphire cover windows, which are series connected and individually loaded near short circuit conditions. Two cells are used to minimize temperature sensitivity. In order to make use of the full range of the telemetry system (± 0.250 volts) the cells are biased in the reverse direction by an ultrastable voltage regulator so that when not illuminated a voltage of approximately $+0.250$ volt is provided. As the illumination increases, the voltage output from the detector decreases to an extreme of approximately -0.250 volt at normal solar incidence. The voltage output of this type of detector is essentially a cosine function of the angle of incidence.

3.2.2 Linear Detectors

The second type of detector has been designed to fill in the region near normal incidence where the cosine detector response is nearly flat. It consists of a circular cell inside a cylindrical well and has an output which is nearly a linear

function of angle of incidence from 0° to the design cutoff angle. The linear detectors are also reverse biased to make full use of the voltage range of the telemetry system. Two such sensors are employed. Cutoff angles are nominally 45° and 60° . A DODGE-type detector is shown in Fig. 3-19.

A typical calibration curve is shown in Fig. 3-20.

3.2.3 Bias Voltage Regulator

Bias voltage for all detectors is provided by an ultrastable voltage regulator of special design. Output of the regulator is 6.455 volts $\pm 0.1\%$ over a temperature range of -25°F to $+145^\circ\text{F}$ with a supply voltage ranging from 9 to 12 volts.

3.2.4 Detector Construction

The heart of the detector is a $5/16$ inch diameter N/P silicon solar cell. The cell has titanium-silver sintered contacts which have been solder dipped. Electrical "N" contact is made to the solar cell by soldering the cell into a Kovar-"A" mask that reduces the exposed active area to a circle of 0.191 inch in diameter. The mask also provides mechanical reference surfaces to align the detector within the outer aluminum housing. The "P" contact is made to the cell by soldering a Kovar-"A" tab to the rear face. Kovar-"A" was selected for the contact material since its coefficient of thermal expansion is almost identical to that of silicon over a broad range of temperatures. This design has allowed the detectors to survive repeated quenches in liquid nitrogen from initial temperatures in excess of 200°F . The cells are protected from particle irradiation by a UV grade sapphire window that has a thickness of 0.030 inch. No adhesive is employed between this window and the solar cell detector. The window is bonded to the anodized aluminum outer housing to preclude darkening adhesives from degrading the sensor output.

NOT REPRODUCIBLE



**Fig. 3-19 DODGE TYPE SOLAR ATTITUDE
DETECTOR**

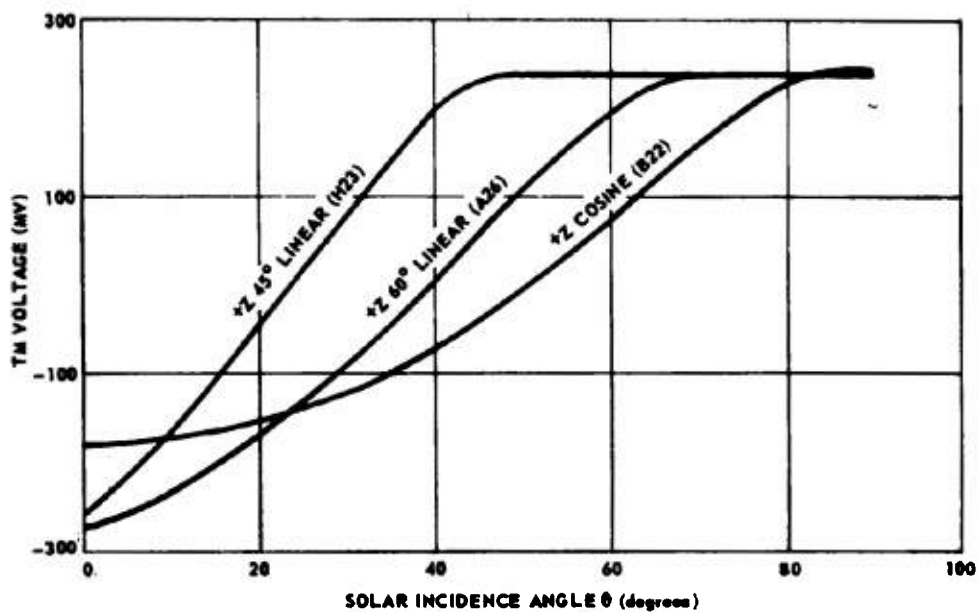


Fig. 3-20 DODGE +Z AXIS SOLAR ATTITUDE DETECTOR OUTPUT AT 77° F
AS A FUNCTION OF SOLAR INCIDENCE ANGLE (PRELAUNCH CALIBRATION)

Wire connections soldered to the Kovar contacts are brought up to a terminal board within the aluminum housing in order to provide strain relief. The terminal board is bonded to the outer aluminum housing. The board is also used to seat the Kovar mask (with cell) against the upper flange in the aluminum housing. The entire assembly is then mounted to an aluminum base on which a printed circuit board is mounted. The printed circuit board has terminals to which resistors and leads are soldered. No wires are soldered directly to the board. Redundant ground leads are provided from all sensors.

3.2.5 Detector Calibration

The telemetered output of a DODGE detector in millivolts is given by:

$$(1) \quad V_{TM} = V_d - k_m k_\theta k_t V_c$$

Where:

V_d - dark reference voltage (mv)

k_m - correction to mean solar intensity

k_θ - correction for solar incidence angle

k_t - correction for detector temperature

V_c - unbiased detector voltage calibration at normal incidence and 77°F (mv)

Calibration of the detector was performed both in natural sunlight and in a laboratory solar simulator employing tungsten and xenon lamps to simulate space sunlight in both intensity and spectral distribution.

3.2.5.1 Normal Incidence Calibration

The calibration constant V_c is defined as the voltage across the cell at 25°C under normal incidence illumination in space at mean solar intensity of 140 mw/cm². This calibration is performed through the use of a laboratory solar

simulator manufactured by Optical Coating Laboratory, Santa Rosa, California. Values obtained for V_c and V_d for each of the DODGE detectors are provided in Table 3-2.

3.2.5.2 Calibration for Output With Variations in Incidence Angle

The calibration of k_θ vs θ was performed in an APL designed collimating tube which "tracks" the sun to an accuracy of 0.1° . The detector under test was mounted on a rotary tilt table at the base of the collimating tube. The table was tilted through known angles with the collimating tube axis while monitoring the detector output. The results were repeated for several solar azimuths by rotating the table and repeating the procedure in order to verify that each detector output was independent of solar azimuth. Table 3-3 gives the results of this calibration for both the cosine and linear detectors.

3.2.5.3 Temperature Calibration

The effect of temperature upon detector output was investigated through the use of the laboratory simulator and natural sunlight. The results of this calibration (k_t) as obtained for the DODGE satellite are given in Table 3-4. The temperature for each detector is obtained from the telemetered output of a sensistor mounted on the solar panel near the detector.

3.2.5.4 Correction to Mean Solar Intensity

Due to the ellipticity of the earth's orbit around the sun, the solar intensity is a function of Day Number (D). The variation in intensity is approximately +3.5% about the mean of 140 mw/cm^2 . The correction to mean solar intensity (k_m) is very closely approximated by

$$k_m = 1.0 - 0.035 \cos \left[\frac{360}{365} (D-1) \right]$$

3.2.6 In-Orbit Performance

The DODGE cosine analog solar attitude detectors have demonstrated excellent performance in orbit. The yaw error attributable to the solar

TABLE 3-2
DODGE SOLAR ATTITUDE DETECTORS
PRELAUNCH CALIBRATION CONSTANTS

Sensor	Channel	V_d (mv)	$V_c @ 77^\circ F$ (mv)
+X Cosine	B 20	244	432
+Y Cosine	B 21	244	425
+Z Cosine	B 22	244	423
-X Cosine	B 23	244	421
-Y Cosine	B 24	244	453
-Z Cosine	B 25	244	431
+X 60° Linear	A 24	236	456
+Y 60° Linear	A 25	234	466
+Z 60° Linear	A 26	236	508
-X 60° Linear	A 24	236	475
-Y 60° Linear	A 25	234	482
-Z 60° Linear	A 26	236	464
+X 45° Linear	H 20	236	444
+Y 45° Linear	H 21	235	450
+Z 45° Linear	H 23	236	496
-X 45° Linear	H 20	236	452
-Y 45° Linear	H 21	235	499
-Z 45° Linear	H 23	236	460

TABLE 3-3
DODGE SOLAR ATTITUDE DETECTORS NORMALIZED DETECTOR OUTPUTS
AS A FUNCTION OF SOLAR INCIDENCE ANGLE

Angle θ (Degrees)	Cosine k_{θ}	60° Linear k_{θ}	45° Linear k_{θ}
0	1.000	1.000	1.000
5	0.996	0.970	0.915
10	0.985	0.921	0.816
15	0.966	0.861	0.698
20	0.940	0.797	0.570
25	0.906	0.723	0.443
30	0.862	0.644	0.325
35	0.810	0.550	0.202
40	0.745	0.455	0.083
45-	0.671	0.356	0.013
*48	0.625	0.297	0.000
50-	0.591	0.260	
55	0.500	0.164	
60	0.404	0.079	
65	0.300	0.020	
*69	0.218	0.000	
70	0.200		
75	0.110		
80	0.042		
85	0.008		
*88	0.000		

*Sensor cut off angles.

Table 3-4

DODGE SOLAR ATTITUDE DETECTORS
TEMPERATURE CORRECTION FACTORS

Temperature (°F)	Cosine k_t	45°, 60° Linears k_t
50	1.000	1.007
60	1.000	1.005
70	1.000	1.002
*77	1.000	1.000
80	1.000	0.999
90	1.000	0.992
100	1.000	0.985
110	0.999	0.976
120	0.998	0.967
130	0.997	0.957
140	0.995	0.944
150	0.992	0.930
160	0.988	0.913
170	0.980	0.896
180	0.970	0.876
190	0.955	0.852
200	0.930	0.820
210	0.905	0.778

*Datum Temperature = 77°F

sensors is typically $\pm 2^\circ$. Only one in-orbit calibration has been required since launch. Because of the excellent performance of this design on both DODGE and GEOS-2, it has been standardized for all future APL satellites.

3.3 The Use of the Vector Magnetometer System in Attitude Detection

The use of vector magnetometer data in conjunction with solar aspect data (from analog sun sensors) is a well-established technique for satellite attitude detection at low satellite altitudes. It is used regularly in the Navigation Satellite Program, in the GEOS series of satellites, in the Direct Measurement Explorer (DME-A) satellite, and in others. One uses a mathematical model of the earth's field to determine the field orientation in space, then the satellite data are used to find the satellite orientation in space. This process obviously depends on the accuracy and reliability of the mathematical model of the field.

At low altitude (i.e., 0 to 5000 n.mi.) the magnetic field is dominated by earth-bound current systems that are fairly stable and predictable. Mathematical models of the field in this region are believed to be generally reliable to an accuracy of 100 to 500 gamma (1 gamma = 10^{-5} oersted). At DODGE altitude of 18,200 n.miles, these same models predict a field of only 100 to 200 gamma. Obviously the accuracy and reliability of the available models are not adequate at the DODGE altitude. Furthermore the field is no longer primarily due to earth-bound current systems, but depends to a significant extent on current systems in the magnetopause, that region where the solar wind and the earth's field interact.

One of the secondary objectives of DODGE is to learn more about the field at high altitude for purposes of mathematical modeling and possible attitude determination. This effort has been seriously hampered by the spurious variable biases in the magnetometer data, discussed previously in Section 2.2.3.1. The available mathematical models predict that the local magnetic field will be

predominantly north in direction, and ranging from 100 to 200 gamma. This prediction has been grossly confirmed by DODGE. When the satellite is three-axis stabilized the sensor aligned with the north-south axis generally shows the stronger component of field and generally positive northward. At certain times during the day when bias effects dominate this may be true.

The general observation that the field is northward has been used for gross attitude determination when the satellite was tumbling and TV pictures of the earth were unavailable. The magnetometer data were also used as a reliable indication of satellite rotation rates during the initial despin phase after injection into orbit.

3.4 DODGE Attitude Detection Procedure

3.4.1 Pitch and Roll Determination - Reduction of Televised Earth Pictures

In the DODGE attitude rotation sequence, pitch and roll are uniquely defined by the location of the satellite subpoint in the television picture. The subpoint is rarely identifiable as a geographic feature in the picture. However, it is mathematically related to the earth's horizon which is readily identified. Consequently, the earth's horizon is first located in order to determine pitch and roll.

Figs. 3-21 and 3-22 illustrate the transparent overlays used to establish the coordinate grids for 22° and 60° pictures, respectively. The dotted outline is the portion of the stack visible in each picture, and the circles correspond to reticle marks. The grid lines are separated by 0.2 inch. For an angular displacement, α , from picture center, the linear displacement in inches is $7.88 \tan \alpha$ in the 22° picture and $2.77 \tan \alpha$ in the 60° picture.

The effect of displacement of the camera axis from the local vertical is shown in Fig. 3-23. As the local vertical angle increases, the horizon outline becomes more elliptical and the subpoint moves away from ellipse center.

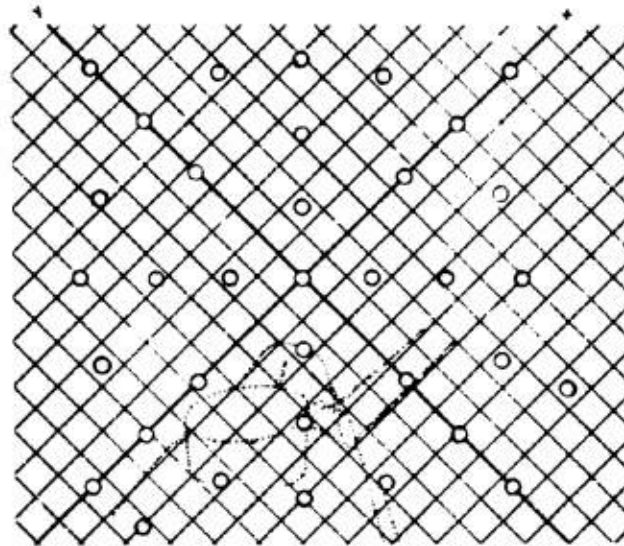


Fig. 3-21 .COORDINATE GRID TEMPLATE FOR 60° CAMERA

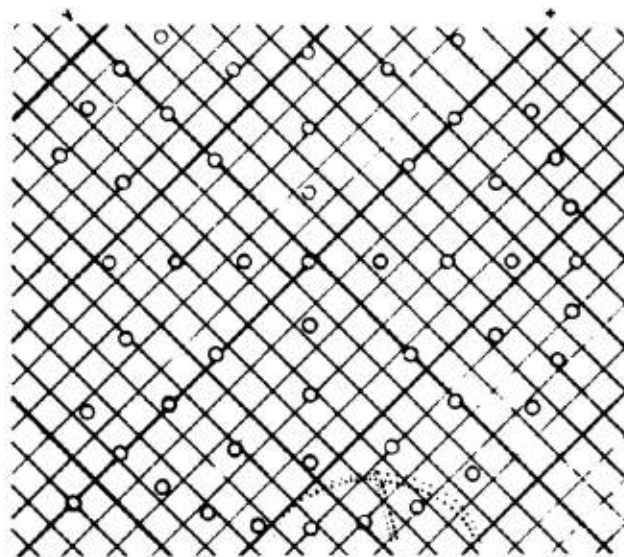


Fig. 3-22 COORDINATE GRID TEMPLATE FOR 22° CAMERA

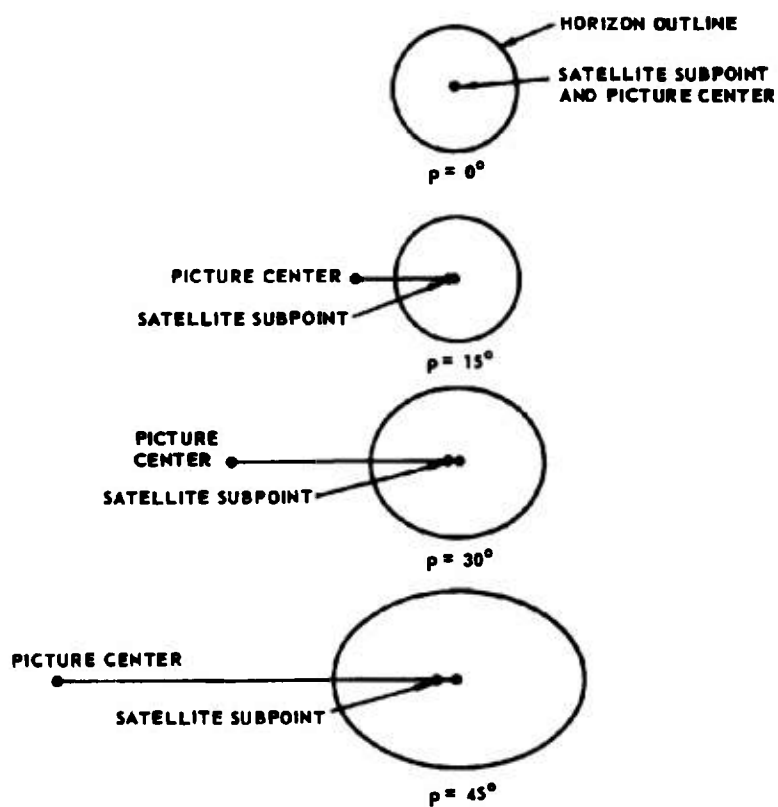


Fig. 3-23 TYPICAL HORIZON-SUBPOINT OVERLAYS
FOR VARIOUS LOCAL VERTICAL ANGLES

Prior to launch, separate horizon-subpoint overlays were made for local vertical angles from 0° through 10° in 1° steps and 15° through 45° in 5° steps. However, after a few passes the circular (0°) overlay was used exclusively to facilitate rapid reduction of pictures during satellite operations. The maximum error introduced into pitch and roll determination by this process is 1.4° at a local vertical angle of 45° . At 30° the error contribution is 0.7° . Although this error can be corrected mathematically, it has not been found necessary to do so.

The satellite subpoint can be located to $+0.05$ inch for local vertical angles less than 25° . This corresponds to $+0.3^\circ$ for the 22° picture and $+1.0^\circ$ for the 60° picture. For local vertical angles between 25° and 45° , the accuracy degrades to $\pm 2^\circ$ for the 60° picture.

Location of the satellite subpoint in picture coordinates is shown in Fig. 3-24. Pitch and roll may be determined either from a pre-computed table or as part of the DODGE Attitude (DATT) computer program. DATT is implemented on both the CDC-3200 computer at APL station 502 and the IBM-7094 in the APL computer center.

3.4.2 Yaw Determination

3.4.2.1 Operational Method Using Analog Solar Attitude Detectors

Once pitch and roll are known, a vector known in body and orbit coordinates and not parallel to the local vertical is required to determine yaw. Except for brief periods around satellite local noon and midnight, the sun vector fits this requirement. The orbit coordinates of the sun vector are generated within the computer program. The body coordinates are obtained from the cosine analog solar attitude detectors (see paragraph 3.2). The accuracy of the yaw angle determination is approximately $\pm \frac{2^\circ}{\sin \mu}$, where μ is the angle between the sun vector and the local vertical. Near satellite local noon, the yaw becomes indeterminate. Near local midnight, yaw determination



NOT REPRODUCIBLE

DODGE TV PICTURE TAKEN WITH 60° CAMERA
AT 10:33 AM EDT ON 1 OCTOBER 1967

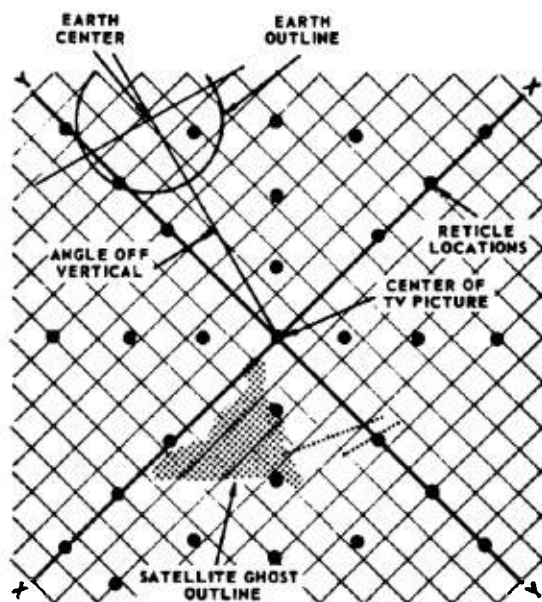


Fig 3-24 REDUCTION OF DODGE TELEVISION PICTURE OF EARTH

is academic because the camera shutter is inhibited when the sun is in the field of view (see paragraph 3.1).

3.4.2.2 Alternate Method Using Terminator Cusps

The use of the earth's terminator line to determine yaw is not straightforward. The mathematics appears to be hopelessly complex and the terminator is poorly defined on the surface of the earth.

However, the terminator cusps which occur at the intersection of the terminator and horizon can be located in the picture. The mathematics for these two points is reasonably simple. A computer program was implemented to predict the locations of the cusps in the picture. Inverse pitch and roll transformations were applied to the cusp picture coordinates. The angle by which the predicted cusps had to be rotated to coincide with the transformed cusps was yaw.

This method was tried during the sixth and eighth APL passes. However, the yaw angles disagreed by as much as 10° with those obtained from the analog solar attitude detectors. The most likely source of error is imprecise location of the cusps either from terminator irregularity or poor picture resolution. This method cannot be used at local noon or local midnight when there are no terminator cusps.

3.4.2.3 Alternate Method Using Identifiable Geographic Features

Yaw can be determined from the picture coordinates of identifiable geographic features. Inverse pitch and roll transformations are applied to the picture coordinates of identifiable features. The predicted picture coordinates can be calculated by hand or computer. As with the terminator cusp method, the rotation angle required to align predicted and transformed coordinates is yaw.

This procedure was attempted on a picture of Africa from APL pass eight. Approximately nine prominent points such as Gibraltar, Benghazi, the

Sinai Peninsula tip, and Cape St. Vincent on the Portugal Coast were identified. The rms yaw was 1° , and the mean value differed from that determined from analog solar attitude detector data by 2° .

The identifiable feature method works at satellite noon. However, since it is time consuming, it is not suitable for support of satellite operations. This method is best suited for intensive study of selected pictures.

3.4.3 Data Reduction

DODGE attitude sensor data are reduced on a real time basis at APL station 502. For every 60° picture and every 22° picture which contains the earth or is shutter inhibited, the following data are transferred to punched cards:

- a. Greenwich Mean Time. The year, day, and time in hours and minutes.
- b. Picture Data. If the earth is visible in the picture the subpoint coordinates and camera (22° or 60°) are entered. If the earth is not visible, a code is entered to indicate whether the earth is not in the 60° field of view, the 60° camera is inhibited, both cameras are inhibited or the 60° picture is unusable.

The DATT program on the CDC-3200 then calculates the geographic location of the satellite subpoint and the libration angles pitch, roll, yaw, in-plane, and cross-plane. If attitude is not available, the reason (shutter inhibit, no sun data, etc.) is printed in the appropriate data column. The plots of these angles are kept current to support satellite operations.

The attitude data collected above must be edited and corrected prior to dissemination as a pass report. This is done by the Data Reduction Project of the Instrumentation Development Group. The punched cards are run on the IBM 7094. In

addition to generating a printout of the libration angles, the 7094 also generates punched cards which contain the libration angles, solar data, and magnetometer data in a format suitable for an automatic data plotter. An additional set of cards is generated to serve as an input to any computer programs that require DODGE attitude data as an input.

The final plots are then annotated with the significant events (such as boom operations) that affect attitude. These plots along with the computer data printout are disseminated as a DODGE pass report.

3.4.4 Summary and Conclusions

The use of televised earth pictures and analog solar aspect sensors to determine DODGE attitude has been extremely successful. This method has worked so well that it has not been necessary to resort to any contingency procedures. The television cameras have taken 10,000 pictures without a failure. Although the picture quality is degraded while the inverter is on, attitude can still be determined. The solar attitude detectors have exhibited reliable and accurate operation since launch. The DODGE and GEOS-2 missions have shown this solar sensor design to be particularly useful in attitude detection.

One important advantage of the television camera is that total attitude can be obtained from the picture of the earth. Pitch and roll are obtained from the tables, and yaw is obtained by rotating the picture until the terminator or some identifiable feature is correctly aligned. This has often been done to obtain "quick-look" coarse yaw when attitude detection at Station 502 is not current.

3.5 References

- 3.1. Thompson, T., "The DODGE Television System," APL Technical Digest, Vol. 6, No. 5, May-June 1967.

- 3-2. Beal, R. C., "Design and Performance of the DODGE Cameras," APL Technical Digest, Vol. 6, No. 5, May-June 1967.
- 3-3. Schenkel, F. W., "Photometric and Optical Considerations in the DODGE Satellite TV Camera Design," *ibid.*
- 3-4. Beal, R. C., "The Electronic Design of the DODGE Camera Heads," TG-963, February 1968.

BLANK PAGE

4. ELECTRIC POWER SYSTEM

4.1 Solar Array

4.1.1 Design Characteristics

The electrical power for operation of the DODGE satellite is derived from approximately 6000 silicon solar cells distributed on 20 body mounted solar panels, Fig. 4-1. Each solar cell is a 2cm x 2cm, 12 mil thick, N on P solar cell of nominal 10 ohm-cm base resistivity. A 6 mil thick Corning 0211 glass microsheet cover slide, with "blue" filter and antireflective coating, was bonded to each solar cell with Sylgard 182 adhesive. The primary purpose of the cover slide is to protect the cell against damage due to particle irradiation in the space environment.

Each solar panel is configured with series-parallel matrices of cells to enhance the reliability of the array. The array is subdivided into four distinct arrays as shown in Fig. 4-2. The start of life power available from each array is as follows:

Array	Average Power (watts)	Maximum Instantaneous (watts)
Main	18	25
Auxiliary 1	14	21
Auxiliary 2	10	19
Command	3	5

As can be noted in Fig. 4-2, the main array is permanently connected to the main bus while the auxiliary 1 and auxiliary 2 arrays may provide power to either the main bus or resistive heaters upon ground command. The command array supplies power directly to one of two redundant command converters. The relatively small but separate command array thus insures that the command system will be maintained operative even with a voltage fault on the main bus.

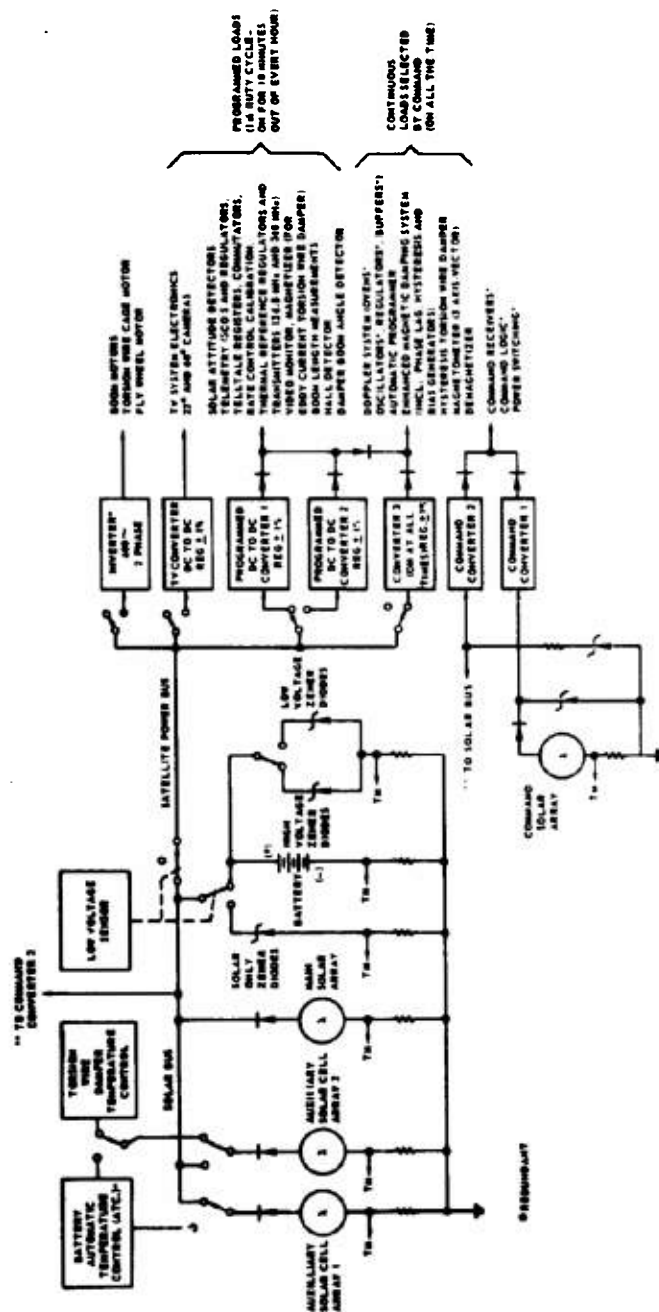


Fig. 4-1 BLOCK DIAGRAM OF SATELLITE ELECTRICAL SYSTEM

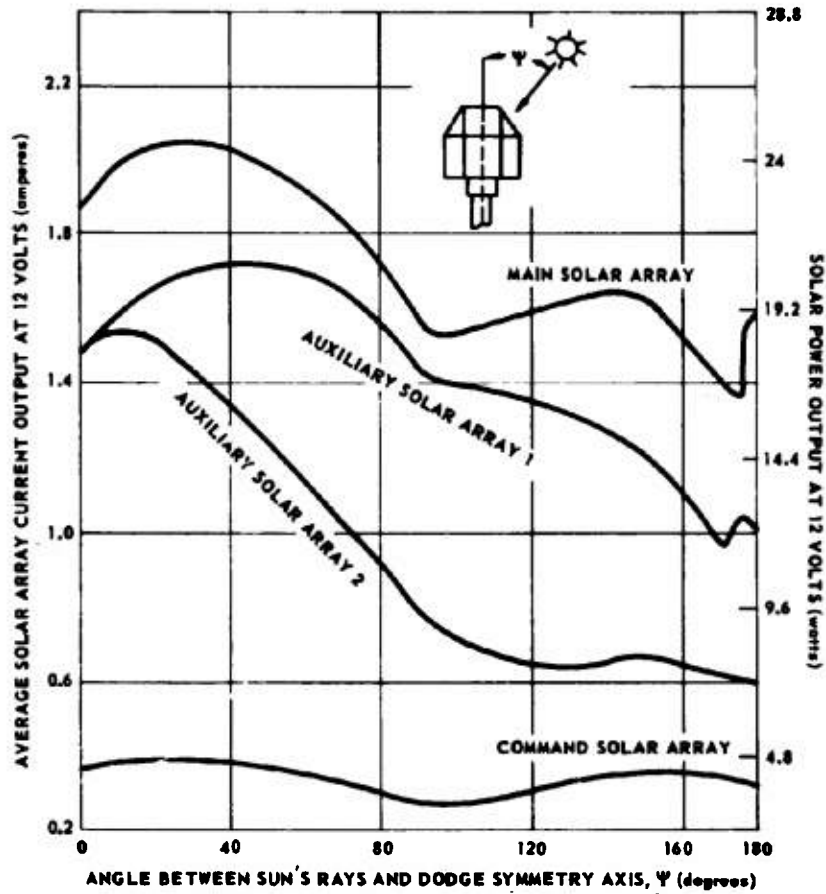


Fig. 4-2 PREFLIGHT DATA FOR DODGE SOLAR CELL ARRAY

Each array is comprised of 40 cells in series. The main and command array operating voltage is approximately 12 volts due to voltage clamping by the main battery and/or zener diodes. The auxiliary arrays are similarly loaded at 12 volts when supplying the main bus. The rather low design operating voltage of 0.3 volts per series solar cell was chosen to insure adequate array performance at the predicted maximum solar panel temperatures of 250°F.

Fig. 4-3 illustrates the predicted start of life output from each of the four DODGE solar arrays as a function of sun angle (ψ) with the satellite symmetry axis. This figure indicates the average output from each array. It does not include, however, the range of outputs possible due to solar azimuth variations and shadowing of panels by booms and the stack assembly.

4.1.2 In-Orbit Performance

The solar array was fabricated using molybdenum interconnectors rather than the more conventional copper types. It was determined during thermal vacuum testing (cycling from -120°C to +90°C) that the molybdenum interconnector frequently separated from the cell at the solder joint. Less frequently, one or more of the corners of a cell would break. The failure was repaired by running a copper jumper wire from each interconnecting tab to the cell. The breakage of the solar cells however, was not prevented by this repair. While this was not a catastrophic type of failure, it was expected to result in a small loss in power at the beginning of life due to thermal cycling.

Fig. 4-4 illustrates data gathered on the performance of the main solar array shortly after spacecraft stabilization was achieved. The data are somewhat noisy. This scatter is thought to be due to some combination of the following three effects:

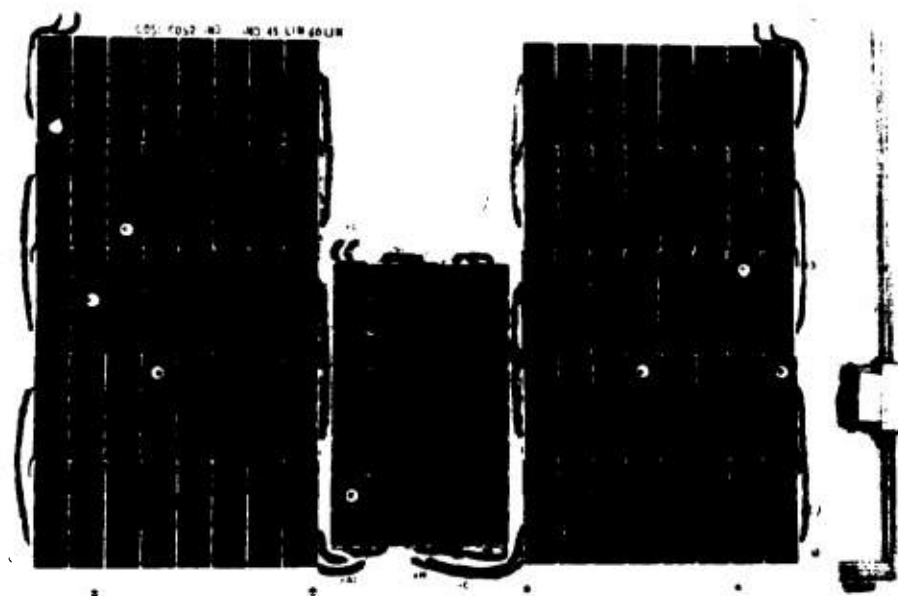


Fig. 4-3 DODGE +X EQUATORIAL SOLAR PANEL

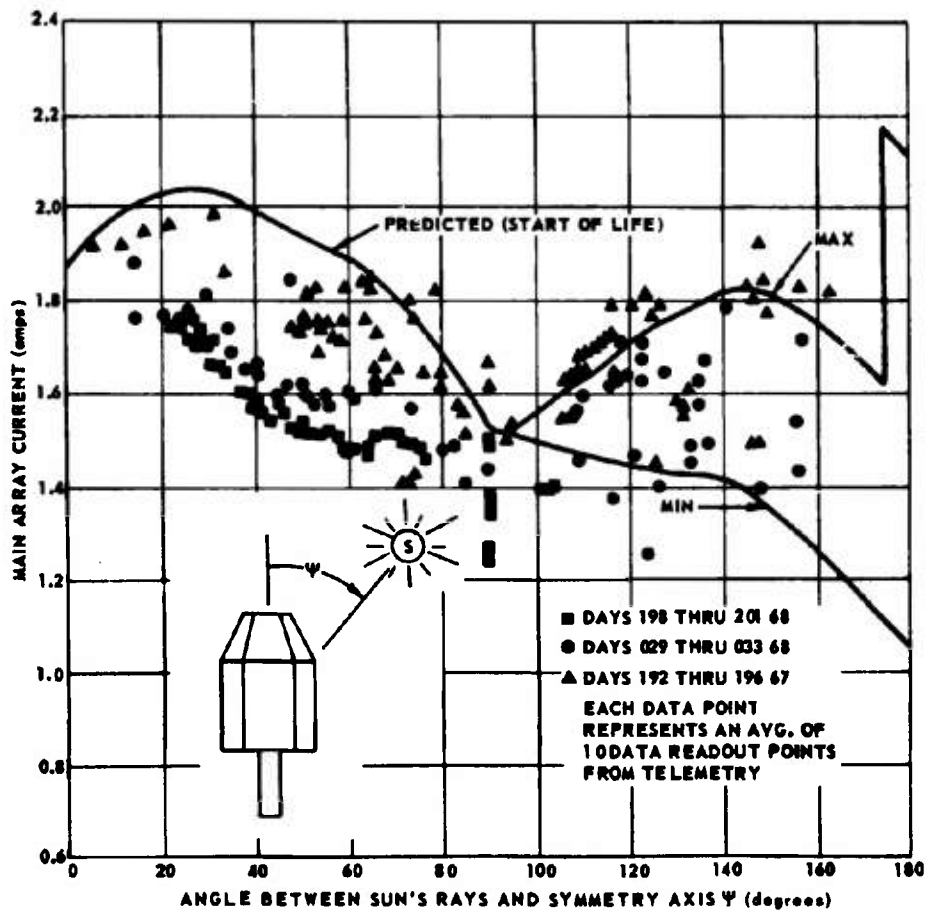


Fig. 4-4 DODGE SOLAR ARRAY CURRENT (MAIN CIRCUIT)

- a. Shading due to spacecraft boom and/or stack assembly.
- b. Temperature variations on solar panels (-107°C to $+116^{\circ}\text{C}$)
- c. Solar cell breakage due to launch environment and/or thermal cycling.

A loss of approximately 3% in main array current during the first 15 days in orbit is most probably attributable to cell breakage. Data taken approximately 200 and 400 days after launch are also included in Fig. 4-4. The rather large spread in data at ψ angles greater than 90° is due to the shadowing of polar panels by the stack assembly.

Fig. 4-5 is a plot of the DODGE main solar array output as a function of time on a logarithmic scale. Each point represents an average of 30 data points received from the telemetry system when the solar incidence angle (ψ) was between 30° and 40° as measured by the +Z solar aspect sensor. During the first four months in orbit there was a solar array degradation of approximately 7%. After 400 days in orbit, the array degraded approximately 15.5%. This degradation may be ascribed to (a) cell breakage due to thermally induced stresses and (b) bulk damage due to particle irradiation. It is difficult, if not impossible, to separate the two effects. Since unpredictable solar flare events are the prime producers of damaging particles, long range predictions of solar array degradation cannot be made. The degradation in array performance to date, although reducing power system performance capability, has not significantly affected the overall operation of the spacecraft.

4.2 Battery

4.2.1 Design Characteristics

The DODGE battery is comprised of eight hermetically sealed cylindrical nickel cadmium cells

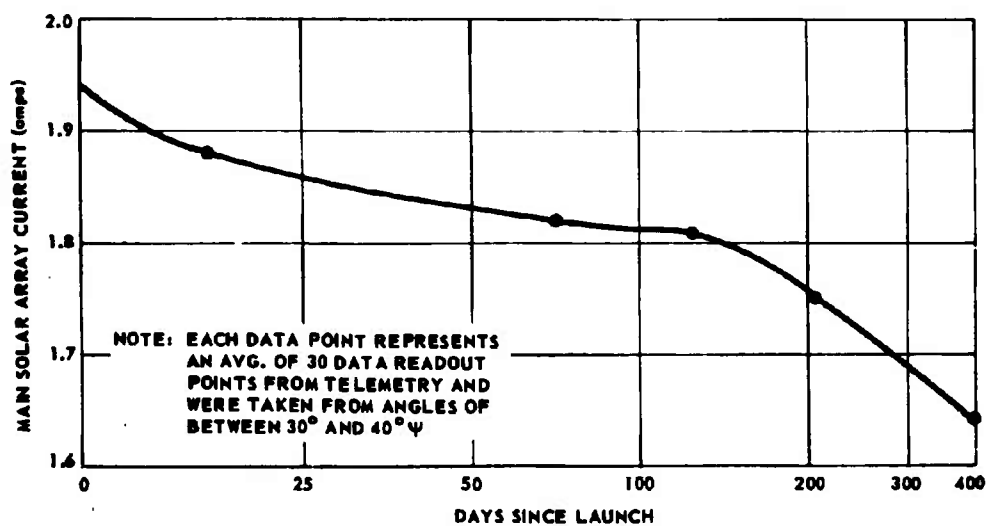


Fig. 4-5 DODGE MAIN SOLAR ARRAY CURRENT VERSUS TIME

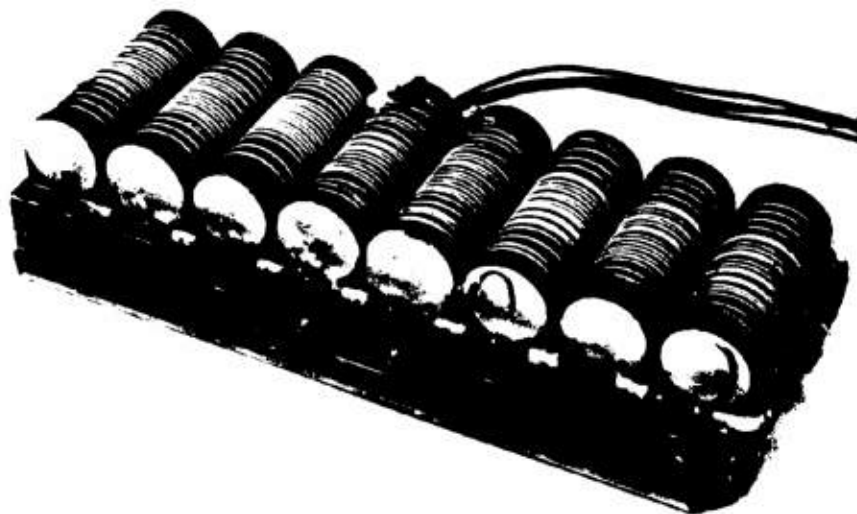
connected in series. The capacity of the battery is nominally 5.5 ampere-hours and nominal operating voltage is 10.7 v at 77°F. Each cell is 1.3 inches in diameter by 3.5 inches long and weighs 0.5 pound. The battery assembly, Fig. 4-6, weighs 6 pounds and incorporates zener diodes for limiting battery voltage as well as automatic temperature control elements. When enabled, the battery automatic temperature control (ATC) units provide heat to the battery assembly when the battery temperature drops below 54°F. The power for heating is derived from either or both the auxiliary 1 or auxiliary 2 arrays. Resistive heating elements are wound around each cell housing as shown in Fig. 4-6. The battery is designed to undergo continuous charge-discharge cycles at temperatures ranging from 45°F to 80°F.

Fig. 4-7 summarized the total experimental capacity available from the battery as a function of discharge voltage and discharge current. These data apply over the design operating temperature range of 45°F to 80°F. Approximately 4.5 ampere hours are available from the battery when it is discharged at 3 amperes to a voltage level of 8.8 volts.

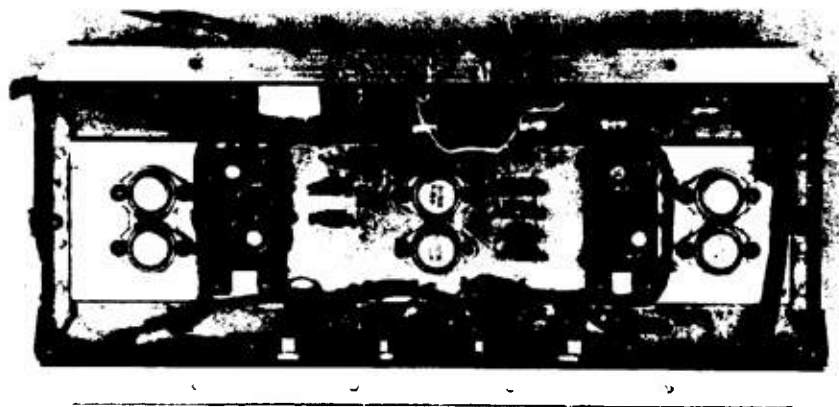
4.2.2 In-Orbit Performance

The DODGE battery performance has been normal in all respects. It has operated satisfactorily, supplying peak demands in excess of solar array capability while the spacecraft is in sunlight and total spacecraft demands during periods of solar eclipse. The battery has, for the major portion of its life, been operated within its design limits of 45° to 80°F. These limits have been exceeded for brief periods by approximately 15°F. These conditions are rectified by employing battery ATC or by adjusting the overcharge rate through the addition or removal of various noncritical spacecraft loads. Data on typical battery performance are provided in Fig. 4-8.

THE JOHNS HOPKINS UNIVERSITY
APPLIED PHYSICS LABORATORY
SILVER SPRING MARYLAND



TOP VIEW



BOTTOM VIEW

Fig. 4-6 DODGE SATELLITE BATTERY

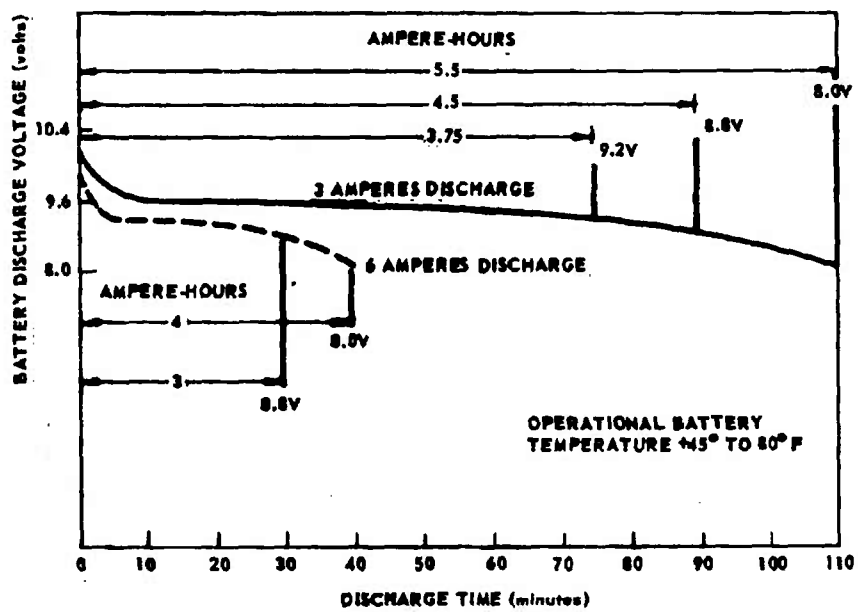


Fig. 4-7 DODGE BATTERY CAPACITY MEASUREMENTS

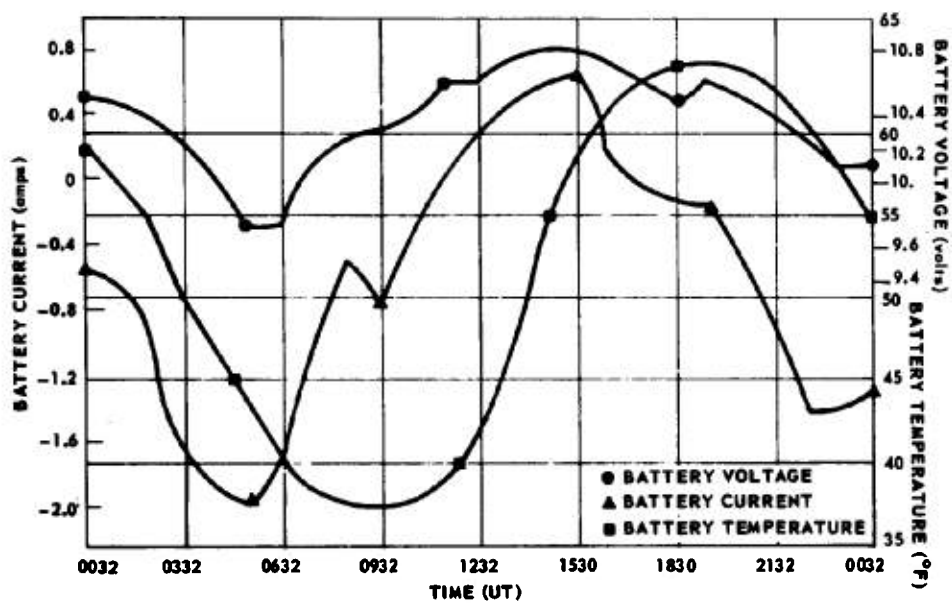


Fig. 4-8 DODGE BATTERY PERFORMANCE DATA DAY 234, 1968

4.3 Voltage Limiting

4.3.1 Low Voltage Sensing Switch

The battery discharge in the DODGE spacecraft is automatically discontinued when its voltage degrades to 8.8 volts. This protection against possible cell polarity reversal is afforded by a low voltage sensor which automatically disconnects the loads from the main bus when the voltage drops to 8.8 volts. The sensor also removes the battery from the main bus so that excessive battery charge rates will not be produced by the removal of loads from the main bus. The low voltage sensing switch has been actuated on several occasions during periods of high demand. Actuation occurred at the set point of 8.8 volts.

4.3.2 High Voltage Zeners

High voltage limiting is accomplished by placing zener diodes across the main battery in order to bypass excessive current that would otherwise cause the battery to overvoltage. The zeners are mounted in the battery housing to provide good thermal coupling to the battery cells. In this manner the energy dissipated as heat in the zeners helps to maintain a stable battery temperature. The upper battery voltage limit established by the high voltage zener is 12.5 volts. The zeners have performed satisfactorily.

4.4 Converters and Inverters

The satellite contains six DC to DC converters and two DC to AC inverters. Fig. 4-1 shows schematically their usage in the power system. The programmed DC to DC converter furnishes five regulated voltages (± 10.7 , $+4.0$, -32.1 , and $+21.4$ volts) to operate several programmed loads (telemetry, transmitter, and attitude detection circuitry). An additional programmed converter may

be commanded in to perform these same functions should it be desired or required. The overall converter efficiency is approximately 85%. The satellite contains a separate converter (#3) to supply regulated voltages (+10.7, -32.1, and +21.4 volts) and to continuously operate attitude control equipment (i.e. magnetometer, demagnetizer, and damping systems), the automatic programmer and doppler circuitry. The TV converter is designed to produce +1% regulated voltages (+100, +12, +4, and +500 and +6.3 volts) to operate the 22° and 60° TV cameras and electronic systems. Two independent command converters, one powered by the battery bus and the other by the 3 watt solar array, supply three voltages (+22.1, +10.7 and +4.7 volts) to the command loads (i.e. redundant receivers, logic, and power switching circuitry). The 150 volt converter produces the high voltage used to charge a capacitor that in turn actuates the magnetizer coils. Either one of two DC to AC inverters may be selected to supply power (2 phase 400 cycles, 52 volts peak to peak) to the booms, torsion wire, and flywheel motors.

The performance of each of the converters and inverters has been within design specifications.

5. TELEMETRY SYSTEM

5.1 System Design

DODGE with its complex damping and stabilization experiments and attitude sensing devices uses a telemetry system with one 76-channel and two 38-channel commutators. These 152 channels include six PCM registers that provide 90 bits of telltale data. The 38-channel commutators telemeter primarily satellite attitude data, and the 76-channel commutator telemeters primarily satellite housekeeping functions. The data are transmitted on 136.8 MHz and 240 MHz carrier frequencies.

The telemetry system and television system are turned on once each hour when the programmer, an ancillary portion of the satellite command system, is operating. These systems are sequenced through several fixed operating modes for 10 minutes and then are automatically turned off. This automatic mode of operation is an important part of the satellite system operation. Since the spacecraft is in a near-synchronous orbit, the time of one pass is approximately 12 days. The satellite will therefore spend long periods over ground stations that do not have the complex command capability required to operate the satellite command system. The automatic turn-on each hour will allow these ground stations to monitor the satellite while it is not in view of APL or other suitable equipped ground stations. The spacecraft cannot be turned on and left on over these ground stations because the battery will not sustain the constant load. It will, however, sustain the 1/6-hour duty cycle provided by the automatic mode.

The programmer operates the spacecraft through the command system. It operates the necessary relays to turn the satellite on and to select the desired information for transmission during each time period. If it is desired that the spacecraft not be exercised each hour, or if the sequence of events must be changed for some reason, the programmer may be commanded off.

The programmer also produces a timing burst from which two or more ground stations working in conjunction can obtain satellite tracking information. The ground stations contain equipment that very accurately determine the time of the phase change.

The programmer clock is the 5 MHz oscillator in the doppler tracking system. Therefore, all the times and the frequencies generated by the programmer are known very precisely.

The telemetry system is instrumented essentially as shown in Fig. 5-1.

The three commutators receive clock pulses at 3.18 Hz from the TM rate control unit, which divides down from a 814 Hz tuning fork oscillator. The commutators divide this rate by four to produce a commutation rate of 1.258 seconds per step. This results in a frame time of about 47.8 seconds for each of the 38-channel commutators and about 95.6 seconds for the 76-channel commutator. Each of the three commutators may be stopped independently by command. A fourth command is available to stop all three commutators simultaneously on the same channel. This command is used in several instances, such as with the magnetometers where the X, Y, and Z axes outputs were placed on corresponding channel numbers of each of the three commutators. Consequently, during normal operation data from each of the three magnetometers are sampled and read out simultaneously. With a single command the three commutators may be stopped for continuous, simultaneous monitoring of the three magnetometer outputs.

The six telltale registers are essentially identical to those used for GEOS and DME-A satellites. Each register contains 15 bits, cumulatively providing 90 data bits. There is a telltale indicating the status of each of the paired commands, with telltales ordered consecutively to correspond with the command numbers, thus facilitating operational procedures. The TM rate control unit provides synchronization and bit rate clock pulses to each telltale register.

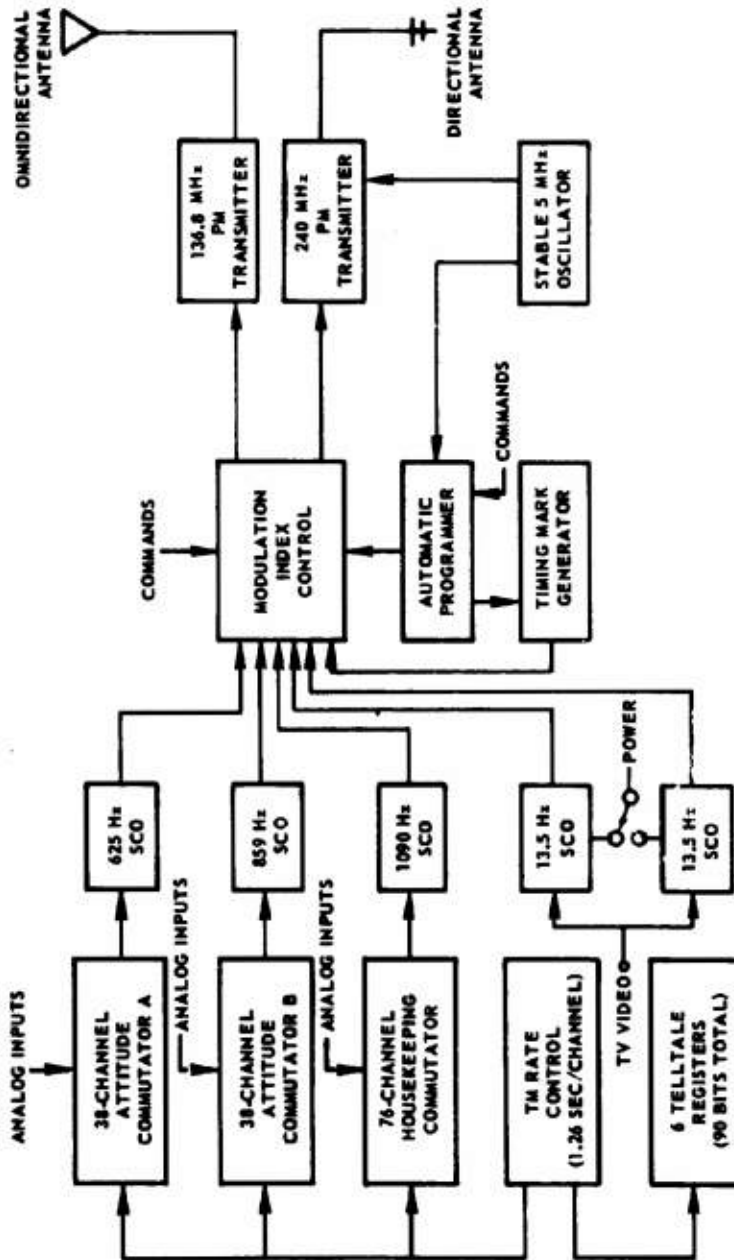


Fig. 5-1 BLOCK DIAGRAM OF THE TELEMETRY SYSTEM FOR THE DODGE SATELLITE

The output of each commutator goes to a separate subcarrier oscillator (SCO). For this payload the DCS constant bandwidth series of subcarriers was selected. The center frequencies chosen were 625, 859, and 1090 Hz. The frequency deviation for each of these SCOs is +62.5 cycles. Since the information frequencies and deviations are identical for these SCOs, each of the three corresponding ground station discriminators will have a threshold at the same input signal-to-noise ratio and provide equal output improvements. The output low pass filters available for use in the discriminators are the linear phase type with 6 Hz cutoff for analog data and 20 Hz cutoff for the telltale data.

The two additional SCOs are for transmitting the video signals from the television cameras. Included with the video signals are the picture frame sync and color-filter wheel position data. These two SCOs have center frequencies of 13.5 Hz and are deviated +40%. These two identical SCOs are used in a redundant configuration, with power being applied to the desired unit by command.

The modulation index control takes the output signals from the SCOs and the timing marker generator and switches them in a variety of combinations to the two phase-modulated telemetry transmitters, as indicated in Fig. 5-2. While selecting these combinations, it simultaneously inserts the proper attenuation networks to achieve the desired phase deviation for the PM transmitters. In each of the several operating modes, the peak phase deviation is $\pm 80^\circ$. The internal switching relays are controlled by command. Some of these relays are also controlled by the automatic programmer. The TM system operating modes are defined in Table 5-1.

The two phase-modulated transmitters obtain their inputs from the modulation index control. The phase modulators are integral parts of the transmitters and have a deviation sensitivity of 4 μ amps rms per radian peak. The carrier frequency of the 240 MHz transmitter is controlled by either of a redundant pair of ultrastable 5 MHz crystal oscillators with -20 parts per

TABLE 5-1
DODGE TELEMETRY MODULATION MODES

Mode	136 MHz Transmitter	240 MHz Transmitter	Telldates				Programmer and Command Positions			
			2-4 P58	4-12 57	4-13 C58	4-14 C59	57	C58	P58	59
1	Att & Hk	TV	0	0	0	0	B	B	B	B
2	TV	Att & Hk	0	0	0	1	B	B	B	A
3*	Att & Hk	Hk	0	0	1	0	B	A	B	B
4*	Hk	Att & Hk	0	0	1	1	B	A	B	A
5	Att & Hk	TV	0	1	0	0	A	B	B	B
6	TV	Att & Hk	0	1	0	1	A	B	B	A
7*	Att & Hk	Hk	0	1	1	0	A	A	B	B
8*	Hk	Att & Hk	0	1	1	1	A	A	B	A
9*	Att, Hk, & TV	TV	1	0	0	0	B	B	A	B
10*	TV	Att, Hk, & TV	1	0	0	1	B	B	A	A
11	Att, Hk, & TV	Hk	1	0	1	0	B	A	A	B
12	Hk	Att, Hk, & TV	1	0	1	1	B	A	A	A
13*	Time	TV	1	1	0	0	A	B	A	B
14*	TV	Time	1	1	0	1	A	B	A	A
15	Time	Hk	1	1	1	0	A	A	A	B
16	Hk	Time	1	1	1	1	A	A	A	A

*These modes can be obtained only through Programmer Operation.

- Note:
1. Hk - 76-channel housekeeping commutator.
 2. Att - Both 36-channel attitude commutator A and 36-channel attitude commutator B.
 3. TV - Either the main TV system SCO or the auxiliary TV system SCO may be on depending on the position of Command 20, which is indicated by Telldate 2-5 (20A, TT high - 20B, TT low).
 4. Telldate States - 1 - High (long)
0 - Low (short)
 5. Relay K1 is operated by both the command system (C57) and the automatic programmer and its state is indicated by TT 4-12. See Fig. 5-1.

TABLE 5-1 (continued)

DODGE TELEMETRY MODULATION MODES

- Note: 6. Relays K2 and K3 are operated together by the command system (C58). However, only K2 (but not K3) is operated by the automatic programmer. Consequently, K2 and K3 can become out of phase as a result of automatic programmer operation. The state of K2 is indicated by TT 2-4 and that of K3 by TT 4-13. See Fig. 5-1.
7. Relay K4 is operated only by the command system (C59) and its state is indicated by TT 4-14. See Fig. 5-1.
8. Relay K5 is operated only by the command system (C20) and its state is indicated by TT 2-5. This relay switches power to either the main TV SCO or the auxiliary TV SCO. Command 20 also enables the auxiliary TV system converter. See Fig. 5-1.

million offset. The RF output power is about 8 watts, which is fed to a directional turnstile antenna having left-hand circular polarization, 7-db gain with respect to a linear isotropic antenna, and a 60° 3-db beamwidth.

The 136.8 MHz transmitter's carrier frequency is controlled by a self-contained crystal without supplemental environmental control. The RF output power is about 10 watts and is fed to a pair of quarter-wave whip antennas that provide an essentially omnidirectional radiation pattern with a representative gain of about -3 db with respect to a linear isotropic antenna.

The timing mark generator provides a square wave signal at about 324.5 Hz (divided down from the stable 5 MHz oscillator) to the transmitters through the modulation index control. When operated in the continuous mode, this generator puts out bursts of 128 cycles each, about every 3.2 seconds. After the 126th cycle of each burst, there is a 180° phase shift followed by two more cycles, Fig. 5-3. Correlation of the reception by various ground stations of this phase reversal provides a capability of locating and tracking the satellite. This tracking technique is supplemented by doppler tracking of the ultra-stable carrier of the 240 MHz transmitter and also by somewhat less refined antenna-pointing techniques.

The automatic programmer is essentially a long divider chain operating from the stable 5 MHz oscillator. From this continuous division process, signals at a variety of precise time intervals are obtained. These signals are used to perform various switching functions automatically throughout the spacecraft. Specifically, this automatic programmer is used to turn the spacecraft on every hour and send back data in the following sequence as indicated in Fig. 5-4: (1) about 200 seconds of telemetry, (2) a timing mark generator burst for 0.4 second, (3) a TV picture taken with the wide (60°) camera and simultaneously the TM data for 200 seconds, (4) another 0.4-second timing burst, (5) a TV picture taken with the narrow angle (20°) camera, which has the selectable color filters that are automatically advanced from

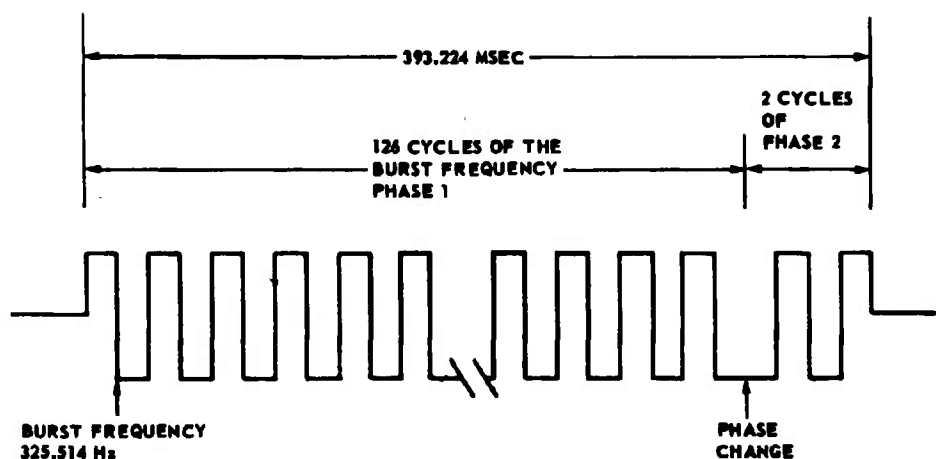


Fig. 5-3 DODGE TIME BURST WAVEFORM



Fig. 5-4 DODGE AUTOMATIC MODE TIMING DIAGRAM

picture to picture, along with the TM data for 200 seconds, (6) another 0.4-second timing burst, and then (7) turn off of the spacecraft (including transmitters) for the remaining 50 minutes of each hour. At the end of this time the programmer automatically causes the preceding sequence to be repeated. The time at which the satellite's hour starts can be set by command. The automatic programmer may also be overridden by command to provide exclusively manual operation of the spacecraft.

The function of each telemetry channel and the full scale values are listed in Tables 5-2, 5-3, and 5-4. The six telltale registers that indicate in a 2-position signal the state of many of the satellite systems are listed in Table 5-5 with a brief explanation of the high and the low indications. The channels containing the telltale data are read out redundantly on separate commutators. This redundancy increases the reliability of the system.

5.2 In-Orbit Performance

Operationally, the telemetry system has met all design objectives. It has responded to all commands and transmitted the requested information. It has successfully operated in its various modes, demonstrating its unique characteristic, flexibility.

The excellent television data received are discussed in Section 9, and plots of the attitude data received are included in Appendix A of this report.

TABLE 5-2
DODGE TELEMETRY FUNCTIONS
(Attitude Commutator A)

<u>Channel</u>	<u>Function</u>	<u>Full Scale Value</u>
1	+ Calibrate	0.25 V
2	0 Calibrate	0.25 V
3	- Calibrate	-0.25 V
4	Main Bus Voltage	15.00 V
5	PCM Teletale No. 1	0.25 V
6	Command Converter No. 2, +22V Tap Voltage	+25.00 V
7	Main Converter, 4V Tap Voltage	+5.00 V
8	Main Converter, 32V Tap Voltage	-50.00 V
9	PCM Teletale No. 2	0.25 V
10	No. 1 Auxiliary Solar Array Voltage	+25.00 V
11	No. 2 Auxiliary Solar Array Voltage	+25.00 V
12	+Z Boom Length	0.25 V
13	+X+Z (Times) Boom Length	0.25 V
14	-X+Z (Times) Boom Length	0.25 V
15	+Y Boom Length	0.25 V
16	-X+Y Damper Boom Length	0.25 V
17	Z Axis DC Amplifier Output Current	0.25 V
18	Y Axis DC Amplifier Output Current	0.25 V
19	X Axis Magnetometer Output	10.00 V
20	Y Axis Magnetometer Output	10.00 V
21	Z Axis Magnetometer Output	10.00 V
22	Magnetizer Capacitor Voltage	+145.0 V
23	Oscillator Regulator Voltage	-15.00 V
24	X Axis 60 Degree Linear SAD	0.25 V
25	Y Axis 60 Degree Linear SAD	0.25 V
26	Z Axis 60 Degree Linear SAD	0.25 V
27	Battery Cell Temperature	0.25 V

TABLE 5-2 (continued)
DODGE TELEMETRY FUNCTIONS
(Attitude Commutator A)

<u>Channel</u>	<u>Function</u>	<u>Full Scale Value</u>
28	Main Converter, +10V Tap Voltage	+15.00 V
29	Main Converter, -10V Tap Voltage	-15.00 V
30	22 Degree TV Camera 500V Supply Voltage	+750.0 V
31	60 Degree TV Camera Filament Current	+2.5A
32	22 Degree TV Camera Filament Current	+2.5A
33	X Axis Magnetometer Output Expanded	0.25 V
34	60 Degree TV Camera Illumination	+2.50 V
35	60 Degree TV Camera Housing Temperature	0.25 V
36	+ Calibrate	+0.25 V
37	+ Calibrate	+0.25 V
38	+ Calibrate	+0.25 V

TABLE 5-3
DODGE TELEMETRY FUNCTIONS
(Attitude Commutator B)

<u>Channel</u>	<u>Function</u>	<u>Full Scale Value</u>
1	- Calibrate	-0.25 V
2	0 Calibrate	0.25 V
3	+ Calibrate	+0.25 V
4	Battery or Solar Zener Current	25.00 A
5	PCM Teiltale No. 3	0.25 V
6	Command Solar Array Current	-0.75 A
7	Stand-by Converter Input Current (Offset) Current Sensing Amplifier	+3.00 A
8	TV Converter Input Current (Offset) Current Sensing Amplifier	+1.50 A
9	PCM Teiltale No. 4	0.25 V
10	Main Converter Input Current (Offset) Current Sensing Amplifier	+10.00 A
11	Receiver No. 1 AGC Voltage Spcl.	0.25 V
12	-Z Boom Length	0.25 V
13	-X-Z (Times) Boom Length	0.25 V
14	+X-Z (Times) Boom Length	0.25 V
15	-Y Boom Length	0.25 V
16	+X-Y Damper Boom Length	0.25 V
17	PCM Teiltale No. 5	0.25 V
18	X Axis DC Amplifier Output Current	0.25 V
19*	Y Axis Magnetometer Output	10.00 V
20	+X Cosine Solar Attitude Detector	0.25 V
21	+Y Cosine Solar Attitude Detector	0.25 V
22	Z Cosine Solar Attitude Detector	0.25 V
23	-X Cosine Solar Attitude Detector	0.25 V

Note: *Telemetered on more than one commutator.

TABLE 5-3 (continued)
DODGE TELEMETRY FUNCTIONS
(Attitude Commutator B)

<u>Channel</u>	<u>Function</u>	<u>Full Scale Value</u>
24	-Y Cosine Solar Attitude Detector	0.25 V
25	-Z Cosine Solar Attitude Detector	0.25 V
26	Spare	0.25 V
27	FM Book Temperature	0.25 V
28	TV Shutter Capacitor Voltage	+125.0 V
29	PCM Teletale No. 6	0.25 V
30	TV System 4V Supply Voltage	+5.00 V
31	60 Degree TV Camera Focus Voltage	+75.0 V
32	22 Degree TV Camera Focus Voltage	+75.0 V
33	Y Axis Magnetometer Output Expanded	0.25 V
34	22 Degree TV Camera Illumination	+2.50 V
35	22 Degree TV Camera Housing Temperature	0.25 V
36	- Calibrate	-0.25 V
37	- Calibrate	-0.25 V
38	- Calibrate	-0.25 V

TABLE 5-4
DODGE TELEMETRY FUNCTIONS
(Housekeeping Commutator)

<u>Channel</u>	<u>Function</u>	<u>Full Scale Value</u>
1	+ Calibrate	+0.25 V
2	0 Calibrate	0.25 V
3	- Calibrate	-0.25 V
4	Main Solar Array Current	-2.50 A
5*	PCM Teletale No. 1	0.25 V
6*	Main Bus Voltage	+15.00 V
7	Overvoltage Zener Current Current Sensing Amplifier	2.50 A
8*	Battery or Solar Zener Current Current Sensing Amplifier	10.00 A
9*	PCM Teletale No. 2	0.25 V
10	No. 1 Auxiliary Solar Array Current	-2.00 A
11	No. 2 Auxiliary Solar Array Current	-2.00 A
12	Inverter Input Current	+5.00 A
13	Inverter Phase 1 Output Voltage	50.0 V
14	Inverter Phase 2 Output Voltage	50.0 V
15	Hall Detector Output	0.25 V
16	Receiver No. 2 AGC Voltage	0.25 V
17	Receiver No. 1 Video Monitor Spcl.	0.25 V
18	+Y Slant Panel Temperature	0.25 V
19*	Z Axis Magnetometer Output	10.00 V
20	X Axis 45 Degree Linear SAD	0.25 V
21	Y Axis 45 Degree Linear SAD	0.25 V
22	+Z Solar Attitude Detector Temperature	0.25 V
23	Z Axis 45 Degree Linear SAD	0.25 V
24	Solar Attitude Detector Regulator Voltage	+7.50 V

Note: *Telemetered on more than one commutator.

TABLE 5-4 (continued)
DODGE TELEMETRY FUNCTIONS
(Housekeeping Commutator)

<u>Channel</u>	<u>Function</u>	<u>Full Scale Value</u>
25	+Z Solar Attitude Detector Temperature	0.25 V
26	1 x 2 P/N 12 mil Li Doped 6 mil F.S. Hoffman	-0.25 V
27	1 x 2 N/P 16 mil 1 ohm-cm 12 mil F.S. Heliotek	-0.25 V
28	1 x 2 N/P 16 mil 1 ohm-cm Integral Glass Hoffman	-0.25 V
29	2 x 2 N/P 14 mil 10 ohm-cm 20 mil F.S. Hoffman	-0.25 V
30	2 x 2 N/P 14 mil 10 ohm-cm 6 mil F.S. Hoffman	-0.25 V
31	2 x 2 N/P 8 mil 1 ohm-cm 3 mil F.S. Heliotek	-0.25 V
32	1 x 2 N/P 16 mil 1 ohm-cm 6 mil F.S. Heliotek	-0.25 V
33	Solar Science Experiment Temperature	0.25 V
34	Main Converter, +22V Tap Voltage	+25.00 V
35	Main Converter, -22V Tap Voltage	-25.00 V
36	- Calibrate	-0.25 V
37	- Calibrate	-0.25 V
38	- Calibrate	-0.25 V
39	- Calibrate	-0.25 V
40	0 Calibrate	0.25 V
41	+ Calibrate	+0.25 V
42	Dewar Oven Temperature	0.25 V
43*	PCM Telltale No. 3	0.25 V
44	Rate Control Book Temperature	0.25 V
45	Thermal Reference Regulator No. 1 + Voltage	+0.50 V
46	Thermal Reference Regulator No. 1 - Voltage	-0.50 V

Note: *Telemetered on more than one commutator.

TABLE 5-4 (continued)
DODGE TELEMETRY FUNCTIONS
(Housekeeping Commutator)

<u>Channel</u>	<u>Function</u>	<u>Full Scale Value</u>
47*	PCM Teletale No. 4	0.25 V
48	Thermal Reference Regulator No. 2 + Voltage	+0.50 V
49	Thermal Reference Regulator No. 2 - Voltage	-0.50 V
50	+X Equatorial Panel Temperature	0.25 V
51	-X Equatorial Panel Temperature	0.25 V
52	+Y Equatorial Panel Temperature	0.25 V
53	-Y Equatorial Panel Temperature	0.25 V
54	Magnetometer Sensor Temperature	0.25 V
55*	PCM Teletale No. 5	0.25 V
56	136 MHz Transmitter Temperature	0.25 V
57	240 MHz Transmitter Temperature	0.25 V
58	Battery Mounting Plate Temperature	0.25 V
59	+Z Boom Motor Temperature	0.25 V
60	-Z Boom Motor Temperature	0.25 V
61	-Y Boom Motor Temperature	0.25 V
62	Eddy Current Damper Vane Temperature	0.25 V
63	-Y Slant Panel Temperature	0.25 V
64	Dual Command Receiver Temperature	0.25 V
65	TV Converter Temperature	0.25 V
66	50 Degree TV Camera Temperature	0.25 V
67	22 Degree TV Camera Temperature	0.25 V
68	60 Degree TV Camera 500V Supply Voltage	+750.0 V
69	60 Degree TV Camera Target Voltage	+15.0 V
70	22 Degree Camera Target Voltage	+15.0 V
71	Z Axis Magnetometer Output Expanded	0.25 V
72	Flywheel Motor Temperature	0.25 V

Note: *Telemetered on more than one commutator.

TABLE 5-4 (continued)
DODGE TELEMETRY FUNCTIONS
(Housekeeping Commutator)

<u>Channel</u>	<u>Function</u>	<u>Full Scale Value</u>
73	Quad 2 Bottom Panel Temperature	0.25 V
74	+ Calibrate	+0.25 V
75	+ Calibrate	+0.25 V
76	+ Calibrate	+0.25 V

TABLE 5-5
DODGE TELLTALE REGISTER FUNCTIONS

Number		Telltale	
TT	CMD	High	Low
1-01	1	Main Power On Via Cmd. 1	Main Power on Via Cmd. 60
1-02	2	Main Converter No. 1	Main Converter No. 2
1-03	3	Battery Mode	Solar Only Mode
1-04	4	Low Voltage Sensor In	Low Voltage Sensor Out
1-05	5	Stand-by Converter On	Stand-by Converter Off
1-06	6	Aux. Array No. 1 to ATC No. 1	Aux. Array No. 1 to Main Bus
1-07	7	Aux. Array No. 2 to ATC (B/D)	Aux. Array No. 2 to Main Bus
1-08	8	Aux. Array No. 2 to ATC No. 2(B)	Aux. Array No. 2 to Damper ATC
1-09	9	Enhanced Magnetic System On	Enhanced Magnetic System Off
1-10	10	Oscillator and Reg. No. 1	Oscillator and Reg. No. 2
1-11	11	Oscillator Oven No. 1	Oscillator Oven No. 2
1-12	12	136 MHz Transmitter On	136 MHz Transmitter Off
1-13	13	240 MHz Transmitter On	240 MHz Transmitter Off
1-14	14	Transmitters on Low Power	Transmitters on High Power
1-15	15	Spare	Spare
2-01	16	TV Converter Disable	TV Converter Enable
2-02	17	TV Scan Normal	TV Scan Fast Expanded
2-03	18	Cameras Protected From Sun	Cameras Not Protected From Sun
2-04		Mod Index Rly. K2 in Pos. A	Mod Index Rly. K2 in Pos. B
2-05	20	TV Sco No. 2	TV Sco No. 1
2-06	21	Flywheel Motor Enabled	Flywheel Motor Disabled
2-07		Payload Unseparated	Payload Separated
2-08	23	Magnetometer On/Demag. Off	Magnetometer Off/Demag. On
2-09	24	Magnetic Spin/Despin Enable	Enhanced Mag. Damping Enable
2-10	25	Spin Torque Positive	Spin Torque Negative
2-11	26	Select Enhanced Hysteresis Damping	Select Phase Lag Damping
2-12	27	Phase Lag Sample Automatic	Phase Lag Time Step and Hold

TABLE 5-5 (continued)
DODGE TELLTALE REGISTER FUNCTIONS

Number	TT	CMD	Telltale	
			High	Low
2-13	28	Enhanced Hysteresis-G High-3 Hour	Enhanced Hysteresis-G High-3 Hour	Enhanced Hysteresis-G Low-6 Hour
2-14	29	Enable XZ Fixed Mag. Moment	Enable XZ Fixed Mag. Moment	Disable XZ Fixed Mag. Moment
2-15	30	Select Fixed XZ Mag. Moment	Select Fixed XZ Mag. Moment	Select Variable XZ Mag. Moment
3-01	31	Damper Boom Angle Detector On	Damper Boom Angle Detector On	Damper Boom Angle Detector Off
3-02	32	Damper Cage Motor Enable	Damper Cage Motor Enable	Damper Cage Motor Disable
3-03	33	+Z Boom Enable	+Z Boom Enable	+Z Boom Disable
3-04	34	-Z Boom Enable	-Z Boom Enable	-Z Boom Disable
3-05	35	+X+Z (Times) Boom Enable	+X+Z (Times) Boom Enable	+X+Z (Times) Boom Disable
3-06	36	-X-Z (Times) Boom Enable	-X-Z (Times) Boom Enable	-X-Z (Times) Boom Disable
3-07	37	-X+Z (Times) Boom Enable	-X+Z (Times) Boom Enable	-X+Z (Times) Boom Disable
3-08	38	+X-Z (Times) Boom Enable	+X-Z (Times) Boom Enable	+X-Z (Times) Boom Disable
3-09	39	+Y Boom Enable	+Y Boom Enable	+Y Boom Disable
3-10	40	-Y Boom Enable	-Y Boom Enable	-Y Boom Disable
3-11	41	-X+Y Damper Boom Enable	-X+Y Damper Boom Enable	-X+Y Damper Boom Disable
3-12	42	+X-Y Damper Boom Enable	+X-Y Damper Boom Enable	+X-Y Damper Boom Disable
3-13		Boom(s) Extend	Boom(s) Extend	Boom(s) Retract
3-14	44	Select Inverter No. 1	Select Inverter No. 1	Select Inverter No. 2
3-15	45	Inverter Power On	Inverter Power On	Inverter Power Off
4-01	46	Fixed Z Mag. Moment Negative	Fixed Z Mag. Moment Negative	Fixed Z Mag. Moment Positive
4-02	47	Z Axis Magnetic Moment Fixed	Z Axis Magnetic Moment Fixed	Variable Z Mag. Moment Enable
4-03	48	Magnetic Damping State 1	Magnetic Damping State 1	Magnetic Damping State 2
4-04	49	Magnetizer-Positive Polarity	Magnetizer-Positive Polarity	Magnetizer-Negative Polarity
4-05	50	Magnetizer-High Charge Rate	Magnetizer-High Charge Rate	Magnetizer-Low Charge Rate
4-06	51	Magnetizer Capacitor Discharge	Magnetizer Capacitor Discharge	Magnetizer Capacitor Charge
4-07	52	Hysteresis TW Damper State 3	Hysteresis TW Damper State 3	Hysteresis TW Damper State 4
4-08	53	Square Wave Generator On	Square Wave Generator On	Square Wave Generator Off
4-09	54	TW Hysteresis Damper On	TW Hysteresis Damper On	TW Hysteresis Damper Off
4-10	55	Programmer Enable	Programmer Enable	Programmer Disable

TABLE 5-5 (continued)
DODGE TELLTALE REGISTER FUNCTIONS

Number		Telltale	
TT	CMD	High	Low
4-11	56	High Overvoltage Zener	Low Overvoltage Zener
4-12	57	Timing Marks In	Timing Marks Out
4-13	58	Modulation Mode Select 58A	Modulation Mode Select 58B
4-14	59	Modulation Mode Select 59A	Modulation Mode Select 59B
4-15	60	Main Power On Normally	Main Power On Abnormally
5-01	61	Attitude Commutator A Stop	Attitude Commutator A Start
5-02	62	Attitude Commutator B Stop	Attitude Commutator B Start
5-03	63	Housekeeping Commutator Stop	Housekeeping Commutator Start
5-04	64	All Commutators Stop	All Commutators Start
5-05		TW Damper Caged	TW Damper Cage Indeterminant
5-06		TW Damper Uncaged	TW Damper Cage Indeterminant
5-07		TW Damper Boom Angle Bit 6 1	TW Damper Boom Angle Bit 6 0
5-08		TW Damper Boom Angle Bit 5 1	TW Damper Boom Angle Bit 5 0
5-09		TW Damper Boom Angle Bit 4 1	TW Damper Boom Angle Bit 4 0
5-10		TW Damper Boom Angle Bit 3 1	TW Damper Boom Angle Bit 3 0
5-11		TW Damper Boom Angle Bit 2 1	TW Damper Boom Angle Bit 2 0
5-12		TW Damper Boom Angle Bit 1 1	TW Damper Boom Angle Bit 1 0
5-13		TV Filter Position Ind. Bit 3 1	TV Filter Position Ind. Bit 3 0
5-14		TV Filter Position Ind. Bit 2 1	TV Filter Position Ind. Bit 2 0
5-15		TV Filter Position Ind. Bit 1 1	TV Filter Position Ind. Bit 1 0
6-01		Not Used	Not Used
6-02		Not Used	Not Used
6-03		Not Used	Not Used
6-04		Not Used	Not Used
6-05		Not Used	Not Used
6-06		Not Used	Not Used
6-07		Not Used	Not Used
6-08		Not Used	Not Used

TABLE 5-5 (continued)
DODGE TELLTALE REGISTER FUNCTIONS

Number		Telltale	
TT	CMD	High	Low
6-09	Not Used		Not Used
6-10	Not Used		Not Used
6-11	Not Used		Not Used
6-12	Not Used		Not Used
6-13	Not Used		Not Used
6-14	Not Used		Not Used
6-15	Not Used		Not Used

6. COMMAND SYSTEM

6.1 Description

The DODGE command system consists of a dual command receiver, four command logics, and two separate power (or command) switching matrices. A block diagram of the system is shown in Fig. 6-1. The system is basically the same as the system used successfully in the DME-A and GEOS 1 and 2 satellites.

The command receivers receive and demodulate the AM command information impressed on the VHF carrier. The command logics, known as the TADEx System (Tone-Address-EXecute System), convert the audio outputs from the command receivers into signals suitable for controlling relays in the power switching matrices. To fully appreciate the operation of the command logic it will be helpful to review the requirements of the power switching matrix.

Each magnetic latching relay in the power switching matrix is controlled by set and reset coils which latch the relay "on" or "off" respectively. There are 32 groups of relays, the number in each group determined by the number of contacts required for that function. The resulting 64 coils or groups of coils are arranged in an 8 x 8 matrix, one lead from each coil going to a row, the other lead to a column, Fig. 6-2. Connected to each column is a capacitor bank which can be charged with respect to ground, and each row contains an SCR which can saturate to ground. A given relay coil is pulsed by charging its column capacitor for 0.6 second and then firing its row SCR. (This discussion is somewhat simplified. The actual matrix circuitry contains extensive component-level redundancy.)

The input to the command logic consists of an "address" tone burst followed by 3 "execute" tone bursts. Each tone is 0.5 second long followed by 0.5 second dead time. Hence the total word time (4 tone + 3 dead times) is 3.5 seconds. The

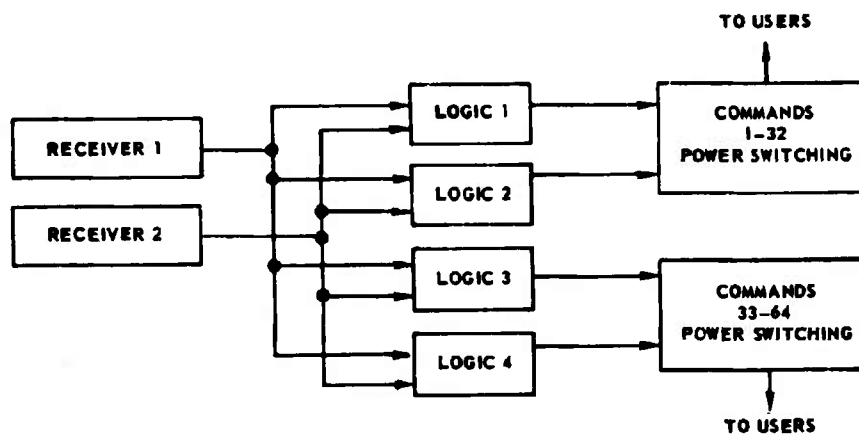


Fig. 6-1 BLOCK DIAGRAM OF DODGE COMMAND SYSTEM

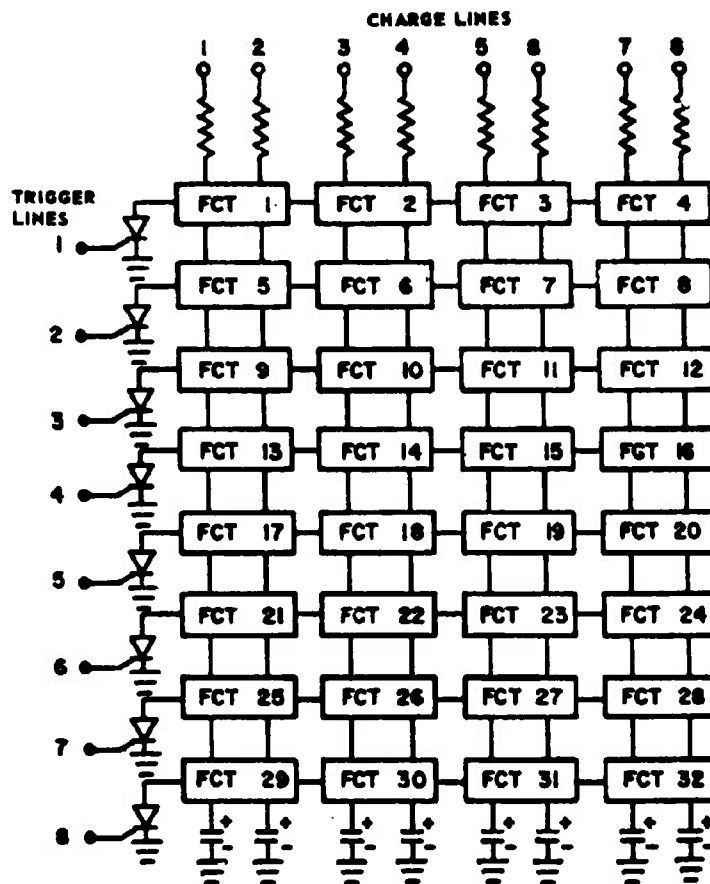


Fig. 6-2 POWER SWITCHING MATRIX

"address" tone gains access to the particular satellite for which the command is intended. Also, where redundant command logics are used, each logic is accessible through a different "address" tone. Each "execute" tone burst is one of four "execute" frequencies. Consequently, with each power switching matrix there are $4^3 = 64$ possible commands corresponding to the $8 \times 8 = 64$ sets of coils required for 32 different ON-OFF relay functions. Two power switching matrices provide for 64 ON-OFF relay functions.

A list of the 64 two-state commands and a description of each are given in Table 6-1 and Section 6-2, respectively.

TABLE 6-1

DODGE COMMAND ASSIGNMENTS

<u>Command</u>	<u>Command Function</u>	<u>Modulator Tones</u>	<u>Telltale No. Ind.</u>
1A	Automatic/Manual Main Power On/Off	2/5 AAA	1-01 High
1B	Automatic/Manual Main Power Off/On	2/5 AAC	1-01 Low
2A	Main Converter No. 1	2/5 CBB	1-02 High
2B	Main Converter No. 2	2/5 CBD	1-02 Low
3A	Battery Mode/LVS Reset	2/5 ADB	1-03 High
3B	Solar Only Mode	2/5 ADD	1-03 Low
4A	Low Voltage Sensor In	2/5 CDA	1-04 High
4B	Low Voltage Sensor Out	2/5 CDB	1-04 Low
5A	Stand-by Converter On	2/5 BCA	1-05 High
5B	Stand-by Converter Off	2/5 BCC	1-05 Low
6A	Aux. Solar Array No. 1 on Main Bus	2/5 FAB	1-06 Low
6B	Aux. Solar Array No. 1 on ATC No. 1 (Bat.)	2/5 DAD	1-06 High
7A	Aux. Solar Array No. 2 on Main Bus	2/5 ABB	1-07 Low
7B	Aux. Solar Array No. 2 on ATC (Bat./Damper	2/5 ABD	1-07 High
8A	Aux. Solar Array No. 2 on ATC No. 2 (Bat.)	2/5 BBB	1-08 High
8B	Aux. Solar Array No. 2 on Damper ATC	2/5 BBD	1-08 Low
9A	Enhanced Magnetic System On	2/5 CDB	1-09 High
9B	Enhanced Magnetic System Off	2/5 CDD	1-09 Low
10A	Oscillator and Regulator No. 1	2/5 ACA	1-10 High
10B	Oscillator and Regulator No. 2	2/5 ACC	1-10 Low
11A	Oscillator Oven No. 1	2/5 CBA	1-11 High
11B	Oscillator Oven No. 2	2/5 CBC	1-11 Low
12A	136 MHz Transmitter Off	2/5 CCA	1-12 Low
12B	136 MHz Transmitter On	2/5 CCC	1-12 High
13A	240 MHz Transmitter On	2/5 ABA	1-13 High
13B	240 MHz Transmitter Off	2/5 ABC	1-13 Low
14A	Transmitters on High Power	2/5 CFA	1-14 Low
14B	Transmitters on Low Power	2/5 CAC	1-14 High

TABLE 6-1 (continued)
DODGE COMMAND ASSIGNMENTS

<u>Command</u>	<u>Command Function</u>	<u>Modulator Tones</u>	<u>Telltale No. Ind.</u>
15A	Spare	2/5 DRB	1-15
15B	Spare	2/5 DED	1-15
16A	TV System Converter Enable	2/5 ADA	2-01 Low
16B	TV System Converter Disable	2/5 ADC	2-01 High
17A	TV System Scan Normal	2/5 BBA	2-02 High
17B	TV System Scan Fast Expanded	2/5 BBC	2-02 Low
18A	TV Cameras Protected by Sun Sensors	2/5 DBA	2-03 High
18B	TV Cameras Not Protected by Sun Sensors	2/5 DBC	2-03 Low
19A	Not Used	2/5 BDA	
19B	22 Degree TV Camera Filter Advance	2/5 BDC	None
20A	TV SCO No. 2	2/5 ECB	2-05 High
20B	TV SCO No. 1	2/5 ECD	2-05 Low
21A	Flywheel Motor Enabled	2/5 EDB	2-06 High
21B	Flywheel Motor Disabled	2/5 EDD	2-06 Low
22A	Set Programmer Start Time/136 OFF	2/5 DCB	None
22B	Magnetometer Calibrate	2/5 DCD	None
23A	Magnetometer Power On/Demagnetizer Off	2/5 DDA	2-08 High
23B	Magnetometer Power Off/Demagnetizer On	2/5 DDC	2-08 Low
24A	Magnetic Spin/Despin Enable	2/5 AAB	2-09 High
24B	Enhanced Magnetic Damping Enable	2/5 AAD	2-09 Low
25A	Spin Torque Positive	2/5 EAB	2-10 High
25B	Spin Torque Negative	2/5 EAD	2-10 Low
26A	Select Enhanced Hysteresis Damping	2/5 CAB	2-11 High
26B	Select Phase Lag Damping	2/5 CAD	2-11 Low
27A	Phase Lag Sample Time Automatic	2/5 CCB	2-12 High
27B	Phase Lag Time Counter Step and Hold	2/5 CCD	2-12 Low
28A	Enhanced Hysteresis-Gain High-3 Hour Hold	2/5 ACB	2-13 High
28B	Enhanced Hysteresis-Gain Low-6 Hour Hold	2/5 ACD	2-13 Low

TABLE 6-1 (continued)
DODGE COMMAND ASSIGNMENTS

<u>Command</u>	<u>Command Function</u>	<u>Modulator Tones</u>	<u>Telltale No. Ind.</u>
29A	Enable XZ Fixed Magnetic Moment	2/5 DCA	2-14 High
29B	Disable XZ Fixed Magnetic Moment	2/5 DCC	2-14 Low
30A	Select Fixed XZ Magnetic Moment	2/5 BAA	2-15 High
30B	Select Variable XZ Magnetic Moment	2/5 BAC	2-15 Low
31A	Damper Boom Angle Detector On	2/5 DDB	3-01 High
31B	Damper Boom Angle Detector Off	2/5 DDD	3-01 Low
32A	Damper Cage Motor Enable	2/5 DAA	3-02 High
32B	Damper Cage Motor Disable	2/5 DAC	3-02 Low
33A	/Z Boom Enable	3/4 AAA	3-03 High
33B	/Z Boom Disable	3/4 AAC	3-03 Low
34A	-Z Boom Enable	3/4 CAA	3-04 High
34B	-Z Boom Disable	3/4 CAC	3-04 Low
35A	/X/Z (Times) Boom Enable	3/4 BCA	3-05 High
35B	/X/Z (Times) Boom Disable	3/4 BCC	3-05 Low
36A	-X-Z (Times) Boom Enable	3/4 DCA	3-06 High
36B	-X-Z (Times) Boom Disable	3/4 DCC	3-06 Low
37A	-X/Z (Times) Boom Enable	3/4 BAA	3-07 High
37B	-X/Z (Times) Boom Disable	3/4 BAC	3-07 Low
38A	/X-Z (Times) Boom Enable	3/4 DAA	3-08 High
38B	/X-Z (Times) Boom Disable	3/4 DAC	3-08 Low
39A	/Y Boom Enable	3/4 ACA	3-09 High
39B	/Y Boom Disable	3/4 ACC	3-09 Low
40A	-Y Boom Enable	3/4 CCA	3-10 High
40B	-Y Boom Disable	3/4 CCC	3-10 Low
41A	-X/Y Damper Boom Enable	3/4 ADA	3-11 High
41B	-X/Y Damper Boom Disable	3/4 ADC	3-11 Low
42A	/X-Y Damper Boom Enable	3/4 ABA	3-12 High
42B	/X-Y Damper Boom Disable	3/4 ABC	3-12 Low

TABLE 6-1 (continued)
DODGE COMMAND ASSIGNMENTS

<u>Command</u>	<u>Command Function</u>	<u>Modulator Tones</u>	<u>Telltale No. Ind.</u>
43A	Boom(s) Extend (Inv. 1)/Retract (Inv. 2)	3/4 CDA	3-13 Spcl.
43B	Boom(s) Retract (Inv. 1)/Extend (Inv. 2)	3/4 CDC	3-13 Spcl.
44A	Select Inverter No. 1	3/4 AAB	3-14 High
44B	Select Inverter No. 2	3/4 AAD	3-14 Low
45A	Inverter Power On	3/4 BBA	3-15 High
45B	Inverter Power Off	3/4 BBC	3-15 Low
46A	Z Axis Fixed Magnetic Moment Negative	3/4 CBA	4-01 High
46B	Z Axis Fixed Magnetic Moment Positive	3/4 CBC	4-01 Low
47A	Z Axis Magnetic Moment Fixed	3/4 DCB	4-02 High
47B	Variable Z Axis Magnetic Moment Enable	3/4 DCD	4-02 Low
48A	Magnetic Damping State 1	3/4 DAB	4-03 High
48B	Magnetic Damping State 2	3/4 DAD	4-03 Low
49A	Magnetizer-Positive Polarity	3/4 BAB	4-04 High
49B	Magnetizer-Negative Polarity	3/4 BAD	4-04 Low
50A	Magnetizer-High Charge Rate	3/4 CCB	4-05 High
50B	Magnetizer-Low Charge Rate	3/4 CCD	4-05 Low
51A	Magnetizer Capacitor Discharge	3/4 ACB	4-06 High
51B	Magnetizer Capacitor Charge	3/4 ACD	4-06 Low
52A	Hysteresis TW Damper State 3	3/4 CAB	4-07 Spcl.
52B	Hysteresis TW Damper State 4	3/4 CAD	4-07 Spcl.
53A	Square Wave Generator On	3/4 DDA	4-08 High
53B	Square Wave Generator Off	3/4 DDC	4-08 Low
54A	TW Hysteresis Damper On	3/4 BCB	4-09 High
54B	TW Hysteresis Damper Off	3/4 BCD	4-09 Low
55A	Programmer Enable	3/4 ABB	4-10 High
55B	Programmer Disable	3/4 ABD	4-10 Low
56A	High Overvoltage Zener (Low Temp.)	3/4 BDA	4-11 High
56B	Low Overvoltage Zener (High Temp.)	3/4 BDC	4-11 Low

TABLE 6-1 (continued)
DODGE COMMAND ASSIGNMENTS

<u>Command</u>	<u>Command Function</u>	<u>Modulator Tones</u>	<u>Telltale No. Ind.</u>
57A	Timing Marks In	3/4 CBB	4-12 High
57B	Timing Marks Out/LVS Reset	3/4 CBD	4-12 Low
58A	Modulation Mode Select	3/4 ADB	4-13 High
58B	Modulation Mode Select	3/4 ADD	4-13 Low
59A	Modulation Mode Select	3/4 CDB	4-14 High
59B	Modulation Mode Select	3/4 CDD	4-14 Low
60A	Manual Main Power On/Off (Normal)	3/4 DBA	4-15 High
60B	Manual Main Power Off/On	3/4 DBC	4-15 Low
61A	Attitude Commutator A Stop	3/4 BBB	5-01 High
61B	Attitude Commutator A Start	3/4 BBD	5-01 Low
62A	Attitude Commutator B Stop	3/4 DBB	5-02 High
62B	Attitude Commutator B Start	3/4 DBD	5-02 Low
63A	Housekeeping Commutator Stop	3/4 BDB	5-03 High
63B	Housekeeping Commutator Start	3/4 BDD	5-03 Low
64A	All Commutators Stop	3/4 DDB	5-04 High
64B	All Commutators Start	3/4 DDD	5-04 Low

6.2 Command Function Descriptions

1A: Automatic/Manual Main Power ON/OFF.

This command or its back-up command 60A, B provides control over the outputs of the two main converters and the output of the regulated TV converter. The command actuates a relay that closes the transistor oscillator base drives in both the master and the slave oscillator in the converters.

1B: Automatic/Manual Main Power OFF/ON.

This command or its back-up command 60A, B opens the base drives of the master and slave oscillators in the two main converters and in the regulated TV converter, thereby turning the converter outputs OFF.

2A: Main Converter No. 1.

2B: Main Converter No. 2.

Commands 2A and 2B switch to either main converter No. 1 or to main converter No. 2 the primary input (+10.7V) derived from the main solar array/main power bus. CAUTION: These commands should be sent ONLY when the main and the TV converters are OFF. (Command 1A, B)

3A: Battery Mode/LVS Reset.

The following remarks are referenced to the Functional Block Diagram, Power Distribution, DODGE.

In "Battery Mode" the main solar array is charging the battery at all times with the possibility that auxiliary solar arrays #1 and #2 may be switched in parallel with the main solar array if desired. Also, with Command 3A in effect the solar arrays are capable of supplying power to the main converters and also to command converter No. 2, the TV converter and the Standby converter.

3B: Solar Only Mode.

This command switches the battery from the main power bus and substitutes a zener diode clamp.

The low voltage sensor (LVS) should be discussed. If low battery voltage is detected by the LVS, it switches Command 3A to Command 3B and additionally removes the converter inputs from the solar arrays, with the exception of command converter No. 2. Command 57B reconnects the +10.7V bus supplying the converters to the solar arrays.

If the LVS executes Command 3B and disconnects the solar arrays from the +10.7V bus the following steps should be taken.

1. Never disconnect the LVS except in most unusual cases. It is a safety device.
2. Turn off the main converters (Command 1A, B or Command 60A, B).
3. Send Command 3A and Command 57B to start charging the battery again. If an abnormally high load is removed from the battery the open circuit voltage should increase toward a more normal value and deactivate the LVS.
4. If the LVS executes Command 3A again it might be necessary to send Command 2A, B to change main converters. Quite possibly the input to one converter may have become shorted.

4A: Low Voltage Sensor IN.

4B: Low Voltage Sensor OUT.

This command enables or disables the low voltage sensor (LVS). Since the LVS is a valuable safeguard against disastrously low battery voltages it should not be disabled except in the event that the unit itself malfunctions. The LVS changes state when battery voltage drops to 9.0V.

5A: Standby Converter ON.

5B: Standby Converter OFF.

Command 5 connects or disconnects the +10.7V input to the standby converter. Because the standby converter supplies power to continuous duty loads only, the command state 5A is normally in effect. These continuous duty loads are: oven, oscillator, regulators, buffer, low TV, enhanced magnetic damping, hysteresis torsion wire damper, and Z-torquing.

6A: Auxiliary Solar Array No. 1 on Main Bus.

6B: Auxiliary Solar Array No. 1 on ATC No. 1 (Battery).

The commands 6A, B switch the output of the auxiliary solar array No. 1 to either the main bus or to the battery automatic temperature control unit No. 1.

7A: Auxiliary Solar Array No. 2 on Main Bus.

7B: Auxiliary Solar Array No. 2 on ATC (Battery/Damper).

This command switches the output of auxiliary solar array No. 2 between the main bus and the automatic temperature control units for the battery or the torsion wire damper.

8A: Auxiliary Solar Array No. 2 on ATC No. 2 (Battery).

8B: Auxiliary Solar Array No. 2 on Damper ATC.

Command 8 has the effect of switching power from Auxiliary Solar Array No. 2 to either Automatic Temperature Control No. 2 for the battery or to the Torsion Wire Damper Automatic Temperature Control. Command 7B must be in effect to enable Command 8.

9A: Enhanced Magnetic System ON.

9B: Enhanced Magnetic System OFF.

This command connects or disconnects the +4.0V and the $\pm 10.7V$ input voltages to the attitude books Nos. 2, 3, and 4. This controls power to the magnetic damping system with the exception of the magnetometers, the demagnetizer, and the magnetic bias generator.

10A: Oscillator and Regulator No. 1.

10B: Oscillator and Regulator No. 2.

This command selects Oscillator and Regulator No. 1 or Oscillator and Regulator No. 2 by switching -32.1V to either.

The ONLY reason to switch from one Oscillator-Regulator to the other is excessive oscillator drift or noise. If a change of oscillator is required there will be a transient drift of oscillation of about four hours duration. Actually the drift will be quite low within a few minutes. The regulator voltage should be -12.400 ± 0.200 volts.

11A: Oscillator Oven No. 1.

11B: Oscillator Oven No. 2.

11A, B allows the choice of two Oscillator-Regulator ovens. This is accomplished by switching a -32.1V input to either oven.

The same rule that applied to switching oscillators holds for switching ovens. ONLY in the event of failure should the ovens be switched.

Temperature variations of $\pm 1/2^\circ C$ mean heater failure, but such a small heater temperature probably could not be seen on the telemetry. If one heater is turned off and the other turned on, a four day frequency drift transient will occur.

If T = outer flask temperature, the limits of temperature regulation of the oscillator by the oven are $-5^{\circ}\text{C} \leq T \leq +48^{\circ}\text{C}$. If the outer flask temperature exceeds these limits it does not necessarily imply destruction of the oscillators, but rather a faster rate of frequency drift. Actually the oscillators can survive 100°C outer flask temperatures.

12A: 136 MHz Transmitter OFF.

12B: MHz Transmitter ON.

Controls the supply voltage to the 136 MHz transmitter. This voltage is -21.4V for low power operation and -32.1V for high power operation.

13A: 240 MHz Transmitter ON.

13B: 240 MHz Transmitter OFF.

The remarks for Command 12A, B apply.

14A: Transmitters on High Power.

14B: Transmitters on Low Power.

This command switches the supply voltage to both the 136 MHz and the 240 MHz transmitters between -21.4V for low power operation and -32.1V for high power operation.

15A: Spare.

15B: Spare.

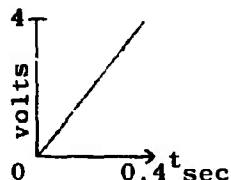
16A: TV System Converter Enable.

16B: TV System Converter Disable.

This command connects or disconnects the +10.7V battery bus from the Regulated TV converter. It also disconnects the +10.7V standby filament voltage to the 60° camera.

17A; TV System Scan Normal.

NORMAL
(Slow)

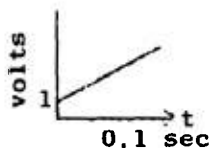


Scan Time:
200 sec. per
frame No. of
Elements:
512 by 512

Horizontal Sweep
Voltage

17B: TV System Scan Fast Expanded.

NORMAL
Fast



Scan Time: 25 sec.
per frame No. of
Elements:
128 per line
256 lines

Horizontal Sweep
Voltage

The samples of the video take place at the same intervals of time for both slow and fast scan modes. Therefore since the horizontal fast scan sweep voltage completes its cycle in $1/4$ of the time of the slow scan sweep and travels $1/2$ the distance, the samples occur twice as far apart in the fast scan case as compared with the sample spacing for the slow scan mode.

Fast scan covers $1/4$ the area of the slow scan faster and takes $1/8$ the time or 25 seconds per frame.

18A: TV Cameras Protected by Sun Sensors.

18B: TV Cameras NOT Protected by Sun Sensors.

The vidicon camera tubes in the TV system are normally protected from the high intensity radiation of the sun by sensors having a somewhat larger field of view than the cameras they are protecting. The effect of a sun sensor sending a signal corresponding to detection of the sun within the field of view of a corresponding camera is to override an open-shutter command. ONLY in the event that the sensors fail should Command 18B be used.

19A: Not Used.

19B: 22° TV Camera Filter Advance.

The 22° field of view TV camera has an eight-position filter wheel that is being used for color work and additionally for minimizing Rayleigh scattering. Three filters, blue, green, and red furnish color information. The remaining five filter wheel positions house a clear opening and four short wavelength cut-off filters that have different cut-off frequencies. These cut-off filters will perform experiments in enhancing black and white picture contrast by successively reducing the effects of Rayleigh scattering which varies as λ^{-4} where λ is the wave-length of light. PCM Telltale No. 5, positions 13, 14, and 15 tells what filter is presently in position in front of the camera. Since the filter position changes (advances to the next position) with shutter closure, the telltale also indicates the type of filter that will be used for the next exposure of the vidicon.

The telltale filter designations and filter functions appear in the following table:

PCM Telltale No. 5

<u>Filter Code</u>	<u>Filter Function</u>	<u>13</u>	<u>14</u>	<u>15</u>
00	Haze 4 (5400 Å cut-off)			
01	Blue			
02	Green			
03	Red			
04	Blank (clear)			
05	Haze 1 (4800 Å cut-off)			
06	Haze 2 (5000 Å cut-off)			
07	Haze 3 (5200 Å cut-off)			

Perhaps an example will best illustrate what the effect of Command 19B will be.

Suppose the filter position was 01 at 30 minutes before the hourly automatic turn-on time of the satellite, and the desired initial position for the next automatic cycle was 04. The procedure would be to send command 55B to disable the automatic programmer and then to send Command 19B three times to go from 01 to 02, 02 to 03, and from 03 to 04. There is necessarily an approximate 10 second delay between commands because of the charging time of the capacitors furnishing the necessary energy to advance the shutter. Now filter 04 is in position for the first exposure of the 22° camera in the automatic cycle. The camera will be erased twice before exposure because the capacitors that actuate the shutter will not be charged when the first command to open the 22° shutter is sent by the programmer. If the manual advancing were not completed by at least 10 seconds before

the automatic programmer turn-on, the capacitors storing energy to open the 22° shutter would not be discharged and the desired filter would be exposed on the already exposed target of the 22° field of view vidicon. This would probably result in a saturated target and no meaningful video for the first frame of the automatic sequence. Since the video signal is not connected to the transmitters in the first 200 seconds of automatic operation this would not be noticed from the ground until the second reading of the 22° camera. Send Command 55A.

20A: TV SCO No. 2.

20B: TV SCO No. 1.

This command supplies power to either of two identical 13.5 kHz subcarrier oscillators that process the video signal from the TV camera system.

21A: Flywheel motor enable/disable.

21B: This command connects/disconnects the two quadrature primary phases of the flywheel with the output of the boom inverter.

22A: Set Programmer Start Time/136 OFF.

In order to reset the programmer the following three steps must be used.

1. Send Command 22A.
2. Turn on the satellite with Command 1A.

Step 2 must be sent within 200 seconds of 1 or else interference will occur between the transmitted commands and the programmer.

Under no circumstances should the satellite be commanded with commands 1 through 32 when the automatic programmer is enabled. Also, if the programmer is not in use it should be disabled at all times. (Command 55B)

After the two command sequence outlined above, the automatic programmer will start automatically once per hour and will run the satellite for 10 minutes and then shut off, unless commanded to do otherwise. The 10 minute ON-time is subdivided as follows. $t = 0$ is the start time.

$t = -77$ seconds	:	TV-vidicon filaments ON
$t = 0$:	Satellite ON
$t = 1.17$:	TV Synch. pulse
$0.4 \leq t \leq 200$:	Attitude, House-keeping func., TV camera erase.
$t = 202.5$:	TV Synch. pulse
$202.1 \leq t \leq 400$:	Attitude, House-keeping, TV 60° scan, TV -22° erase.
$400 \leq t \leq 403.8$:	Time burst, phase changes, TV Synch.
$403.8 \leq t \leq 600$:	Attitude, House-keeping, TV 22° scan, TV 60° erase.
$t = 605.1$:	Satellite OFF.

The time burst waveform consists of 126 cycles of 325.5 Hz square wave of 0° phase followed by two cycles of the same frequency square wave but with 180° phase. This timing burst is used so that tracking information may be obtained.

Note that if the TV system is on fast scan, one erase frame followed by 7 picture-taking frames occur in the first 200 seconds of automatic operation. However, the telemetry channel for the video information is not connected to the transmitters until 200 seconds has elapsed. Thus only 16 frames are actually transmitted if the fast scan mode is used throughout the 10 minute automatic cycle. Command 55A must be sent to enable the automatic programmer.

22B: Magnetometer Calibrate.

This command generates a signal within the Enhanced Magnetic Damping System which allows the magnetometers to be calibrated.

23A: Magnetometer Power ON/Demagnetizer OFF.

This command removes $\pm 10.7V$ from the inputs of the demagnetizer and applies the voltages to the X, Y, and Z magnetometers of the Enhanced Magnetic Damping System. If Command 23A is part of a demagnetizing cycle, it is important to send Command 26B first to decouple the hysteresis generator from the magnetometer outputs and then send Command 23A, thereby eliminating the initial offset that would otherwise be caused by turn-on current transients in the magnetometers. Then send Command 26A to reconnect the magnetometer outputs to the hysteresis generator if enhanced hysteresis damping is desired.

23B: Magnetometer Power OFF/Demagnetizer ON.

Command 23B disconnects $\pm 10.7V$ from the magnetometers and connects it to the demagnetizer. A zero average value alternating signal then degausses the hysteresis generator provided Command 26A is in effect.

24A: Magnetic Spin/Despin Enable.

Command 24A connects the Y electromagnet negatively to the X magnetometer output and the X electromagnet to the Y magnetometer output. Thus, depending on the state of Command 25, the resulting magnetic moment created by the X-axis and Y-axis electromagnets either leads or lags the magnetic field intensity component in the XY plane by 90° .

24B: Enhanced Magnetic Damping Enable.

Command 24B connects the X and Y electromagnets and the Z coil to the output of the 3-axis hysteresis generator through the adder-amplifier corresponding to each axis.

25A: Spin Torque Positive.

Command 24A must be in effect. With Command 25A, the magnetic moments created by the X electro-magnet and the Y electromagnet lead by 90° the X and Y components of the ambient magnetic field.

$$\begin{aligned} M_x &= KH_y & M &= \text{Magnetic Moment} \\ & & H &= \text{Magnetic Field Intensity} \\ M_y &= -KH_x & K &= \text{Gain Factor} \end{aligned}$$

25B: Spin Torque Negative.

Command 24A must be in effect. Command 25B reverses the phase of the magnetic moments of the X and Y electromagnets so that the moments lag the X and Y components of the ambient magnetic field by 90°.

$$\begin{aligned} M_x &= KH_y & M &= \text{Magnetic Moment} \\ & & H &= \text{Magnetic Field Intensity} \\ M_y &= KH_x & K &= \text{Gain Factor} \end{aligned}$$

26A: Select Enhanced Hysteresis Damping.

This command applies $\pm 10.7V$ and $+4V$ to the hysteresis generator and the associated amplifiers. Command 24B must be in effect for Command 26 to be enabled.

26B: Select Phase Lag Damping.

Command 26B removes $\pm 10.7V$ and $+4V$ from the hysteresis generator and applies those voltages to the phase lag generator. The outputs from the phase lag generator are then connected to the 3-axis adders and current amplifiers. Again, Command 24B must be in effect.

27A: Phase Lag Sample Time Automatic.

This command allows the phase lag generator to automatically sample the ambient magnetic field at either three or six hour intervals. Because Torque = $\vec{M} \times \vec{H}$ where \vec{M} is the magnetic dipole moment of a particular satellite axis and \vec{H} is the external

magnetic field intensity, it is desirable to have the vectors M and H nearly orthogonal for maximum damping torque.

Since the natural period of gravity librations is approximately 24 hours, the 6-hour sampling time constant will therefore be a quarter of an oscillation cycle and the M and H vectors will tend to be displaced by 90° from each other.

27B: Phase Lag Time Counter Step and Hold.

Command 27B allows manual sampling of the ambient magnetic field by the phase lag generator. Additionally, leaving Command 27B in effect overrides the automatic 3- or 6-hour samples. In order to set up a 3-hour or a 6-hour sample, Command 27 must be toggled between A and B positions three times after the initial sample for the 3-hour hold and six times after the initial sample for the 6-hour hold.

28A: Enhanced Hysteresis - Gain High - 3 Hour Hold.

Command 28A affects both hysteresis damping and phase lag damping. It selects a high gain operating mode for the amplifiers driving the hysteresis generator from the magnetometers, and also selects a 3-hour automatic sample interval for the phase lag generator.

28B: Enhanced Hysteresis - Gain Low - 6 Hour Hold.

This command selects a low gain mode for the amplifiers driving the hysteresis generator from the magnetometers and selects a 6-hour sample interval for the phase lag generator.

29A: Enable XZ Fixed Magnetic Moment.

29B: Disable XZ Fixed Magnetic Moment.

Command 29 connects or disconnects $\pm 10.7V$ to the magnetic bias generator which in turn may supply the X and Z adders and current amplifiers which drive the X electromagnet and the Z coil.

30A: Select Fixed XZ Magnetic Moment.

This command connects the output of the magnetic bias generator to the input of the X and the Z adders and current amplifiers.

30B: Select Variable XZ Magnetic Moment.

Command 30B connects the outputs of the X and the Z magnetometers to the inputs of the X and the Z adders and current amplifiers.

31A: Damper Boom Angle Detector ON.

31B: Damper Boom Angle Detector OFF.

Command 31 connects or disconnects +10.7V and +21V to the digital damper angle detector.

32A: Damper Cage Motor Enable.

32B: Damper Cage Motor Disable.

This command opens or closes the quadrature primary windings of the damper cage motor which in turn rotates a cam which moves a spring-loaded plunger up and down in a hole in the damper boom thereby preventing damper boom rotation. Command 32 may be sent even though the pin and the hole do not line up because the spring-loading of the pin ensures that no damage can take place. (The initial motion of the cam unlocks the launch lock of the torsion wire assembly.)

33A: +Z Boom Enable (#5 Boom).

33B: +Z Boom Disable.

Command 33 connects or disconnects the two quadrature primary phases of the +Z boom motor with the output of the boom inverter through phase reversing switches.

IMPORTANT: ONLY one pair of opposing boom motors should be enabled at any given time because the boom inverter cannot supply any more power than that required to operate two boom motors. Failure

to observe this restriction can result in the failure of the boom inverter.

34A: -Z Boom Enable (#6 Boom).

34B: -Z Boom Disable.

The information for Command 33 applies.

35A: +X+Z Boom Enable (#1 Boom).

35B: + X+Z Boom Disable.

The information for Command 33 applies.

36A: -X-Z Boom Enable (#3 Boom).

36B: -X-Z Boom Disable.

The information for Command 33 applies.

37A: -X+Z Boom Enable (#4 Boom).

37B: -X+Z Boom Disable.

The information for Command 33 applies.

38A: +X-Z Boom Enable (#2 Boom).

38B: +X-Z Boom Disable.

The information for Command 33 applies.

39A: +Y Boom Enable (#8 Boom).

39B: +Y Boom Disable.

The information for Command 33 applies.

40A: -Y Boom Enable (#7 Boom).

40B: -Y Boom Disable.

The information for Command 33 applies.

41A: -X+Y Damper Boom Enable.

41B: -X+Y Damper Boom Disable.

The information for Command 33 applies. Additionally, the power to the damper boom motor is sent via a transformer; the primary windings and core of which are mounted rigidly on the satellite stack. The secondary windings are connected to the quadrature primary windings of the boom motor. The primary windings of the transformer are connected or disconnected to the boom inverter output by Command 41.

IMPORTANT: The damper boom must be caged before enabling takes place.

42A: +X-Y Damper Boom Enable.

42B: +X-Y Damper Boom Disable.

The comments for Command 41 apply.

43A: Boom(s) Extend (Inv. 1)/Retract (Inv. 2).

This command reverses the phase of the inverter output driving the boom motors. Thus if inverter No. 1 is in use, the enabled booms will be extended. If inverter No. 2 is in use the booms will retract if Command 43A is in effect.

43B: Boom(s) Retract (Inv. 1)/Extend (Inv. 2).

Command 43B reverses the phase of the output of the boom inverter driving the boom motors. If inverter No. 1 is being used the enabled booms will retract if Command 43B is sent. If inverter No. 2 is in operation the enabled booms will extend.

44A: Select Inverter No. 1.

44B: Select Inverter No. 2.

Command 44 selects one of two inverters that drive any enabled booms. The inverters are wired to change the output phases as the inverters are changed. This provides redundancy for Command 43.

45A: Inverter Power ON.

45B: Inverter Power OFF.

Command 45 connects or disconnects the +10.7V input to the boom inverter.

46A: Z-Axis Fixed Magnetic Moment Negative.

46B: Z-Axis Fixed Magnetic Moment Positive.

This command reverses the Z coil leads to +10.7V and to ground.

47A: Z-Axis Magnetic Moment Fixed.

Command 47A connects the Z coil to ground and +10.7V.

47B: Variable Z-Axis Magnetic Moment Enable.

This command connects the Z coil to the output of the Z adder and current amplifier so that the Z coil can be supplied with signals from the magnetic bias generator, the Z magnetometer, the hysteresis generator, or the phase lag generator.

48A: Magnetic Damping State 1.

Command 48A sets the X, Y, and Z adders and current amplifiers into a high gain (X1 voltage) mode. Command 48A allows damping states 3 and 4 depending on whether Command 52B or Command 52A is in effect respectively.

The 4 damping states of the hysteresis torsion wire damper are defined as follows:

Damping State 1:

Command State:	48B, 52B
Damping Torque:	± 20 dyne-cm
Power Dissipated:	0.10 watt

Damping State 2:

Command State:	48B, 52A
Damping Torque:	± 65 dyne-cm
Power Dissipated:	0.45 watt

Damping State 3:

Command State	48A, 52B
Damping Torque:	-130 dyne-cm
Power Dissipated:	0.90 watt

Damping State 4:

Command State:	48A, 52A
Damping Torque:	-250 dyne-cm
Power Dissipated:	3.40 watts

48B: Magnetic Damping State 2.

This command sets the X, Y, and Z adders and current amplifiers into a low gain (X.0.25 voltage) mode. Command 48B allows damping state 1 or 2 depending on the state of command 52. See the information under Command 48A for damping states 1 and 2.

49A: Magnetizer - Positive Polarity.

49B: Magnetizer - Negative Polarity.

Command 49 changes the direction of the eddy current damper magnetizing current from the magnetizer control module.

50A: Magnetizer - High Charge Rate.

50B: Magnetizer - Low Charge Rate.

Command 50 charges a capacitor within the magnetizer control module at two different rates. This is accomplished by switching the output of the magnetizer converter between two possible resistive charging paths.

51A: Magnetizer Capacitor Discharge.

51B: Magnetizer Capacitor Charge.

This command actuates a relay within the magnetizer control module that connects or disconnects the magnetizer winding of the eddy current damper with the capacitor within the

magnetizer control module. The capacitor is thereby discharged, sending current to the eddy current damper changing the magnetization of the hysteretic damper core.

52A: Hysteresis Torsion Wire Damper State 3.

See the data on Damping states appearing under Command 48A. Damping states 2 and 4 are possible with Command 52A in effect.

52B: Hysteresis Torsion Wire Damper State 4.

As may be seen in the data on damping states appearing under Command 48A, damping states 1 and 3 are possible using Command 52B.

53A: Square Wave Generator ON.

53B: Square Wave Generator OFF.

Command 53 connects or disconnects $\pm 10.7V$ from the main converter to the Hall detector electronics and regulated square wave generator. The Hall detector measures the magnetic flux density in the air gap of the horse-shoe magnet of the eddy current damper, and thus measures the damping constant.

54A: Torsion Wire Hysteresis Damper ON.

54B: Torsion Wire Hysteresis Damper OFF.

Command 54 connects or disconnects the standby converter $+10.7$ to the damper.

55A: Programmer Enable.

55B: Programmer Disable.

Command 55 connects or disconnects one line of $+21.4V$ from the standby converter to the automatic programmer. Command 55A must be in effect before Command 22A is effective.

56A: High Overvoltage Zener (Low Temperature).

56B: Low Overvoltage Zener (High Temperature).

Command 56 switches either of two different voltage zener diodes between the main bus (the output of the solar arrays and/or the positive voltage terminal of the battery) and ground through a current limiting resistor. This effectively clamps the supply voltage to the satellite at some maximum value.

57A: Timing Marks IN.

This command connects the output of the timing mark generator to the switches in the Modulation Index control controlled by Commands 58 and 59. It is then possible to obtain timing information on either of the transmitters. (See TM Operating Modes following Commands 58 and 59.)

57B: Timing Marks Out/LVS Reset.

Command 57B disconnects the timing mark generator from the Modulation Index control and substitutes TM and TV inputs. Additionally Command 57B functions as a reset for a switch connecting the solar array outputs to the main power bus. If the low voltage sensor opens the switch, Command 57B as well as Command 3A must be sent to restore the power system to normal operation.

58A, B: Modulation Mode Select.

59A, B:

Commands 57, 58, and 59 select the TM System operating modes as defined in Section 5.

60A: Manual Main Power ON/OFF (Normal).

60B: Manual Main Power OFF/ON.

Command 60 is intended as a back-up for Command 1. It is a redundancy in case Command 1 becomes inoperative.

61A: Attitude Commutator A STOP.

61B: Attitude Commutator A START.

Command 61 stops commutator A on any of its 36 channels so that continuous analog data may be obtained if desired. When sending the TADEx command to stop a commutator it should be remembered that a delay of 4 to 5 seconds occurs between the time of initiating the command and the time that the command actually takes effect because of the 4-tone burst involved. Therefore the command to stop a commutation should be sent 4 channels before the one desired is "up" to be read.

62A: Attitude Commutator B STOP.

62B: Attitude Commutator B START.

The information under command 61 applies.

63A: Housekeeping Commutator STOP.

63B: Housekeeping Commutator START.

The information for Command 61 applies.

64A: All Commutators STOP.

64B: All Commutators START.

The information for Command 61 applies.

6.3 In-Orbit Performance

The satellite command system has operated extremely well. More than 4300 commands have been sent and successfully executed.

A few anomalies have occurred in the DODGE command system but they have not detracted from the usefulness of the system. The following discussion of anomalies is included for historical purposes and completeness of the record on the performance of the command system rather than to indicate serious complications.

The satellite responded properly to all commands until 10 May 1968 when the APL Command and Telemetry Station 502 reported that command anomalies occurred during DODGE's 27th pass, which was to end the next day. Essentially, these anomalies consisted of two commands performed for one requested. The following week a set of test commands was drawn up in an effort to find the cause. On 4 June 1968 an abbreviated version of this test was run. From a practical standpoint it is not possible to exercise the entire command system for a test such as this; there are too many commands that would destroy the spacecraft's attitude or endanger its health. For this reason the information about the anomalous behavior remains very sketchy. The test on 4 June merely confirmed the difficulties encountered during DODGE daily operations.

The DODGE satellite is still serving a useful function in spite of the command difficulties. Since it would be difficult, if not impossible, to determine a failure mechanism even by extensive tests and since such tests would certainly cause loss of stabilization, further tests are not anticipated.

The observed command discrepancies are listed below. The first line, for example, means that when command 55A (programmer enable) is transmitted in addition to enabling the programmer the command system also stops commutator A (Command 61A).

<u>Command Transmitted</u>	<u>Additional Command Executed</u>
55A	61A
55B	58B
57A	61A and 62A
57B	61A
58B	61A
35B	63B
38B	62B
6A	61A
6B	61A
59A	55B
7B	61A

In some cases each time a particular command is sent the additional command is also performed. In other cases the additional command is performed only occasionally.

No assumed failure mode has been able to explain the observations. It is possible that no amount of ground experimentation would uncover the cause of malfunction, and for reasons stated earlier no further analysis is being done.

The difficulties with the command system have not compromised the satellite mission.

7. THERMAL CONTROL SYSTEM

7.1 Description

The DODGE satellite is the first three-axis, gravity-gradient-stabilized spacecraft at near-synchronous altitude. The orbit and stabilization presented two basic problems for the thermal designer. Because of the 22-hour orbit period, the spacecraft presents one of its sides to the sun for long periods of time. For instance, a side panel can be near normal incidence to the sun for more than 3 hours while sunlit for 11 hours each orbit and then be in the satellite shadow viewing deep space for the remaining hours. Large temperature gradients result from these conditions. Another result of the 22-hour orbit is a 75-minute eclipse period. During this period, only thermal capacity prevents the spacecraft from becoming excessively cold. In order to provide a benign environment for the electronics and the experiments, the large thermal gradient had to be reduced, and the sharp temperature drop during eclipse had to be controlled.

Both environmental problems were solved by isolating the solar array panels from the inner structure, which contains the electronics, by controlled conductive paths, e. g., thermal stand-offs. Radiation between the shell and the electronics was reduced as much as possible with multilayer insulation. This technique allows the hot-side panels to re-radiate most of their absorbed solar energy so that only a small amount of heat is conducted to the inner structure. Radiative relief from panel to panel reduced the hot-side peak temperatures as much as possible. This design also results in a long thermal time constant which is needed to retain the temperature during the 75-minute eclipse period.

The battery required separate consideration because of its smaller operating-temperature range. Thermostatically controlled heaters, which were designed to provide 6 watts of heat at 60°F that decrease linearly to 0 watts at 65°F, were installed directly on the cells.

The magnetometer sensor and torsion wire damper support tube (the mast) also presented a thermal design problem. Since the mast was attached directly to the center of the spacecraft, special precautions had to be taken to prevent an intolerable heat leak. The open end of the tube was equipped with two self-closing doors so that heat loss would be minimized but the -Z boom end mass could still pass. In addition, an external cover supported by lacing was fitted around the mast and insulated from it by multilayer insulation.

Due to the complexity of the structure, a large number of nodes was required to construct an accurate thermal analogue. The resulting analytical model consisted of 350 lumped capacity nodes and 650 conductive and radiative resistors. One- and two-dimensional heat conduction techniques were used for the model, and electrical network reduction methods reduced the number of nodes and resistors to an amount compatible with the computer memory capacity. A program was written to calculate the orbital heat inputs to all external surfaces from Kepler data and satellite geometry. Using these heat inputs with the thermal analogue, temperatures were predicted for all limiting orbital environments and satellite operating modes.

A system thermal vacuum test of the spacecraft checked out the spacecraft under orbit conditions and verified the analytical model. Electrical heater panels, which replaced the flight solar array panels, were used to simulate the solar heat loads. The 22-hour orbit was simulated by cycling the electrical heat inputs to these exterior surfaces.

Overall results of the thermal vacuum test agreed well with the analytical predictions, with only a few areas having significant disagreement. A comparison of the predictions with the test results is shown in Fig. 7-1 for the minimum sun orbit case, and the agreement is quite good over the entire orbit.

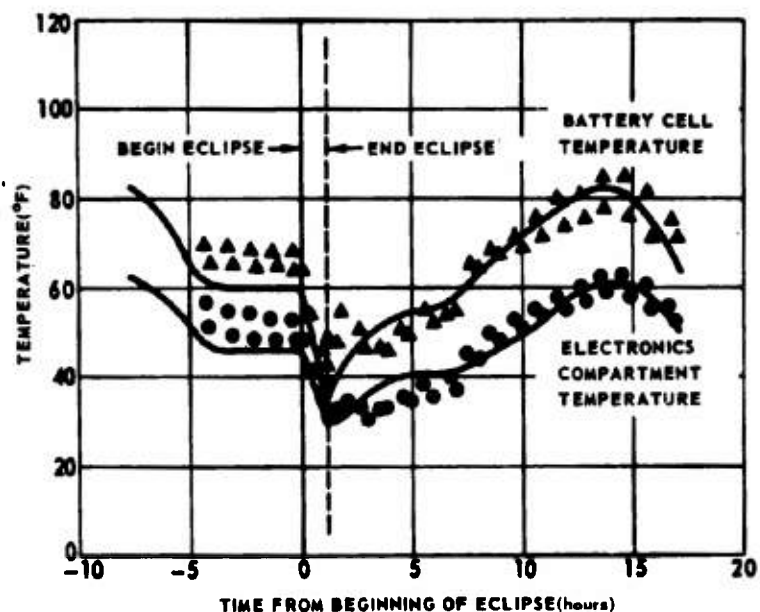


Fig. 7-1 THERMAL VACUUM TEST RESULTS COMPARED WITH ORBIT PREDICTIONS (MINIMUM SUN ORBIT, DAY 81, 1967)

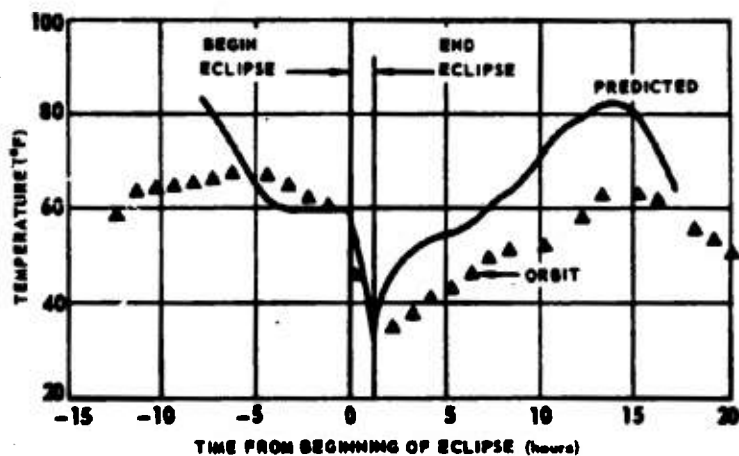


Fig. 7-2 TELEMETERED BATTERY CELL TEMPERATURE COMPARED WITH ANALYTICAL PREDICTION (MINIMUM SUN ORBIT, DAY 284-285, 1967)

During thermal vacuum testing and later in orbit, telemetered internal temperatures were reduced by computer.

7.2 In-Orbit Performance

Of course, the ultimate proof of success of the thermal design is the orbital performance. As an example, a comparison of telemetered battery cell temperatures with the predicted temperature is shown for the cold orbit in Fig. 7-2.

Other internal temperatures have been within the limits observed during thermal vacuum testing. A measure of the effectiveness of the isolation techniques is shown by comparing the observed internal gradient of 30°F with the external gradient of 400°F. During the eclipse period (see Fig. 7-2), internal temperatures dropped about 40°F, indicating that the thermal time constant is about 20 hours. Maximum solar panel temperatures are about +220°F, and the minimum temperatures are -200°F; however, the solar array is loaded in the least temperature-sensitive portion of the I-V curve, and no problems have been observed.

Now that the DODGE satellite has been in orbit for more than a year it is useful to compare the current thermal performance with the initial performance. This comparison can indicate whether thermal control coatings have behaved as predicted and whether the internal power levels remain at the expected levels.

In order to make a valid comparison, times when good stabilization was achieved must be chosen, and for this purpose days 97 through 101, 1968, and 272 through 276, 1967 were picked. These days are close to the times of the vernal and autumnal equinoxes. Shown below in tabular form is a comparison of the maximum and minimum average temperatures for these periods.

Thermistor Location	Days 272 - 276 1967		Days 97 - 101 1968	
	Temperature °F		Temperature °F	
	High	Low	High	Low
Battery Cell	58	34	63	41
240 MHz	63	26	77	21
60° TV	48	31	60	21
FM Book	62	18	71	14
Mag. Sensor	66	15	75	4
Damper Vane	56	22	79	25

It is readily apparent that although some differences exist no significant change in temperature has occurred during this period of about 6 months. This can be attributed to compensating degradation of the solar array and the thermal control coatings. The expected loss in array output due to particle bombardment results in about a 5°F drop in internal temperature which is balanced by the outer shell increase of about 7°F due to thermal control coating degradation. The other possibility is that any change is lost in the experimental accuracy due to measurement and the way the averages are taken.

In either case the conclusion is that thermally the DODGE satellite is still operating satisfactorily; little if any change in the average temperature has occurred. It is not necessary to limit the satellite operation in any of the standard operational modes because of temperature limitations.

BLANK PAGE

8. DOPPLER TRACKING SYSTEM

8.1 Near-Synchronous Orbit Tracking

Before DODGE was launched, APL made a study to determine if a satellite in a near-synchronous orbit of DODGE characteristics could be tracked using doppler data only. The study showed that the satellite could be tracked using doppler data only and that the existing computer programs could be used with only slight modifications.

As the period of the satellite orbit approaches synchronism with earth rotation its doppler signals approach zero. Since the expected doppler signal would be tenuous, at best, it became imperative to investigate probable error sources. Among those investigated were the following:

- a. Ionospheric Refraction - This proved to be the largest error in the system, amounting to an error on the order of 50 km in satellite position.
- b. Satellite Oscillator Drift - Oscillator drift rates on the order of 1 part in 10^{10} /day are within the state-of-the-art and yield errors on the order of 1 km in satellite position determination.
- c. Differential Station Oscillator Drifts - When different stations do not maintain their oscillators relative to the same "standard" their oscillators may drift at different rates thus inducing a tracking error. It was found that differential drift rates of 6 parts in 10^{10} /day could induce errors of 140 km in the tracking.

The theory for tracking a near-synchronous satellite using doppler data is in many ways similar to that for near-earth satellites. The major difference is in the magnitude of the doppler (3 parts in 10^7 as opposed to 3 parts in 10^{10} for near

earth satellites). Additionally, one must allow for significantly more data because of the extended pass length.

Doppler tracking of DODGE serves as the primary source of its orbits and the satellite ephemerides. The tracking program itself provides a measure of both prediction accuracy and tracking accuracy through the changes in the satellite orbit when retracking a predicted orbit over new data.

8.2 DODGE Doppler Data

The station network for collection of DODGE doppler data consists of the following stations:

<u>Station Number</u>	<u>Location</u>
911 (111)	APL, Maryland
008	Sao José Dos Campos, Brazil
112	Smithfield, Australia
013	Misawa, Japan

Some passes were also taken by Station 103 in Las Cruces, New Mexico. All of these stations belong to the TRANET system and their locations are known relative to one another to the order of 60 m (the level of confidence associated with intra-datum ties). This station distribution allows almost constant surveillance of the DODGE satellite in its circuit of the earth.

It has been determined that unless all the station oscillators were maintained, relative to a single standard (WWV), to better than 1 part in 10^{10} per day drift rate, one could expect significant errors in the tracking. To cope with the problem of station oscillator drift, a standard procedure was instituted whereby each station resets its oscillator with WWV at noon local time every day. In addition, records of these corrections were kept so that each station could monitor its own oscillator drift. This resulted in maintenance of station drift rates of less than 1 part in 10^{10} per day. No orbit errors have been directly attributable to this source.

DODGE doppler data are collected in the same manner as near-earth satellite doppler data. That is, the receiving station accumulates a count of positive zero-crossings of a clock frequency during some specified number of cycles of the doppler signal and submits this count, along with the UT time at which the count was started, as raw data to the computing facility. The data are submitted in batches of one point every 4 seconds for spans of 10 minutes or less. A duty cycle in the satellite causes one 10-minute transmission of the satellite's carrier frequency (240 MHz) every hour. Each 10-minute batch is submitted as a separate entity with an identification header. These blocks of data are collected at the computing facility until there is enough data to perform a track. Enough consists of not less than 3 revolutions (about the earth) of the satellite; given 4 stations at 3 passes each, each pass lasting 4.5 days results in 1296, 10-minute blocks of data. At 150 data points per block, the computing program is processing almost 200,000 points per run as a minimum.

8.3 Data Compression

There is obviously a need to compress these data into a representative subset. A 10-minute block of data covers about $(\frac{1}{144})^{\text{th}}$ of the orbital period sine wave (to be explained later) and therefore can be quite adequately approximated by a quadratic. (Fig. 8-1 is a plot of one such 10-minute data block.) A single representative point for each data block is computed by first least squares fitting a quadratic, Q_Y , to the data in the block (eliminating bad or noisy data on a 3σ criterion) and then computing the doppler, Δf_Y , at time t_Y , using the coefficients determined in the fit:

$$\Delta f_Y = Q_Y(t_Y)$$

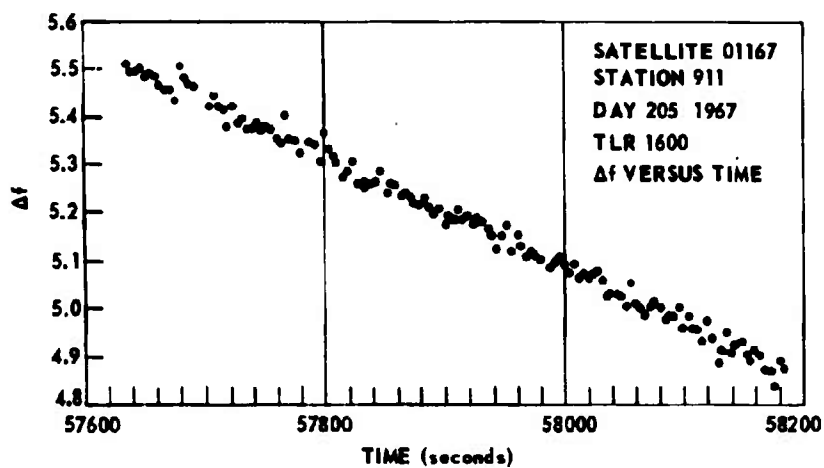


Fig. 8-1 TYPICAL 10-MINUTE BLOCK OF
DODGE DOPPLER VERSUS TIME

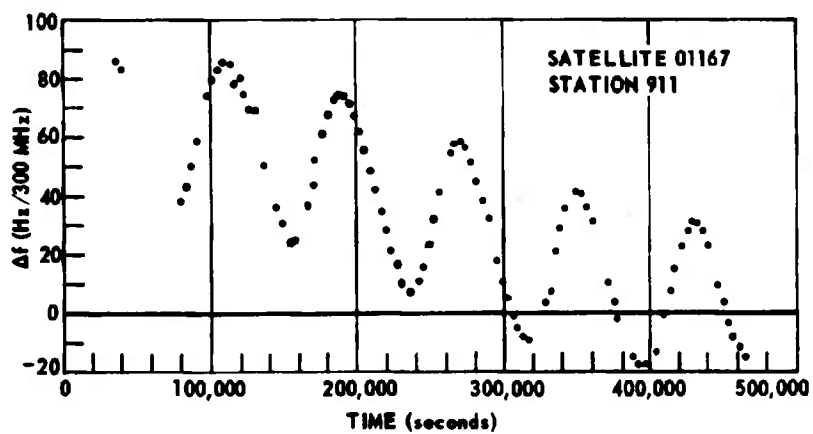


Fig. 8-2 REAL DOPPLER CURVE FROM DODGE PASS:
DAY 214 TO 219, 1967

where

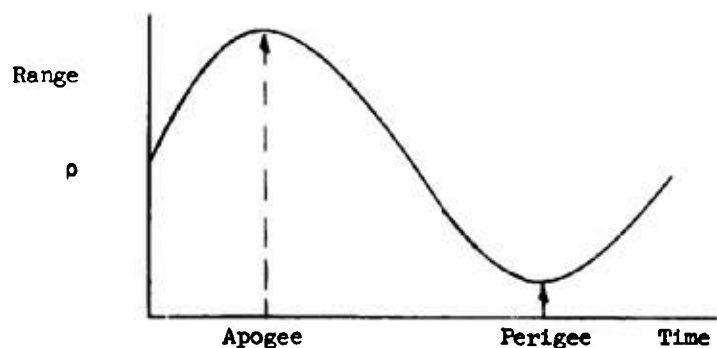
$$t_Y = \frac{t_Y^L - t_Y^F}{2}$$

t_Y^L = time of last data point in the γ th block

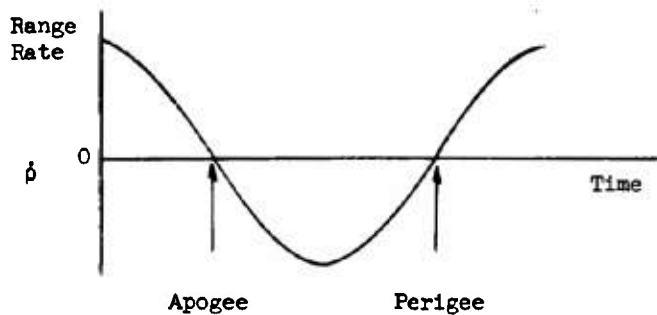
t_Y^F = time of first data point in the γ th block.

By collecting these representative points into groups belonging to the same transit of a given station we generate what we call DODGE "passes." Fig. 8-2 is a plot of a typical DODGE pass.

The doppler curve for a near-synchronous satellite resembles a typical doppler curve with a sinusoid superimposed; where the sinusoid has a period equal to the satellite's period. The sinusoidal oscillation superposed on the typical doppler curve can be understood if one considers a hypothetical satellite fixed in latitude and longitude above the station. If, further, this satellite's orbit has a non-zero eccentricity then its range from the station will vary as they both make one revolution in space. At apogee the satellite will be farthest from the station while at perigee it will be closest.



The range rate will then look like



In the case of a near-synchronous satellite the doppler shift will be a superposition of two physical effects:

- a. The "eccentricity" effect noted above, and
- b. A component resulting from the station-satellite relative motion due to the fact that the satellite's period differs from that of the earth ("classical" doppler curve).

8.4 Tracking Program

The tracking program accepts as input the set of data described in the previous section. All the passes are processed in a batch, i.e., all the data in the batch are fit to a single set of initial conditions, epoched at the beginning of the data span (the span is defined as the time associated with the arc of the trajectory covered by data). The fit is performed by minimizing, in the least squares sense, the doppler residuals with respect to the fitting parameters. The residuals are defined as

$$\Delta^2 f = \Delta f_{\text{exp}} - \Delta f_{\text{th}}$$

where Δf_{exp} is the raw doppler data corrected for transmission delay. Δf_{th} is the theoretical doppler

produced using the known station coordinates for the station under consideration, and the satellite position and velocity obtained by numerically integrating the satellite equations of motion using the current best estimate of the initial conditions. Descriptions of the fitting parameters and the integration scheme are given in Ref. 8.1.

8.5 Tracking Results

Tracking results for DODGE are meager primarily because of the long time constants involved. That is, we have tracked only three times (August 1967 and December 1967, and May 1968 to date)* because orbit accuracies sufficient to meet all apparent needs have been maintained. The current accuracy is well within most of the users' ability to measure the existing errors in satellite position. We have also found that the prediction of satellite position degrades in accuracy very slowly.

An explanation of the measure used to determine the position error (Fig. 8-3) from the tracking results is pertinent.

We use as starting values of the initial conditions that set which has been numerically integrated forward in time from the nearest previous track. If we compare the tracked values with the starting values, i.e., look at total orbit (initial condition) movement, and can, in some way, translate these differences in initial conditions into position differences then we have a measure of the prediction accuracy of the previous track. By translating the final orbit movement (i.e., the changes in the orbit parameters from the next to last and last

*A preliminary track on day 220, 1967 was only partially successful and although the associated Kepler elements were used to produce station antenna pointings (see later section) other aspects of the track are not here included.

KEY:

- = MAY 1968 TRACK ⊙ = TOTAL ORBIT MOVEMENT
- = Δr , ANTENNA POINTING RADIAL ERROR MEAN
- ◆ = $\sigma \Delta r$, STANDARD DEVIATION FOR ANTENNA POINTING DATA
- ◇ = AUGUST TRACK, FINAL ORBIT MOVEMENT
- = DECEMBER TRACK, FINAL ORBIT MOVEMENT
- = DECEMBER TRACK, TOTAL ORBIT MOVEMENT
- △ = ECLIPSE DATA
- ▲ = ECLIPSE DATA WITH EPOCH CORRECTION TO ORBIT

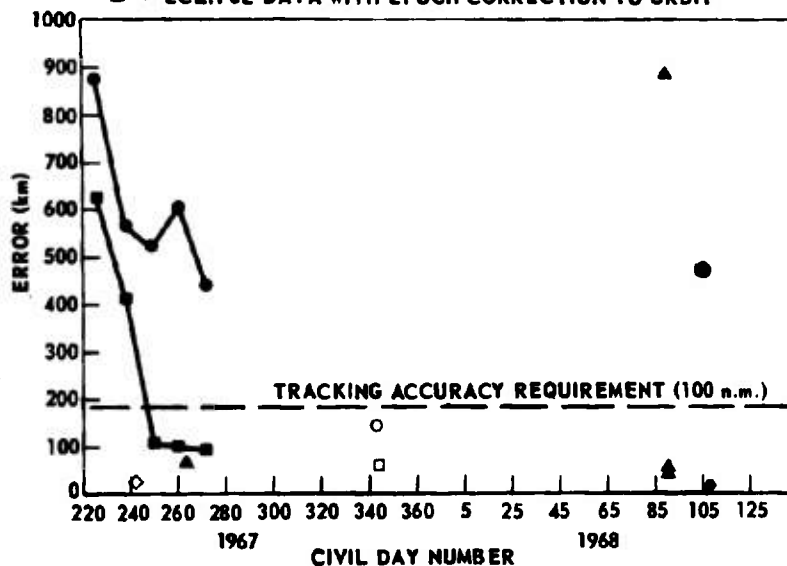


Fig. 8-3 TRACKING ACCURACY MEASURES FROM ALL AVAILABLE SOURCES VERSUS TIME

iterations) in the same manner we get a measure of the accuracy of the fit.

From Ref. 8.2 we find the formulae for the necessary translation:

$$H = \Delta a - \Delta e a \cos M$$

$$C = a(-\Delta i \sin \beta + \Delta \Omega \sin i \cos \beta)$$

$$L = a(\Delta \beta + \Delta \Omega \cos i) + \bar{V} \Delta t_0$$

(The H, L, C coordinates are a right-handed, orthogonal, cartesian basis centered in the satellite with directions:

H = aligned with the radius vector from the earth's center to the satellite

L = normal to H, lying in the orbital plane in the direction of satellite motion

C = lies in the direction of the satellite angular momentum vector.)

where $\beta \approx \omega + M$ and the Δt_0 term has been added since the reference assumes that the values are given at the same epoch and in our case the epochs are different. The total position error, $|\delta \vec{r}|$, is given by

$$|\delta \vec{r}| = [L^2 + H^2 + C^2]^{1/2}$$

It can be shown that these equations also hold when "cycled" Kepler elements (Ref. 1) are used since they are associated with the orbit plane rather than the cartesian frame.

Using the above equations we have converted the orbit changes (both final vs initial and last iteration movement) to equivalent position error for the August and December 1967 and May 1968 tracks.

The August track used data from day 204 through day 238, 1967 and the December track used data from day 204 through day 319, 1967. The May tracking span was from day 108, 1968 to day 141, 1968.

TABLE 8-1
SUMMARY OF ORBIT ERRORS FOR DODGE TRACKS

	August Track		December Track		May Track	
	Final -Initial	Final Movement	Final -Initial	Final Movement	Final -Initial	Final Movement
H(km)	2.0	2.67	-1.55	0.06	-2.88	-.044
C(km)	1.4	4.52	-19.33	19.34	41.01	0
L(km)	1211.9	27.29	142.20	59.85	-434.16	-.007
Total(km)	1211.9	27.79	143.52	62.90	436.10	.004

It should be pointed out that the discrepancy between the final movements of the August and December tracks can be attributed to the fact that the August tracking span was 34 days long while the December tracking span was 115 days long. In any case 63 km is quite good (1.58×10^{-3} radians = $^{\circ}09$).*

8.6 Solar Detector Data

The earth eclipse of the sun as viewed by the satellite can serve as a measure of along track error. The measurements result from a comparison of the predicted eclipse time and the actual eclipse time as determined using TM data. The data consists of the output of a solar detector mounted on the -Z satellite axis. This detector is nearly aligned with the local vertical (the satellite-earth-center line) and points toward the earth when the satellite

*The May track used a considerably shorter span than the December track and it remains to be seen if the orbit will hold as well.

is gravity-gradient stabilized (right-side-up). Without presenting details let us simply point out that the output consists of what is essentially a cosine curve (which can be slightly distorted as a function of attitude). As the satellite enters the shadow of the earth the power output from this detector falls off as though the incident radiation were becoming parallel with the detector face. At the point where the output reaches 1/2 total the satellite is halfway through the penumbra, i.e., half the sun is behind the earth. This coincides with the geometrical shadow entry which is computed analytically. By comparing the predicted time of this event with the time determined from TM data, Δt , we can compute the satellite along track error, L :

$$L = \Delta t |\bar{V}|$$

where

$$|\bar{V}| = \text{average satellite speed} \\ (\approx 3.1609 \text{ km/sec})$$

The geometrical shadow is computed only to a precision of about 3 km since we use the earth's equatorial radius without accounting for a change due to latitude. The precision of the solar detector data is on the order of 15 km when translated into equivalent satellite along track error.

Several eclipses have been analyzed, and the results are contained in Fig. 8-3.

8.7 Antenna Pointings

As a part of DODGE operations, antenna pointing orders are produced using the predicted satellite orbit. As the satellite is acquired the antenna is corrected in pointing direction until maximum signal strength is attained.

A comparison of predicted direction and maximum signal strength direction shows a standard deviation the order of 1 degree but the mean of the radial error is about 0.2 degree (≈ 117 km), which is comparable to the errors

as measured by eclipse and tracking data. The following table lists antenna pointing comparisons for five DODGE passes:

TABLE 8-2
COMPARISON OF ANTENNA POINTINGS WITH DIRECTION
OF MAXIMUM SIGNAL STRENGTH*

<u>Day</u>	$\Delta \bar{r}(\text{km})$ <u>Mean Radial Error</u>	$\sigma_{\Delta r}(\text{km})$ <u>Δr</u>
226**	631.	870.
237	420.	566.
249	105.	520.
260	99.	602.
271	93.	444.

*Table entries are equivalent distances at DODGE altitude in km.

**Produced using preliminary orbit tracked on day 220, 1967.

All the tracking accuracy data available are summarized in Fig. 8-3.

8.8 Conclusions

We have shown that a near-synchronous satellite of DODGE altitude and eccentricity can be tracked using doppler data only. We could maintain accuracy by tracking more often or eliminating the primary error source, 1st order ionospheric refraction.

The major feature of the ionospheric refraction effect at these altitudes (periods) is that the diurnal variation term dominates the geometrical term since the station-satellite relative geometry varies so slowly. Fig. 8-4 is a plot of simulated ionospheric refraction. For comparison the residuals from a DODGE pass are plotted in Fig. 8-5. It is interesting to note the similarity of the two curves. Clearly if two frequencies were being transmitted from the satellite then one could

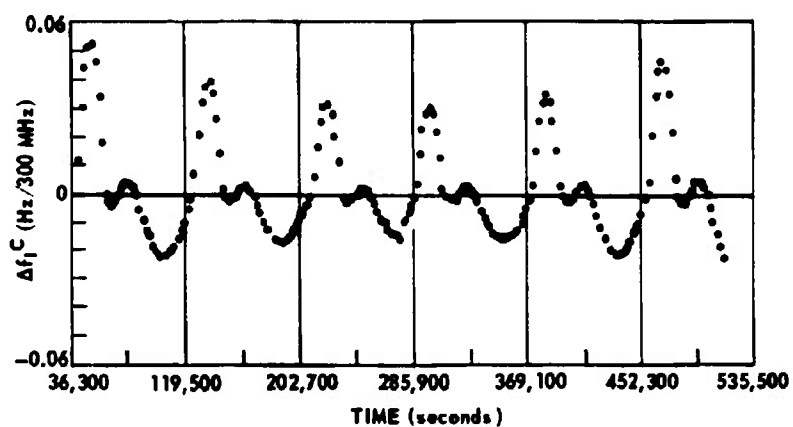


Fig. 8-4 MODELED IONOSPHERIC REFRACTION
CONTRIBUTION TO DOPPLER SIGNAL
FROM A NEAR-SYNCHRONOUS SATELLITE

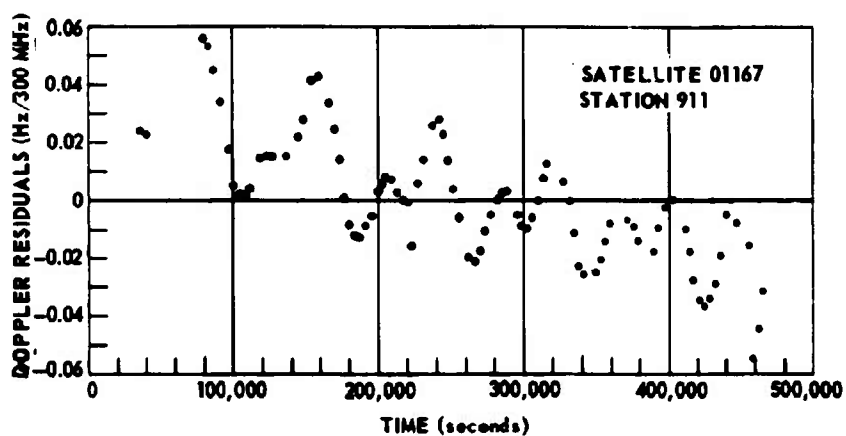


Fig. 8-5 DOPPLER RESIDUALS AFTER TRACKING
FROM DODGE PASS: DAY 214 TO 219, 1967

both track more accurately and perhaps study the diurnal variation of the ionosphere through a study of the extracted 1st order ionospheric refraction.

8.9 References

- 8.1 Holland, B. B., "Doppler Tracking of Near-Synchronous Satellites," APL Report TG 1006, 1968.
- 8.2 Guier, W. H., "Geodetic Problems and Satellite Orbits," Space Mathematics, Part II, Lectures in Applied Mathematics, Vol. 6, The American Mathematical Society, 1966, p. 198.

9. GROUND STATIONS OPERATION

9.1 APL Command and Telemetry Station

The APL Command and Telemetry Station (Station 502) is the center of DODGE ground station operations. Telemetry (TM) and television (TV) data are received with the station's 60-foot dish antenna. The data from real-time passes as well as data collected at other stations are processed at Station 502. Functionally the station, as it relates to the DODGE satellite, may be considered in three sections as shown in Fig. 9-1.

The RF and analog section is responsible for real-time communications with the satellite; which includes reception, demodulation, and recording of the TM and TV data, and command control of the satellite system. The composite demodulated signal from the main receiver consists of the output of the satellite's three TM subcarrier-oscillators (SCO's) and the TV SCO. The TM SCO signals are demodulated and displayed on one or more analog chart recorders. The composite signal of all four SCO's is also routed to the digital and video sections for processing. Control of the command antenna and transmitter is also a part of the main control room function. Command tones can be initiated manually from a command generator in the control room or by the computer. The command mode is selected at the command position in the main control room.

The digital section is responsible for digitizing the analog TM SCO signals and processing these data for display on a high speed line printer. The three TM SCO signals are demodulated with appropriate discriminators and the output signals are sampled under control of the CDC 3200 computer. Each channel of each commutator is converted to engineering units for printout on the line printer and recording on digital magnetic tape. The computer can also provide satellite commands. This capability is particularly useful when accurate timing of commands is required.

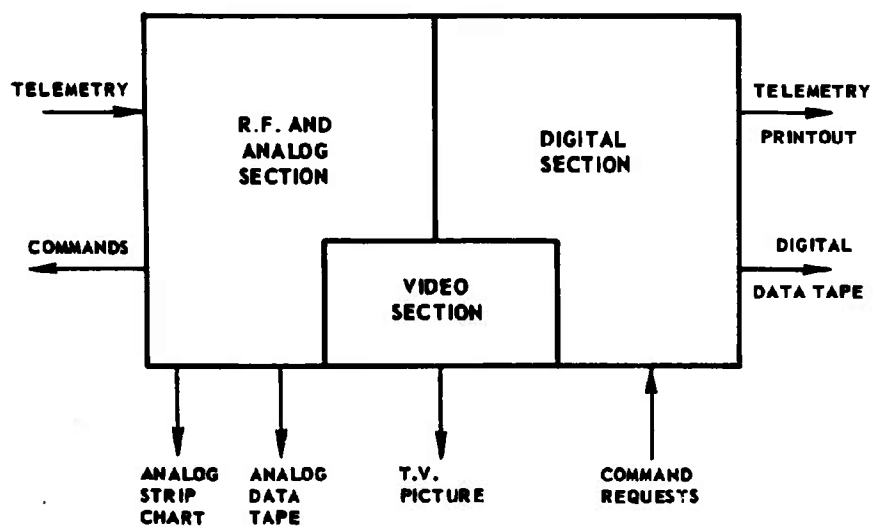


Fig. 9-1 STATION 502 FUNCTIONAL DIAGRAM

When the computer is not on-line for processing of the DODGE TM data it is employed for special reduction of the TM data, for processing of the attitude data, and for processing of special TV data.

The video section demodulates the TV SCO signal and records its output on the DODGE TV Reproducer. The picture reproduction equipment has one real-time and two non-real-time modes of operation. One of the non-real-time modes is identical to the real-time mode except that the input signal is supplied from a playback of an analog magnetic tape recording. The second non-real-time mode uses the station computer for control of the picture reproducer. Attitude data are generally obtained from pictures processed by the real-time processing equipment. Computer processing is generally restricted to pictures of special interest.

9.1.1 Operating Modes

The most common DODGE operations performed at the station are hourly turn-ons (satellite in automatic programmed mode), boom operations, picture taking sequences, and magnetometer runs.

In the programmed mode of operation the satellite turns itself on for 10 minutes every hour. The data from these turn-ons are received and processed by Station 502 whenever the DODGE satellite is in view (approximately 5 of 12 days). The main receiver output is recorded on magnetic tape, and analog chart recordings of the TM data are made in the RF and analog section. The digital section processes, records on digital tape, and prints out the real-time TM data for each turn-on. The TV data from one programmed turn-on include 60-degree and 22-degree pictures,

which are processed in real time in the video section. Immediately following a turn-on, the digital data tape is processed to perform computations on the data for specific non-real-time analyses for each of several scientists and engineers. Following the non-real-time TM processing an attitude program is run, which combines measured data from the real-time pictures and TM data from the solar aspect detectors, to compute the three attitude angles.

During boom operations the satellite is commanded on continuously and real-time data are received and processed as in the programmed mode. The scientist or engineer conducting the operation monitors the data outputs to determine the exact state and position of the satellite. When the proper time for the boom operation is reached the TM subcommutator is stopped on the channel which monitors boom length. This channel has the output of a spool counter superimposed on a voltage analog of the boom length. The discriminator output of this channel is connected to a preset counter, and the preset counter is connected to the command control. When the reset button on the counter is pushed a command is sent which starts the boom inverter. As the boom motor runs the spool counter pulses are counted on the counter and when the preset count is achieved it automatically causes a command to be sent to turn off the boom inverter. After the boom lengths have been adjusted the strip chart recordings of the TM data are carefully reviewed to check the operation, and the TM commutators are started to check the condition of the satellite.

Continuous picture sequences are generally taken near satellite noon at times when the satellite attitude is such as to allow all or most of the earth to be visible in the 22-degree

picture. When good signal conditions exist, both TV and TM data are transmitted and the ground station processing of the data is identical to that done in the programmed mode. When the signal conditions are not favorable the satellite modulation system can be commanded to a TV-only condition to improve the reception quality. At these times the computer can be used to digitize TV pictures on-line. In all cases the real-time video processing system is employed, and the data are recorded on magnetic tape for later computer processing as required.

Special magnetometer data runs are usually taken with the DODGE satellite for several hours before and after satellite noon whenever the satellite is in view of Station 502. For this mode the three TM subcommutators are stopped on each magnetometer (X, Y, and Z axis) and monitored continuously. Once each hour the commutators are started, and the TV system is enabled to check the status of the satellite system. These status checks are approximately equivalent to a programmed turn-on and as such require roughly 10 minutes. Usually the satellite programmer is disabled during these periods.

The DODGE satellite has a great deal of flexibility with regard to its operating mode. Therefore the ground station operations discussed above are not all-inclusive. The remainder of this discussion is devoted to types of data and their formats, a basic hardware description of the station, and a description of the software used for TM processing. Software for the CDC 3200 as related to attitude processing or picture processing is discussed in Section 10 of this report.

9.1.2 Data Output

9.1.2.1 Analog Strip Charts

Analog data from three constant bandwidth subcarrier oscillators via the RF system are reduced to the form for presentation on the brush pen recorder. Fig. 9-2 shows a typical strip chart recording of DODGE telemetry. The subcarrier oscillator frequencies are 625 Hz, 859 Hz and 1090 Hz. All deviate plus or minus 62.5 Hz. Each subcarrier is commutated and the "A" and "B" commutator nomenclature refers to the 625 Hz and the 859 Hz, respectively. The 1090 Hz subcarrier is referred to as the "H" or housekeeping commutator.

9.1.2.2 Analog Data Tapes

All data in the form of the composite TM and TV are recorded on half-inch analog magnetic tape. Also recorded are the WWV signals, a main-frame sync clock signal for playback of TV pictures, a 12.5 kHz reference signal, the NASA 36 bit time code generator data, and all command tones transmitted to the satellite.

9.1.2.3 Telemetry Printouts

Printed records of processed data are produced by the CDC 3200 computer for both real and non-real time data. The format is similar for both types of data consisting of a heading giving the data source, station, year, and time, telltale states expressed in statements, time, and data quality on the left margin, and three columns of channel values. The primary difference being that only the channels requested are printed for the non-real time data. A sample real time printout is shown in Fig. 9-3, and a sample non-real time printout is shown in Fig. 9-4. The various portions of the printouts are further described as follows.

At the top of the printout are the states of all the telltales in each of the five telltale registers at the end of the previous data frame. If the states of the telltales are being monitored by the computer, an asterisk will be used to denote

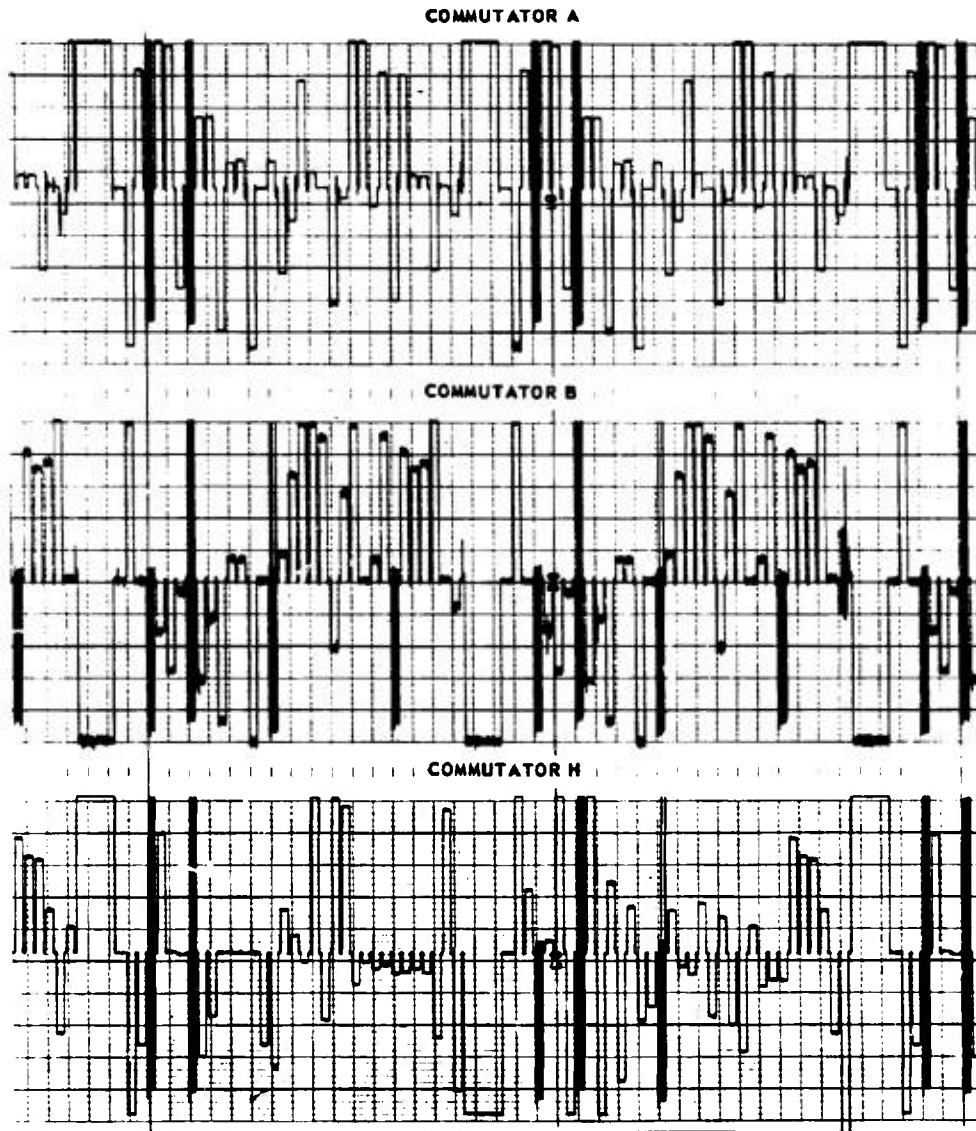


Fig. 9-2 ANALOG STRIP CHART RECORDING

THE JOHNS HOPKINS UNIVERSITY
APPLIED PHYSICS LABORATORY
BALTIMORE, MARYLAND

DATA SOURCE OF LINK STATION 502 YEAR 68 DEV 256 TIME 193608 7

TELLTALE STATUS AT END OF LAST DATA FRAME

TELLTALE REGISTER 1	TELLTALE REGISTER 2	TELLTALE REGISTER 3	TELLTALE REGISTER 4	TELLTALE REGISTER 5
AUTO-MAIN MAIN RUN ON MAIN CONVERTER NO.2 RAIIRRT MODE LO-VOLT SENSOR IN SIAMMT CONV ON	TV SYS CONV ENABLE TV SYS SCAM NORMAL TV CAMERA PHOTOCLIP MOD INDR R-LAY POS A TV SCO NO 1	DMPR ROOM ANGL DET OFF DMPR CADR MTR DISARLED +2 ROOM DISARLED +2 ROOM DISARLED +2 TIMES ROOM DISARLED	FIXED 2 MAG MOMENT MFG VAR 2 MAG MNT MAGNETIC DAMPING STATE 1 MAGNETIZER NEGATIVE MAGNETIZER CHG RT LO	ATII COMM A START ATII COMM B START H COMM START ALL COMMUTATIONS START TV DMPR INDETERMINATE
AUX SOL ARY 1 ON RAIN BUS AUX SOL ARY 2 ON RAIN BUS AUX 5 A 2 ON DMPR ATC ENHANCED HIG 4YS ON OSC AND RFA NO 2	FLYWHEL DISARLE RAYLDAI SEPARATED HABN ON DF MAG OFF ENHNC MAG DMPR FIBLO SPIN THROUGH POSITIVE	-X -2 TIMES ROOM DISARLED -X -2 TIMES ROOM DISARLED -X -2 TIMES ROOM DISARLED -Y ROOM DISARLED	MAGNETIZER CAR DISCHG HYSTERESIS TV DMPR SY 4 SQUART WAVE GEN OFF TV HYST DAMPER OFF RHOHAMMER PHARLED	TV DMPR UNCAWFO TV DMPR RM ANGL RIT 0 0 TV DMPR RM ANGL RIT 5 0 TV DMPR RM ANGL RIT 4 0 TV DMPR RM ANGL RIT 3 0
OSCILLATOR OVEN NO 1 136 MHZ ENTER OFF 264 MHZ ENTER ON ENTERS ON LO RWR UNMISSIOMFI	RHASE LAG DAMPING PH LAS SAMPLE AUTO FINHAMPER HYST LOW GRIN EZ FIFEN MAG MNT DISARLE SEL BY HAR MOUNT FIFEN	-X -Y DMPR ROOM DISARLED -X -Y DMPR ROOM DISARLED ROOMS DETRACT SELCT INVERTER 2 INVERTED DMPR OFF	OVERVOLTAGE ZFNER LOW TIMING MARKS OUT MOD MODE SEL 49A MOD MODE SEL 49A MAIN ROVER ON NORMAL	TV DMPR RM ANGL RIT 2 0 TV DMPR RM ANGL RIT 1 0 TV FITR DMS RIT 3 0 TV FITR DMS RIT 2 A TV FITR DMS RIT 1 1

MINUTE ANGLE NOT VALID

O COMMUTATOR						R COMMUTATOR						H COMMUTATOR						
TIME	FXC	CH	FUNCTION	MV	ENGR	UNT	CH	FUNCTION	MV	ENGR	UNT	CH	FUNCTION	MV	ENGR	UNT		
193647	7	A	CALIBRATE	180.0	240	VLT	1	A	CALIBRATE	180.0	240	VLT	1	A	CALIBRATE	180.0	240	VLT
193648	2	A	CALIBRATE	180.0	240	VLT	2	A	CALIBRATE	180.0	240	VLT	2	A	CALIBRATE	180.0	240	VLT
193649	3	A	CALIBRATE	180.0	240	VLT	3	A	CALIBRATE	180.0	240	VLT	3	A	CALIBRATE	180.0	240	VLT
193649 999	4	A	MAIN BUS VOLT	178.9	14.0	VLT	4	A	MAIN BUS VOLT	178.9	14.0	VLT	4	A	MAIN BUS VOLT	178.9	14.0	VLT
193650	5	A	MAIN BUS VOLT	178.9	14.0	VLT	5	A	MAIN BUS VOLT	178.9	14.0	VLT	5	A	MAIN BUS VOLT	178.9	14.0	VLT
193650 999	6	A	MAIN BUS VOLT	178.9	14.0	VLT	6	A	MAIN BUS VOLT	178.9	14.0	VLT	6	A	MAIN BUS VOLT	178.9	14.0	VLT
193651	7	A	MAIN BUS VOLT	178.9	14.0	VLT	7	A	MAIN BUS VOLT	178.9	14.0	VLT	7	A	MAIN BUS VOLT	178.9	14.0	VLT
193651 999	8	A	MAIN BUS VOLT	178.9	14.0	VLT	8	A	MAIN BUS VOLT	178.9	14.0	VLT	8	A	MAIN BUS VOLT	178.9	14.0	VLT
193652	9	A	MAIN BUS VOLT	178.9	14.0	VLT	9	A	MAIN BUS VOLT	178.9	14.0	VLT	9	A	MAIN BUS VOLT	178.9	14.0	VLT
193652 999	10	A	MAIN BUS VOLT	178.9	14.0	VLT	10	A	MAIN BUS VOLT	178.9	14.0	VLT	10	A	MAIN BUS VOLT	178.9	14.0	VLT
193653	11	A	MAIN BUS VOLT	178.9	14.0	VLT	11	A	MAIN BUS VOLT	178.9	14.0	VLT	11	A	MAIN BUS VOLT	178.9	14.0	VLT
193653 999	12	A	MAIN BUS VOLT	178.9	14.0	VLT	12	A	MAIN BUS VOLT	178.9	14.0	VLT	12	A	MAIN BUS VOLT	178.9	14.0	VLT
193654	13	A	MAIN BUS VOLT	178.9	14.0	VLT	13	A	MAIN BUS VOLT	178.9	14.0	VLT	13	A	MAIN BUS VOLT	178.9	14.0	VLT
193654 999	14	A	MAIN BUS VOLT	178.9	14.0	VLT	14	A	MAIN BUS VOLT	178.9	14.0	VLT	14	A	MAIN BUS VOLT	178.9	14.0	VLT
193655	15	A	MAIN BUS VOLT	178.9	14.0	VLT	15	A	MAIN BUS VOLT	178.9	14.0	VLT	15	A	MAIN BUS VOLT	178.9	14.0	VLT
193655 999	16	A	MAIN BUS VOLT	178.9	14.0	VLT	16	A	MAIN BUS VOLT	178.9	14.0	VLT	16	A	MAIN BUS VOLT	178.9	14.0	VLT
193656	17	A	MAIN BUS VOLT	178.9	14.0	VLT	17	A	MAIN BUS VOLT	178.9	14.0	VLT	17	A	MAIN BUS VOLT	178.9	14.0	VLT
193656 999	18	A	MAIN BUS VOLT	178.9	14.0	VLT	18	A	MAIN BUS VOLT	178.9	14.0	VLT	18	A	MAIN BUS VOLT	178.9	14.0	VLT
193657	19	A	MAIN BUS VOLT	178.9	14.0	VLT	19	A	MAIN BUS VOLT	178.9	14.0	VLT	19	A	MAIN BUS VOLT	178.9	14.0	VLT
193657 999	20	A	MAIN BUS VOLT	178.9	14.0	VLT	20	A	MAIN BUS VOLT	178.9	14.0	VLT	20	A	MAIN BUS VOLT	178.9	14.0	VLT
193658	21	A	MAIN BUS VOLT	178.9	14.0	VLT	21	A	MAIN BUS VOLT	178.9	14.0	VLT	21	A	MAIN BUS VOLT	178.9	14.0	VLT
193658 999	22	A	MAIN BUS VOLT	178.9	14.0	VLT	22	A	MAIN BUS VOLT	178.9	14.0	VLT	22	A	MAIN BUS VOLT	178.9	14.0	VLT
193659	23	A	MAIN BUS VOLT	178.9	14.0	VLT	23	A	MAIN BUS VOLT	178.9	14.0	VLT	23	A	MAIN BUS VOLT	178.9	14.0	VLT
193659 999	24	A	MAIN BUS VOLT	178.9	14.0	VLT	24	A	MAIN BUS VOLT	178.9	14.0	VLT	24	A	MAIN BUS VOLT	178.9	14.0	VLT
193660	25	A	MAIN BUS VOLT	178.9	14.0	VLT	25	A	MAIN BUS VOLT	178.9	14.0	VLT	25	A	MAIN BUS VOLT	178.9	14.0	VLT
193660 999	26	A	MAIN BUS VOLT	178.9	14.0	VLT	26	A	MAIN BUS VOLT	178.9	14.0	VLT	26	A	MAIN BUS VOLT	178.9	14.0	VLT
193661	27	A	MAIN BUS VOLT	178.9	14.0	VLT	27	A	MAIN BUS VOLT	178.9	14.0	VLT	27	A	MAIN BUS VOLT	178.9	14.0	VLT
193661 999	28	A	MAIN BUS VOLT	178.9	14.0	VLT	28	A	MAIN BUS VOLT	178.9	14.0	VLT	28	A	MAIN BUS VOLT	178.9	14.0	VLT
193662	29	A	MAIN BUS VOLT	178.9	14.0	VLT	29	A	MAIN BUS VOLT	178.9	14.0	VLT	29	A	MAIN BUS VOLT	178.9	14.0	VLT
193662 999	30	A	MAIN BUS VOLT	178.9	14.0	VLT	30	A	MAIN BUS VOLT	178.9	14.0	VLT	30	A	MAIN BUS VOLT	178.9	14.0	VLT
193663	31	A	MAIN BUS VOLT	178.9	14.0	VLT	31	A	MAIN BUS VOLT	178.9	14.0	VLT	31	A	MAIN BUS VOLT	178.9	14.0	VLT
193663 999	32	A	MAIN BUS VOLT	178.9	14.0	VLT	32	A	MAIN BUS VOLT	178.9	14.0	VLT	32	A	MAIN BUS VOLT	178.9	14.0	VLT
193664	33	A	MAIN BUS VOLT	178.9	14.0	VLT	33	A	MAIN BUS VOLT	178.9	14.0	VLT	33	A	MAIN BUS VOLT	178.9	14.0	VLT
193664 999	34	A	MAIN BUS VOLT	178.9	14.0	VLT	34	A	MAIN BUS VOLT	178.9	14.0	VLT	34	A	MAIN BUS VOLT	178.9	14.0	VLT
193665	35	A	MAIN BUS VOLT	178.9	14.0	VLT	35	A	MAIN BUS VOLT	178.9	14.0	VLT	35	A	MAIN BUS VOLT	178.9	14.0	VLT
193665 999	36	A	MAIN BUS VOLT	178.9	14.0	VLT	36	A	MAIN BUS VOLT	178.9	14.0	VLT	36	A	MAIN BUS VOLT	178.9	14.0	VLT
193666	37	A	MAIN BUS VOLT	178.9	14.0	VLT	37	A	MAIN BUS VOLT	178.9	14.0	VLT	37	A	MAIN BUS VOLT	178.9	14.0	VLT
193666 999	38	A	MAIN BUS VOLT	178.9	14.0	VLT	38	A	MAIN BUS VOLT	178.9	14.0	VLT	38	A	MAIN BUS VOLT	178.9	14.0	VLT
193667	39	A	MAIN BUS VOLT	178.9	14.0	VLT	39	A	MAIN BUS VOLT	178.9	14.0	VLT	39	A	MAIN BUS VOLT	178.9	14.0	VLT
193667 999	40	A	MAIN BUS VOLT	178.9	14.0	VLT	40	A	MAIN BUS VOLT	178.9	14.0	VLT	40	A	MAIN BUS VOLT	178.9	14.0	VLT
193668	41	A	MAIN BUS VOLT	178.9	14.0	VLT	41	A	MAIN BUS VOLT	178.9	14.0	VLT	41	A	MAIN BUS VOLT	178.9	14.0	VLT
193668 999	42	A	MAIN BUS VOLT	178.9	14.0	VLT	42	A	MAIN BUS VOLT	178.9	14.0	VLT	42	A	MAIN BUS VOLT	178.9	14.0	VLT
193669	43	A	MAIN BUS VOLT	178.9	14.0	VLT	43	A	MAIN BUS VOLT	178.9	14.0	VLT	43	A	MAIN BUS VOLT	178.9	14.0	VLT
193669 999	44	A	MAIN BUS VOLT	178.9	14.0	VLT	44	A	MAIN BUS VOLT	178.9	14.0	VLT	44	A	MAIN BUS VOLT	178.9	14.0	VLT
193670	45	A	MAIN BUS VOLT	178.9	14.0	VLT	45	A	MAIN BUS VOLT	178.9	14.0	VLT	45	A	MAIN BUS VOLT	178.9	14.0	VLT
193670 999	46	A	MAIN BUS VOLT	178.9	14.0	VLT	46	A	MAIN BUS VOLT	178.9	14.0	VLT	46	A	MAIN BUS VOLT	178.9	14.0	VLT
193671	47	A	MAIN BUS VOLT	178.9	14.0	VLT	47	A	MAIN BUS VOLT	178.9	14.0	VLT	47	A	MAIN BUS VOLT	178.9	14.0	VLT
193671 999	48	A	MAIN BUS VOLT	178.9	14.0	VLT	48	A	MAIN BUS VOLT	178.9	14.0	VLT	48	A	MAIN BUS VOLT	178.9	14.0	VLT
193672	49	A	MAIN BUS VOLT	178.9	14.0	VLT	49	A	MAIN BUS VOLT	178.9	14.0	VLT	49	A	MAIN BUS VOLT	178.9	14.0	VLT
193672 999	50	A	MAIN BUS VOLT	178.9	14.0	VLT	50	A	MAIN BUS VOLT	178.9	14.0	VLT	50	A	MAIN BUS VOLT	178.9	14.0	VLT
193673	51	A	MAIN BUS VOLT	178.9	14.0	VLT	51	A	MAIN BUS VOLT	178.9	14.0	VLT	51	A	MAIN BUS VOLT	178.9	14.0	VLT
193673 999	52	A	MAIN BUS VOLT	178.9	14.0	VLT	52	A	MAIN BUS VOLT	178.9	14.0	VLT	52	A	MAIN BUS VOLT	178.9	14.0	VLT
193674	53	A	MAIN BUS VOLT	178.9	14.0	VLT	53	A	MAIN BUS VOLT	178.9	14.0	VLT	53	A	MAIN BUS VOLT	178.9	14.0	VLT
193674 999	54	A	MAIN BUS VOLT	178.9	14.0	VLT	54	A	MAIN BUS VOLT	178.9	14.0	VLT	54	A	MAIN BUS VOLT	178.9	14.0	VLT
193675	55	A	MAIN BUS VOLT	178.9	14.0	VLT	55	A	MAIN BUS VOLT	178.9	14.0	VLT	55	A	MAIN BUS VOLT	178.9	14.0	VLT
193675 999	56	A	MAIN BUS VOLT	178.9	14.0	VLT	56	A	MAIN BUS VOLT	178.9	14.0	VLT	56	A	MAIN BUS VOLT	178.9	14.0	VLT
193676	57	A	MAIN BUS VOLT	178.9	14.0	VLT	57	A	MAIN BUS VOLT	178.9	14.0	VLT	57	A	MAIN BUS VOLT	178.9	14.0	VLT
193676 999	58	A	MAIN BUS VOLT	178.9	14.0	VLT	58	A	MAIN BUS VOLT	178.9	14.0	VLT	58	A	MAIN BUS VOLT	178.9	14.0	VLT
193677	59	A	MAIN BUS VOLT	178.9	14.0	VLT	59	A	MAIN BUS VOLT	178.9	14.0	VLT	59	A	MAIN BUS VOLT	178.9	14.0	VLT
193677 999	60	A	MAIN BUS VOLT	178.9	14.0	VLT	60	A	MAIN BUS VOLT	178.9	14.0	VLT	60	A	MAIN BUS VOLT	178.9	14.0	VLT
193678	61	A	MAIN BUS VOLT	178.9	14.0	VLT	61	A	MAIN BUS VOLT	178.9	14.0	VLT	61	A	MAIN BUS VOLT	178.9	14.0	VLT
193678 999	62	A	MAIN BUS VOLT	178.9	14.0	VLT	62	A	MAIN BUS VOLT	178.9	14.0	VLT	62	A	MAIN BUS VOLT	178.9	14.0	VLT
193679	63	A	MAIN BUS VOLT	178.9	14.0	VLT	63	A	MAIN BUS VOLT	178.9	14.0	VLT	63	A	MAIN BUS VOLT	178.9	14.0	VLT
193679 999	64	A	MAIN BUS VOLT	178.9	14.0	VLT	64	A	MAIN BUS VOLT	178.9	14.0	VLT	64	A	MAIN BUS VOLT	178.9	14.0	VLT
193680	65	A	MAIN BUS VOLT	178.9	14.0	VLT	65	A	MAIN BUS VOLT	178.9	14.0	VLT	65	A	MAIN BUS VOLT	178.9	14.0	VLT
193680 999	66	A	MAIN BUS VOLT	178.9	14.0	VLT	66	A	MAIN BUS VOLT	178.9	14.0	VLT	66	A	MAIN BUS VOLT	178.9	14.0	VLT
193681	67	A	MAIN BUS VOLT	178.9	14.0	VLT	67	A	MAIN BUS VOLT	178.9	14.0	VLT	67	A	MAIN BUS VOLT	178.9	14.0	VLT
193681 999	68	A	MAIN BUS VOLT	178.9	14.0	VLT	68	A	MAIN BUS VOLT	178.9	14.0	VLT	68	A	MAIN BUS VOLT	178.9	14.0	VLT
193682	69	A	MAIN BUS VOLT	178.9	14.0	VLT	69	A	MAIN BUS VOLT	178.9	14.0	VLT	69	A	MAIN BUS VOLT	178.9	14.0	VLT
193682 999	70	A	MAIN BUS VOLT	178.9	14.0	VLT	70	A	MAIN BUS VOLT	178.9	14.0	VLT	70	A	MAIN BUS VOLT	178.9	14.0	VLT
193683	71	A	MAIN BUS VOLT	178.9	14.0	VLT	71	A	MAIN BUS VOLT	178.9	14.0	VLT	71	A	MAIN BUS VOLT	178.9	14.0	VLT
193683 999	72	A	MAIN BUS VOLT	178.9	14.0	VLT	72	A	MAIN BUS VOLT	178.9	14.0	VLT	72	A	MAIN BUS VOLT	178.9	14.0	VLT
193684	73	A	MAIN BUS VOLT	178.9	14.0	VLT	73	A	MAIN BUS VOLT	178.9	14.0	VLT	73	A	MAIN BUS VOLT	178.9	14.0	VLT
193684 999	74	A	MAIN BUS VOLT	178.9	14.0	VLT	74	A	MAIN BUS VOLT	178.9	14.0	VLT	74	A	MAIN BUS VOLT	178.9	14.0	VLT
193685	75	A	MAIN BUS VOLT	178.9	14.0	VLT	75	A	MAIN BUS VOLT	178.9	14.0	VLT	75	A	MAIN BUS VOLT	178.9	14.0	VLT
193685 999	76	A	MAIN BUS VOLT	178.9	14.0	VLT	76	A	MAIN BUS VOLT	178.9	14.0	VLT	76	A	MAIN BUS VOLT	178.9	14.0	VLT
193686	77	A	MAIN BUS VOLT	178.9	14.0	VLT	77	A	MAIN BUS VOLT	178.9	14.0	VLT	77	A	MAIN BUS VOLT	178.9	14.0	VLT
193686 999	78	A	MAIN BUS VOLT	178.9	14.0	VLT	78	A	MAIN BUS VOLT	178.9	14.0	VLT	78	A	MAIN BUS VOLT	178.9	14.0	VLT
193687	79	A	MAIN BUS VOLT	178.9	14.0	VLT	79	A	MAIN BUS VOLT	178.9	14.0	VLT	79	A	MAIN BUS VOLT	178.9	14.0	VLT
193687 999	80	A	MAIN BUS VOLT															

THE JOHNS HOPKINS UNIVERSITY
APPLIED PHYSICS LABORATORY
SILVER SPRING, MARYLAND

DATA FOR LES

PAGE 1

DATA TAPE PLAYBACK STATION 902 YEAR 88 DAY 256 TIME 193204 2

TELEMETRY REDUCTION PROGRAM

TELLTALE STATES AT END OF LAST DATA FRAME

TELLTALE REGISTER 1	TELLTALE REGISTER 2	TELLTALE REGISTER 3	TELLTALE REGISTER 4	TELLTALE REGISTER 5
AUTO-MAN MAIN PWR ON MAIN CONVERTER NO.2 *BATTERY WIND LOW-VOLT SENSOR IN STANBY CONV ON	TV STS CONV ENABLF *TV STS SCAM UNNORMAL *TV CAMERA PROTECTED *MOD INDEX RELAY POS N TV SCN NO 1	DMPR ROOM ANGL DET OFF DMPR CAP MTR DISARLEO *Z ROOM DISARLEO *A *Z TIMES ROOM DISARLEO	FIXED Z MAG MOMENT NFN VAR Z MAG MNT MAGNETIC DAMPING STATE 1 MAGNETIZER NERATIVE MAGNETIZER CHN RT LO	*ATTI COMM A START ATTI COMM R START *COMM START *ALL COMMUTATORS START TR DMPR [UNDEF]MNT
AUX SOL ARY 1 ON MAIN BUS AUX SOL ARY 2 ON MAIN BUS AUX 5 A 2 ON DMPR AT FINANCFO MAG SYS ON OSC AND REG NO 2	*FLYWHEEL DISARLF PAYLOAD SEPARATED MAGN CM DEMAG OFF ENHND MAG DMPL FIMLO *SPIN TORQUE POSITIVE	*X *Z TIMES ROOM DISARLF *X *Z TIMES ROOM DISARLF *Y ROOM DISARLF *Y ROOM DISARLF	MAGNETIZER CAP DISCHG HYSTERESIS TR DMPR ST A SQUARED WAVE GEN OFF TR MYSY DAMPER OFF PROGRAMMER FRARLEO	TR DMPR UNCAEPI TR DMPR RM ANGL RIT A 4 *TR DMPR RM ANGL RIT 5 0 TR DMPR RM ANGL RIT A 0 TR DMPR RM ANGL RIT 7 0
OSCILLATOR OVEN NO 1 130 MHZ XMTTR OFF 240 MHZ XMTTR ON UNITS ON TO PWR UNASSIGNED	PHASE LAG DAMPING *PM LAG SAMPLE AUTO FINANCFO MYSY LOW GAIN *Z FIXED MAG MNT DISARLF *SEL 17 MAG MOMENT FIXED	*X *Y DMPR ROOM DISARLF *X *Y DMPR ROOM DISARLF BOOMS RETRACT SELECT INVERTER 2 INVERTER POWER OFF	OVERVOLTAGE ZENER LOW TIMING MARKS OUT MOD MODE SEL 544 MOD MODE SEL 544 MAIN POWER ON NORMAL	TR DMPR RM ANGL RIT 7 0 TR DMPR RM ANGL RIT 1 0 *TR DMPR RM ANGL RIT 3 1 TV FLTR POS RIT 2 0 TV FLTR POS RIT 1 1

TIME	FAC	CH	FUNCTION	NU	FNDR	UNT	CH	FUNCTION	NU	FNDR	UNT	CH	FUNCTION	NU	FNDR	UNT
193215	555	4	MAIN BUS VOLT	177	10.0	VLT	25	-Z COS 540°	243	-100.0	DEG	8	RAT ON SOL ZENER 1	-4	-100.0	AMP
193247	555	27	RATT CELL TEMP	-30	41.5	DEG	27	FM ROOM TEMP	-3	90.1	DEG	42	DEWAR TEMP	03	155.0	DEG
193300	54						22	-Z COS 540°	113	44.3	DEG	44	RATE CTRL BK TEMP	-14	44.4	DEG
193315	534	4	MAIN BUS VOLT	177	10.0	VLT	25	-Z COS 540°	154	44.3	DEG	44	130 MHZ XMTTR TEMP	34	70.0	DEG
193316	544	27	RATT CELL TEMP	-30	43.5	DEG	27	FM ROOM TEMP	-19	94.4	DEG	47	240 MHZ XMTTR TEMP	6	42.1	DEG
193318	55						22	-Z COS 540°	114	45.2	DEG	48	RATT MNT PLTF TEMP	-24	41.0	DEG
193320	4											12	INVERT INPUT 1	0	40.2	AMP
193335	4											72	FLYWHEEL MTR TEMP	-132	47.0	DEG
193400	55	4	MAIN BUS VOLT	177	10.0	VLT	25	-Z COS 540°	234	-100.0	DEG					
193403	55	27	RATT CELL TEMP	-29	41.0	DEG	27	FM ROOM TEMP	-2	90.0	DEG					
193406	5						22	-Z COS 540°	119	44.9	DEG					
193420	555	4	MAIN BUS VOLT	177	10.0	VLT	25	-Z COS 540°	237	-100.0	DEG	8	RAT ON SOL ZENER 1	0	40.0	AMP
193409	555	27	RATT CELL TEMP	-29	41.0	DEG	27	FM ROOM TEMP	-1	90.0	DEG	42	DEWAR TEMP	03	155.0	DEG
193411	55						22	-Z COS 540°	120	45.1	DEG	44	RATE CTRL BK TEMP	-14	44.4	DEG
193424	555	4	MAIN BUS VOLT	177	10.0	VLT	25	-Z COS 540°	243	-100.0	DEG	44	130 MHZ XMTTR TEMP	37	70.0	DEG
193427	55	27	RATT CELL TEMP	-29	41.0	DEG	27	FM ROOM TEMP	-8	90.0	DEG	47	240 MHZ XMTTR TEMP	72	47.7	DEG
193429	54						22	-Z COS 540°	122	45.3	DEG	48	RATT MNT PLTF TEMP	-24	41.0	DEG

DATA FOR LES

DAY 256 TIME 193404

PAGE 2

TIME	FAC	CH	FUNCTION	NU	FNDR	UNT	CH	FUNCTION	NU	FNDR	UNT	CH	FUNCTION	NU	FNDR	UNT
193521	4											12	INVERT INPUT 1	0	40.2	AMP
193546	5											72	FLYWHEEL MTR TEMP	-132	47.0	DEG
193702	555	4	MAIN BUS VOLT	176	10.0	VLT	25	-Z COS 540°	243	-100.0	DEG	8	RAT ON SOL ZENER 1	-4	-100.0	AMP
193704	555	27	RATT CELL TEMP	-29	41.0	DEG	27	FM ROOM TEMP	-5	90.0	DEG	42	DEWAR TEMP	03	155.0	DEG
193707	54						22	-Z COS 540°	124	45.4	DEG	44	RATE CTRL BK TEMP	-13	44.4	DEG
193708	554	4	MAIN BUS VOLT	176	10.0	VLT	25	-Z COS 540°	243	-100.0	DEG	44	130 MHZ XMTTR TEMP	37	70.0	DEG
193709	554	27	RATT CELL TEMP	-29	41.0	DEG	27	FM ROOM TEMP	0	90.0	DEG	47	240 MHZ XMTTR TEMP	74	46.4	DEG
193709	54						22	-Z COS 540°	124	45.7	DEG	48	RATT MNT PLTF TEMP	-24	41.7	DEG
193707	4											12	INVERT INPUT 1	0	40.2	AMP
193722	4											72	FLYWHEEL MTR TEMP	-132	47.0	DEG
193734	555	4	MAIN BUS VOLT	176	10.0	VLT	25	-Z COS 540°	244	-100.0	DEG	8	RAT ON SOL ZENER 1	-4	-100.0	AMP
193734	554	27	RATT CELL TEMP	-29	41.0	DEG	27	FM ROOM TEMP	0	90.0	DEG	42	DEWAR TEMP	03	155.0	DEG
193737	54						22	-Z COS 540°	131	46.2	DEG	44	RATE CTRL BK TEMP	-12	44.4	DEG
193738	554	4	MAIN BUS VOLT	176	10.0	VLT	25	-Z COS 540°	244	-100.0	DEG	44	130 MHZ XMTTR TEMP	39	71.1	DEG
193739	554	27	RATT CELL TEMP	-16	47.0	DEG	27	FM ROOM TEMP	11	90.2	DEG	47	240 MHZ XMTTR TEMP	77	46.1	DEG
193741	4						22	-Z COS 540°	130	46.1	DEG	48	RATT MNT PLTF TEMP	-24	41.4	DEG
193741	4											12	INVERT INPUT 1	0	40.2	AMP
193745	4											72	FLYWHEEL MTR TEMP	-132	47.0	DEG

Fig. 9-4 NON-REAL TIME TELEMETRY PRINTOUT

telltale that are not in the expected state. The asterisk will appear immediately to the left of the printed statement for a particular telltale. The expected state of a telltale may be determined in one of two ways:

- a. by a telltale card read into the computer. This sets an expected state (high or low) for one or more telltales,
- b. by sending commands with the computer, each command having an associated telltale which is expected to be in a certain state after the command has been sent.

Time read from the station time code generator is displayed as a 6 digit number including, from left-to-right, hours - 2 digits, minutes - 2 digits, and seconds - 2 digits. It represents the Universal, or Zulu, time at which the line of data was printed.

The Q factor is a measure of the quality of the received data. More specifically it is a measure of the noise on the data channel. The three digit number includes a digit for each commutator (from left-to-right A, B, and H) which has a value from 1 to 5. The larger the number, the higher the quality of the data. The noise is measured by taking the summation of the absolute values of the differences between successive data readings on a particular channel, and then dividing by the number of samples.

$$\text{NOISE} = \frac{\sum v_m - v_{m+1}}{\# \text{ Samples}}$$

The following table is used to arrive at the printed numbers.

<u>NOISE</u>	<u>Q FACTOR</u>
0-4 millivolts	5
4-8 millivolts	4
8-12 millivolts	3
12-16 millivolts	2
greater than 16 millivolts	1

Each commutator is calibrated independently at the beginning of each frame of data by manipulating the plus, zero, and minus calibrate channels. The received value of the plus calibrate is equated to +0.250 volt, the zero calibrate channel to 0.000 volt, and the minus calibrate channel to -0.250 volt. Then the slope and offset (m and b terms) are found for positive and for negative data. Once this has been accomplished the calibrated data (y) for each channel of the data frame may be found from the raw data (x) by the following calibration equations:

$$y_+ = m_+ x + b_+ \quad \text{for positive data}$$

$$y_- = m_- x + b_- \quad \text{for negative data}$$

The data of the non-digital telemetered channels are computed both as unscaled millivolts and as engineering units. Each channel is initially calibrated. The calibrated value is the printed millivolt value. Engineering unit conversion depends upon the type of data, i.e., linear or nonlinear. If the data are for a linear channel, the engineering unit value is computed by multiplication by a specific reverse attenuation factor. Data for a nonlinear channel are converted to engineering units by performing a linear interpolation between points from a lookup table. The appropriate units (volt, amp, etc.) are printed along with the data value in engineering units.

Digital (telltale) channels are printed out in binary. A "1" indicates a "high" telltale and a "0" indicates a "low" telltale. If the telltales are being monitored, an arrow will be printed immediately below any telltale in the register that is not in the expected state.

9.1.2.4 Digital Data Tapes

All DODGE telemetry data processed by the 3200 computer are recorded on digital magnetic tape. This includes real time data and analog tape playbacks of data taken at other tracking stations. The recorded data include:

- a. exact time of synchronization with the telemetry signal.
- b. calibration data for each commutator.
- c. each channel value in millivolts.
- d. each channel value in engineering units.
- e. data quality.

The digital tapes are recorded in binary (odd parity) at a density of 556 bits per inch, which allows approximately two months of real time data to be recorded on one reel of tape. The tapes are divided into files, each file containing records for one spacecraft turn-on or continuous run of data. Each record contains the data for one frame of commutators A and B and 1/2 frame of commutator H. Two or more consecutive file marks are used to indicate the end of the data on a particular tape.

9.1.2.5 TV Picture Data

In the normal mode of operation two pictures are transmitted from the DODGE satellite each hour. A typical set of pictures, one from the 60° camera and one from the 22° camera is shown in Fig. 9-5. These pictures were taken at 1330 UT on Day 255, 1968. A large part of the DODGE mast structure is visible in the 60° picture. The mast and antenna are used in conjunction with the camera reticle marks to aid in measuring the satellite attitude. Since the reticle marks are black, they can only be seen along the mast or on the earth. The reticle marks are more clearly seen on the 22° picture. The white horizontal

NOT REPRODUCIBLE



60° CAMERA-1333 GMT DAY 255



22° CAMERA-1337 GMT DAY 255

Fig. 9-5 REAL TIME TV PICTURES

lines result from the scan characteristic of the cameras. A full discussion of the camera characteristics and the method employed for attitude determination is given in Section 3.1 of this report.

9.1.3 Hardware

9.1.3.1 RF and Analog Hardware

Signals from the DODGE satellite are received via the 60 foot dish antenna on 136 MHz or 240 MHz. They pass through a low noise figure pre-amplifier and are then converted down to 3.25 MHz by an Electrac Model 520 Converter and fed into a phase lock demodulator (tracking filter). The output of the demodulator is the composite TM and TV which in turn is passed on to the digital section as well as to the video section, to the analog magnetic tape recorder, and to the inputs of the discriminators. The discriminators further process the composite waveform, and each in turn produces an analog output to drive the brush recorder, the end result of which is an analog strip chart (see Fig. 9-6).

Commands to the satellite can be controlled via the computer or manually by using a TADEx command modulator. All commands transmitted to the satellite are recorded on the analog tape recorder. Selection of modulation control is done in the operations room.

9.1.3.2 Digital Hardware

A block diagram of the station hardware is shown in Fig. 9-7. The telemetry subcarriers are separated and converted to analog signals by the 625, 859, and 1090 Hz discriminators. The outputs of these discriminators have a range of ± 10 volts. The computer samples these analog signals one at a time by switching the multiplexer to the desired signal and reading it in through the analog-to-digital converter. The analog signals may also be displayed directly on the pen recorder.

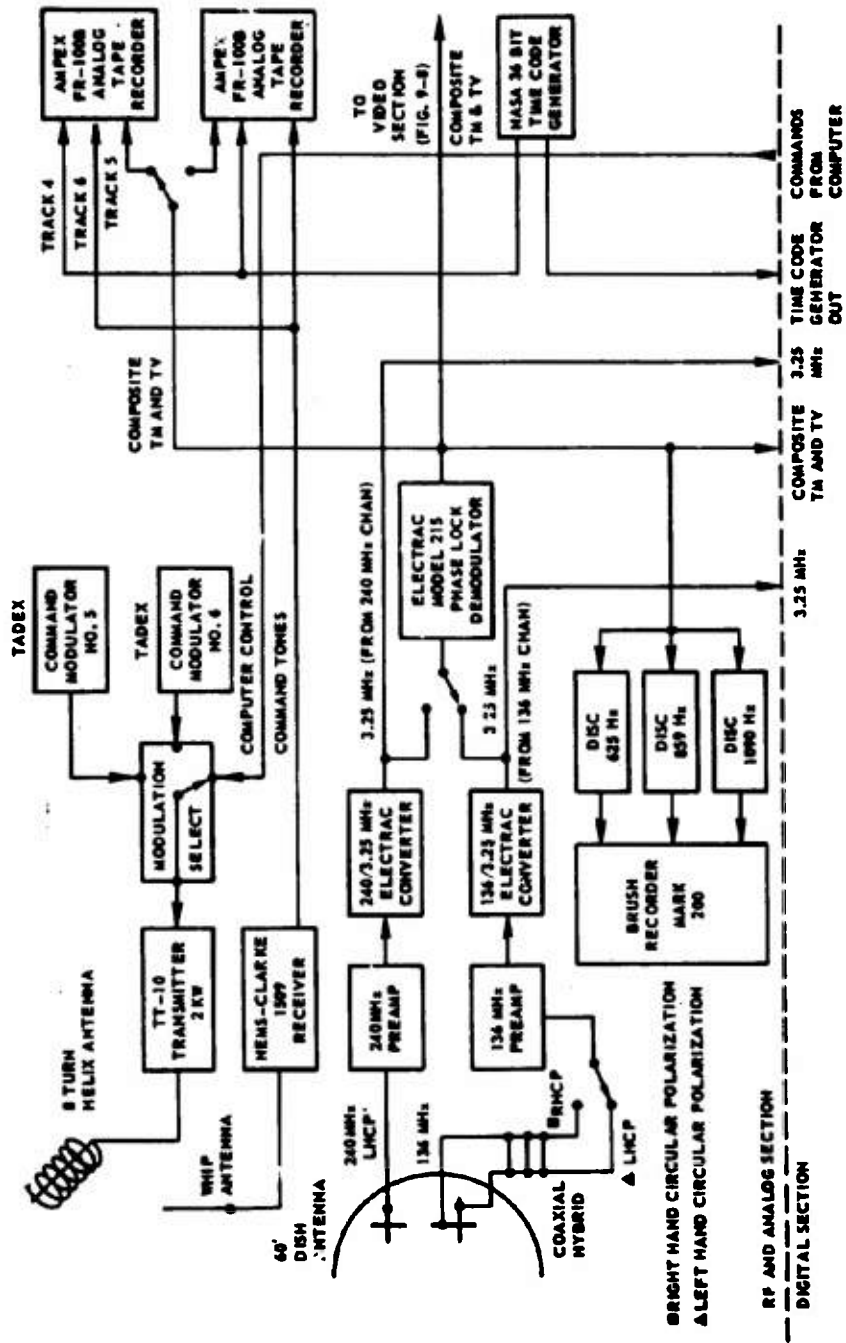


Fig. 9-6 RF AND ANALOG SECTION HARDWARE

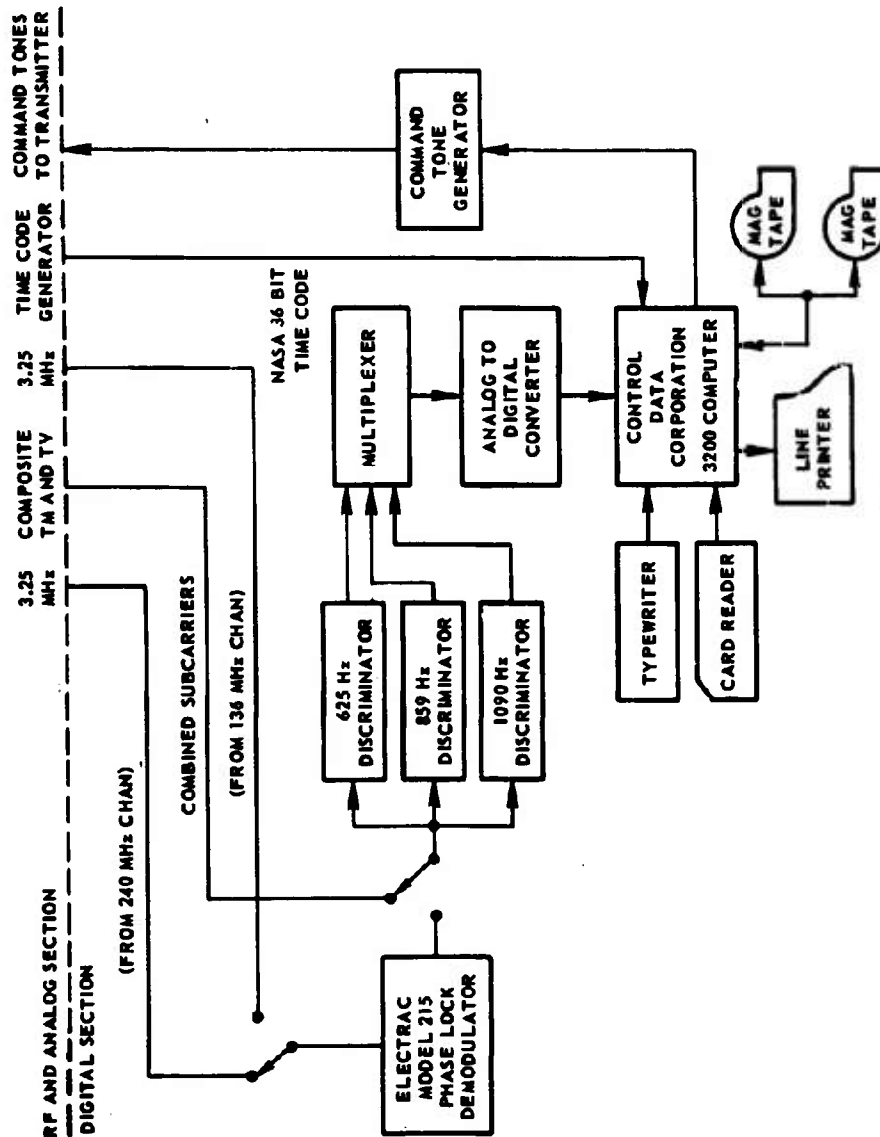


Fig. 9-7 DIGITAL SECTION HARDWARE

The discriminator gains are set so that the upper and lower band edges of the received telemetry signal produce approximately +8 volt outputs. Then the data may over-range by 25% before the +10 volt limits are reached. This setting also gives a resolution within the computer of better than 0.5 millivolt.

The analog-to-digital (A/D) converter will accept the +10 volt input and digitize it to an 11 bit binary number (10 data bits plus one sign bit) representing a total of $\pm 2^{10}$ or ± 1024 binary states.

The A/D converter is capable of 10,000 conversions per second. The rate of conversion is controlled by the computer, and generally data that change rapidly are sampled at a faster rate than data which change slowly.

Data calibration and conversion to engineering units are carried out in the computer and the results are displayed on the line printer in an easy to read format. All data are also stored in a compact form on a magnetic tape mounted on one of the digital magnetic tape units. The other digital magnetic tape unit and the card reader are used for program loading under control of the console typewriter.

The UT day number and time of day are read in from the NASA 36-bit Time Code Generator. This time is used to identify both the stored data and the data being printed.

Commands are initiated by the computer from requests made via the console typewriter or the card reader. The computer controls the command tone generator, which is a set of audio oscillators corresponding to the frequencies of the Tone Address Execute (TADEX) command system. These tones are used to modulate the carrier which is then transmitted to the satellite.

The only component of the digital section not yet discussed is the analog magnetic tape recorder. This is used as a backup simply to record the subcarriers along with the time and commands. This tape may then be used to play the signal back into the system to recover any data that may have

been lost. It is also very valuable in program debugging, allowing a recorded signal from the satellite to be played back into the system.

9.1.3.3 TV Recovery System Hardware

A block diagram of the DODGE TV recovery system is shown in Fig. 9-8. The input signal to the system includes the 13.5 kHz DODGE video sub-carrier-oscillator (SCO) signal, which originates in the RF and analog section, either from the main receiver for real-time operations, or from an analog tape recorder for non-real-time operations. A second non-real-time mode of operation is provided through a computer interface. This configuration is discussed in Section 10 of this report.

Referring to the block diagram, the sync tone demodulator recognizes the beginning of a picture from the data and initiates the sweep generator. It also decodes the camera mode data that are added to the video signal. The code is entered on the picture record as a series of bars along the picture edge. The discriminator demodulates the frequency modulated SCO signal; its output is the camera video signal. The video signal is transformed by the video processor into the appropriate range for the image module; an antilogarithmic conversion is included at this point. The sweep generator provides the necessary signals to position the image module cathode ray tube (CRT) beam to the proper position for video presentation. The brightness of the CRT is controlled by the level of the video from the video processor. The camera mode data are added to the video signal in the video combiner for presentation in the image module. The image module consists basically of a CRT, optics, and a film system which converts the video and sweep signal inputs to a hard copy picture record of the TV data. Polaroid film is used for the output picture to take advantage of its rapid and dry processing capabilities. Fig. 9-9 is a photograph of the DODGE TV reproduction equipment. The two racks on the left house the sync tone demodulator, discriminators, sweep generators, and the video processor. Also mounted in these racks are monitoring equipments, part of the computer interface equipment, a simulator for equipment testing, and a tracking

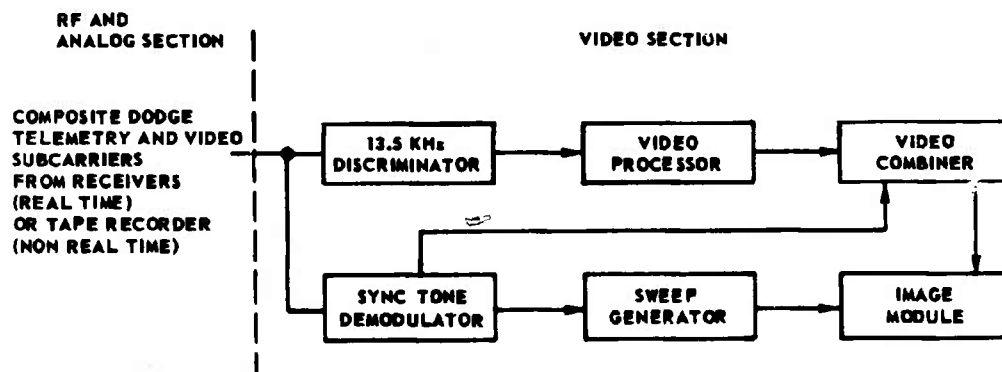


Fig. 9-8 VIDEO SECTION HARDWARE

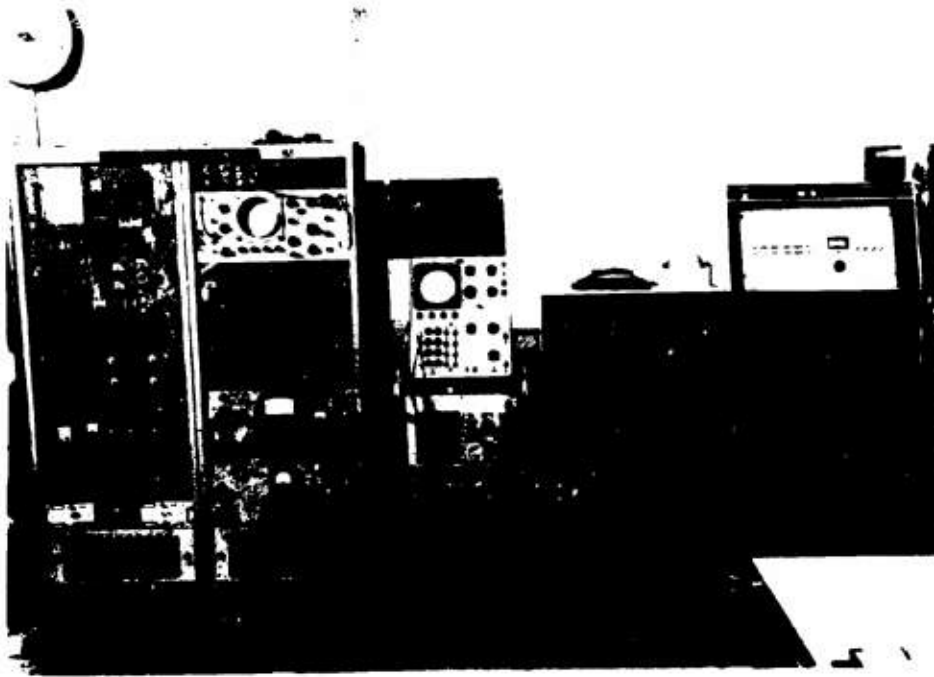


Fig. 9-9 DODGE TV REPRODUCTION EQUIPMENT

filter for tape clock signal recovery. The equipment console on the right is the image module. The patch panel directly behind and above the oscilloscope between the reproducer equipments, provides the interconnections between the equipments and the interconnection to the main control room and the computer room.

9.1.4 Software

9.1.4.1 Programming Approach

The three commutators that make up the full DODGE telemetry system have many modes of operation. They may be in synchronism with each other, out of sync (one or more commutators), or any or all of the commutators may be stopped on any channel. Further, the A and B commutators may be turned off while data are received on the H commutator only. The number of these possibilities is large enough to make a single unified program to recover data in all cases difficult to write. One aspect of the data is that it has a very slow rate (the low pass filters in the discriminators are 12 Hz and still pass all the signal components). This rate allows for a considerable number of machine instructions to be executed for each channel of data. A decommutation program capable of recovering data from any of the three commutators was written, and duplicates were made to form a program of three parts, capable of recovering data from the three commutators of the DODGE spacecraft. The three decommutation programs are time multiplexed in the computer as the data are processed. Because the three parts can run independently, the difficulties of lack of synchronism or a stopped commutator do not affect the total reduction program. The computer has an internal clock that is used to provide the timing for the program once a fiducial time is determined from the data stream.

These three programs operate completely separately from one another and communicate to the printout and command routines via common storage areas in core.

The signals from DODGE are received via an RF signal and are detected and passed to the FM discriminators that produce PAM (Pulse Amplitude Modulated) signals as their output. These data are multiplexed, under computer control, as the input to an A/D converter which converts the data to binary numbers for input to the computer. The conversion process is controlled by the computer. Rapidly changing data are sampled more rapidly than slowly varying data. Commands are initiated by the computer which controls the modulation and timing of the command tone modulator. Station time is input to the computer continuously in order that printouts and operations will be correlated with time. Data display devices include a printer capable of printing 500 lines per minute, with each line being 136 characters in width, an 8-channel pen recorder, and associated digital-to-analog (D/A) converters. The real-time system receives control inputs via the console typewriter or card reader. Commands, data monitor information, etc., are entered in this manner.

9.1.4.2 Real-Time Decommutation Program

The real-time decommutation and command program accomplishes acquisition, scaling, conversions, and display of the telemetered data as well as control of the sending of commands. The program is stored on magnetic tape and loaded via the operating monitor program after being requested by the operator on the typewriter. Control cards containing telltale monitor information (i.e., the telltales to be monitored and their expected states) may then be entered via the card reader. A general flow chart of the program is shown in Fig. 9-10.

The program initially searches for the frame synchronization marker, which is also a calibration channel. Other calibrate channels immediately follow, and the $y = mx + b$ calibration equations are formed from the three calibrate channels (See Fig. 9-11). The trailing edge of the last calibrate is defined as the master frame time. All data following within the frame are sampled at predetermined times with respect to this master frame time.

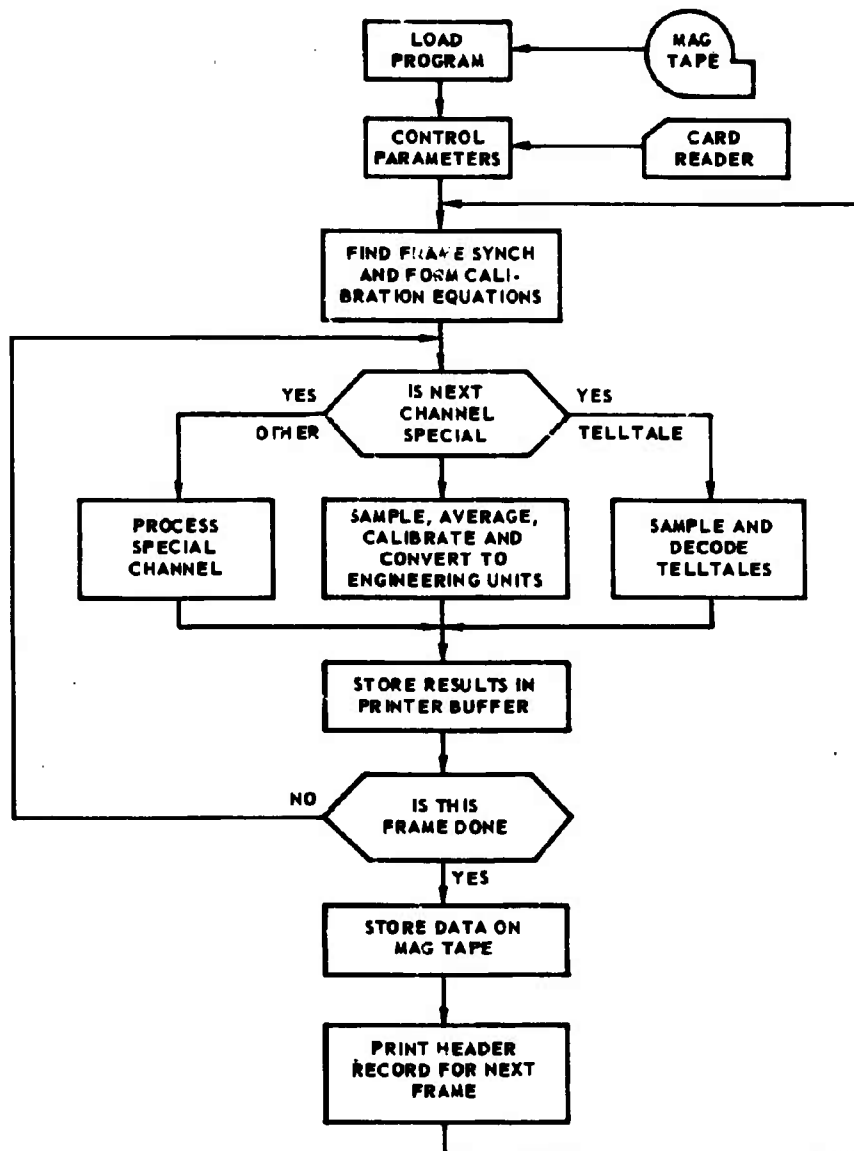
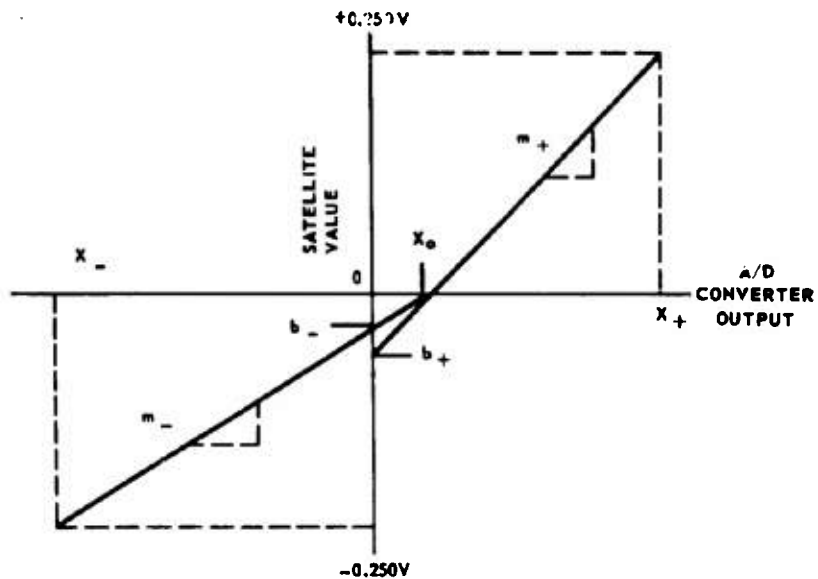


Fig. 9-10 SIMPLIFIED FLOW CHART REAL TIME PROGRAM



For Positive Data Channels:

$$y_+ = m_+ x + b_+$$

$$m_+ = \frac{.250}{x_+ - x_0}$$

$$b_+ = m_+ x_0$$

For Negative Data Channels:

$$y_- = m_- x + b_-$$

$$m_- = \frac{.250}{x_0 - x_-}$$

$$b_- = m_- x_0$$

Fig. 9-11 COMPUTATION OF CALIBRATION EQUATIONS

The values of the data channels are determined by sampling and averaging a number of samples from each channel. This average is then calibrated and converted to engineering units. In addition, a noise measurement is taken on each channel. As the data are processed they are immediately displayed on the line printer; the printout includes time, channel name, the millivolt and the engineering values of the data, and the quality factor.

At the end of each frame of data, all data collected during that frame are transferred to digital magnetic tape. This tape may then be used as a data source tape for non-real time data analysis.

Sampling of the data and the control of commands are accomplished through use of the real time clock interrupt system. The computer contains an internal real time clock that is continuously updated each millisecond and which contains an associated interrupt when the current clock time equals a preselected time. Several time interrupts may be programmed ahead and are queued by a time interrupt subroutine.

Commands are entered via the typewriter or card reader. Single commands or a series of commands may be specified. A delay time between individual commands within a sequence may be specified to within one millisecond accuracy. If no delay is specified, the commands are sent 3 1/2 seconds apart when a sequence of commands is being executed. Command timing is generated by the time interrupt system.

9.1.4.3 Sequential Operation of the Deconvolution Program (Refer to Fig. 9-12)

1. While searching for initial frame synchronization (the positive calibrate channel) the program samples the data each 10 milliseconds continuously until 300 consecutive samples have been received with amplitude in excess of half full scale from the A/D converter. The

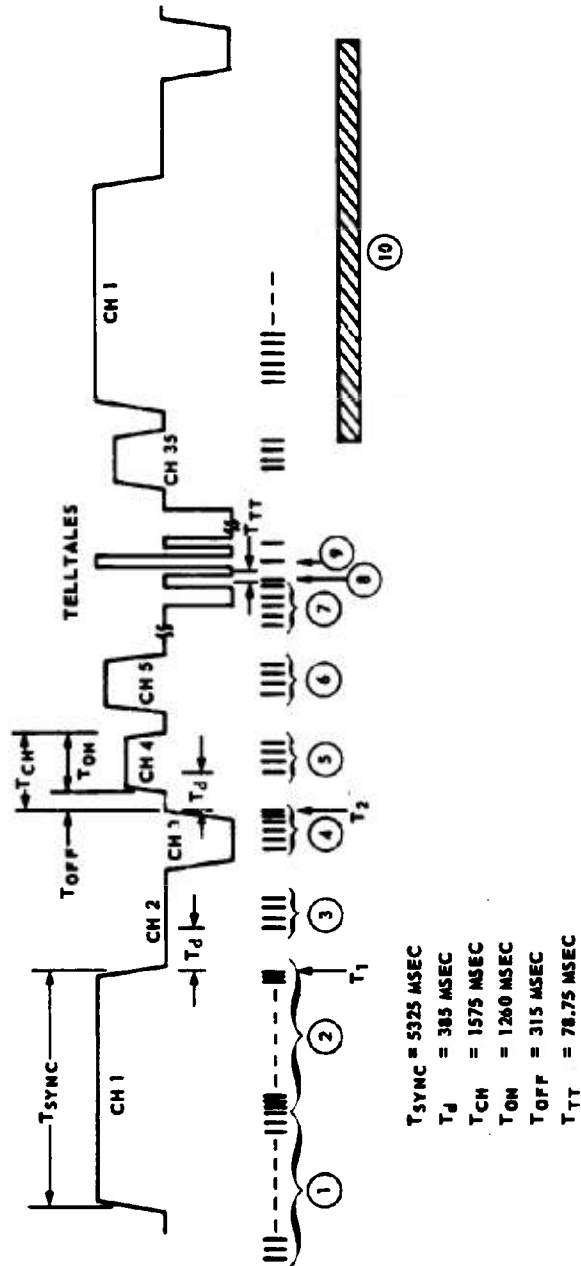


Fig. 9-12 DODGE DECOMMUTATION PROGRAM TIMING

discriminator gain is adjusted so that the positive and negative calibrate channels swing the discriminator to roughly +80% of its full output with a corresponding output of the A/D converter). Once the positive calibrate channel is recognized the sum of the samples is averaged. This is the positive calibrate to be used in the formulation of the calibration equations.

2. During the remaining time for the positive calibrate channel, the channel is sampled each 3 milliseconds in search of its trailing edge. Once the trailing edge is detected (3 consecutive samples less than one-half the value of the positive calibrate) the time T_1 is saved. The sampling of the zero and minus calibrate channels will be referenced to T_1 .
3. Following a delay time T_d , (equal to the channel off time (315 ms) plus an additional delay of 110 milliseconds into the following channel) the zero calibrate channel is sampled each 10 milliseconds until 70 samples are accumulated. The accumulated total is then averaged and the result saved for the calibration equation computation.
4. After another delay T_d , the minus calibrate channel is sampled and averaged. Now that all necessary inputs are available the $y = mx+b$ calibration equations are computed. All future data channels will be modified by this equation. The remainder of the negative channel is sampled each 3 milliseconds until the trailing edge (3 consecutive samples less than one-half the amplitude of the channel value) is detected. This time T_2 , is the master frame time. All subsequent data channels will be sampled at a predetermined time with respect to T_2 .

5. A delay T_d is initiated before sampling channel 4. Before sampling begins, the channel time (T_{CH}) is added to the current time. This is the time at which the following channel will be sampled. Then the current channel (channel 4) is sampled, averaged, calibrated, and a noise test is made. The results are then printed on the line printer.
6. Channel 5 and the remaining channels, with the exception of the telltale channels, are handled in a like manner.
7. During a telltale channel, no delay (T_d) is used, and the program searches for the initial telltale dwell time. Timing begins from the trailing (positive going) edge of the dwell interval.
8. A delay of $1/4 T_{TT}$ (the telltale period) is initiated and a single sample is taken. A threshold test (less than 50 millivolts = "0", more than 50 millivolts = "1") is made and the decoded value of the telltale is stored.
9. The program delays by T_{TT} and the following telltale is sampled and decoded. This process continues until all telltales have been decoded.
10. When the last channel of the frame has been sampled, the entire frame of data is written on digital magnetic tape for future non-real time processing. After the tape dump is completed, the header record for the next frame of data is printed. This entire process is completed before the first channel of the next frame so the real time printing process is not interrupted. While the tape dump and the header record print operations are in

progress in the background, frame synchronization is detected and calibrates are processed in the foreground all under interrupt control.

9.1.4.4 DODGE Non-Real Time Program

The DODGE non-real time program is used to print abstracts of the DODGE telemetry for various users. The data are taken from the data tape written by the real time program. Control of the non-real time program is via cards. These cards are punched, one for each data point that is to appear in the abstract. There are two control cards, one for the start of the deck that contains the name of the user (or any other 80 characters of information) and one used to close a deck for a given abstract. Between these two control cards there may appear any number cards that have two numbers separated by at least one blank or a comma. The numbers are integers and specify the commutator and channel desired. The data abstracted from the tape are in engineering units. The engineering units, however, may or may not be the units that appear on the real-time printout. There are two types of channels that have computation performed on the millivolt readings (which are on the data tape) to improve the accuracy of the data for the non-real time printout. These are the magnetometer and solar attitude detector channels. The data tape has the data in engineering units, millivolts and the noise factors for each data measurement. The slopes and offsets and the calibrate readings are also included but the DODGE NON-REAL TIME PROGRAM does not use these data.

9.1.4.5 Data Tape File Handling Program

The DODGE data tape is a collection of many data transmission intervals. These are normally 10 minutes in length but can be much longer. The data are collected during a single local overhead pass lasting for approximately five days. At the end of this period the data collected are merged to a larger master tape that will contain as many as four "Passes." The program that allows

the tape to be merged and manipulated is called DDT (DODGE Data Tape). It has several options. These options include:

- a. listing the beginning and end times for all data files on the tape.
- b. copying portions of one data tape onto another.
- c. merging two data tapes into one.

9.1.5 Performance Evaluation

All the hardware and software programs described above have operated in a satisfactory manner, and all the data obtained from DODGE have been successfully processed and made available for study of the DODGE performance.

9.2 DODGE Satellite Time Tracking System

9.2.1 Description

Earth synchronous spacecraft in circular orbits cannot be tracked by doppler methods due to the lack of relative motion between the observer and the spacecraft. A suggestion by R. R. Newton of APL for "range tracking" through recognition of timing bursts emitted by the spacecraft has been implemented with the DODGE satellite to test this concept. As implemented, the DODGE satellite transmits timing bursts at fixed intervals on a 240 MHz carrier derived from a stable oscillator; these time bursts are detected at several ground tracking stations. The time at which the bursts are seen at a tracking station yields range information when combined with similar data from other tracking stations, all of which must maintain time to a common reference.

- a. The accuracy with which remotely separated clocks can be maintained to a common standard.
- b. The signal to noise ratios in the time burst recovery equipment.

- c. The accuracy with which equipment delays can be measured and controlled.
- d. The number of measurements available, either through simultaneous recordings of a single burst by several tracking stations, or through reception of sequences of coherent bursts having a fixed spacing.
- e. Range errors due to refraction by the ionosphere and the troposphere.

Accuracy requirements were set at 20 microseconds peak to peak bias error with a standard deviation of 10 microseconds rms or better for all equipment-contributed errors. The bias error limit of 10 microseconds at any station includes errors in setting and maintaining the epoch of the station reference clock, errors in measuring and reporting signal delay time in station equipment, and variations in the phase path from the VLF station from one mean noon to another. The 10 microsecond rms deviation limit is shared between delay measurement accuracy and the rms error in data points recovered from the satellite. A time and frequency control experiment, carried out at tracking Station 103, Las Cruces, and the APL Time and Frequency Standards Laboratory indicated that the time and frequency accuracy requirement could be met, at least in the continental U.S.

Four stations of the TRANET, 008 - Brazil; 013 - Japan; 112 - Australia; and 111 - Howard County were selected to participate in the DODGE tracking trails. With the concurrence of NavAirSysCmd, arrangements were made with the Physical Science Laboratory, New Mexico State University, for modification of station equipment to receive 240 MHz signals from the DODGE satellite and produce the proper input signals to operate an APL designed Time Recovery System, and to record the time of recognition of the time burst from the satellite with 1 microsecond resolution.

9.2.2 Establishing An Epoch

In order for remotely located clocks to maintain time to better than about 10 micro-seconds, an epoch must be established at each station with respect to a common reference, and a common clock rate reference must be used. Since atomic frequency standards were not available at any of the tracking stations considered, it was necessary to use VLF standard transmissions to relate the various clocks to a common clock rate. The choice of VLF stations lay between NLK - 18.6 kHz, which can be tracked by all stations, and OMEGA, which required a split in the network with 013 Japan and 112 Australia monitoring 13.6 kHz transmissions from Haiku, Hawaii and 008 Brazil monitoring 13.6 kHz (later 12 kHz) from Trinidad. In the first case the APL Time and Frequency Facility had been monitoring 18.6 kHz; in the case of OMEGA, it was necessary to begin monitoring 13.6 kHz transmissions from Haiku and to arrange with U. S. Naval Observatory to receive results of NAVOBS monitoring of 12 kHz TRINIDAD. The lower frequency and superior phase stability of OMEGA made it the better choice. Since the 13.6 kHz OMEGA frequency is time shared between the four operating OMEGA stations, it was necessary to construct gating units that short the antenna terminals of the receiver except during the time interval in which the desired station is transmitting.

At the tracking station, the phase-lock VLF receiver produces a 100 kHz signal which is coherent with the received VLF signal. This signal drives a "coherent" clock, Fig. 9-13 which is used as the station's time reference. Phase differences between the VLF signal and local oscillator are logged hourly together with measurements between the several clocks. Coherent clock epoch is established by portable clock and serves as the station time reference. The nighttime diurnal phase shift is circumvented by using the coherent clock as a reference only during daylight hours for the VLF path, and by correcting for the effect of local oscillator frequency offset for 24 hour spans between mean noon for the particular VLF path. Day to day variations in the phase path

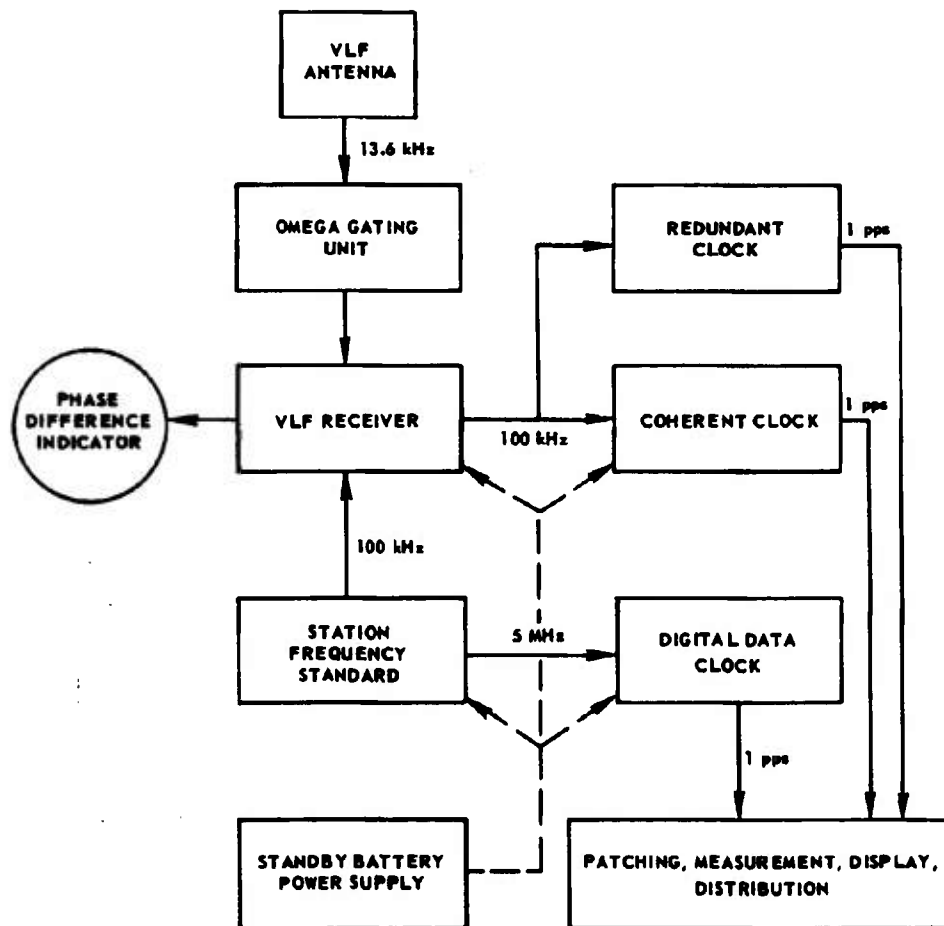


Fig. 9-13 TYPICAL STATION CLOCK SYSTEM

length at mean noon, in the absence of unusual phase perturbations, are thought to contribute about 3 microseconds uncertainty. Deviation of the OMEGA VLF signals from UTC has been negligibly small. Thus the station reference is driven at approximately the UTC rate, and it remained only to establish an epoch. This was accomplished by time transfers using precision portable clocks. During 1967 each of the tracking stations involved was visited not less than twice with a portable clock. Time transfers made by the U. S. Naval Observatory using atomic clocks are said to be accurate to a few microseconds. Time transfers made with the APL crystal clock are generally less accurate, Ref. 9-1.

In practice, standby battery power supplies and redundant clocks are also necessary to safeguard against loss of epoch due to power failures or clock malfunctions.

9.2.3 Time Recovery Accuracy vs. Signal to Noise Ratios

The timing burst emitted by the satellite consists of 126 full cycles of a 325.514323 Hz square wave followed by a phase reversal and two full cycles at the same frequency. Total duration of the burst is 393 milliseconds, and the burst occurs at approximately 200 second intervals for 10 minutes out of each hour. The burst appears as 60° phase modulation on both 240 MHz and 136.8 MHz.

On the ground, the DODGE Time Recovery System (DTRS) uses a narrow bandwidth filter to greatly increase the signal to noise ratio. The phase reversal is detected by comparing the input and output of the filter. Because of the narrow filter bandwidth, the output signal continues at its original phase immediately after the phase reversal, and the input and output signals differ in phase by 180 degrees. The phase reversal detector, which compares the filter input and output signal, is used to enable the next cycle out of the filter output to trigger a time measurement. In this way, a white noise bandwidth corresponding to the filter bandwidth is achieved.

It can be shown that for 10 μ sec rms accuracy a signal to noise ratio of +34 db is required. The available signal power is -120 dbm using 10 db gain antennas and the noise density is estimated at -165 dbm/cycle. The noise bandwidth at the input to the filter is 1300 Hz and the maximum s/n at the input to the filter is approximately +15 db. We allow a 9 db system margin and assume that the available signal to noise ratio at the input to the filter is +6 db. These figures imply a filter bandwidth of 8 cycles or less. A lower limit on the filter bandwidth is determined by the allowable variations in phase delay through the filter due to changes in the center frequency of the filter with temperature, and changes in the frequency of the burst tone due to residual doppler effects. The filter bandwidth chosen was $2.4 \pm .1$ cycles, and the filter itself was installed in an oven to maintain it within one degree of a constant temperature over an ambient temperature range of 0 to 50°C.

9.2.4 Measurement and Stability of Equipment Delays

The propagation delay time from the time of receipt of a timing burst at the antenna to the instant the burst is recognized and recorded must be known so that it can be subtracted from the raw data in the process of calculating range to the satellite. A time burst generator was incorporated with the DODGE time recovery system. When the burst generator is driven by the station frequency standard and the burst initiated by the station clock 1 per second pulse, the burst is coherent with the station clock and an exact measure of the equipment delay is possible by modulating an RF test beacon with the burst and measuring the interval between start of the burst and the time the burst is recognized.

During the evaluation of the DTRS, extensive tests (Ref. 9-2) were made to determine system propagation delay as a function of RF signal level, receiver loop bandwidth, receiver tuning, AC line voltage variations, and temperature

variations. All tests tend to show that hourly equipment delay variations from a daily mean value probably do not exceed 2 microseconds rms. A long term drift of about 1 microsecond per day has been observed.

9.2.5 Tracking Results

Although a substantial amount of raw timing data have been acquired since the launch of DODGE, analysis has been limited to examination of first differences. In normal operation a sequence of three timing data points is transmitted once each hour. Reception of all three points yields two first differences. First difference values for a selected 5-day period of a DODGE pass over Station 112, Australia were plotted and a curve was fitted to these values by trail and error, Fig. 9-14. The 22-hour period of the final term of the equation is a good approximation of the orbital period and represents the north-south excursions from the equator as the orbit is traversed. The term $5/12 x - 4.5 \sin \pi/60 x$ represents an approximation to the standard doppler curve (broken line). The approximation is only fair. A better fit should yield a lower rms than the 7.7 microseconds obtained with the present curve. The rms fit clearly indicates that the timing data acquired meet the accuracy requirement set for this test and should be suitable for orbit computation.

9.3 References

- 9-1. APL/JHU Quarterly Report, Space Programs, U-SQR/67-2, April-June 1967.
- 9-2. C. H. Buerkle, "Evaluation of DODGE Time Recovery System Using ITTL and Space General Receivers at TRANET Station 103 - Final Report, Contract No. N0w 62-0604-C 230519 Task I," Physical Science Laboratory, New Mexico State University, July 1967.

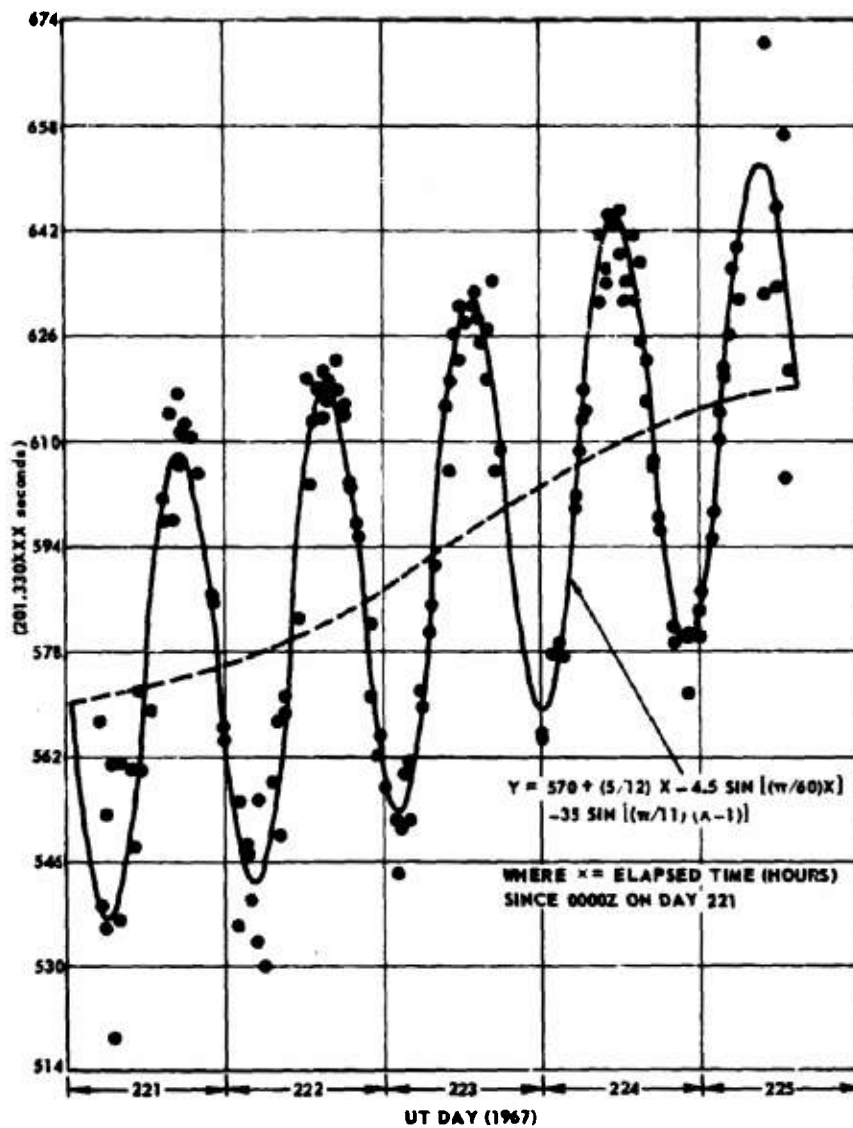


Fig. 9-14 STATION 112 DODGE TIMING POINTS FIRST DIFFERENCES

BLANK PAGE

10. TV PICTURE STUDY

The objectives of the DODGE picture study are: (a) to provide an effective means for data handling and storage, (b) to correct flaws in the picture data, (c) to analyze the multispectral data, and (d) to establish an efficient data file such that further studies of the picture data can be conveniently carried out.

Since the picture characteristics of the DODGE cameras were of secondary importance, and the time and budget were limited, a minimum of calibration data were obtained on the completed camera system before launch. Also, the picture reproducing equipment was not available until shortly before launch. As a result, most of the processing programs and procedures had to be developed after launch, and the picture characterization and calibrations were necessarily delayed. At the present time, programs have been written that satisfy, to a large degree, the first two objectives stated above. However, methods for compact data storage are currently being investigated and a final storage format has not been established. Analysis of the multispectral picture data has been limited primarily to obtaining color balance for several color pictures.

The overall effort to date has been directed primarily toward generation of a processing library, characterization and gray scale calibration of the camera data, and the establishment of a dark room facility for the photographic processing of the DODGE pictures, with particular emphasis on color processing. In addition to the computer processing effort, an optical processing technique has been studied and employed for filtering of the picture data.

10.1 Processing System

The availability of the CDC 3200 computer facility made it possible to study the DODGE video information by computer methods. Computer hardware and software were prepared in

order that the computer system (The APL CDC 3200 Real Time Satellite Data Processor) could be used to acquire, process, and display the DODGE video data.

The advantages of computer processing the video data are as follows:

- a. the video data frame can be conveniently ordered and stored on digital tape with efficient picture packing density. Stored in this manner, video frames or portions thereof, can be easily recovered for processing.
- b. Any number of processes may be applied on a frame of data by repeated re-entry of the data into the computer.
- c. Sophisticated processes such as spatial filtering, editing, etc., may be applied since the computer can examine the data character of a given picture by area.
- d. Mathematical conversions and processes are conveniently performed by a computer.
- e. Since the data are ordered uniformly, the data from one frame may be compared with that of another frame on an element by element basis.
- f. A video frame is easily displayed numerically for evaluation by engineering personnel.
- g. Data compression and subsequent archives storage is conveniently handled by computers.

10.1.1 Hardware Configuration

A block diagram of the computerized DODGE video processor is shown in Fig.10-1.

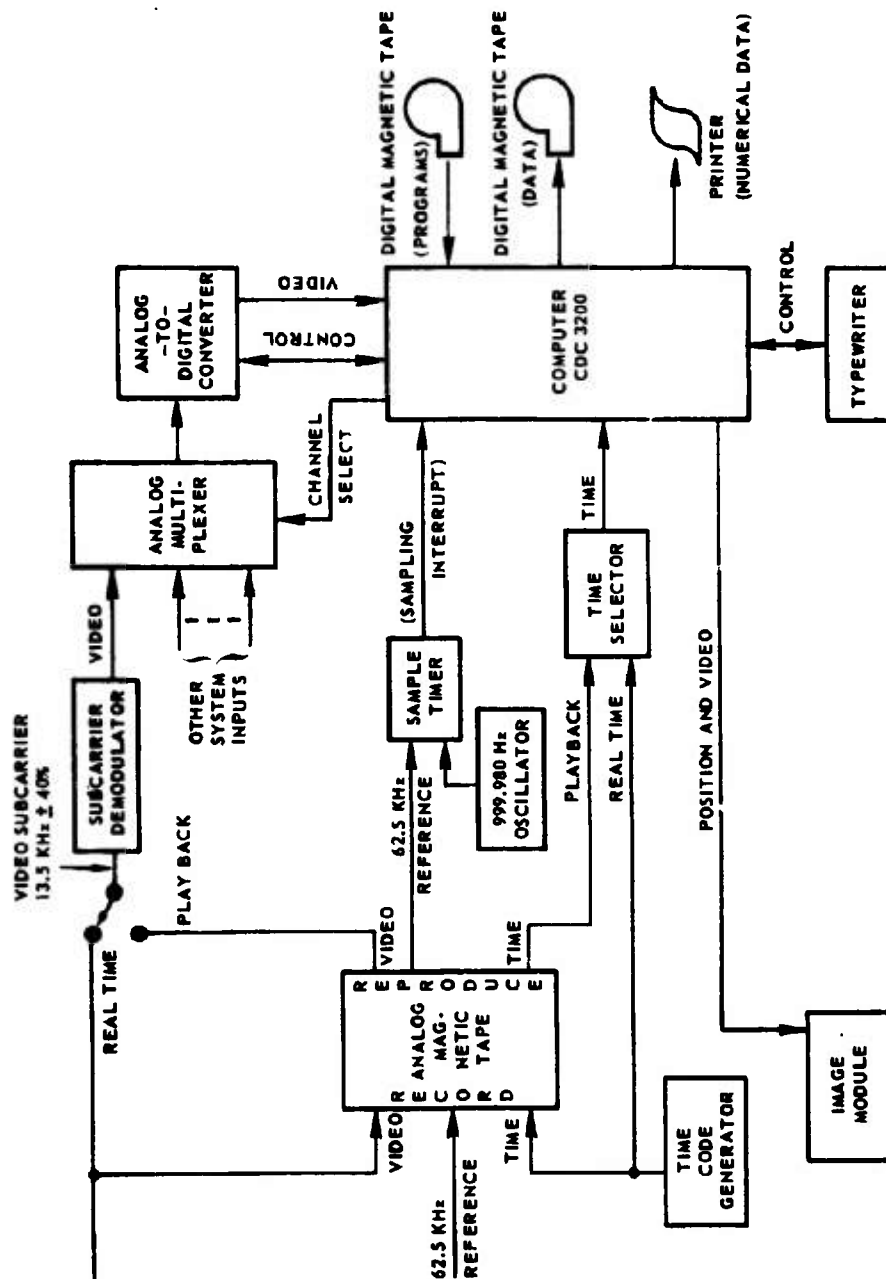


Fig. 10-1 BLOCK DIAGRAM OF DODGE VIDEO PROCESSOR

The APL real time satellite data processor, a system utilized in the prelaunch evaluation and post launch data recovery of all Laboratory satellites, was used to process and study the DODGE video data on a non-interference (with real time satellite operations) basis.

The system includes a control data corporation (CDC) Model 3200 computer system incorporating 8,192 words of core memory, two input-out channels, and a priority interrupt system. Standard computer peripherals include two digital magnetic tape units with 41,000 bytes (a byte here is defined as a 6 bit computer sub-word) per second transfer rate each, a 500 line per minute, 136 column printer, a 1200 card per minute card reader (not shown) and an input-output typewriter.

The system as shown in the figure is only a part of the total system available, and indicates only those system components necessary for DODGE picture processing.

Input to the system is the DODGE video subcarrier (13.5 khz + or - 40 percent, either real time, or from data prestored on an analog data tape. The incoming data are demodulated by a FM discriminator (a data control systems Model GFD-13 with a 13.5 khz + or - 40 percent bandpass filter and a 1200 Hz low pass output filter) that recovers the DODGE video signals and places the data on an input channel of the analog multiplexer. The analog multiplexer, under real time computer control, selects the DODGE video input channel to be digitized for input to the computer. The analog-to-digital converter samples the analog video and converts this signal to an 11 bit signed digital number for computer input. The start of a single conversion process is initiated by the computer, the converter then notifies the computer when the data sample has been converted and is ready for computer input, and the data are then transferred to the computer for processing.

The computer achieves video frame synchronization (detects the beginning of a video picture) by software. However, there is no timing

information transmitted within the video signal following the frame synchronization data (The video frame consists of a continuous analog signal), and therefore sampling intervals must be determined by the ground processor. The sampling periods used to construct the video signal in the satellite were derived from a 999,980 Hz master oscillator with the proper countdown divider to produce the approximately 1200 Hz sampling frequency. The spacecraft system was essentially duplicated on the ground for real time operations. The sample timer shown on Fig. 10-1 generates the sampling frequencies. A 999,980 Hz crystal oscillator is used, and its frequency is properly divided to generate the computer sampling information. Once started by the computer, the sample timer sends an interrupt signal (a signal alerting the computer to the occurrence of an event external to the computer) to the computer each time the input video data are to be sampled.

The computer system is normally used for DODGE telemetry processing in real time and therefore video processing must be deferred. The video data are stored on an analog data tape along with a reference frequency and time. The reference frequency is required to eliminate the effects of the tape motion (uneven tape motion causes irregularities in the recovered analog video signal). During playbacks, the computer sampling process is essentially slaved to the reference frequency on the tape. Sampling is then always directly related to tape motion and is always in synchronism with the data stored on the tape. The reference frequency used is approximately 62.5 kHz (it is actually derived by dividing the 999,980 Hz crystal oscillator frequency by 16). The input frequency to the sample timer (which is computer selectable) is either 999,980 Hz for real time operations or 62.5 kHz for analog tape playbacks (non-real-time). The output of the timer is always maintained the same i.e., the DODGE video sampling frequency, by computer control of the timing unit internal logic.

Time of year (day number, hours, minutes, and seconds) is also input to the computer in order that the processed video frame be tagged with time of occurrence. Time input is either from the station time code generator (real time) or from the pre-recorded time track on the analog data tape.

The data input to the computer is formatted and transferred, line by line, to a digital magnetic computer tape for subsequent processing by the video processing routines, which require the data to be formatted on a digital data tape.

The data collection process is then one of digitizing the input video, each sample corresponding to a video element, grouping these elements into lines, and transferring these data, line by line, to a digital data tape.

Once the video data are recovered and processed, results are displayed on the video image module, a CRT video reproduction system that records video data on film. The computer transmits positional information (X and Y coordinates) and video intensities to the image module.

The remaining hardware as illustrated in Fig. 10-1 includes a digital magnetic tape unit for program input, a printer for numeric display of picture content, and a typewriter for operator-computer communications.

10.1.2 Software Description

Computer programs developed during the video study can be grouped into the following categories:

- a. Synchronization and input conversion.
- b. Repair and quality enhancement.
- c. Video display routines.
- d. Analysis of picture content.
- e. Data handling, conversion, and storage.

10.1.2.1 Synchronization and Input Conversion

Programs were developed to acquire, synchronize, and store the digital equivalent of the analog input video. Two programs to accomplish this, IVIN and FBSYNC, have the following characteristics.

TVIN

The video data are sampled rapidly in search of frame synchronization which is achieved when the first negative-going transition of the initial two-line identification and synchronization record is detected. Once synchronization has been detected, internal timing is derived to sample and decode the identification record (camera and filter data). At the same time, the actual time at which frame synchronization is detected is stored. Time, camera data, and certain information describing the format of the data records to follow, are stored as a header (identification) record on the digital data tape.

Once the identification data have been decoded and stored, the program activates the sample timer which controls the sampling process throughout the remainder of the video frame. A marker from the timer causes the program to be interrupted and control to be transferred to a routine which samples the video data. After sampling and subsequent transfer to the computer, the data are scaled 0 - 5 volts (in order that the data correspond to the data of the DODGE video system in the spacecraft) in a 24 bit computer word with 12 integer and 12 fractional bits. Successive elements are accumulated in a data buffer in the computer memory until a full line (256 or 512 elements) has been stored. Then, the entire line is transferred to digital magnetic tape from one data buffer while a second data buffer begins to fill with the next line. The program continues to sample, scale, and store the data until the entire frame has been collected. Then a file mark is written at the end of the magnetic tape records to indicate the termination of the video data for

that particular frame. Meanwhile, the program begins to search for synchronization of the following video frame (if any).

A digital data file (one complete video frame) is depicted in Fig. 10-2. The tape file begins with the identification record, is followed by either 256 or 512 individual line records, and is terminated by a file mark.

FBSYNC

Certain data inputs are from data tapes collected at the Indian Ocean Station and the NASA Station at Ororral, Australia. These tapes are different from those collected at APL in that the 62.5 kHz reference frequency is not recorded. In order to maintain frame synchronization throughout the data frame, the ability to resynchronize the program with each individual line was developed. This program, called FBSYNC (fly-back synchronization) is identical to TVIN with the exception that it derives line synchronization from the fly-back pulse. The data tape generated by FBSYNC is identical to that produced by TVIN.

10.1.2.2 Repair and Quality Enhancement

Computer routines that fall into this category remove objectionable line structure, random and systematic noise, and smooth the data to improve its appearance. Following are descriptions of these routines, which are called, LINREP, LSF, TVPLTR, and BLKREF.

LINREP (Line Repair) removes line structure and random noise from a video frame of data. The program initially scans the input frame (on digital magnetic tape) and computes and stores the individual line averages (the average value of all elements along a single line) and stores these averages in a table in the memory. Data from this table will be used to compute all line structure removal operations.

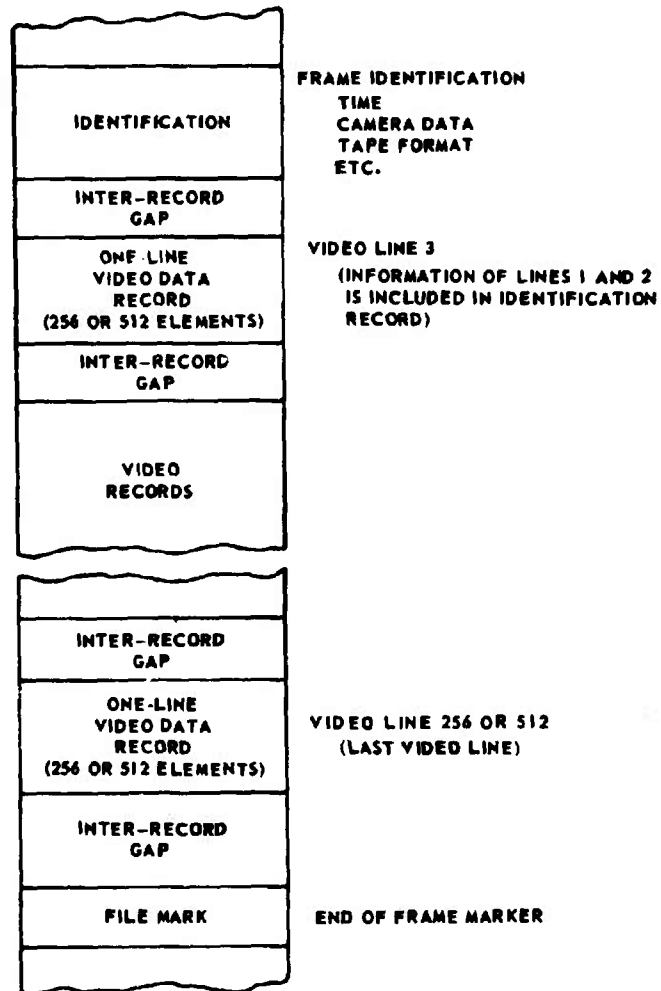


Fig. 10-2 CONVENTIONAL DIGITAL DATA TAPE FORMAT

The following manipulations are performed on the table of line averages.

- a. The averages of lines $32N-2$ and $32N+1$ are averaged and stored as the averages of lines $32N-1$ (where N is referred to as the line number).
- b. The averages of lines $4N-1$ and $4N+1$ are averaged and stored as the averages of lines $4N$.
- c. The modified line average table as computed above is then edited with out of tolerance line averages being replaced by the average of their adjacent neighbors.
- d. The ratios of the modified line average table (Produced by a, b, and c above) and the original line average table are computed and stored in a third table, the gain correction table.
- e. The modified line average table is then filtered by a low pass running average filter.
- f. The differences between the filtered table and the original line average table are computed and stored as the line correction table.
- g. The data frame is then read in, line by line, and each element of a given line is manipulated by multiplication of the gain correction table and the addition of the line correction table corresponding to that line. The resultant elements are recorded, line by line, on a digital data tape of the conventional format.

In addition to the line structure correction described above, the program reduces the effects of random noise by an edit routine.

The intensity of a particular element is compared with that of its immediate neighbors and if they differ by a preset threshold, the element being edited is modified to agree with neighboring elements.

LSF (Line Scan Filter) this program is a two dimensional correlation filter which compares the average scene brightness in the region of the point to be corrected, and the average of the scan line containing the point. The difference between the scene average and the line average is applied as the correction to the filtered element. The filter applies a weighted filter matrix (7 elements by 7 elements in dimension) to a corresponding data matrix within the video frame. The filter and data matrices are multiplied to the filtered value of the central (middle) data element. The filter then moves to the adjacent data element and the operation is repeated. The program produces a data tape of the conventional format.

The LSF program contains an option that detects system noise within a frame. System noise here is defined to be a systematic frequency superimposed upon the original image. The noise may be extracted from the image by application of a cross-correlation filter to each element within the video frame. The cross correlation filter is defined as

$$\text{Filter} = A \cos 2 \pi (Hx + Ky)$$

A = Maximum Noise Amplitude (Measured)

H = Horizontal Noise Component (Measured)

K = Vertical Noise Component (Measured)

X,Y = Spatial Position of Element Being Filtered.

Through unrelated functionality to LSF, the system noise detection routine handles the data in a manner very similar to LSF and therefore it is convenient to group the two routines into a single program. The horizontal and vertical noise

components are first determined through analysis of a raw (unprocessed) video photograph and the equation above is used to produce a 7 by 7 element system noise filter.

Once computed, the matrix is implemented in the same manner as the line scan filter described above. The routine produces a digital tape which contains only the system noise information. (The result of the above equation). The data stored on this tape are then subtracted, element by element, from the original data tape to produce a noise free data tape, once again, of conventional format.

TVFLTR (TV Filter) is a high frequency recovery filter which slides a weighted filter along a video data line, filtering one element at a time. The filter computes the following for each data element

$$\begin{aligned}\text{Filtered Element} = & 0.4(N-2) - 1.0(N-1) \\ & + 2.4(N) - 1.0(N+1) \\ & + 0.4(N+2)\end{aligned}$$

Where N refers to the position in the line of the filtered element.

The output of TVFLTR is a digital data tape of the conventional format.

BLKREF (Black Reference) reduces the effects of contouring from the spacecraft camera by subtracting, from a frame of data on an element by element basis, the content of a totally black reference picture. The program computes for each element

$$\text{VOUT} = \text{VIN} - \text{VREF} - \text{VBLACK(IN)} + \text{VBLACK(REF)}$$

WHERE

VIN = The Input Data Element

VREF = The Corresponding Video Element
of the Black Reference Frame

VBLACK(IN) = The Black Level of the
Input Frame

VBLACK(REF) = The Black Level of the
the Referenced Frame (Pre-
stored Constant)

Initially the data tape containing the picture to be processed is examined to determine the black level of that frame. Then, as the frame under process is once again read into the computer, each element of the input frame is modified by the above equation. The results are stored in conventional format on a digital data tape.

10.1.2.3 Video Display Routines

Two computer programs, TVOUT (TV Output) and TVDISP (TV Display), control the presentation of video data on the image module (CRT photographic reproducer). The image module controls Z-axis modulation by either of two modulation methods

- a. Analog modulation in which the duration of the video unblanking pulse is held constant while the amplitude of the Z-axis data is varied.
- b. Pulse width modulation where the duration of the unblanking pulse is varied while the voltage level is held constant.

The programs TVOUT and TVDISP are functionally similar, the former controls the analog modulation mode, while the latter involves pulse width modulation. In either case, the data prestored on digital data tape (of the conventional format) is processed to derive video intensity levels to be output to the image module. Segmented transfer curves relating spacecraft camera voltages to image module input intensities are derived from a study of the video data, particularly the data in the regions of the colored sections of the ball. These segmented curves are described in tabular format in the computer memory. Interpolation routines are used to generate image module intensities from video elements referenced in camera voltage (as stored on the digital data tape).

In addition to the video data, alpha-numeric data describing the identity (time, camera data, etc.) are recorded on the film to tag each processed picture.

10.1.2.4 Analysis of Picture Content

Programs, TVSTAT, TVLST, and a special option of TVOUT are used to present the content of a video data frame in graphical and numerical form.

TVSTAT (TV Statistic) computes and displays the following information on the printer.

- a. A graphical display of the distribution of elements within a particular data frame.
- b. A tabular listing of line averages and their first and second differences.
- c. A graph of deviation from the frame average of each individual line average.

The program initially enters the data from the digital data tape, and line by line, computes the stores in a table in memory, the average of each line. At the same time, each element is examined and stored in a position in a distribution table according to its intensity. The distribution table is divided into 50 equally spaced steps, each representing an intensity spread of 0.1 volt.

When the entire frame has been processed in the above manner, the distribution table is formatted and displayed graphically on the line printer. Then, the first and second differences are computed, formatted, and printed. Also computed and printed at this time is a threshold bar graph indicating the magnitude of the difference between successive second differences. Finally, the difference between each line average and the overall frame average is computed and graphically formatted and printed.

TVLST (TV List) lists, numerically on the printer, the content of a particular video data frame. It has two modes of operation.

- a. The video data line is sampled 16 (equally displaced) times, these samples are printed, along with the line number, as a single printed line.
- b. All video elements are printed. In this case, a video line represents several printed lines (a maximum of 16 elements can be accommodated along a single printer line) which are appropriately tagged with line number.

TVOUT (previously discussed in Section 10.1.2.3) includes a special option that analyzes a given area of a video frame statistically. A particular area (a squared sector of adjacent elements) is first defined, and the elements within the region are processed in the following manner.

- a. The average and standard deviation of all elements within the region are computed and printed.
- b. An intensity distribution graph is plotted on the printer.
- c. The region under study is outlined (framed) on the normal TVOUT video photograph.

10.1.2.5 Data Handling, Conversion, and Storage

The computer programs used for data handling, conversion, and storage of data includes LOGTV, HIRES, and TVDT.

LOGTV is a logarithmic conversion routine that relates DODGE video information on either side of the logarithmic amplifier in the spacecraft video system. It has two modes of operation.

a. Convert data in logarithmic format to anti-logarithmic data by the following equation

$$VOUT = 0.1 (10 \text{ EXP } VIN/2.5)$$

b. Convert data in anti-logarithmic format to logarithmic data by the following equation

$$VOUT = 2.5 \text{ LOG (BASE 10) (VIN/0.1)}$$

In either of the cases above, a digital data tape of the conventional format is produced.

HIRES (High Resolution) expands a conventional digital data tape by a factor of two in each (x and y) direction to produce an expanded (1024 by 1024 element) frame, also stored on digital data tape.

The program inputs two adjacent video lines from the input tape, and expands these by averaging adjacent elements to produce an intermediate element. This intermediate element is merged with the original line to create a high resolution line. Two adjacent high resolution lines are then manipulated by a similar process (in this case corresponding elements of adjacent lines are averaged) to create an intermediate high resolution line. The two high resolution lines are then recorded on the output tape. The next line is then read from the input tape and the above process is repeated until the entire frame has been converted.

The expanded output tape, generated by the Hires program, is directly compatible with the required input format of the video display routines, TVOUT and TVDISP.

TVDT (TV Data Tape) is a data tape handler, processed video pictures are normally stored on digital data tapes, several video frames on each data tape. The program, TVDT accomplishes the following functions:

- a. Single or multiple video frames may be added to a digital data tape.
- b. Specific video frame(s) may be extracted from the data tape.
- c. A video data tape may be edited.
- d. The identification of each video frame stored on a particular data tape may be conveniently recovered and listed on the printer.

10.2 Picture Characterization

Before the DODGE picture characteristics can be considered, it is necessary to establish a reference definition for the ideal picture. Fundamentally a picture attempts to reproduce a scene exactly as it would be seen by a human observer. While useful for descriptive purposes, such a definition provides a poor reference for camera system evaluation. For our purposes, a picture is a one to one mapping of brightness contours, as viewed from a point in space over an angular field of view and projected on a plane perpendicular to the viewing direction, to density contours on a photographic plate. The reference to a point in space in this definition implies an unlimited angular resolution capability. Brightness and density are defined in the normal photometric sense. The difficulties and somewhat arbitrary nature of the definitions dealing with brightness and picture are necessary since such terms deal with human sensation and interpretation. Note, that from a geometric standpoint, a pin-hole camera is an ideal camera.

In a photographic camera the geometric performance is determined by the mechanical precision of the camera and lens. The photometric response is limited by the lens transmission characteristics and by the chemistry of the photosensitive materials. A television camera has the same geometric limitations as a photographic camera and in addition, geometric distortions that result from inaccuracies of the scan system. The photometric response is

similarly limited by the lens, or more generally the optics (all elements of the optical path such as filters), and by the physics of the sensor.

Resolution is limited by every component of the system. Even in a perfect lens, resolution is limited by the lens aperture due to the wave character of light (diffraction limit). In most cases the primary resolution limitation of a TV system results from the scanning beam characteristics in both the optical to electronic transfer of the camera, and the electronic to optical transfer of the reproducer system. In some cases film grain can be an important resolution limit of a system.

When we refer to characterization of the DODGE picture, the limitations of all parts of the system are important. However since the reproduction equipment is available for calibration and adjustment and does not have the weight and power constraints of the camera system, most of the picture limitations are set by the camera. Distortions of a geometric or photometric nature and resolution limitations are the factors which degrade a picture from the ideal.

10.2.1 Camera Limitations

Fig. 10-3 is shown as a reference for discussion of the camera distortions.

This particular picture has been digitized and the video range has been adjusted to result in a pleasing presentation, but it is otherwise representative of an uncorrected picture. The most prominent flaw is seen to be the horizontal white line structure. On more careful examination a non-uniformity is detected in the black background, and a bright spot can be seen at the lower right of the color reference ball. The general tapering off of the background could be either an optics or vidicon characteristic and is likely the result of both. The bright spot is known to be a blemish on the vidicon photosurface. Also, particularly across the upper part of the earth a diagonal line structure can be observed. This interference is believed to result from the vibration of the



Fig. 10-3 AN UNCORRECTED DODGE PICTURE

vidicon electrodes brought about by the shock of the shutter action. These three distortions are the major positional photometric discrepancies. The line structure also produces small scale geometric distortions, but there appears to be very little large scale geometric distortion.

To understand the nature of the line structure it is necessary to consider the nature of the vidicon and the scan system. The operation of the vidicon is discussed in Section 3.1, but it should be recalled here that the video output signal results from recharging an area of the vidicon target which has been previously discharged by the action of the optical image. The electron scanning beam has a cross-section which is generally gaussian. Therefore as each element of the target is discretely sampled by the readout beam all the adjacent elements are also slightly recharged. If the sampling is geometrically uniform over the whole target, the beam overlap is constant and the video data are not affected by the scan system.

If however, a nonuniform step is taken by the sampling beam there will be level shift in the video output. For example, if the beam position step is less than normal, the relative overlap with the previously discharged area will increase and the signal level will decrease.

If the scan step is larger than normal the relative overlap with the discharged area will decrease and the signal output level will increase. In the DODGE cameras the horizontal sweep voltage is an analog ramp and the video sampling is controlled by very accurate timing. As a result very uniform sampling distribution is accomplished in this direction. If this were not true the picture would also be marked with a series of vertical lines. The vertical sweep signal is a staircase type generated by a digital-to-analog (D/A) converter. The horizontal lines in the picture result from the nonuniform sampling distribution in this direction.

Geometric distortions are in reality not produced by either the camera or reproducer scan system, but by the difference between the geometry of these scans. Of course, the natural and normal practice is to attempt to produce a linear scan geometry for both cameras and reproducers. With this in mind a scan system is considered responsible for geometric distortions to the extent that the scan geometry is not linear. Therefore the non-uniform steps of the vertical scan also produce a geometric distortion. The localized character and small degree of this distortion make it difficult to detect. However, a careful examination of the pictures of the earth's edge shows it to have a slightly ragged character as a result of this scan distortion. No careful tests have been carried out to determine the degree of large scale (i.e., more continuous) forms of geometric distortion. These distortions can result from nonlinear sweep signals, or nonlinear magnetic field deflection geometry, or can be produced by the camera optics.

There are two overall types of photometric distortions unlike the positionally dependent types discussed above. In the strict sense, none of the DODGE pictures can represent brightness contours since the vidicon spectral response is not the same as the standard visual response defined by photometric purposes. However, the response of the vidicon in the red region of the spectrum is similar to the visual response, and in combination with one of the haze filters a good approximation of the visual response is achieved. The comparison between this camera position and the visual response is shown in Fig. 10-4. Relative brightness data can also be approximated quite well from the green channel of the color separations. Another form of photometric distortion results from the nonlinear response of the vidicon. That is, the vidicon signal output is not linearly related to the face plate illumination.

As noted previously all the camera components contribute to the resolution limitations. However, the principal limitation is set by the fact that the vidicon and beam sampling to a 512 line raster. It should be noted that the

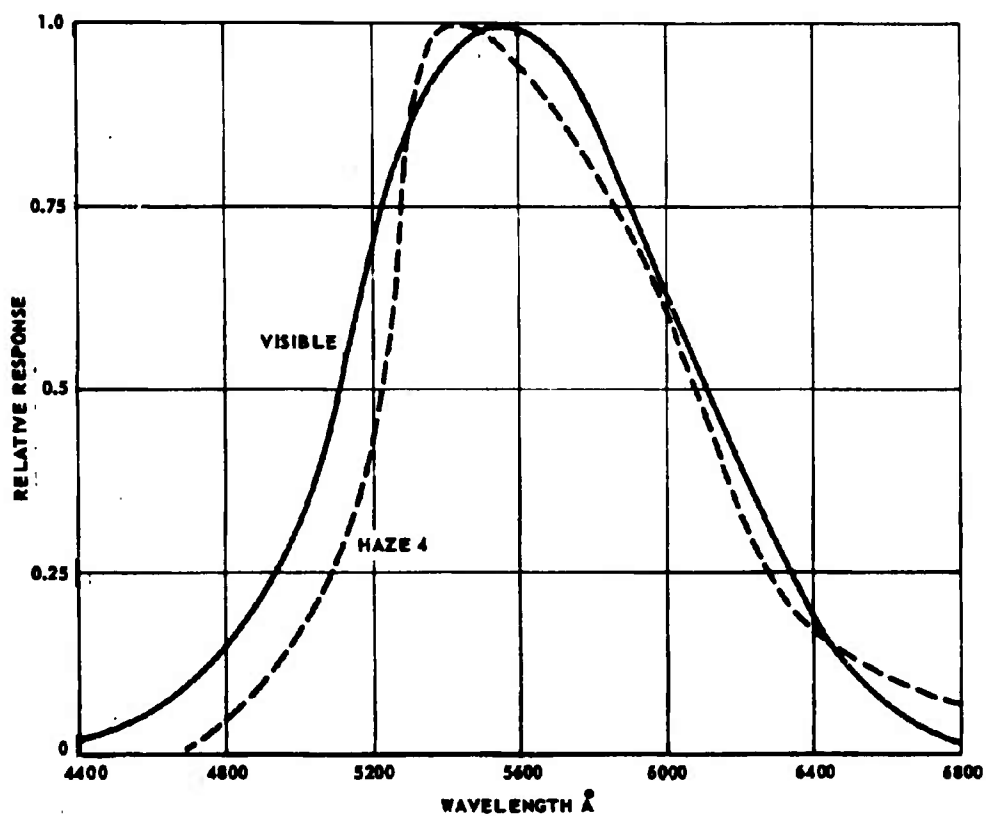


Fig. 10-4 COMPARISON OF THE DODGE CAMERA "HAZE 4" POSITION AND THE STANDARD VISUAL RESPONSE

vidicon limiting resolution at the center of the tube is slightly greater than the sampling density. However, even on the tube axis the response at the sampling density is below 20%. The limiting resolution of an image tube is defined as that spatial frequency at which the black to white signal output is 5-10% of its low frequency value. The setting of the percentage at which the limiting resolution is defined is arbitrary, and if there were no noise limitation for the camera, frequency response would actually be unlimited. The camera noise characteristic and the saturation level set a limit on the dynamic range of the brightness data.

10.2.2 Reproducer Limitations

Generally the picture reproducer has all the same types of limits as the camera. Basically, the reproducer consists of a cathode ray tube (CRT), optics (a lens and mirror), and a film for storage. The film used is Polaroid P/N 55, which has the convenience of immediate "dry" processing when only positives are required, and a simple "wet-but-not-dark" processing provides negatives as well. The resolution capability of the full system including the negative is approximately 2000 lines. The scanning system is fully digital and the linearity is such that no scan distortions of a geometric or photometric nature are apparent.

The primary limitation of the reproducer is that the voltage to density transfer is not constant. A closed loop control can be installed in the reproducer which monitors the output of the CRT and retains a constant brightness. This control in combination with a method of beam modulation which is controlled by accurate timing signals can produce a constant voltage to CRT brightness transfer. However, the film response is not controllable in the same sense. Another advantage of the closed loop control of the CRT results from the ability of this system to provide a high degree of uniformity. Figs. 10-5 and 10-6 show the voltage to negative density transfer of the DODGE picture reproducer. The first figure shows the result of a warm up test.

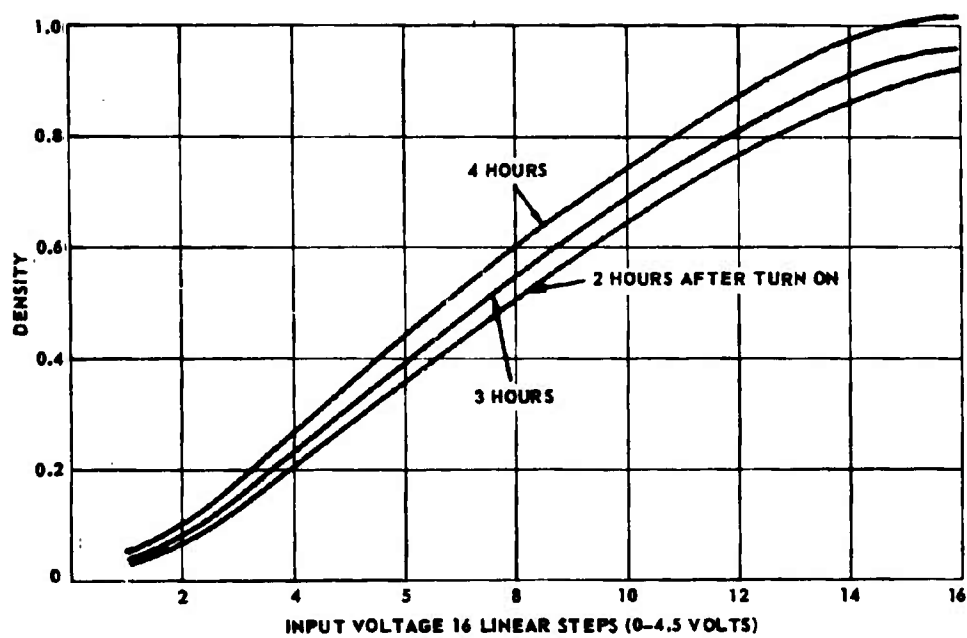


Fig. 10-5 REPRODUCER WARM-UP CHARACTERISTIC

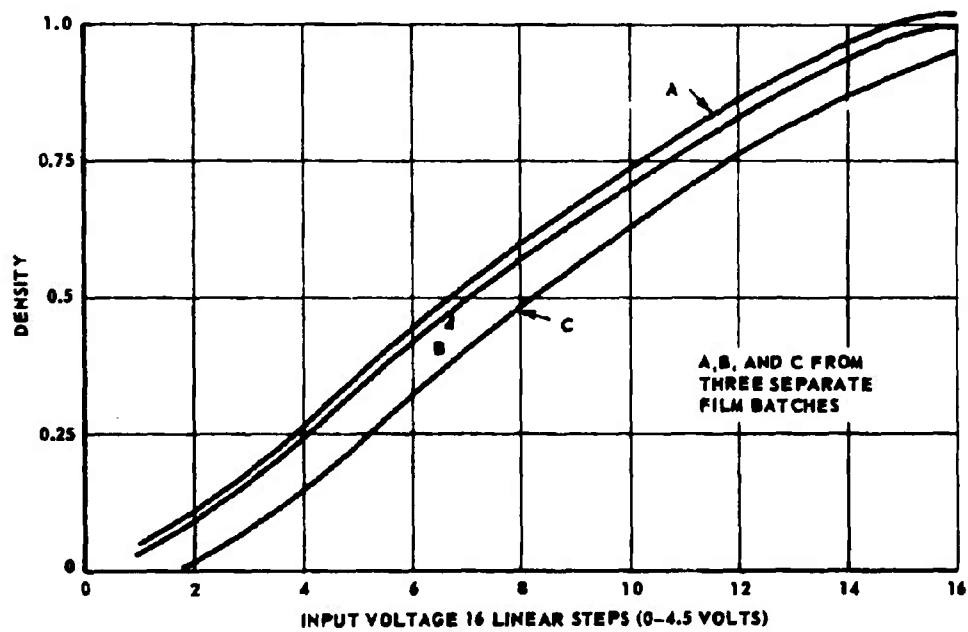


Fig. 10-6 REPRODUCER FILM BATCH VARIANCE

The second figure indicates the variations for films from three different batches. The most different of the three was the oldest and had also been out of the package longest. These plots establish two other points. First, the voltage to density transfer is approximately linear over a wide range, and second, the P/N 55 negative has a limited density range. With this density range a linear brightness to density transfer will limit the data range to 10:1. This limit can be overcome by using a nonlinear brightness to density transfer for producing the negative and the inverse transfer in the printing process. It might be noted here that the reflective density range of the P/N 55 positive is about 2 (100:1 range).

10.3 Data Analysis

The analysis of the camera data has thus far been mainly concerned with providing information as an aid to designing and evaluating methods for picture correction, and for photometric calibration. Most of the picture distortion analysis effort has been concerned with the line structure problem, and the photometric analysis has been limited primarily to establishing a transfer curve for producing a properly balanced color reference picture.

10.3.1 Picture Distortion

Fig. 10-7 is the data distribution corresponding to the uncorrected picture shown in Fig. 10-3. In this plot, which is a part of the line printer output from the TVSTAT program, the number of elements (plotted with an asterisk-increasing left to right) is printed at the left next to the element value. The number of elements is interpreted as the number of video elements of the picture having a voltage between the indicated value and the next value. For example, the first number 1010 means that there are 1010 picture elements within the picture having a voltage (at the camera output) between 0.0000 and 0.0998 volts.

The large number of elements at this lowest value is a result of the flyback pulse of the camera which contributes two near-zero elements

24 BIT ELEMENTS

0

FILTER *

22

CAMERA ANGLE *

SCAN TYPE = SLOW

AVERAGE VALUE OF ALL ELEMENTS = 2.4411

TIME = 100 16 11 08

ELEMENT VALUE NUMBER DISTRIBUTION

0.6000	1010
0.6004	540
0.1997	520
0.2005	240
0.3994	630
0.4002	520
0.5991	610
0.6000	560
0.7008	760
0.8006	1190
0.9005	1240
1.0003	2010
1.1003	2550
1.2000	3200
1.3000	3840
1.4077	4170
1.5074	4030
1.6075	1521
1.7073	3863
1.8072	9381
1.9070	10719
2.0069	26901
2.1068	25414
2.2066	22023
2.3065	14720
2.4062	8107
2.5062	5392
2.6060	7427
2.7059	12708
2.8057	16744
2.9056	16954
3.0054	16046
3.1053	17054
3.2051	14010
3.3050	9885
3.4048	6312
3.5047	2820
3.6046	1103
3.7044	415
3.8043	1560
3.9041	670
4.0039	650
4.1039	290
4.2036	50
4.3034	0
4.4033	0
4.5033	0
4.6031	0
4.7029	0
4.8028	0

Fig. 10-7 DATA DISTRIBUTION FOR PICTURE OF FIGURE 10-3

for each line. The first and highest peak in the distribution represents the black level of this picture. The actual earth data are seen to vary between approximately 2.2 and 4.2 volts. This distribution represents the output of the camera and includes the transfer of the logarithmic amplifier of approximately one volt per decade. It is clear from the distribution that the line structure does not cause saturation of the modulation system.

Fig. 10-8 is the second page output of the TVSTAT program. The data shown here are the line number, the average voltage of each line, and the first and second differences of the line average table. On the right is a threshold table. An asterisk is printed in a column whenever the voltage threshold at the top of that column is exceeded by the first difference. The third section of this print-out is a plot of the deviation of the line average from the frame average. A two page section of this plot is shown in Fig. 10-9. Note how clearly the line structure is indicated by this plot. Referring to the picture corresponding to this plot (Fig. 10-3), line 256 is the white line directly below the horizontal row of reticle marks, and line 192 is the brightest line above line 256. The fainter white line between lines 192 and 256 is line 224, and an equal distance above line 192 is another faint white line (line 160). Examination of the line average plot shows, in addition to this major line structure, other line structures with periods as short as 4 lines. Another interesting feature of the line structure is that lines 64, 192, 256, 320, and 448 are major lines whereas lines 128 and 384 are not. Recalling the discussion of the vertical scan system of Section 10.2, it is not hard to understand that the line structure has periods which are binary numbers. The fact that the average of lines 128 and 384 deviates from a smooth curve less than the average of: lines 62, 192, 256, 320, and 448 indicates that the voltage output of the camera scan D/A converter corresponding to the eighth bit is nearly equal to the output corresponding to the sum of all the previous bits plus a voltage equal to one normal step. The first time this bit is activated is for line 128; the second time is for line 384. The white lines at each multiple of 64

LINE	LINE AVERAGE	FIRST DIFFERENCE	SECOND DIFFERENCE	THRES1 0.0150	THRES2 0.0312	THRES3 0.0625	THRES4 0.1250	THRES5 0.2500	THRES6 0.5000	THRES7 0.7500
2	2.3090	2.3090	2.3090
3	1.6337	-0.6753	-2.8342
4	2.5581	0.9244	1.3077
5	1.7812	-0.7769	-1.4375
6	1.6447	-0.1365	0.5366
7	1.6850	0.0403	0.1500
8	1.6531	0.0290	0.0088
9	1.7241	0.0710	0.0822
10	1.7424	0.0183	-0.0159
11	1.7739	0.0312	0.0154
12	1.6280	0.0546	-0.0234
13	1.8364	0.0080	-0.0490
14	1.6384	-0.0059	-0.0139
15	1.6550	0.0241	0.0300
16	1.6079	0.0329	0.0088
17	1.6840	0.0760	-0.0230
18	1.9074	0.0695	-0.0005
19	1.9211	0.0137	0.0041
20	1.9809	0.0597	0.0466
21	1.9751	-0.0056	-0.0657
22	1.9019	0.0069	0.0117
23	2.0027	0.1002	0.0134
24	2.0264	0.0244	0.0041
25	2.0104	-0.0160	-0.0324
26	2.0210	0.0105	0.0125
27	2.0412	0.0202	0.0174
28	2.0781	0.0371	0.0166
29	2.0570	-0.0207	-0.0578
30	2.0551	-0.0022	0.0199
31	2.0864	0.0314	0.0337
32	2.1833	0.0964	0.0556
33	2.1091	-0.0742	-0.1786
34	2.0835	-0.0256	0.0485
35	2.0974	0.0139	0.0395
36	2.1394	0.0425	0.0295
37	2.1181	-0.0205	-0.0650
38	2.1194	0.0005	0.0210
39	2.1277	0.0078	0.0014
40	2.1521	0.0246	0.0166
41	2.1304	-0.0220	-0.0496
42	2.1411	0.0108	0.0327
43	2.1516	0.0108	0.0060
44	2.1907	0.0383	0.0275
45	2.1601	-0.0306	-0.0682
46	2.1504	-0.0090	0.0206
47	2.1677	0.0188	0.0206
48	2.1951	0.0285	0.0117
49	2.1804	-0.0261	-0.0544
50	2.1784	0.0080	0.0349
51	2.2017	0.0232	0.0144
52	2.2204	0.0193	-0.0034
53	2.2041	-0.0166	-0.0351
54	2.1974	-0.0069	0.0091
55	2.2040	0.0104	0.0173

Fig. 10-8 PAGE 2 OF TVSTAT OUTPUT

THE JOHNS HOPKINS UNIVERSITY
APPLIED PHYSICS LABORATORY
SILVER SPRING, MARYLAND

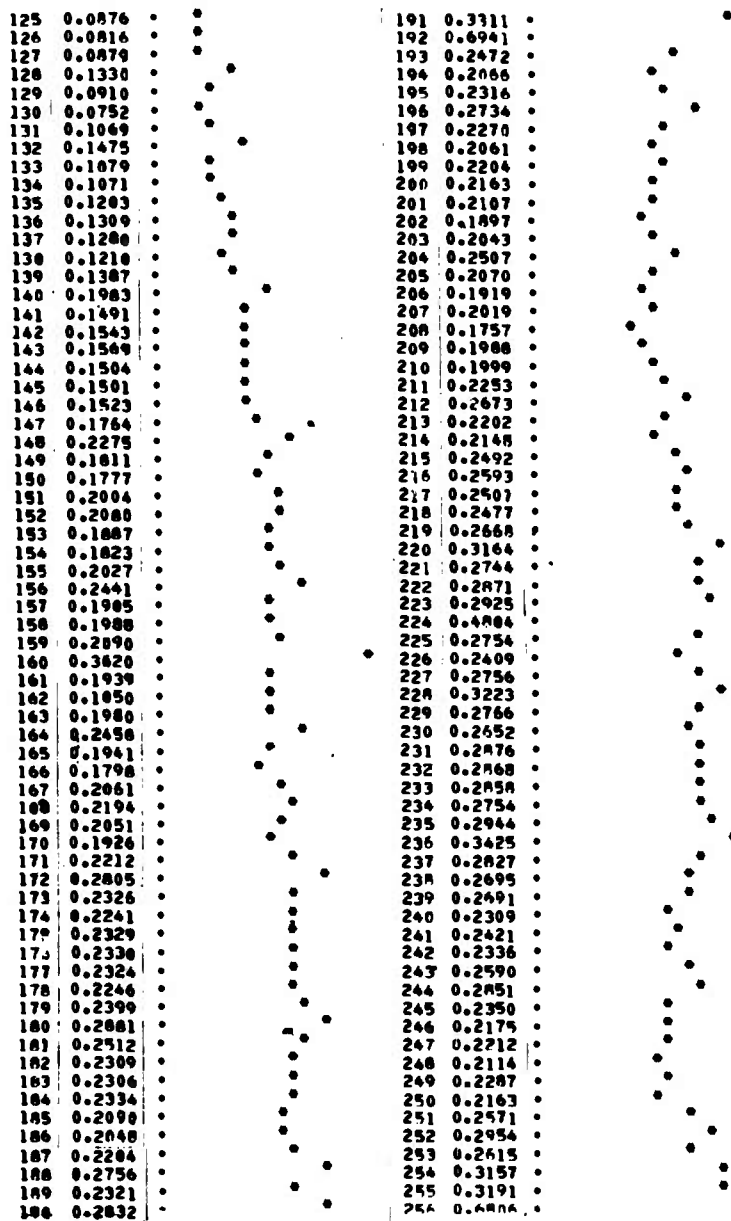


Fig. 10-9 SECTION OF THE LINE AVERAGE GRAPH FROM TVSTAT

(except 128 and 384) indicate that the voltage corresponding to the seventh bit of the scan converter is greater than the sum of all previous bits plus one normal step. Bits 3,6, and 9 also contribute to larger than normal steps. Bits 4 and 5 provide less than normal steps resulting in a black line structure.

10.3.2 Photometric Calibration

As noted above the photometric calibration has been limited to obtaining a monitor transfer to make possible a properly balanced color picture. Basically the method consists of measuring the camera voltage corresponding to the painted sectors of the color reference bass (the -2 end mass). These measurements are made on the green channel. Measurements have also been made of the brightness of each of the laboratory paint samples through a green filter (duplicate of the camera filter-a flight spare) with solar illumination. These two measurements make possible the construction of an "in-flight" brightness to voltage transfer for the camera. This transfer combined with the monitor voltage to density transfer provides the necessary information to shape the system brightness to density transfer. The system transfer is shaped by a camera voltage to monitor voltage transfer in the TVOUT program. Measurement of the reference ball voltages is made with the aid of the FRAME option in TVOUT. Fig. 10-10 shows the monitor output for this option. The square section outlines in white on the end mass is the region being measured. The measurement output from the line printer consists of the average, the standard deviation, and a distribution plot corresponding to the video elements within the square outline on the picture.

10.4 Picture Correction Procedures

The basic goal of the various correction procedures is to normalize the DODGE picture data for photometric interpretation. Since optimum packing of the data on magnetic tape can be realized only after the major line structure is removed, the

NUMBER STA 512 DAY 108 TIME 16 11 A UT 22 DEC CAM FAZE 4 F110 SLOW
 YCHTR = 222 YCHTR = 176 DIMENSION = 4 NUMBER OF ELEMENTS = 63
 AVERAGE OF ALL DATA POINTS 0.020
 STANDARD DEVIATION 0.001

FRAME DATA DISTRIBUTION

INTENSITY	NUMBER
0.020	1
0.050	0
0.060	1
0.070	1
0.075	1
0.080	2
0.085	2
0.090	7
0.095	6
0.100	7
0.105	4
0.110	3
0.115	3
0.120	5
0.125	1
0.130	0
0.135	1
0.140	1
0.145	1
0.150	1

NOT REPRODUCIBLE

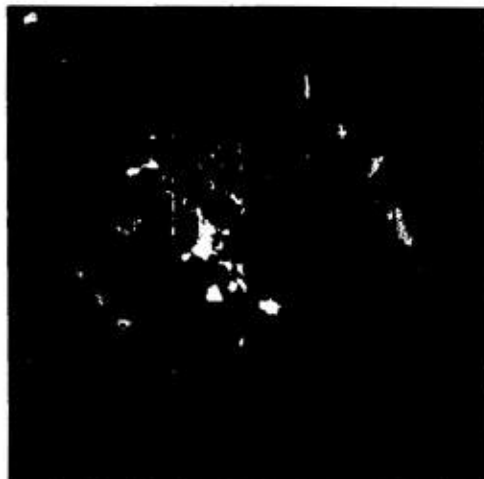


Fig. 10-10 OUTPUT OF FRAME

correction process is important to the method of picture storage. It thus influences the general data handling plan and establishment of a digital magnetic tape file of the DODGE pictures. Providing such a file is one of the prime objectives of the picture study.

The general plan for handling pictures is to select those pictures from the real time picture file (attitude data file) which are considered to contain useful picture data. The analog tapes containing the selected pictures are played back and a digital tape is produced. These tapes are then processed to remove the major line structure and stored in the magnetic tape file. The prestorage processing reduces the data range for more efficient packing and permits the establishment of a useful picture library, while experimentation is continuing on methods of correction. In addition to this experimentation, other forms of special processing will be undertaken. Study of data compression techniques, methods of picture data display, and "in-flight" performance evaluation of the camera system, are a few of the areas where further special processing can be useful.

10.4.1 Prestorage Processing

Methods have been designed to remove the major line structure, reduce the background nonuniformity, and remove random noise errors from the pictures. Before any processing is undertaken the raw data are converted from their logarithmic form to a linear format. Fig. 10-11 is an uncorrected picture and its data distribution after the antilogarithmic conversion. This is the same picture shown in Fig. 10-3, and the distribution can be compared to Fig. 10-7 which relates to the logarithmic data. This picture, which is used throughout this discussion, is the green part of a color picture taken 22 September 1967. Fig. 10-12 shows the picture and its data distribution after the background correction. The next step in the process removes the random noise errors and corrects the line structure.

NOT REPRODUCIBLE

TIME = 100 16 11.00 SCAN TYPE = SLOW CAMERA ANGLE = 22 FILTER = 0 24 HIT ELEMENTS
AVERAGE VALUE OF ALL ELEMENTS = 1.2849

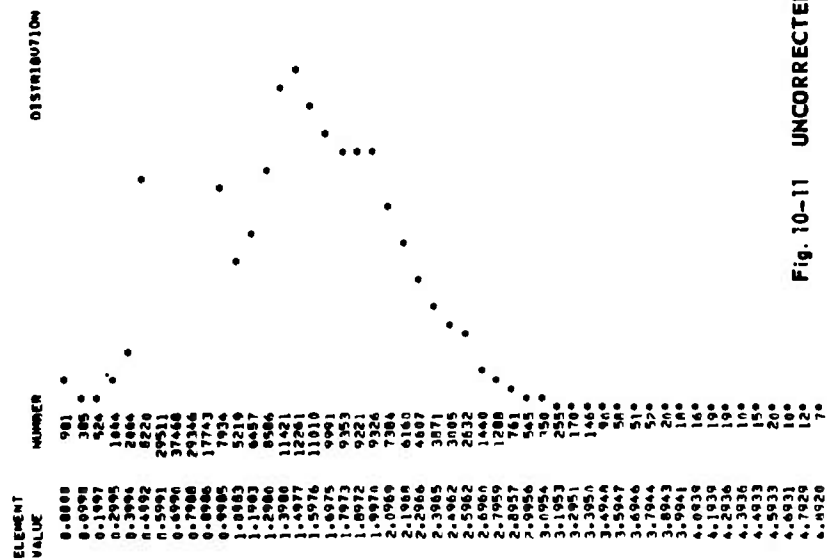


Fig. 10-11 UNCORRECTED PICTURE AND ITS DATA DISTRIBUTION

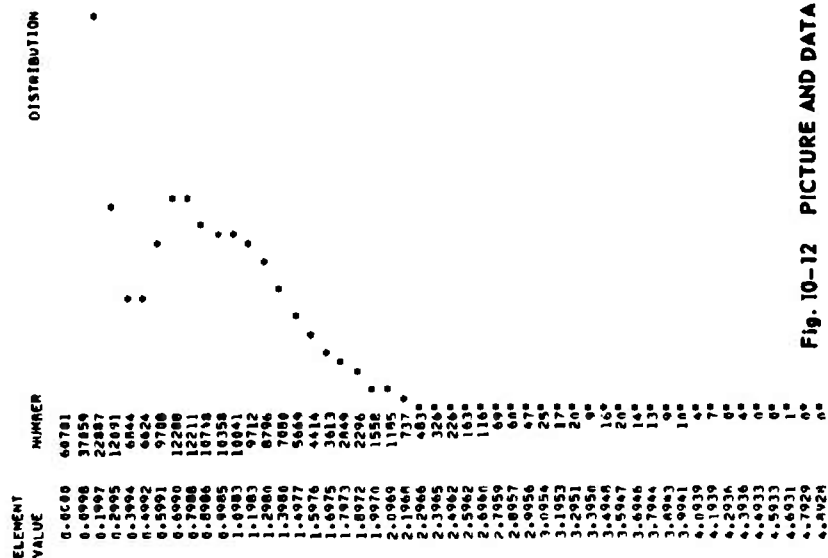
NOT REPRODUCIBLE

24 BIT ELEMENTS

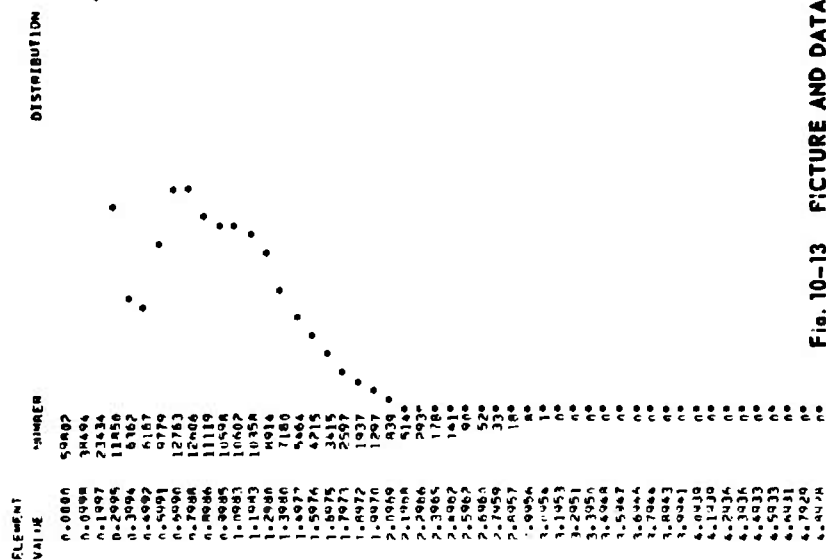
FILTER = 0

CAMERA ANGLE = 22

TIME = 108 16 11 08
AVERAGE VALUE OF ALL ELEMENTS = 0.6147



TIME = 108.1A 11.3A SCAN TYPE = SLOW
AVERAGE VALUE OF ALL ELEMENTS = 0.4017
CAMERA ANGLE = 22 FILTER = 0 20 HIT ELEMENTS



NOT REPRODUCIBLE



Fig. 10-13 PICTURE AND DATA DISTRIBUTION AFTER PRESTORAGE CORRECTIONS

Random noise corrections are accomplished by noting a large single element change in the data. Such spikes are generally the result of a poor signal to noise condition or the result of an interfering signal. In the scan direction the noise components frequently obscure more than one element. However, in the vertical direction noise is almost always restricted to a single element width. The method of correction simply replaces the identified noise element by the average of the adjacent elements. The threshold is set such that no scene detail one element in extent is identified as noise. This is possible since the tube response at this high frequency is restricted to less than 20% of a low frequency black to white transition. Noise components, on the other hand, usually result in large signal level changes.

Line corrections are made under the assumption that the line average of a picture should be a slowly varying function of a generally continuous nature. The nonuniformities of the line average structure are modified by establishing a new line average function smoothed by replacing the displaced averages, resulting from the larger scan errors, by the average of the adjacent lines. A gain correction is computed from the ratio of the corrected average and the original average, and each element of the displaced lines is multiplied by the corresponding gain correction. With the larger errors reduced, the line averages are filtered through use of a digital RC filter and a bias adjustment, equal to the difference of the line averages before and after filtering, is added to each line. The effect of these corrections is to alter the gain and bias on a line by line basis such that the line average function varies slowly and smoothly. This form of correction has no effect on the high frequency data in the scan direction. In the cross-scan direction, modification of the high frequency response is possible but very unusual. The result of these corrections is shown in Fig. 10-13. The shift in distribution in the region above 1.8 volts results from the shifting of the white picture lines into their proper range (Compare to Fig. 10-12). It is important to note that this line correction procedure restores the actual line data to their

proper relationship in the picture. It is not a method for replacing a bad line. The output picture from this process is shown again enlarged in Fig. 10-14 for comparison with Fig. 10-3.

10.4.2 Special Processing

Several special processing programs have been written and tested which are either outside the picture correction category or are not suitable to, or ready for the standard correction process. The line scan filter (LSF) program is a general program which removes structure related to inaccuracies in the scan system. The general nature of this program is less suitable to correcting the large scale deviations in the DODGE pictures than the method currently in use. This program has been used with success after the preprocessing routine. It is currently not part of the standard process due to its relatively long running time. However, it may be incorporated into a new standard process later.

The high resolution (HIRES) program is a special program which is not within the correction category. This program expands a DODGE picture to 1024 elements in each direction by generation of intermediate elements which are the average of the adjacent elements. The purpose of this program is to allow monitor reproduction without further degradation of the original picture resolution. That is, if the monitor spot size is adjusted to produce continuous grays, the resolution of the monitor is approximately the same as the camera, and the picture resolution is reduced by both. With the 1024 x 1024 picture format, spot size overlap can be employed on the monitor to produce continuous grays without significantly reducing the picture resolution from the 500 line limit set by the camera. High frequency corrections have been limited to relatively few tests and more analysis is necessary before this type of correction can be a part of the normal process. A filter program (TVFLTR) is available for one type of high frequency enhancement, but the parameters have not been adjusted for best results.

NOT REPRODUCIBLE

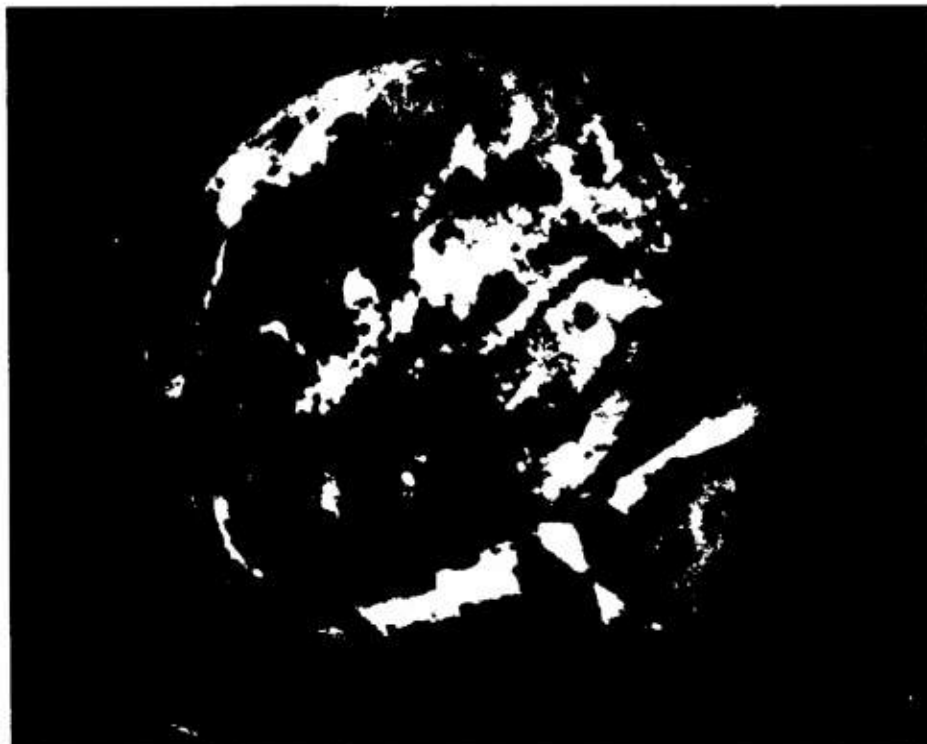


Fig. 10-14 ENLARGED PICTURE AFTER PRESTORAGE CORRECTIONS

10.5 Photographic Procedures

A special dark room has been set up for the purpose of producing prints from the Polaroid negatives obtained from the TV reproducer. Special emphasis has been put on establishing a technique for producing color pictures. The method which has proved most satisfactory is to make an enlargement directly from the three negatives, each exposed separately through the proper color filter. Registration is accomplished on a test print mounted in a frame on the enlarger table. Step by step, the method is as follows:

- a. Place the test print in the registration frame and position the "blue" negative in the enlarger head.
- b. Manually position the registration frame such that the projected image is in register.
- c. In complete darkness place the color paper in the registration frame and slide the blue filter into position. Expose the paper and return it to dark storage.
- d. Place the test print in the frame again and position the "green" negative. Repeat the above procedure.
- e. Repeat again for the red exposure.
- f. Process the print by the normal methods.

An experienced operator can produce a print by this method with a Kodak rapid color processor in 20 to 30 minutes.

To check the color fidelity of the picture, measurements are made on the color reference ball in the picture with a color densitometer. Similar readings have been made on the paint samples. Each paint color is measured through each filter resulting in a matrix of nine measurements.

A measurement is made on a white portion of the print and is used to normalize the difference between the reflectance of the white paint sample and the white portion of the print. A difference matrix is computed from the color matrix for the paints and the color matrix for the prints. A null matrix would result if the print were perfect. The matrix which results for any real picture indicates the variance required in the balance in order to produce the desired result. A large series of variations was attempted with the same print in an attempt to minimize the color difference matrix. The best result obtained has been retained as a color reference for comparisons with other processing methods.

Another method of color balance has also been attempted in which each step in the process was independently calibrated. The photographic calibrations in combination with the monitor and camera calibrations discussed above were all combined in an effort to improve on the first result. To date, the initial method has still provided the best result.

10.6 Optical Processing

Although the primary picture processing effort is directed toward digital techniques, a limited amount of experimentation has been carried out on optical processing techniques. The heart of the optical processing system is a two dimensional optical Fourier transformation. Fig. 10-15 is a schematic of the basic optical system. Coherent light is passed through a transparency of the picture being processed and then through a lens. The intensity distribution at the focal point of this first lens is an optical analog of the two dimensional Fourier transform of the input picture. For a simple example consider a clear transparency at the object plane. In this case, the collimated light into the first lens results in a single point of light at the focal plane, this represents

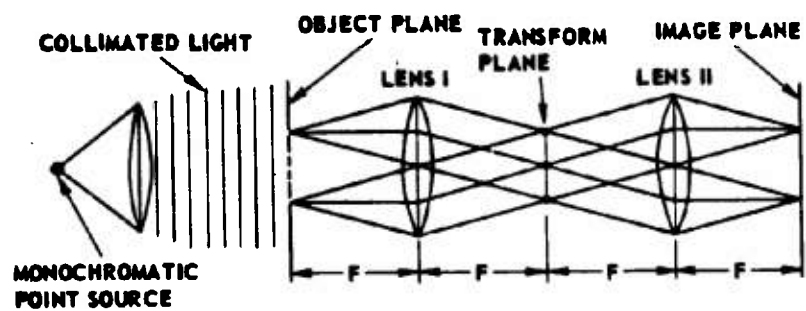


Fig. 10-15 SCHEMATIC OF BASIC OPTICAL SYSTEM

the zero frequency component of the input transparency. An input transparency with a series of horizontal lines will result in a series of vertical dots at the focal plane due to interference between the vertically distributed coherent light sources as viewed from different angles by the input lens. These dots are an optical analog of the spatial frequency distribution of the horizontal lines. A second lens, located as shown in the basic schematic, transforms the intensity distribution at the central focal plane back to an image of the input picture at the second focal plane. The lens system as shown is a simple one to one transfer. However, due to the coherent nature of the input light, the frequency characteristic of the input picture is represented at the central focal plane. Filtering at this point can remove undesirable frequency components from the output image.

The method as applied to the removal of line structure in a DODGE picture is illustrated in Fig. 10-16. Relative to the locations shown in Fig. 10-15, a transparency of the input picture is located at the object plane. The Fourier transform of the picture is obtained at the transform plane, where it is filtered as shown. The output picture is recorded on film at the image plane. The figure clearly shows the removal of the line structure. The use of optical Fourier processing has a wide range of application beyond the example given here. A more complete discussion is given in Ref. 10-1.

10.7 References

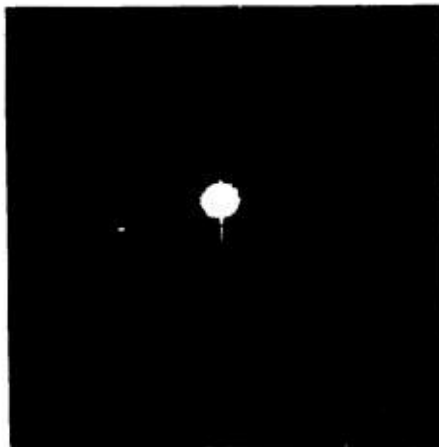
- 10-1 F. W. Schenkel, "Fourier Transform Optical Image Processing", Quarterly Report - Space Programs U-SQR/68-2, April-June 1968.



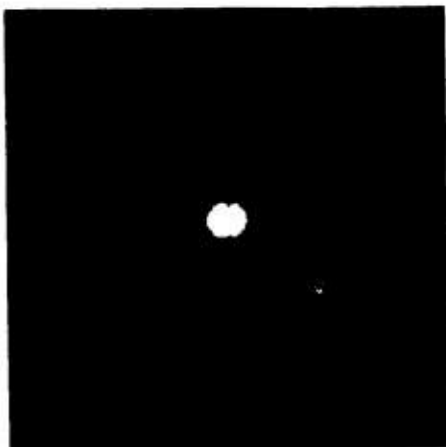
NOT REPRODUCIBLE



INPUT PICTURE



FOURIER TRANSFORM



FILTERED FOURIER TRANSFORM



OUTPUT PICTURE

Fig. 10-16 OPTICAL LINE REMOVAL

11. MAGNETIC FIELD MEASUREMENTS

About 1 May 1968, experiments were started for a study of quasi-sinusoidal geomagnetic micropulsations (a class of temporal variations of the magnetic field) and for an additional investigation of the DODGE magnetic anomaly. In both cases auxiliary data are desirable, and collaborative efforts were established with (a) the University of California at Los Angeles, which has a magnetic experiment aboard the synchronous satellite ATS-I; and (b) ESSA/ITSA, Boulder, Colorado, which has a set of ground stations.

When DODGE is within telemetry range of the APL/JHU Howard County Station, the satellite is commanded to measure continuously the vector magnetic field for four hours each day. Data are being acquired when the satellite is at and near the following longitudes:

- a. 210°E , for comparison with results obtained by the ATS-I satellite and by the ground stations at College, Alaska, and Maui, Hawaii.
- b. 275° to 285°E , for comparison with the ground data from Great Whale River, Canada; Byrd, Antarctica; and Lima, Peru.

Sampling at other longitudes is being programmed to achieve coverage over the range 210° to 360°E at times when the magnetic variations are present.

The micropulsations frequently appear. An example is shown in Fig. 11-1. Here, X, Y, and Z represent respectively the approximately northward, eastward, and downward components of the geomagnetic field; each component is normalized to the value existing at 1735 UT 14 June. In this case, the micropulsations are mainly in the Y component and are almost linearly polarized in the plane normal to the geomagnetic field of origin

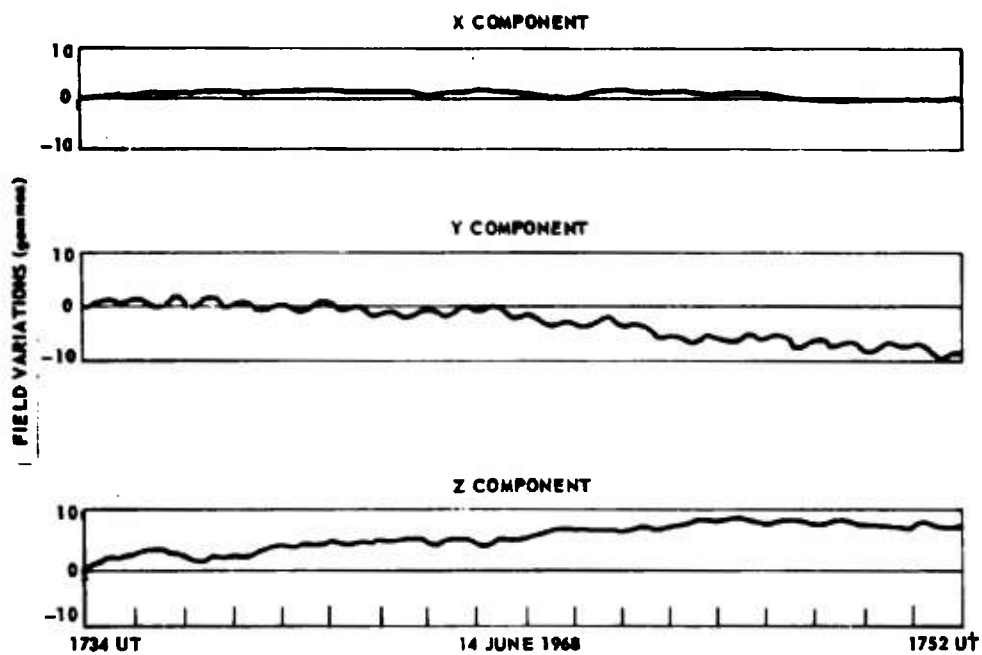


Fig. 11-1 AN EXAMPLE OF GEOMAGNETIC MICROPULSATIONS

internal to the earth. The peak-to-peak amplitude is about 5 gammas (1 gamma = 10^{-5} gauss) and the period about 40 seconds.

Computer programs for data analysis are being "debugged." It is expected that new results will be forthcoming in the following areas: the influence of the satellite on the field as detected by the magnetometers; the fundamental modes of the magnetosphere and their excitation by the solar wind; propagation of micropulsations across as well as along the geomagnetic field lines.

12. CONCLUSIONS

Itemized below are the most significant conclusions which have been derived from the DODGE satellite experiment.

- a. Two-axis and three-axis gravity-gradient stabilization is achievable at synchronous altitude.
- b. Three-axis stabilization can be achieved with the use of multiple booms, and improved yaw stabilization can be achieved with the use of booms plus an angular momentum flywheel.
- c. Computer simulations which can predict the motions of gravity stabilized satellites have been developed.
- d. The magnetometer system on board the satellite has a systematic error caused by some interaction with the spacecraft. This interaction is certainly influenced by the attitude of the spacecraft relative to the sun.
- e. In spite of the deficiency in the magnetometer system mentioned in d above, the magnetic sample-hold damping system has proven to be an effective means for removing satellite libration.
- f. With the magnetic sample and hold system on the DODGE satellite the best stabilization achieved to date has been approximately 2° rms in pitch, 2.5° rms in roll, and 10° rms in yaw (during Pass 8 and most of Pass 41). This condition was not maintained however for any considerable length of time. Without the flywheel running, disturbances in the attitude are usually initiated by large disturbances in yaw. When the flywheel is on, yaw stability is distinctly improved and never becomes unstable.

- g. The satellite always shows improved stabilization when the sun line is contained in the orbit plane. This is undoubtedly a result of a lower level of solar radiation pressure disturbance during this time. This is predicted by the computer simulations.
- h. Measurements of boom bending confirm that the magnitude of the bending as theoretically calculated is close to being correct, however a small hysteresis effect in boom bending has been observed which was not considered by any prior investigators. A lack of straightness has been observed in the one boom on which this measurement could be made. Although the boom was the straightest available within the existing state-of-the-art and was within design specifications, it still deviated by 1.2° from being straight. The combined effects of lack of straightness, hysteresis in boom bending, and the boom bending itself are probably the reasons why the DODGE satellite does not more accurately achieve three-axis gravity-gradient stabilization. These deviations from the theoretical model of boom bending also account for the fact that computer prediction of satellite attitude has been accurate in magnitude over many days but after more than 1-1/2 days a phase discrepancy in the attitude motions is usually observed.
- i. The torsion wire damper boom system has never appeared to be effective in damping DODGE satellite oscillation. This is possibly due to the fact that there is an appreciable angular bias from the rest position of the damper boom.

Listed below are several conclusions regarding the technological aspects of the DODGE satellite which are significant:

- a. Extendible boom units using 400 Hz, AC, hysteresis synchronous motors are exceedingly reliable for repeated operations in the space environment. A total of more than 200 such operations on individual booms have been performed in the first year of satellite operation.

- b. Television cameras are an excellent means for attitude determination.
- c. Color photography of the earth using color filters has been shown to be practical and reliable.
- d. The DODGE telemetry system, in which the rf power can be altered, the information bandwidth can be altered, the transmitted frequency can be changed, and a directional or an omnidirectional antenna can be selected, has proven to be exceedingly valuable for obtaining data from experimental satellites.

In summary, the DODGE satellite has achieved its primary objective of obtaining gravity-gradient stabilization at near-synchronous altitude. Usually the attitude alignment is poorer than desired. This is undoubtedly due to some unknown interaction between the satellite and its magnetometers. In the case of the torsion wire damper, the lack of damping observed is probably due to an angular bias offset that has been observed in flight.

On the DODGE satellite it was not convenient to place the magnetometer sensors as far from the satellite body as would be desired. If this were done on another spacecraft, particularly a satellite with a single boom, dumbbell configuration, and an angular momentum flywheel for yaw control, one could expect that accuracies of better than 1° peak angle each in roll, pitch, and yaw could be achieved at synchronous altitude.

13. BIBLIOGRAPHY

1. Andren, C. F.: "DODGE Main and Standby Converters." APL report U-SQR/66-1, January-March, 1966.
2. Andren, C.: "Regulated DR to DC Converters." APL report U-SQR/65-3, July-September, 1965.
3. Aspnes, J. D.: "Vidicon Camera Tube Evaluation." APL report U-SQR/66-1, January-March, 1966.
4. Bainum, P. M., Anand, D.K., and Mackison, D. L.: "Perturbations and Lyapunov Stability of a Multiple Connected Gravity-Gradient Satellite at Synchronous Altitude," Fifth U. S. National Congress of Applied Mechanics, Paper No. 242, June 14-17, 1966.
5. Bainum, P. M., Anand, D. K., and Mackison, D. L.: "Lyapunov Stability and Solar Perturbations of a Passively Damped Gravity-Gradient Satellite," APL report TG-854, September 1966.
6. Bainum, P. M.: "On the Motion and Stability of a Multiple Connected Gravity-Gradient Satellite with Passive Damping," APL report TG-872, January 1967; also Ph.D. Dissertation The Catholic University of America, December 1966.
7. Bainum, P. M., and Mackison, D. L.: "Gravity-Gradient Stabilization of Synchronous Orbiting Satellites," The British Interplanetary Society Spring Meeting, April 1967; also to appear in The Journal of the British Interplanetary Society, December 1968.
8. Beal, R. C.: "Design and Performance of the DODGE Cameras," APL Technical Digest, Vol. 6, No. 5, May-June, 1967.
9. Beal, R. C.: "DODGE TV Camera Head Electronics," APL report U-SQR/66-1, January-March, 1966.

10. "DODGE Operations Plan by Space Development Department," APL report SDO 2077, June 1967.
11. Dozsa, J. R.: "DODGE TV Camera Sequencer (Main System)," APL report U-SQR/66-1, January-March, 1966
12. Dozsa, J. R.: "DODGE TV Tape Clock Unit," APL report U-SQR/68-1, January-March, 1968.
13. Dunn, J. T.: "DODGE Field Operations," APL report U-SQR/67-3, July-September, 1967.
14. Fischell, R. E.: "A Gravity-Gradient Satellite Experiment at Synchronous Altitude," 2nd IFAC Symposium on Automatic Control in Space, September 1967.
15. Fischell, R. E.: "The DODGE Satellite," AIAA/JACC Guidance and Control Conference, 15 August 1966.
16. Harrison, J. S.: "DODGE Spacecraft Telemetry Reduction Program," APL report U-SQR/67-1, January-March, 1967.
17. Heins, R. J.: "DODGE TV Power Supply," APL report U-SQR/66-3, July-September, 1966.
18. Hickerson, R. L.: "DODGE Attitude Determination," APL report U-SQR/67-3, July-September, 1967.
19. Holland, Bruce B.: "Doppler Tracking of Near-Synchronous Satellites," APL report TG-1006,
20. Holland, Bruce B.: "Doppler Tracking of Near-Synchronous Satellite (DODGE)," AAS/AIAA Astrodynamics Special Conference, AAS Paper No. 68-128, 3-5 September 1968.
21. Holland, B. B., and Hook, B. J.: "DODGE Doppler Tracking," APL report U-SQR/67-3, July-September, 1967.
22. Hull, W. E.: "Torsion Wire Damper System for DODGE Satellite," APL report U-SQR/66-3, July-September, 1966.

23. Hull, W. E., and Howard, D. M.: "Boon End-Mass Lock Assembly," APL report U-SQR/66-3, July-September, 1966.
24. Loessi, J. C.: "The DODGE Programmer," APL report U-SQR/66-2, April-June, 1966.
25. Mackison, D. L.: "Analysis of Time-Delay Magnetic Damping of Spacecraft Librations in Near-Synchronous Equatorial Orbits," APL report TG-916, June 1967.
26. Mackison, D. L., and Bainum, P. M.: "Magnetic Sample-and-Hold Damping of a Gravity-Gradient Stabilized Satellite," accepted for presentation at The Air Force Gravity-Gradient Symposium, Aerospace Corporation, (Orbital Results Session), December 3-5, 1968.
27. Marsh, L. B.: "DODGE TV Reproduction Console," APL report U-SQR/67-1, January-March, 1967.
28. Marsh, L. B., and Pokorny, A. J.: "DODGE Television Reporducer" (U), APL report TG 277-11 (C), APL Accomplishments, FY 1967.
29. Marsh, L. B., and Pokorny, A. J.: "DODGE TV Reproduction System," APL report TG-1014, September 1968.
30. Marsh, L., and Pokorny, A.: "DODGE TV Reproducer Station Manual."
31. Marshall, E. L., Mobley, F. F., and Thompson, T.: "DODGE Satellite" (U), APL report TG 277-11 (C), APL Accomplishments, FY 1967.
32. Milne, J. S.: "DODGE Satellite Environmental Tests," APL report U-SQR/66-1, January-March, 1966.
33. Milne, J. S.: "DODGE Satellite Environmental Tests," APL report U-SQR/67-1, January-March, 1967.
34. Milne, J. S.: "DODGE Satellite Environmental Tests," APL report U-SQR/67-2, April-June, 1967.

35. Mobley, F. F.: "Enhanced Magnetic Damping System," APL report U-SQR/66-3, July-September, 1966.
36. Mobley, F. F.: "Gravity Stabilization and Damping of DODGE Using the Magnetic Sample and Holding System," APL report U-SQR/67-3, July-September, 1967.
37. Mobley, F. F.: "Gravity-Gradient Stabilization Results from the DODGE Satellite," AIAA 2nd Communications Satellite Systems Conference, No. 68-460, 9 - 10 April 1968.
38. Mobley, F. F., Brown, R. D., and Ford, J. A.: "Eddy-Current Damper for Torsion-Wire System," APL report U-SQR/66-3, July-September, 1966.
39. Mobley, F. F., and Fischell, R. E.: "Orbital Results from Gravity-Gradient Stabilized Satellites," APL report TG-826, October 1966.
40. Morrison, J., Tossman, B. E., and Mobley, F.: "DODGE-RAE Satellite Attitude Dynamics Analog Simulation," APL report U-SQR/66-1, January-March, 1966.
41. Mullens, D. G.: "DODGE Command System Test Program," APL report U-SQR/67-1, January-March, 1967.
42. Pardo, P. P.: "A Description of the Digital Attitude Simulation," APL report TG-964, February 1968.
43. Pisacane, V. L.: "Three-Axis Stabilization of a Dumbell Satellite by a Small Constant-Speed Rotor," APL report TG-855, October 1966.
44. Pisacane, V. L., Guier, W. H., Pardoe, P.P.: "Dynamical Equations for the Position and Attitude of a Spacecraft with Time Dependent Mass and Mass Properties," APL report TG-919, June 1967.

45. Pisacane, V. L., Pardoe, P. P., and Whisnant, J. M.: "Simulation of the Attitude Stabilization of the DODGE Spacecraft with Time-Lag Magnetic Damping," APL report TG-949, October 1967. (XVIII Congress--International Astronautical Federation, Belgrade, Yugoslavia, September 1967)
46. Pokorny, A. J.: "DODGE Telemetry Ground Support." APL report U-SQR/66-3, July-September, 1966.
47. Samburoff, S., and Thompson, T.: "DODGE TV Camera Head Mechanical Design," APL report U-SQR/66-1, January-March, 1966.
48. Schenkel, F. W.: "DODGE Satellite Color Television Capabilities," APL report U-SQR/66-1, January-March, 1966.
49. Schenkel, F. W.: "Filtering for Rayleigh Scattering in the 22" FOV Color-Black and White Television Camera," APL report U-SQR/66-1, January-March, 1966.
50. Schenkel, F. W.: "Illumination and Sun Sensor Significance," APL report U-SQR/65-3, July-September, 1965.
51. Schenkel, F. W.: "Illumination and Sun Sensor for DODGE Satellite," APL report U-SQR/66-4, October-December, 1966.
52. Schenkel, F. W.: "Photometric and Optical Consideration in the DODGE Satellite TV Camera Design," APL Technical Digest, Vol. 6, No. 5, May-June, 1967.
53. Seylar, G. R.: "Telemetry System for the DODGE Satellite," APL report U-SQR/66-2, April-June, 1966.
54. Sloan, R. F.: "A Time-Lag Generator for the DODGE Attitude Stabilization System," APL report U-SQR/66-3, July-September, 1966.
55. Sloan, R. R.: "A Time-Lag Generator for Spacecraft Magnetic Damping Systems," APL report TG-965, January 1968.

56. Smola, J. F., Howard, D. M., and Radford, W. E.: "DODGE Extendible Boom Operations," APL report U-SQR/67-3, July-September, 1967.
57. Spedden, E. H., Jr.: "Modular Satellite Telemetry System," APL report U-SQR/65-4, October-December, 1965.
58. Spedden, E. H., Jr.: "Modular Satellite Telemetry System," APL report U-SQR/66-1, January-March, 1966.
59. Stephens, R. A.: "Solid State 240 Mc/s Ground Receiving System Preamplifier for DODGE Satellite," APL report U-SQR/66-2, April-June, 1966.
60. Stott, D.D.: "DODGE TV-CDC 3200 Computer System," APL report U-SQR/67-2, April-June, 1967.
61. Thompson, T.: "The DODGE Television System," APL report U-SQR/66-1, January-March, 1966.
62. Thompson, T.: "The DODGE Television System," APL Technical Digest, Vol 6, No. 5, May-June, 1967.
63. Thompson, T.: "DODGE TV System," APL report U-SQR/67-3, July-September, 1967.
64. Thompson, T.: "Picture Geometry and Photometry for the DODGE Television System," APL report U-SQR/66-1, January-March, 1966.
65. Thompson, T.: "System Geometry for the DODGE Television System," APL report U-SQR/66-1, January-March, 1966.
66. Thompson, T., and Beal, R. C.: "A Slow Scan Television System for Attitude Measurement at Synchronous Altitudes," APL report TG-993, April 1968; Supplement to IEEE Transactions on Aerospace and Electronic Systems, Vol. AES-3, No. 6 (November 1967), pp. 72-79; reprint issued 8 December 1967.
67. Thompson, T., and Beal, R.: "Evaluation of the DODGE Camera System," APL report U-SQR/67-1, January-March, 1967.

68. Tossman, B. E.: "Hysteresis Generator for Enhanced Magnetic Damping System," APL report U-SQR/66-3, July-September, 1966.
69. Tossman, B. E.: "Magnetic Hysteresis Damper," APL report U-SQR/66-3, July-September, 1966.
70. Tossman, B. E.: "Performance of Enhanced Magnetic Hysteresis System in Removing Spin and Tumble of DODGE," APL report U-SQR/67-3, July-September, 1967.
71. Vanderslice, J. L.: "DODGE Satellite Libration Dynamics," APL report U-SQR/65-4, October-December, 1965.
72. Weaver, K. F.: "Historic Color Portrait of Earth From Space," National Geographic, Vol. 132, No. 5, November 1967, p. 726.
73. White, P. E. P., and Dunnell, C. A.: "Portable Clock Time Transfers to Station 008 Brazil, 013 Japan, and 112 Australia," APL report U-SQR/67-2, April-June, 1967.
74. Wilson, L.: "DODGE Power System," APL report U-SQR/67-3, July-September, 1967.
75. Wilson, L.: "DODGE Satellite Power System," APL report TG-978, May 1968.
76. Wingate, C. A., Flieger, H. W., and Nordeen, R. D.: "DODGE Thermal Design" (U), APL report TG 277-11 (C), APL Accomplishments, FY 1967.
77. Wingate, C. A., Jr., and Flieger, H. W., Jr.: "Thermal Design and Performance of DODGE Spacecraft," APL report U-SQR/67-3, July-September, 1967.
78. Zitterkopf, D. L.: "DODGE TV Video Test Pattern Generator," APL report U-SQR/67-1, January-March, 1967.

UNCLASSIFIED
Security Classification

DOCUMENT CONTROL DATA - R & D		
<i>(Security classification of title, body of abstract and indexing annotation must be entered when the overall report is classified)</i>		
1. ORIGINATING ACTIVITY (Corporate author) The Johns Hopkins University, Applied Physics Lab. 8621 Georgia Avenue Silver Spring, Maryland		2a. REPORT SECURITY CLASSIFICATION Unclassified
		2b. GROUP
3. REPORT TITLE DODGE Satellite Performance, 1 July 1967--1 October 1968, Volumes A and B--		
4. DESCRIPTIVE NOTES (Type of report and inclusive dates)		
5. AUTHOR(S) (First name, middle initial, last name) Space Development Department		
6. REPORT DATE January 1968	7a. TOTAL NO. OF PAGES 569	7b. NO. OF REFS 115
8a. CONTRACT OR GRANT NO. NOw 62-0604-c	9a. ORIGINATOR'S REPORT NUMBER(S) TG-1034A and TG-1034B	
b. PROJECT NO.		
c.	9b. OTHER REPORT NO(S) (Any other numbers that may be assigned this report)	
d.		
10. DISTRIBUTION STATEMENT This document has been approved for public release and sale; its distribution is unlimited.		
11. SUPPLEMENTARY NOTES		12. SPONSORING MILITARY ACTIVITY Naval Air Systems Command
13. ABSTRACT In Volume A of this report the mission of the Department of Defense Gravity Experiment (DODGE) satellite program is defined, the design of each of the satellite systems is briefly described, and the performance of each of the systems from the time the satellite was launched into orbit on 1 July 1967 to 1 October 1968 is described in detail. The systems include attitude control, attitude detection, electric power, telemetry, command, thermal control, and doppler tracking. It also includes ground station operations. The report summarizes the magnetic field measurements made to date and the performance of the satellite's attitude control systems. It presents conclusions on the attitude performance and on how well the objectives of the mission were met. Volume B is an Appendix and contains pitch-roll, yaw, and in-plane-cross-plane plots for APL passes 2 through 39 and ORRORAL passes 2, 9, 14, 16, and 17.		

DD FORM 1473
1 NOV 65

UNCLASSIFIED
Security Classification

UNCLASSIFIED

Security Classification

14.

KEY WORDS

Angular momentum flywheel
Colored earth pictures
Dual television camera system
Extendible booms
Gravity gradient stabilization
Magnetic damping
Magnetic stabilization
Manual damping
Near-synchronous
Torsion wire damping

UNCLASSIFIED

Security Classification